UNIVERSITY OF SOUTHAMPTON

ASSESSMENT OF ANKLE ARTHRODESIS WITH INTERNAL FIXATION USING FINITE ELEMENT ANALYSIS

Ana Alonso Vázquez

A thesis submitted in partial fulfilment of the requirements for the degree of

Doctor of Philosophy

SCHOOL OF ENGINEERING SCIENCES

Bioengineering Sciences Research Group

April 2003

UNIVERSITY OF SOUTHAMPTON
ABSTRACT
FACULTY OF ENGINEERING AND APPLIED SCIENCES
BIOENGINEERING SCIENCE RESEARCH GROUP
Doctor of Philosophy

ASSESSMENT OF ANKLE ARTHRODESIS WITH INTERNAL FIXATION USING FINITE ELEMENT ANALYSIS

by Ana Alonso Vázquez

Ankle arthrodesis has been the gold standard surgical treatment for painful and disabling ankle diseases whose symptoms do not respond to conservative treatment. Despite improvements and new techniques that have resulted in high levels of performance, cases of fusion failure are still reported. Initial stability at the fusion site is believed to be one of the main mechanical factors affecting the outcome of the arthrodesis. Biomechanical studies have tried to establish the best way to achieve a rigid fixation, by comparing the gross motion between the tibia and the talus when using different fixation techniques. However, little is know about the mechanical response of ankle arthrodesis constructs at the fusion site. The purpose of this research was to use the finite element method as a comparative tool to assess the initial stability at the fusion site of ankle arthrodesis constructs internally fixed with screws.

Digital image-based finite element models of ankle arthrodesis constructs were built and subjected to the load cases most likely to affect the ankle in the postoperative period. Mesh refinement and sensitivity analyses were performed upon a reference model. Two joint surface preparation techniques (preserved and flat cut joint contours) were compared in ankle constructs fixed with two and three screws in different configurations. Normal and poor bone quality were simulated. The initial stability was assessed by measuring the relative micromotions between the tibia and the talus at the fusion site, as well as examining the bone strain distributions.

Preserved joint contours predicted better initial stability at the fusion site and a more uniform distribution of loads in the bones than resected joint surfaces. With two-screw fixation, regardless of the surface preparation technique, inserting the screws at 30 degrees relative to the long axis of the tibia and crossing them above the fusion site predicted the best performance. Increasing the insertion angle and lowering the crossing level caused an overall decrease in the stability at the fusion site. Three-screw fixation predicted better initial stability, a more uniform distribution of loads in the bones and a lower risk of bone failure than two-screw fixation. Adding a third screw anteriorly produced, overall, a better performance than adding the screw posteriorly. As compared to the normal quality bone, large decreases in stability at the fusion site were predicted when different levels of poor bone quality were simulated. Even the most stable two-screw configuration predicted low levels of stability and regions at risk of bone failure, suggesting the need for a third screw.

This research should be seen as a step towards the use of finite element modelling as a tool to provide additional information to the orthopaedic surgeon during the preoperative planning of ankle arthrodeses. Model limitations must be borne in mind when considering a direct transfer of the findings of this research into the clinical situation. Nevertheless, the results of these finite element analyses have shown the importance of the surface preparation technique and the screw orientation on the initial stability of the ankle arthrodesis construct at the fusion site. The differences obtained between the models may well be the difference between success and failure of the ankle arthrodesis.

A Tim y a mis padres, Isidoro y Benilde.

LIST OF CONTENTS

LIST OF FIGURES

LIST OF TABLES

ACKNOWLEDGEMENTS

I would like to mention the following that have helped me and contributed, in one way or another, to this thesis.

Dr Mark Taylor, who trusted me from the beginning, has skilfully guided my academic progress and has built an ideal research environment.

Dr Henrik Lauge-Pedersen, who has kept me aware of the clinical realities and has managed to achieve the invaluable dialogue between our two disciplines. I believe this type of multidisciplinary collaboration to be essential for any progress in this field.

All my colleagues within the Bioengineering Sciences Research Group. Whilst we have exchanged valuable ideas and helped each other with our individual project, they have also given me the chance to learn about other cultures. And even in my grumpy moments, they have made me smile (except for that frisbee).

Dr Luis Gómez Pellico and all my former colleagues from the Departamento de Ciencias Morfológicas (Universidad de Alcalá, Spain), who introduced me to the wonderful workings of the human body and transmitted to me a passion for human anatomy.

Tim, my companion, my love. Despite all my changing moods, he has given me his unconditional support, always being very understanding, tolerant and generous.

My parents, brothers and sisters, all the rest of my family and my dear friends, just for always being beside me.

Finally, I want to acknowledge the Medical Faculty (Lund University), the Swedish Medical Research Council (Project 09509), the Swedish Foundation for Strategic Research and the School of Engineering Sciences (University of Southampton) for funding this research.

Thanks to all of you.

Me gustaría nombrar aquí a todos aquellos que me han ayudado y, de una forma o de otra, han colaborado en la realización de esta tesis.

Dr. Mark Taylor, quien confió en mi desde el principio, guiándome con destreza en mi desarrollo académico y proporcionando un ambiente de trabajo ideal.

Dr. Lauge-Pedersen, quien me ha mantenido siempre consciente de las realidades clínicas y ha sido capaz de lograr ese diálogo inestimable entre nuestras dos disciplinas. Creo firmemente que este tipo de comunicación multidisciplinar es imprescindible para cualquier avance en este campo.

Todos mis compañeros del Bioengineering Sciences Research Group. A la vez de intercambiar valiosas ideas y ayudarnos mutuamente en nuestros respectivos proyectos, me han dado la oportunidad de conocer otras culturas. Me han hecho sonreir incluso en mis momentos de mal humor (excepto quizás con aquel frisbee).

Dr. Luis Gómez Pellico y todos mis antiguos compañeros del Departamento de Ciencias Morfológicas (Universidad de Alcalá), quienes me iniciaron en el maravilloso mundo del cuerpo humano y su funcionamiento, transmitiéndome su pasión por la anatomía humana.

Tim, mi compañero, mi amor. A pesar de todos mis cambios de humor, me ha dado su apoyo incondicional y ha sido siempre muy comprensivo, tolerante y generoso.

Mis padres, mis hermanos y hermanas, todo el resto de mi familia y mis queridos amigos, sencillamente por estar siempre a mi lado.

Finalmente, quiero agradecer a la Medical Faculty (Universidad de Lund), al Swedish Medical Research Council (Project 09509), al Swedish Foundation for Strategic Research y a la School of Engineering Sciences (Universidad de Southampton) por financiar este trabajo.

Muchas gracias a todos.

INTRODUCTION

The computational analysis of orthopaedic problems arises from the need to complement *in vivo* and *in vitro* experiments aimed at enlarging the body of knowledge that will help to address specific clinical needs. This obviously requires a multidisciplinary approach. Thus, before the objectives of this research on ankle arthrodesis are discussed, a brief description of the anatomy and function of the ankle joint is presented in Chapter 1, followed by an overview of the structure and material properties of bone in Chapter 2. Chapter 3 introduces the clinical aspects of ankle arthrodesis, with its indications, techniques and results. Despite the numerous techniques available and the improvements in the clinical outcome of ankle arthrodesis, significant failure rates are still being reported. Biological and mechanical factors act together to produce a given outcome. Chapter 4 looks at the mechanical factors that may affect the outcome of ankle arthrodesis. It becomes clear that stability at the fusion site achieved at the time of surgery plays a key role in the success or failure of the arthrodesis procedure. Given the limitations of the *in vitro* experiments designed to assess this initial stability, the use of computational models emerges as a suitable alternative.

The assessment of the initial stability of ankle arthrodesis with internal fixation using finite element analysis starts in Chapter 5. This describes the modelling procedure followed and the results from a number of tests performed upon a reference model to determine its robustness. Information regarding the benefits in terms of initial stability of different arthrodesis techniques and screw configurations could help the surgeon to choose the option most likely to produce the desired outcome. Thus, Chapter 6 and Chapter 7 compare the initial stability of two joint surface preparation techniques and the effect of changing the configuration of the screws. Ankle arthrodesis is often performed in patient populations with pathologies that affect the quality and mechanical integrity of their bones. To get closer to this clinical scenario, a comparison between a selection of the models studied in the previous chapters is performed in several cases of simulated poor bone quality in Chapter 8. Finally, a critical discussion of the finite element analyses performed is presented, followed by recommendations for future developments.

Chapter 1

ANATOMY AND FUNCTION OF THE ANKLE JOINT

The ankle joint, also called the talocrural joint, is the joint of the lower limb that connects the leg and the foot. Its special configuration and location provide both stability and mobility, making the ankle joint essential in weight-bearing and force transmission that occurs during locomotion.

1.1 ANATOMICAL REFERENCE FRAME

In order to describe the location, orientation and movement of the human body in three-dimensional space, three orthogonal planes are used as the anatomical reference system (Figure 1.1). Consider the body in the anatomical position, i.e. in erect posture, with the arms hanging along the sides of the body and the palms looking forwards. The *sagittal plane* is the vertical antero-posterior plane that passes through the centre of the trunk, dividing the body to two sides. The *frontal plane* (also known as coronal plane) is the vertical plane perpendicular to the sagittal plane. The *transverse plane* is the horizontal plane perpendicular to both the sagittal and the frontal plane. Any parallel plane to any of these three planes is referred to by the same name.

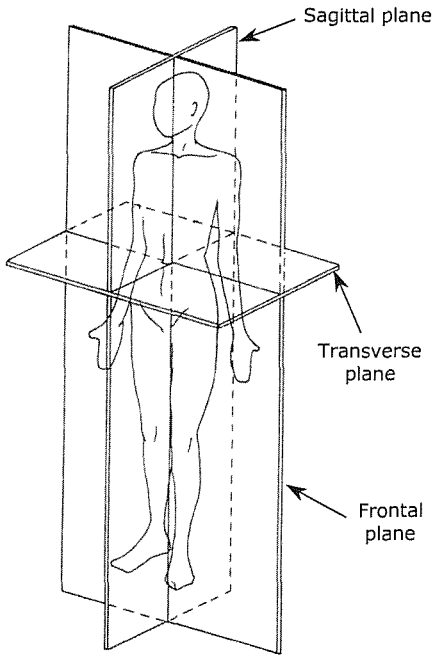

Figure 1.1 Anatomical planes *(Modified from Palastanga et al.[121])*.

The intersection of the sagittal and frontal planes is called the *longitudinal axis* of the body. The terms *superior* and *inferior* describe the levels along this axis of parts or structures of the body. The intersection of the sagittal and transverse planes determines the *antero-posterior axis*. The relations of structures with the front or back of the body or limbs are described with the terms *anterior* (or *ventral*) and *posterior* (or *dorsal*) respectively. The intersection of the frontal and transverse planes gives the *transversal axis*. The terms *medial* and *lateral* describe being nearer or further from the sagittal plane along this axis. With regard to the limbs, *proximal* and *distal* refer to the near and far positions from the trunk, respectively.

1.2 DESCRIPTION OF THE ANKLE JOINT

The ankle joint is formed by the distal ends of the two bones of the leg (tibia and fibula) and the proximal bone of the tarsus of the foot (talus). A brief description of these bones will be given here. For a more detailed description of these bones, as well as the ankle joint and its function, refer to the numerous texts available, such as Basmajian [4], Draves [41], Sarrafian [142], Norkin and Levangie [116] and McMinn et al.[102].

1.2.1 Ankle bones

Both the tibia and the fibula are long bones, with a long shaft (diaphysis) and proximal and distal ends (epiphyses). The distal epiphysis of the tibia enlarges from the diaphysis, presenting three main features related to the ankle joint (Figure 1.2): The inferior part or *tibial plafond*, which is wider anteriorly and contains a concave articular surface facing downwards towards the talus; the most distal part of the tibia, the *medial malleolus,* on the medial side, whose lateral surface is covered with an articular facet, continuous with that of the tibial plafond; and the *fibular notch* on the lateral side, which is the site of the distal tibiofibular joint. The diaphysis of the fibula is thinner than the tibial diaphysis, expanding distally to the *lateral malleolus* (Figure 1.2). The lateral malleolus lies more inferior and slightly posterior than the medial malleolus. On its medial surface there is a triangular articular facet for articulation with the talus.

The talus is a small bone with three main parts: the body, the neck and the head (Figure 1.3). The superior part of the *body* of the talus (talar dome) is wider anteriorly and its mostly covered by three articular facets for articulation with the tibia and fibula (two on each side and a trochlear surface at the top). The body of the talus also articulates with the tarsal bone underneath it (the calcaneus), forming the subtalar joint. The *neck* of the talus is the narrower part that connects the anterior part of the body with the head of the talus. The *head* presents a rounded anterior surface, which is covered with a facet for articulating with the navicular bone, another tarsal bone, forming the talonavicular joint. Due to the orientation of the neck, the head of the talus lies anterior and medial to the body of the talus.

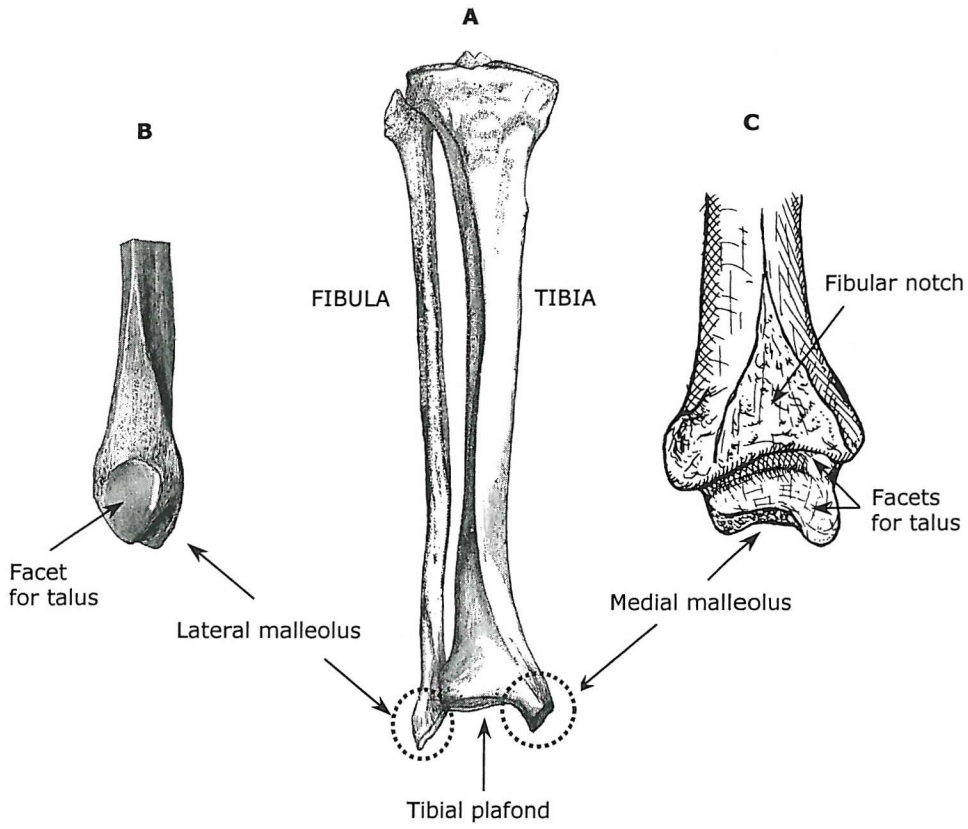

Figure 1.2 **A** Anterior view of the tibia and fibula from a right leg. **B** Detail of the distal part of the diaphysis of the fibula and the lateral malleolus (medial view). **C** Detail of the distal end of the tibia (lateral view) *(A and B modified from Gray [53]; C modified from Draves [41]).*

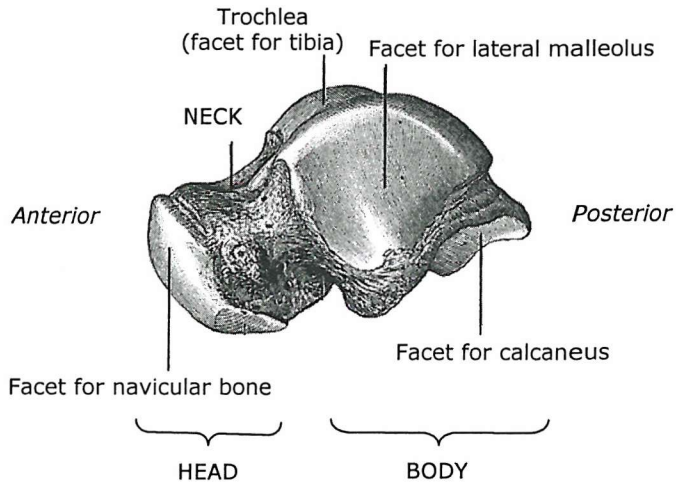

Figure 1.3 Lateral view of a left talus *(Modified from Gray [53]).*

1.2.2 Joint anatomy

The ankle joint is classified as a synovial joint. It comprises a joint cavity lined with articular cartilage over the articular facets and synovial membrane over the rest. Synovial fluid provides lubrication, reducing friction between the contacting surfaces. A fibrous capsule encloses all these structures, isolating the joint from the outside and keeping the bones together. Extra-articular ligaments reinforce the capsule in specific areas.

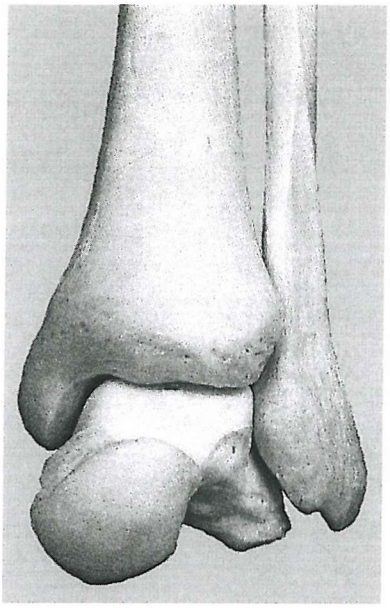

Figure 1.4 Anterior view of the bones of a left ankle joint.

The tibia and fibula form a concave cavity, called the *mortise*, into which the talus fits (Figure 1.4). The articular facets present on the tibia and fibula form an almost continuous joint surface for articulating with the corresponding three articular facets on the talar dome. The superior face of the talar body is covered by a trochlear surface that articulates with the tibial plafond. It is convex from anterior to posterior and slightly concave from medial to lateral. As well as the tibial plafond, the trochlea is wider anteriorly than posteriorly. The medial and lateral borders of this articular surface are continuous with the medial and lateral articular surfaces. On the medial side of the talar dome, there is a comma-shaped articular surface for articulating with the medial malleolus of the tibia. A concave triangular surface covers the lateral side of the talar body for articulating with the triangular articular surface present on the lateral malleolus of the fibula.

The distal ends of the tibia and fibula are joined by a fibrous joint or syndesmosis, the distal tibiofibular joint. This joint allows very small movements between the two bones; it varies slightly the dimensions of the ankle mortise during ankle motion to adapt it to the varying width of the talar trochlea.

1.2.2.1 Ankle joint ligaments

The ligaments of a synovial joint are major stabilizing structures and help to maintain the integrity of the joint, limiting the range of motion and constraining certain undesirable movements. At the ankle joint, two main groups of ligaments reinforce the articular complex, connecting the malleoli with the talus and adjacent tarsal bones (Figure 1.5).

The medial collateral ligament or *deltoid ligament* connects the medial malleolus to several tarsal bones, and consists of several bands whose number and description is somewhat controversial in the literature. As shown in Figure 1.5 A, there are three bands: the *naviculotibial ligament*, running anteriorly towards the navicular bone; the *calcaneotibial ligament*, from the medial malleolus down to the calcaneus; and the *posterior talotibial ligament*, running posteriorly down to the talus. Some authors also describe a deeper layer with two bands: the *deep anterior talotibial ligament* and the *deep posterior talotibial ligament*.

The lateral collateral ligament (Figure 1.5 B) is less extensive and weaker than the medial ligament; it has three components originating from the lateral malleolus: the *anterior talofibular ligament*, running anteriorly to the talar neck; the *calcaneofibular ligament*, attaching to the calcaneus; and the *posterior talofibular ligament*, running posteriorly towards the back of the talus.

Closely related with the ankle ligaments are the *crural tibiofibular interosseous ligament* and the *anterior* and *posterior tibiofibular ligaments*. They are strong ligaments, part of the distal tibiofibular joint, that keep the distal ends of tibia and fibula together, preserving the integrity of the ankle mortise (Figure 1.5 B).

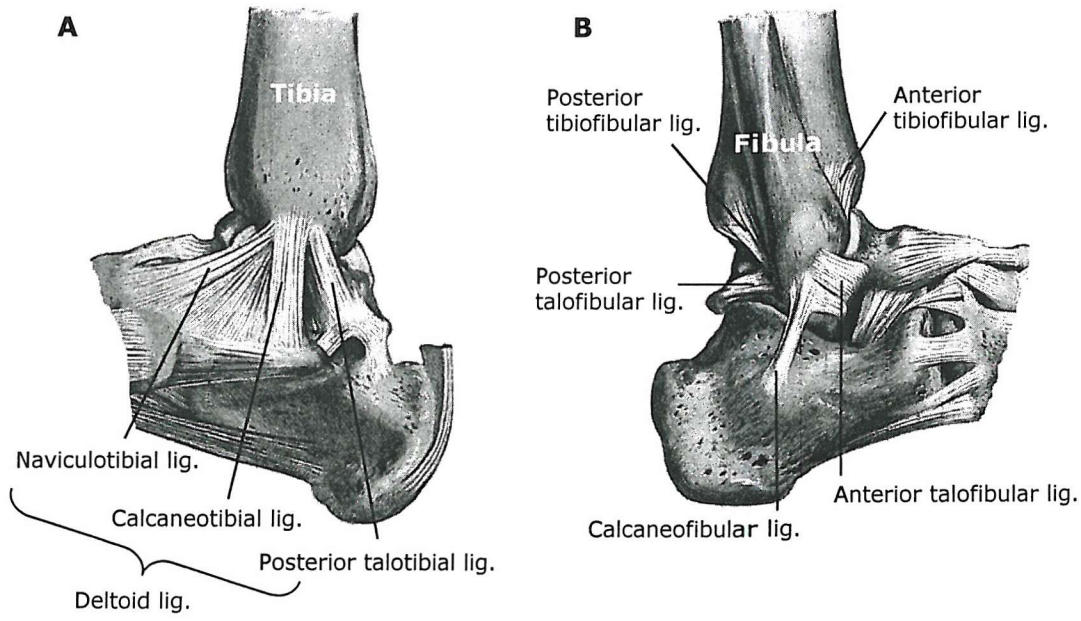

Figure 1.5 A Medial view of the ankle joint with the medial collateral ligaments. **B** Lateral view of the ankle joint with the lateral collateral ligaments *(Modified from Gray [53])*.

1.3 ANKLE JOINT FUNCTION

1.3.1 Axis of rotation and mobility

Regarding its function, the ankle joint is classified as a diarthrodial joint. Traditionally, the ankle joint has been considered as a hinge joint, allowing the rotation of the talus relative to the shank around a fixed single axis [41,132]. This single axis is usually described as passing transversally through the ankle, approximately at the level of the tips of the malleoli. Relative to the longitudinal axis of the foot, it is externally rotated in the transverse plane and slopes downwards from medial to lateral. The direction of the axis results in ankle motion across the three reference planes (Figure 1.6). Plantar flexion and dorsiflexion are the major movements, though small degrees of internal/external rotation and inversion/eversion are also allowed. (Note: internal/external rotation is also called adduction/ abduction; inversion/eversion is also called varus/valgus).

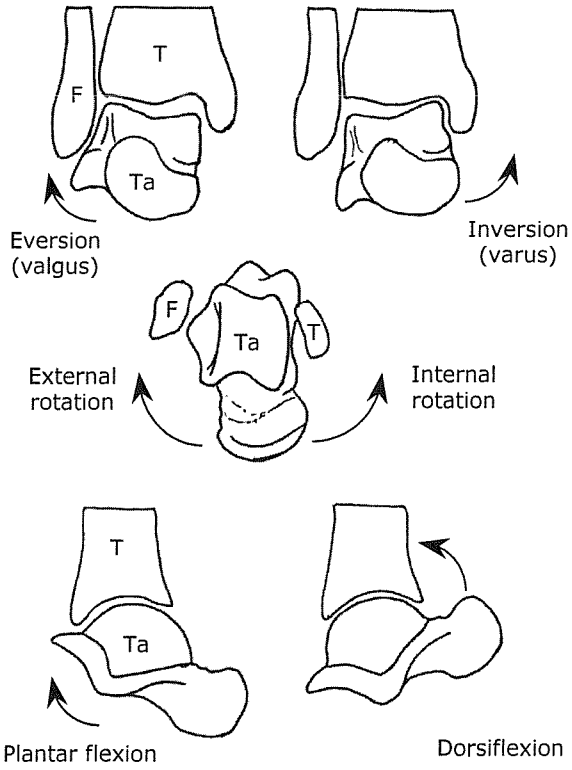

Figure 1.6 Rotational movements of the talus relative to the shank (T=tibia, F=fibula, Ta=talus), showed top to bottom in the frontal, transverse and sagittal planes respectively.

More recently, several studies have reported changes of the talocrural joint axis throughout the range of movement [88,94,149], pointing out the fact that the normal motion of the talocrural joint involves sliding as well as rolling. All this suggests that considering the ankle joint as a fixed hinge joint could well mean an over-simplification of the real ankle kinematics.

With regards to the range of motion of the ankle joint, results from different studies show a certain degree of variation. These differences are apparently caused by the different methodologies used and by individual variations. It is worth noting the lack of standard joint coordinate systems to describe the motion of the human joints. Despite recent efforts to address this problem [171], no standard ankle joint coordinate system has

yet been established and different coordinate systems have been used when assessing ankle motion. Therefore, ranges of motion referred to by the same name in different studies can describe slightly different motions depending on the coordinate systems employed in each case. Values between 20º and 50º of plantarflexion and between 10º and 25º of dorsiflexion have been reported, as well as just a few degrees (less than 10º) of external/internal rotation and inversion/eversion [41,80,88,142].

The complex movements of the foot related to the shank involve several joints of the foot in addition to the talocrural joint. In particular, the talocrural joint is closely related to two other joints of the foot: distally to the *subtalar joint* (between inferior face of the talus and superior face of the calcaneus) and anteriorly to the *transverse tarsal joint* (which includes the *talonavicular joint* and the *calcaneocuboid joint*). Generally, the term "ankle joint complex" is used to describe the structure formed by the ankle and subtalar joints. Although most of the gross motion between the foot and the shank takes place at the ankle joint complex, other joints of the foot contribute to it in different degrees. In the global motion of the foot relative to the shank, a combination of dorsiflexion, eversion and external rotation is called pronation. On the other hand, supination is a combination of plantar flexion, inversion and internal rotation. The various joints of the foot and ankle complex contribute in different degrees to these combined motions and, therefore, the range of motion of the foot relative to the shank in any direction is larger than that of the talocrural joint.

Several cadaver specimen experiments and *in vivo* roentgen stereophotogrammetric studies have reported the contribution of the various joints to the motion between the leg and the foot [80,93,149]. The major motion occurring at the ankle joint is plantar flexion/dorsiflexion and it takes place mainly during the plantar flexion/dorsiflexion of the foot relative to the shank. Yet again, differences in terminology and methodology have led to some inconsistency when describing the motion of the ankle as a result of the motion of the foot relative to the shank. In this way, for instance, Kitaoka et al.[80] found that some degree of dorsiflexion occurred at the ankle joint when the foot was pronated, as well as smaller amounts of external rotation and eversion. When the foot was supinated, they observed a small amount of dorsiflexion and a smaller amount of inversion at the ankle. In contrast, Leardini et al.[88] observed ankle dorsiflexion coupled with external rotation and supination, and plantar flexion coupled with internal rotation and pronation (it seems as if they called supination/pronation that which has been considered above as eversion/inversion).

1.3.2 Muscles acting on the ankle joint

The muscles that act on the ankle joint are those with origins in the leg and insertions upon the foot. These muscles and their tendons cross the ankle joint at different positions relative to the ankle joint axis. Since there are no muscle attachments to the talus, they indirectly cause ankle motion by acting on other bones and joints of the foot.

The muscles that control the motions of the talocrural joint belong to the three muscular compartments of the leg: anterior compartment, lateral compartment and posterior compartment. Most of these muscles present tendinous extensions, which enter the foot under the cover of several retinacula. Considering their position relative to the ankle axis indicates the function of each muscle. Name, function and position of the main muscles acting on the talocrural joint are shown in Table 1.1 and Figure 1.7.

The muscles of the anterior compartment of the leg are dorsiflexors of the talocrural joint as they lie anterior to the ankle axis. The *tibialis anterior* is the main dorsiflexor. They also contribute to the inversion/eversion and internal/external rotation of the foot relative to the shank. The muscles of the lateral and posterior compartments act as plantar flexors of the ankle joint, being the *triceps surae* the main plantar flexor, followed by the *flexor digitorum longus*. They also contribute in different degrees to the relative movements of the foot relative to the shank.

Table 1.1 Function of the main muscles acting upon the ankle joint.

Leg compartment	Muscle name	Function *
Anterior	Tibialis anterior	**DF**, INV, IR
	Extensor hallucis longus	DF, INV, IR
	Extensor digitorum longus	DF, EV, ER
Lateral	Peroneus longus	ER, EV, PF
	Peroneus brevis	ER, EV, PF
Posterior	Triceps surae	**PF**, IR, INV
	Flexor hallucis longus	IR, INV, PF
	Flexor digitorum longus	PF, IR, INV
	Tibialis posterior	IR, INV, PF

* DF=dorsiflexion, PF=plantar flexion, INV=inversion, EV=eversion, IR=internal rotation, ER=external rotation. Plantar flexion/dorsiflexion refers to the talocrural joint. Inversion/eversion and rotation refer to the motion of the foot relative to the leg. Functions appear in order of importance; bold indicates main plantar flexor or dorsiflexor of the talocrural joint.

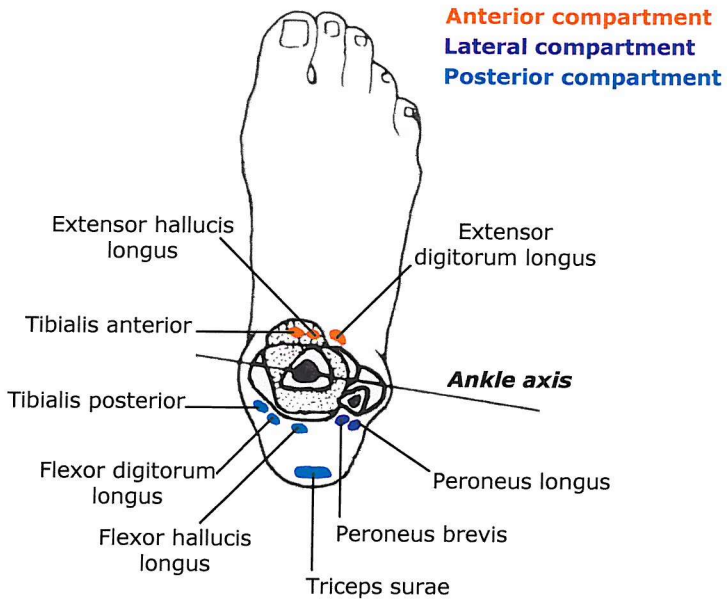

Figure 1.7 Position of the muscles and tendons crossing the ankle joint relative to the ankle axis. Talus is shown dotted, tibia and fibula in blue *(Modified from Czerniecki [29]).*

1.3.3 Forces and moments acting on the ankle joint

During locomotion, the foot and ankle complex are subjected to functional demands that include force absorption and force transmission. Thus, large forces and moments act on the ankle joint, with a combination of internal forces – caused by the action of the muscles upon the skeletal segments and the viscoelastic properties of the joints and their surrounding soft tissues, and external forces – gravitational, inertial and ground reaction forces.

In vivo direct and non-invasive measurements of the forces acting at the talocrural joint are not available. Motion analysis systems provide ranges of motion, velocities and accelerations between the shank and the foot during locomotion, and predict the forces and moments acting on the foot and ankle complex. They are based on relatively simple models of the body segments and joints. Using the kinematic data, the ground reaction forces measured in force platforms and anthropometric data as inputs, they predict the forces and moments acting at the different joints. However, they do not consider the internal forces generated by the muscles. They are widely used in the clinical practice to assess normal and pathological gait patterns. Only through mathematical or invasive approaches is it possible to treat the ankle joint and the subtalar joint separately. Therefore, these systems consider the ankle complex as a single unit. Typical kinematic

and kinetic data of the ankle complex obtained from motion analysis systems are shown in Figure 1.8 and Figure 1.9, where the moments were normalised with respect to the weight and height of the subjects.

More complex mathematical models have tried to predict the forces and moments acting on the joint of the lower extremities. Detailed anthropometric data, as well as data obtained from motion analysis systems and force platforms or *in vitro* experiments, were used as inputs. Muscle forces and joint reaction forces were usually considered as the unknown variables, leading to a statically indeterminate system of equilibrium equations. Various methods to overcome this problem were followed, assuming simplifications such as muscle grouping on functional grounds or minimization of different variables such as the sum of all the muscle forces. However, the limitations of the models might have led to inaccurate magnitudes.

Seireg and Arkivar [147] presented a purely mathematical 3D model of the lower extremity, assuming certain arbitrary limb segment motion patterns. The ankle motion was defined as a one degree of freedom (DOF) system, referring to the relative motion between shank and foot. They reported a peak reaction force of 5.2 times body weight (BW) (peak vertical component approx 5 BW, peak posterior component approx 2.2 BW and peak medial-lateral approx 1 BW). Stauffer et al.[154] analysed the force and motion of the ankle joint in a 2D model, also assuming a single DOF between the shank and the foot. They predicted a peak compressive force between 4.5 and 5.5 BW (mean 4.73 BW) and a peak posterior shear force of 0.8 BW. The results of this study are often mentioned and used in the literature, despite the limitation of being a 2D analysis of a joint whose axis of motion seems to require a 3D approach, leaving aside the fact that it only considered the gross motion between leg and foot.

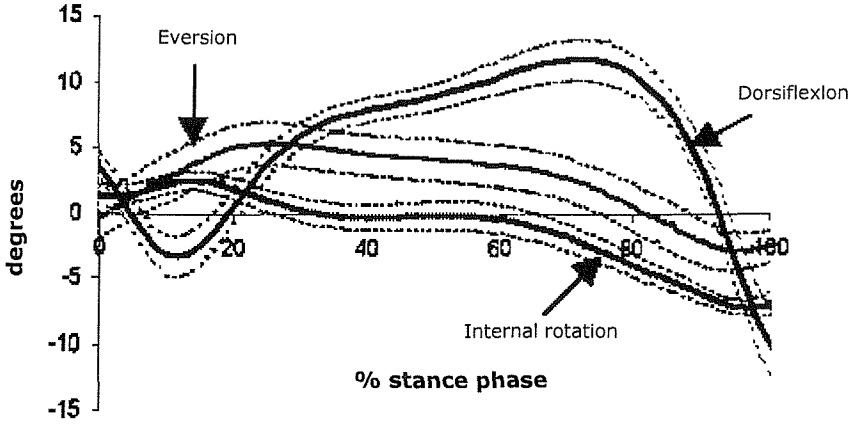

Figure 1.8 Ankle complex kinematics (mean ± 95% confidence) during the stance phase of the gait cycle (stance phase = period during which the foot is in contact with the floor). Positive values are dorsiflexion, eversion and external rotation *(Modified from Hunt et al.[63])*.

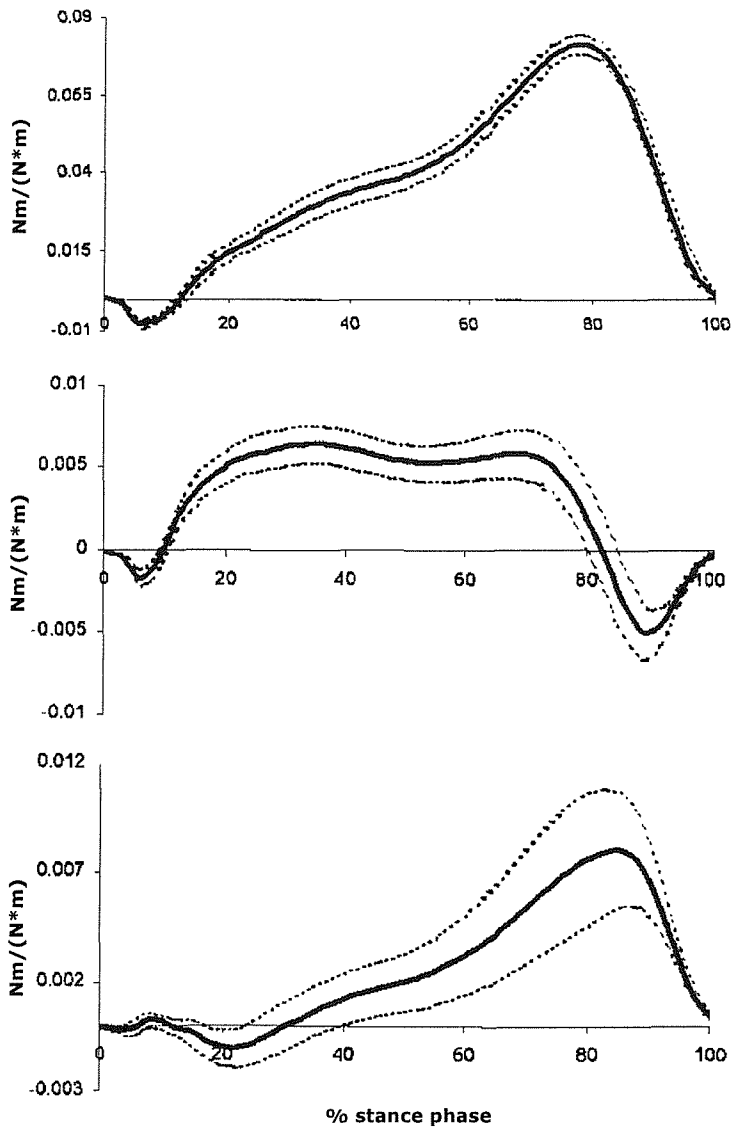

Figure 1.9 Ankle complex moments (mean ± 95% confidence) during the stance phase of the gait cycle *(Modified from Hunt et al.[63])*.

Röhrle et al.[139] presented a more complex model for a 3D analysis of the hip, knee and ankle during walking. The ankle joint also represented the relative motion between shank and foot but had two DOF, allowing inversion-eversion in addition to plantar flexion-dorsiflexion. They predicted considerably lower values than Seireg and Arkivar [147]. They reported a peak force across the shank-foot complex between 3 and 3.8 BW for various gait velocities (peak vertical force of 3.18 BW, peak posterior force of 1.41 BW and peak lateral force of 0.1 BW, for an average gait velocity and with respect to a global coordinate system).

Only two references have been found that consider the isolated behaviour of the talocrural joint. Procter, in his PhD thesis [131], performed a very detailed study of ankle biomechanics, whose main results were later summarized in Procter and Paul [132]. They studied the talocrural and the subtalar joints separately. Like Röhrle et al.[139], they considered plantar flexion-dorsiflexion and inversion-eversion but, in this case, each joint was assumed uniaxial, providing a single DOF. They predicted a peak joint force for the talocrural joint of 3.9 BW (2.9-4.7 BW range)(Figure 1.10 A). They also presented the moments at the talocrural joint due to the external forces for one of the subjects studied: peak dorsiflexor/plantar flexor moments = 110Nm/30Nm; peak everting/inverting moments = 45 Nm/10 Nm and peak external/internal rotation moments = 25 Nm/5 Nm (Figure 1.10 B). An overall variation of their results of ± 20-25% was estimated due to experimental error, cadaver anthropometric data and individual subject variability. However, they considered that their 3D model produced physiologically feasible solutions, whilst including the main shank muscles and the talocrural and subtalar joints. They planned to further improve the model including ligaments, but no later references have been found.

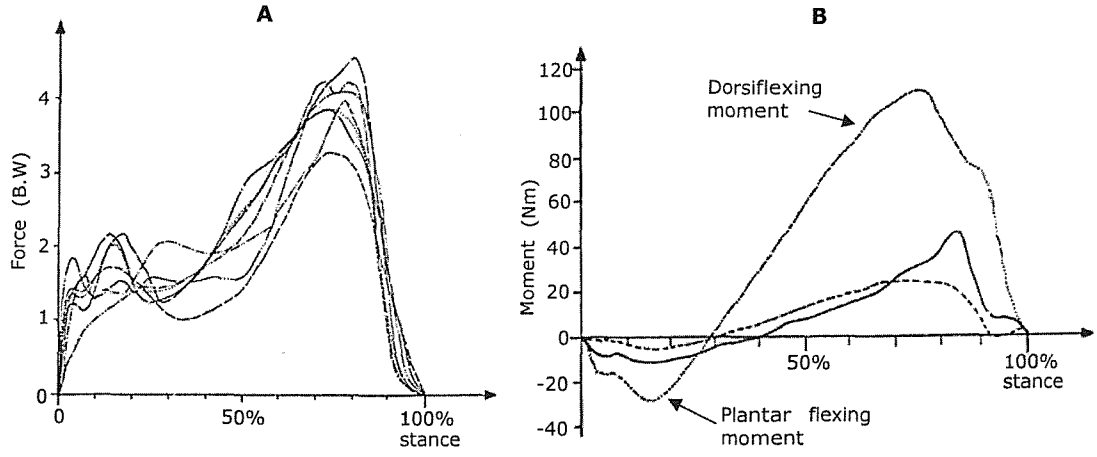

Figure 1.10 **A** Predicted talocrural joint force through the stance phase for the seven subjects studied by Procter [131]. **B** External moments at the talocrural joint through the stance phase for subject number seven. The dashed line represents externally(+)/internally(-) rotating moment and the continuous line everting(+)/inverting(-) moment.

Scott and Winter [145] examined the 3D kinematics and kinetics of the ankle joint complex considering rotations about the talocrural and subtalar joints. They assumed both joints acting as single DOF joints, offering a validation of this assumption. They did not report force values but predicted external moments at both joints for three subjects. In the

case of the talocrural joint, these moments ranged from 83.3 to 117.8 Nm. The predicted moments were described as combination of dorsiflexion-eversion-external rotation and plantar flexion-inversion-internal rotation (probably referring to the global laboratory coordinate system). Unlike previous studies, they did not include in their model the internal forces generated by the muscles. However, they performed an interesting analysis to check the error generated when the talocrural axis is assumed to be perpendicular to the sagittal plane (as happens in 2D analyses). They found a peak overestimation of between 5.9% and 22.6% of the talocrural joint moment and stated that a 2D analysis of the rotation between the leg and the calcaneus cannot separate the contribution due to the talocrural and subtalar joints.

In summary, there is only limited data available for the forces acting on the ankle joint. These data are based on predictions from inverse dynamics simulations and, due to simplifications, the predicted force values may be questionable.

Chapter 2
BIOMECHANICS OF BONE

The main functional demands of bone are support and movement of the body, in addition to the protection of vital internal organs and its role as a major store for calcium. Structure and function of bone have an intrinsic relationship [136], though the precise laws that govern it have not been completely described. However, information about bone structure and its mechanical behaviour is essential for a numerical approach to bone mechanics and modelling of orthopaedic problems.

2.1 DESCRIPTION OF BONE

2.1.1 Bone as a structure

In order to describe the structure of bone, both macrostructure and microstructure need to be considered. At a macroscopic level, ***cortical bone*** (also known as *compact bone*) forms the outer wall of the bones, accounting for about 80% of the skeletal mass. It comprises the diaphysis and the thin shell that surrounds the epiphyses of long bones and the outer wall of the rest of bones. Spongy ***cancellous bone*** (also referred to as *trabecular bone*) forms the inner regions of the bones, excluding the medullary cavity present in the shaft of long bones (see Figure 2.1). Except for the articular surfaces, bones are covered by a fibrous membrane called *periosteum*, which contains blood vessels, nerves and an inner layer of bone cells. It provides nutrition to the bone, allowing for its growth and repair. Another thin membrane with bone cells, the *endosteum,* lines the inner cavities of cancellous and cortical bone and the medullary cavities of long bones.

Cortical bone is a dense solid mass with similarities to fibre-reinforced engineering composites, whereas cancellous bone presents an intercommunicated network of rods, plates and arches (*trabeculae*) with cavities of varying dimensions in between, occupied by bone marrow. The porosity of cancellous bone can vary from 30% to more than 90% [60]. Keaveny et al.[72] classified trabecular bone as a composite, anisotropic, open porous cellular solid. The general assumption is that the direction and orientation of the trabeculae is related to the directions of the stresses imposed on the bones [60]. It has also been suggested that cancellous bone density and its architecture are dependent on the magnitude of the imposed loads and the number of loading cycles. Several parameters such as mean trabecular thickness, percentage anisotropy and bone volume fraction have

been used to quantify the architecture of trabecular bone. In general, there is an area of dense cancellous bone lying underneath articular surfaces, being referred to as *subchondral bone*.

2.1.1.1 Bone microstructure

At a microscopic level, bone is a highly vascularized connective tissue formed by *bone cells* embedded in a fibrous, organic matrix called *osteoid* (mainly made of collagen and some ground substance). This matrix is calcified by mineral salts, which permeate it and give the bone its rigidity and strength. The mineral salts that precipitate around the collagen fibres of the osteoid are mainly hydroxyapatite [$Ca_{10}(PO_4)_6(OH)_2$] crystals and amorphous calcium phosphate. *Osteoblasts* are the bone-forming cells, which secrete the osteoid around them. Derived from the osteoblasts, *osteocytes* are the fully formed bone cells, which lie in individual cavities (*lacunae*) enclosed by the calcified osteoid. Tubular channels called *canaliculi* connect the lacunae and allow the osteocytes to obtain nutrients. *Osteoclasts* are multinucleated giant cells related to bone resorption (see Figure 2.1).

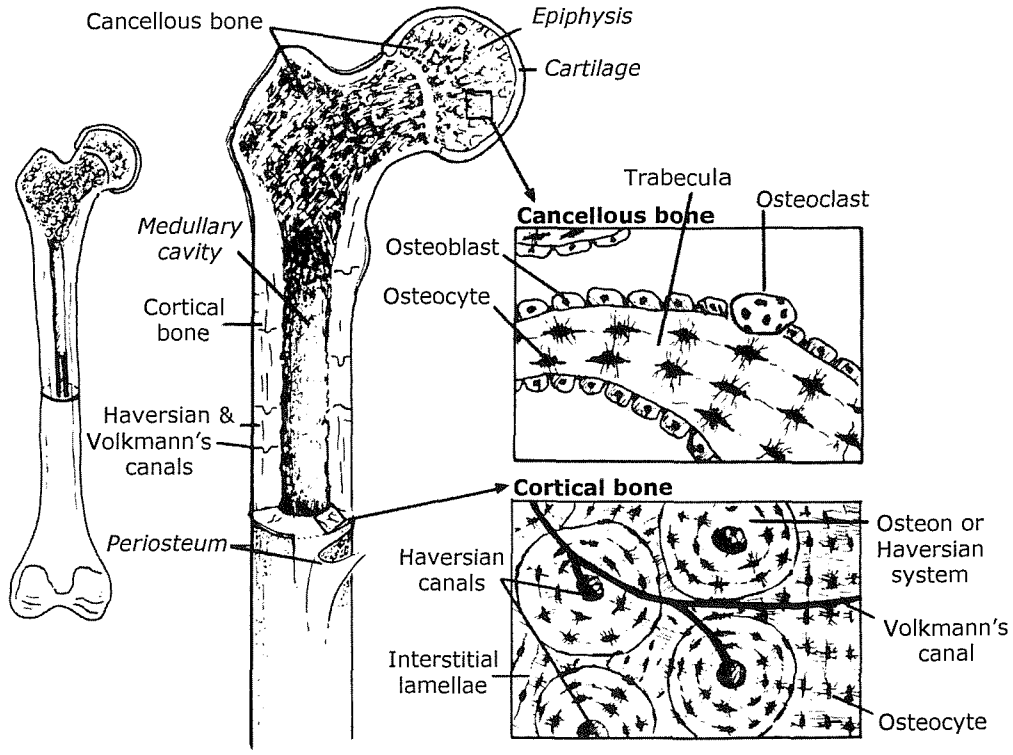

Figure 2.1 Diagram of cortical and trabecular bone in a long bone (femur) *(Modified from Hayes [60])*.

Lamellar bone is mature bone formed by alternating layers (*lamellae*) of bone deposited by the osteoblasts, with a characteristic collagen fibre orientation. In cortical bone, this lamellar bone forms *osteons* or *haversian systems*, lamellar cylinders surrounding a longitudinal vascular canal. Cement lines with a high content of inorganic matrix and little collagen bind the osteons. *Interstitial lamellar bone* fills the areas between the osteons, whereas *circumferential lamellar bone* encloses them, lining the periosteal and endosteal surfaces. In trabecular bone, the individual trabeculae consist primarily of interstitial bone covered by a single layer of osteoblasts and some osteoclasts.

During life, there is a continuous sequence of bone resorption and bone formation carried out by osteoclasts and osteoblasts respectively. This process, called *bone remodelling*, continually changes the architecture of bone and it is involved in bone growth, changes in shape, bone repair, the adjustment of the bone to the mechanical environment and the calcium ion regulation in the body. The strong interaction between the biological processes and the mechanical structure and environment involving bone are still being analysed through a variety of biomechanical studies and mathematical models.

2.1.2 Bone as a material

In addition to the information about bone structure and bone geometry, knowledge of the material properties of bone and the loads affecting it are necessary to understand the mechanical behaviour of the bone as a whole.

Bone is an anisotropic and heterogeneous material, whose properties have been, and are still being, intensely analysed. Experimental techniques have gradually provided more complex characterizations of bone mechanical properties, assuming isotropy, transverse isotropy or anisotropy. These experimental characterizations of bone mechanical properties as a function of bone density, anatomical site or age are being currently complemented by sophisticated engineering analysis tools, seeking a more complete characterization of the complex behaviour of bone [72] (see section 2.2). Both elastic and plastic properties (such as elastic and plastic modulus, yield strain and stress, ultimate stress and strain) have been investigated in the literature for cancellous and cortical bone (see section 2.2). Bone also exhibits viscoelastic behaviour, but in the human physiological range and during normal activities the effect of strain rate (generally below 0.01 s^{-1} [60]) on the mechanical properties of bone is small compared with other factors. Therefore, bone has usually been considered as being elastic or elastic-plastic, except for situations with higher strain rates, such as traumatic events [60,92,112].

The material properties of bone can be defined either at the tissue level or at the apparent level. Tissue properties refer to the level of individual trabeculae. Bone apparent properties represent an average of the properties for a certain volume of bone, considering bone as a continuous material. In the case of cancellous bone, it has been suggested that, in order to provide meaningful apparent properties, this representative volume should include about five trabeculae, measured along any direction (about 3-5 mm) [57].

2.2 BONE MATERIAL PROPERTIES

2.2.1 Direct experimental measurements of bone material properties

A multitude of studies have tried to obtain the apparent material properties of bone by using various experimental techniques. Bone heterogeneity leads to varying apparent properties depending on the anatomic location and on different biological variables, such as gender, age and pathology [38,50,90,100,108]. Therefore, a wide range of values of bone apparent properties can be found in the literature. These values are generally difficult to compare because of the differences in the experimental methods and the specimens considered. For instance, apparent densities of trabecular and cortical bone have been measured using different experimental methods to determine the volume and bone mass of the specimens considered. Values from 50 to 1100 kg m^{-3} for cancellous bone of various degrees of porosity, and about 1800-2100 kg m^{-3} for dense cortical bone have been reported [60,71].

Bone anisotropy makes the apparent mechanical properties strongly dependent on the orientation of the bone microstructure relative to the direction of testing. Materials testing techniques used include compression, tension, bending and torsion, as well as ultrasound measurements. One of the disadvantages of the mechanical tests is that damage of the sample after loading in one direction is likely to affect subsequent measurements in other directions or loading modes. Ultrasound techniques do not damage the samples and the three orthogonal Young's moduli and the three orthogonal shear moduli can be measured from a single specimen. Furthermore, with the appropriate frequency of the wave, it is possible to estimate the modulus of trabecular tissue. However, when using ultrasound techniques to obtain the elastic magnitudes, the assumption of a constant bone density is required; another drawback is the impossibility to measure bone strength or time-dependent properties using ultrasound techniques.

The estimation of the mechanical properties of **cortical bone** is usually done in three principal directions of the specimens (longitudinal, radial and circumferential), with the longitudinal direction usually being parallel to the direction of the osteons. A summary of cortical bone properties is given in Table 2.1. Values between 17 and 21 GPa have been reported for the Young's modulus of cortical bone tested in the longitudinal direction. The longitudinal elastic modulus has been shown to be about 50% greater than the transverse elastic moduli [3,60] and, therefore, cortical bone is generally considered as transversally isotropic. Young's moduli under tension and compression do not seem to differ. Shear moduli are lower than Young's moduli, with values around 5 GPa. The reported values of ultimate stress vary between 51 and 214 MPa, also with higher values in the longitudinal direction than in the transverse directions. Cortical bone strength also depends upon the type of loading (asymmetric behaviour), as compressive strength is greater than tensile strength (see Table 2.1).

Cancellous bone shows a much larger variation in mechanical properties than cortical bone, mainly due to larger variations in its apparent density and the effect of trabecular orientation. A summary of cancellous bone mechanical properties is given in Table 2.2. Cancellous bone also presents a greater dependency upon the anatomic location and loading direction [50,71]. It has been commonly tested in the antero-posterior, medio-lateral and infero-superior anatomical directions of the specimens. More recently, however, it has been suggested that mechanical testing should be performed along the principal directions of the trabecular architecture, because there is strong evidence that the principal directions of cancellous bone are aligned with the trabecular architecture [72].

Young's moduli of cancellous bone from 20 to 5000 MPa have been reported, with no significant differences with respect to the type of loading (i.e. compression and tension). Significant differences, however, have been found when Young's modulus was measured in different directions (i.e. infero-superior as compared to medio-lateral directions) (see Table 2.2). With regards to cancellous bone strength, asymmetric behaviour has been reported in addition to the dependence on loading direction, with lower strength in tension than in compression, and even lower in shear [72]. Mean values of ultimate stress between 2 and 6 MPa have been reported (see Table 2.2). Bone strength has been commonly estimated by means of ultimate stress or yield stress. However, recent findings suggest that the apparent failure behaviour of trabecular bone is much simpler when strain is considered. Axial loading experiments performed on human cancellous bone have suggested that ultimate strain and yield strain can be considered independent of bone density [65,82,92,138]. At least, within a single anatomic site, yield strains can reasonably be considered as homogeneous for uniaxial loading [82,107]. In addition, experiments on bovine cancellous bone have found that uniaxial yield strains are isotropic [15], though these findings still need to be confirmed for human cancellous bone. Asymmetric behaviour of ultimate and

yield strain has been reported, with values for compression and tension ranging from 1.10 to 1.60% for ultimate strain and from 0.61 to 0.85% for yield strain (see Table 2.3).

The Poisson's ratio is another elastic material property, which has not been addressed very often in experimental bone-related studies. A wide range of values has been reported for the Poisson's ration, but there is no information about factors that could affect it, such as anatomic location and strain rate. Nevertheless, in structural analyses the Poisson's ratio of bone is often assumed to be 0.3 [71].

At a tissue level, experimental studies on individual trabecula have obtained values between 1 and 20 GPa for the elastic modulus of trabecular tissue [54,71,134]. This wide range may reflect the difficulty in applying traditional testing methods to obtain mechanical properties at the tissue level. For the same reason, it is difficult to compare cortical tissue and trabecular tissue properties, though it has been suggested that the Young's modulus of trabecular bone tissue is between 20-30% lower than that of cortical bone tissue [54,71].

The experimental determination of bone elastic constants has a considerable number of limitations and problems. Size and shape of the specimens, as well as environmental and testing conditions seem to have affected the results of the available experimental studies [91,112,118]. These experimental errors could explain some of the differences in the material properties of bone reported.

Table 2.1 Human cortical bone. Published values of Young's modulus, shear modulus and ultimate stresses.

Study	Anatomic site	Method	Young's Modulus ± SD (GPa)	Shear Modulus (GPa)	Ultimate stress ± SD (MPa)	Ultimate shear stress (MPa)
Reilly et al[60,133] †	Femur diaphysis	Compression & tension	E_1 **11.5** E_3 **17.1 ± 3.2**	G_3 ‡ **3.3**	S_1(tension) **51** S_1(compression) **133** S_3(tension) **133** S_3(compression) **193**	S_3 ‡ **68**
Ashman et al[3] *	Femur diaphysis	Ultrasonic	E_1 **12.0** E_2 **13.4** E_3 **20.0**	G_{12} **4.53** G_{13} **5.61** G_{23} **6.23**	—	—
Snyder & Schneider[152]	Tibial diaphysis	3-point bending	E **17.5 ± 1.6** range 14.3-21.1	—	S(bending) **214 ± 21** range 178-250	—
Rho et al[134]	Tibial diaphysis	Ultrasonic ξ	E **20.7 ± 1.9**	—	—	—
		Microtensile	E **18.6 ± 3.5**			

Subscripts 1, 2 and 3 refer to the radial, circumferential and longitudinal anatomical directions respectively. † Compact bone considered transversally isotropic. ‡ Torsion around longitudinal axis. * Compact bone considered orthotropic. ξ Assumed constant density of cortical bone = 1817 kg m^{-3}.

Table 2.2 Human cancellous bone. Reported values of Young's modulus, shear modulus and ultimate stress.

Study	Anatomic site	Method	Young's Modulus ± SD (MPa)	Shear Modulus ± SD (MPa)	Ultimate stress ± SD (MPa)
Røhl et al[138]	Proximal tibia	Compression	E_{IS} **485 ± 333**	—	S_{IS} **2.22 ±1.42** range 0.51-5.60
		Tension	E_{IS} **483 ± 323**		S_{IS} **2.54 ± 1.18** range 0.92-5.38
Dalstra et al[31]	Pelvis	Compression	E_1 **59.8 ± 45.2** E_2 **50.1 ± 41.5** E_3 **38.3 ± 39.1**	G_{23} **20.8 ± 17.1** G_{31} **23.5± 18.3** G_{12} **25.2 ± 17.8**	—
Goulet et al[52]	Various	Compression	E_{IS} **287 ± 255** range 16-1113 E_{AP} **173 ± 204** range 6-1524 E_{ML} **123 ± 120** range 1-654	—	S_{IS} **4.63 ± 3.48** range 0.51-14.56 S_{AP} **3.31 ± 3.14** range 0.58-16.00 S_{ML} **2.58 ± 2.19** range 0.10-9.60
Destresse et al[37]	Tibia	Ultrasonic	E range **197-2597**	—	—
Cody et al[22]	Proximal femur	Compression†	E_{IS} **210 ± 162** range 12-1105 E_{AP} **202 ± 211** range 8-2181 E_{ML} **161 ± 135** range 6-945	—	S_{IS} **6.47 ± 5.37** range 0.38-28.64 S_{AP} **4.14 ± 3.73** range 0.23-14.70 S_{ML} **3.59 ± 3.42** range 0.22-16.69
Rho et al[134]	Proximal tibia	Ultrasonic‡	E **14800 ± 1400**	—	—
		Microtensile‡	E **10400 ± 3500**		

Subscripts IS, AP and ML refer to the infero-superior, antero-posterior and medio-lateral anatomical directions of the specimens, respectively. Subscripts 1, 2 and 3 refer to the specimens' material principal directions. † IS orientated in the primary compressive trabecular direction. ‡ Values for individual trabeculae. For the ultrasonic testing, a constant density of trabecular bone = 1764 kg m^{-3} was assumed.

Table 2.3 Human cancellous bone. Reported values of yield strain and ultimate strain.

Study	Anatomic site	Method	Yield strain ± SD (%)	Ultimate strain ± SD (%)
Røhl et al[138]	Proximal tibia†	Compression	—	**1.11 ± 0.63** range 0.30-2.79
		Tension	—	**1.55 ± 0.49** range 0.89-2.52
Kopperdahl & Keaveny[82]	Vertebra†	Compression	**0.84 ±0.06** range 0.75-0.95	**1.45 ±0.33** range 0.96-2.30
		Tension	**0.78 ±0.04** range 0.71-0.88	**1.59 ±0.33** range 1.09-2.51
Morgan & Keaveny[107]	Proximal tibia‡	Compression	**0.73 ±0.06**	—
		Tension	**0.65 ±0.05**	—
	Femoral neck‡	Compression	**0.85 ±0.10**	—
		Tension	**0.61 ±0.03**	—

† Loading along the supero-inferior anatomical directions of the specimens. ‡ Loading direction aligned with the principal trabecular orientation within each specimen.

2.2.2 Derived bone material properties

An alternative to the direct measurement of mechanical properties of bone is the use of relationships between these mechanical properties and other physical parameters, which are, in principle, easier to obtain. Numerous attempts have been made to find valid relationships between bone density measurements and bone mechanical properties such as elastic constants, strength and fracture risk. Bone density measures and bone mechanical properties estimated experimentally have been correlated using statistical models. Despite the strong and statistically significant correlations found, the precise form of such relationships remains controversial, and there is not an established model that can be applied without regard to the type of bone, the anatomical location and the age of the patient. This is the case for the numerous relationships reported between bone apparent density and bone Young's modulus and strength, a summary of which is given in Table 2.4.

Because *in vivo* direct characterization of bone physical parameters is a difficult task, alternative means are commonly used. Non-invasive techniques, such as computed tomography (CT)[†], photon absorptiometry and magnetic resonance (MR) scanning, allow quantification of bone density and bone structure, both *in vivo* and *in vitro*. Significant high correlations have been reported between CT values and cancellous bone apparent density [20,65,74,98,135]. Worse correlations have been reported in the case of cortical bone [135,152], maybe due to the narrow range of cortical densities; it has been suggested that CT can only accurately measure cortical bone density if the cortex thickness exceeds 2-2.5 mm [56]. CT values and mechanical properties, such as Young's modulus and strength, have also shown significant correlations [6,20,22,65,98,138]; as with bone density, the precise form of the relationships between them remains controversial.

Measures of bone density have provided reasonable estimates of mechanical properties, such as bone stiffness or strength, and so they have been widely used both in clinical practice and biomechanical studies, especially with regard to cancellous bone. However, bone density did not explain all of the variability in the measured bone elastic constants (see Table 2.4) nor did it account for the bone tissue architecture and, therefore, bone anisotropy. Structural parameters were expected to explain some of the variance in the elastic properties not explained by density measures alone [20,73]. More recent studies have investigated the effect of the inclusion of such structural parameters in combination with bone density in the relationships with elastic constants, showing different degrees of improvement in the variability explained [71,72]. In any case, a global form of the relationships between elastic properties and bone density and structural parameters

[†] See Appendix A for a description of computed tomography.

remains unknown. Maybe there is not sufficient knowledge to explain the reported differences and the fact that some of the variance of the elastic constants still remained unexplained.

Recently, advanced computational models (high-resolution finite element models) have been designed as an alternative to obtain information about bone properties. Representing the trabecular structure in detail and assuming isotropic and homogenous behaviour of the trabecular bone tissue, they seem to produce good predictions of apparent elastic properties [69], and high correlations between bone density and structural parameters and apparent elastic properties [166]. The use of such techniques has been extended to the study of bone failure, with high levels of performance [115], showing its potential to assess strength behaviour. Niebur et al.[115] even stated that this kind of computational models, when using uniform tissue modulus and asymmetric tissue failure strains, "have reached a level of fidelity that qualifies them as surrogates for destructive mechanical testing of real specimens". However, most of these studies have been performed using non-human bone specimens and the validity of the results for human bone in general remains to be seen. In addition, further research is needed to better understand the effect of bone tissue properties on the apparent properties of bone.

Table 2.4 Linear and non-linear relationships between bone apparent density (ρ), Young's modulus (E) and strength (S).

Study	Type of bone	Anatomic site	$E = a + b\rho$	(r^2)	$E = a\rho^b$	(r^2)	$S = a + b\rho$	(r^2)	$S = a\rho^b$	(r^2)
Carter and Hayes[13]**	Trabecular*	Tibia & femur	–		$2875\ \rho^3$	–	–		$52\ \rho^2$	–
Hvid et al[65]**	Trabecular	Proximal tibia	$-99.4+1689\rho$	(0.57)	$2132\ \rho^{1.46}$	(0.61)	$-1.14+18.99\rho$	(0.74)	$25.3\ \rho^{1.49}$	(0.80)
Snyder & Schneider[152]ξ	Cortical	Tibial diaphysis	$-23.5E9+21.91E9\rho$	(0.55)	$1E9.59\ \rho^{2.39}$	(0.56)	$-189.9+217.1\rho$	(0.45)	$1E1.81\ \rho^{1.93}$	(0.46)
Linde et al[91]**	Trabecular	Proximal tibia	–		$1624\ \rho^{1.32}$	(0.49)	–		$25.4\ \rho^{1.6}$	(0.56)
Keller[73]ξ	Cortical $\rho \geq 0.5$	Femur	$-6.79+11\rho$	(0.56)	$3.31\ \rho^{2.36}$	(0.68)	$-64.9+113\rho$	(0.86)	$43.9\ \rho^2$	(0.89)
	Trabecular	Spine	$-0.007+0.203\rho$	(0.54)	$0.757\ \rho^{1.94}$	(0.70)	$-0.971+16.9\rho$	(0.74)	$97.9\ \rho^{2.3}$	(0.79)
Keyak et al[74]**(ash ρ)	Trabecular	Proximal tibia	–		$33900\ \rho^{2.20}$	(0.84)	–		$137\ \rho^{1.88}$	(0.91)
Rho et al[135]	Cortical†	Femur	$-6.142+0.014\rho$	(0.77)	–		–		–	
		Tibia	$-3.842+0.013\rho$	(0.53)						
	Trabecular††	Distal femur	$-384+5.27\rho$	(0.91)	$0.82\ \rho^{1.27}$	(0.95)	–		–	
		Proximal tibia	$-326+5.54\rho$	(0.95)	$0.51\ \rho^{1.37}$	(0.96)				

In all the studies, the loading direction ran along the longitudinal axis of the tested bones. * Human and ovine specimens. ** ρ (g cm^{-3}), E (MPa), S (MPa). ξ ρ (g cm^{-3}), E (GPa), S(MPa). † ρ (kg m^{-3}), E (GPa). †† ρ (kg m^{-3}), E (MPa).

2.2.3 Factors affecting bone material properties

2.2.3.1 Age and gender

It is generally accepted that there is a relationship between increasing age and change of bone material properties, which leads to a decrease in the mechanical integrity of bone. Mosekilde [108] stated "age by itself is the major determinant of vertebral bone strength, mass and microarchitecture". These changes are a result of aging alone or associated pathologies (e.g., osteoporosis).

Bone mass seems to reach a peak before the age 30, with higher peak values in men than in women. After reaching this peak, bone mass remains relatively stable and, then, starts to decline. Higher rates of bone loss have been observed in women than in men, especially after the menopause. Around age 90, women may have lost 20% of their peak cortical bone mass and 40-50% of their peak trabecular mass, whereas men at the same age may have lost 5% and 10-25% of cortical and trabecular bone mass respectively [174]. Additionally, geometry, composition and gross architecture of bone may also change with age, as a result of bone remodelling. Normal age-related changes include decreases in cortical thickness, trabecular bone density and connectivity. Men seem to have an age-related compensatory increase in bone size; women after the age of menopause seem to have a higher tendency for disconnection of the trabecular network than men [108]. All these changes have a noticeable effect on bone mechanical properties.

Regarding cancellous bone, Ding et al.[38] performed axial compression tests on tibial cancellous bone from donors aged from 16 to 83 years to determine its mechanical properties, density and mineral and collagen content. They reported a decrease of apparent density, Young's modulus, strength, ultimate strain, failure energy (energy absorption to failure) and collagen density from about age 60, whereas trabecular tissue density and mineral concentration remained almost constant (Figure 2.2). They suggested that the loss of trabecular bone substance was the main cause of this decrease in mechanical properties, rather than a decrease in the quality of the substance itself.

McCalden et al.[100] studied age-related changes in the compressive strength of distal femoral cancellous bone and their relationship with changes in density and trabecular architecture. They reported a significant decrease in bone density and compressive strength (ultimate stress) with age (specimens from 20 to 102 years), with no significant gender differences (Figure 2.3). The decrease of compressive strength was approximately 8.5% per decade. In this study, density accounted for around 90% of the variations in

strength, suggesting that changes in trabecular architecture played only a small independent role, with the exception of the mean thickness of the trabecular plate. However, they noted that the effect of density and microstructure on mechanical properties had only been assessed in one direction and it could be different in other directions.

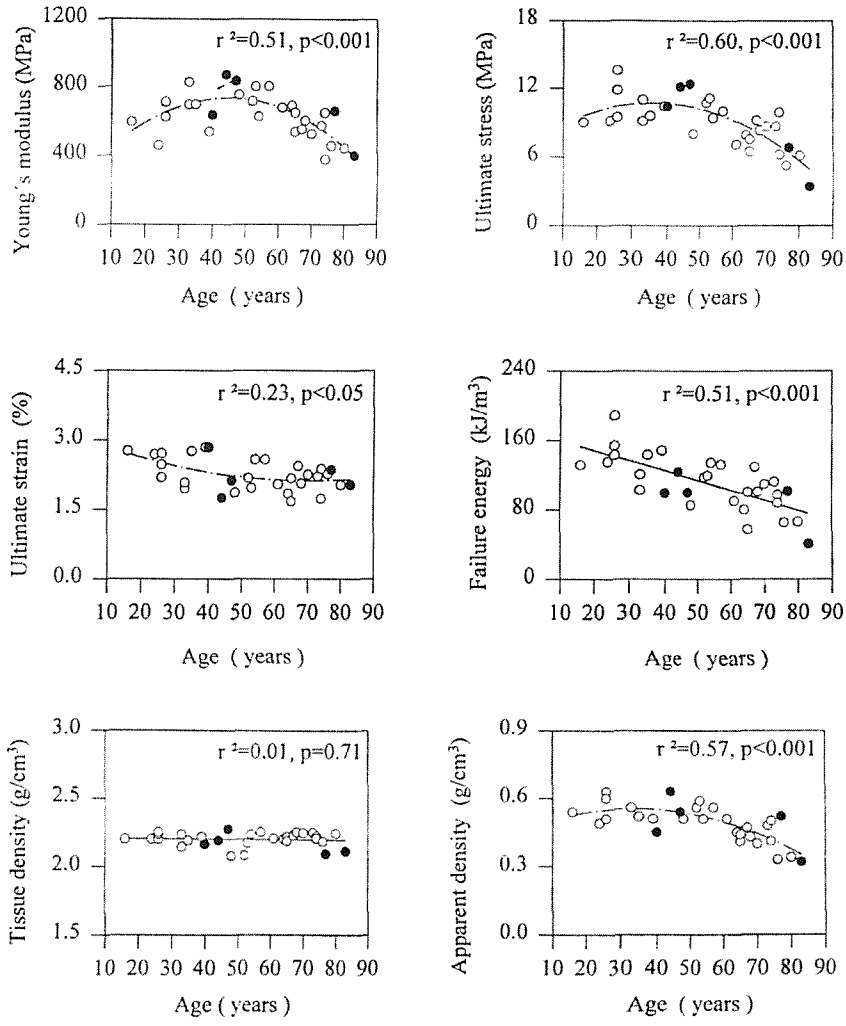

Figure 2.2 Changes of the material properties of tibial trabecular bone with age. • = female, ○ = male *(From Ding et al.[38])*.

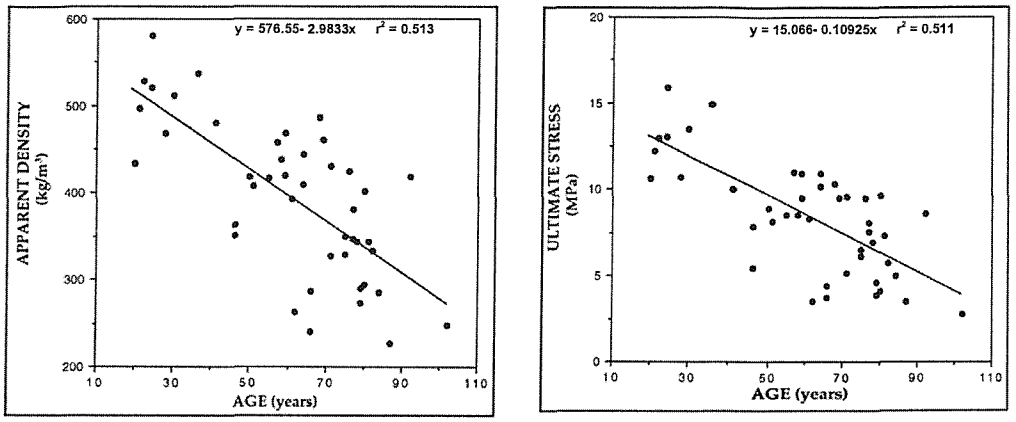

Figure 2.3 Changes in apparent density and strength with age in femoral cancellous bone *(From McCalden et al.[100])*.

With regard to cortical bone, Burstein et al.[11] determined the mechanical properties of human femoral and tibial cortical bone for a population ranging from 21 to 86 years. No significant gender-related differences were found in age-grouped specimens. With increasing age, femoral cortical bone showed a progressive but slow degradation in its mechanical properties, except for an increase of the plastic modulus (slope of the plastic portion of the stress-strain curve). Strength values decreased at approximately 2% per decade, but no significant changes were observed in the elastic modulus. However, tibial cortical bone did not show any regular change in its mechanical properties, except for the ultimate strain and energy absorption. McCalden et al.[99] reported that strength, ultimate strain and failure energy were inversely and linearly correlated with age, decreasing by 5%, 9% and 12% per decade, respectively. They also found little change of Young's modulus with age. Increase of porosity was found to account for 76% of the reduction of the strength of cortical bone. Zioupos & Currey [177] also found a steady and significant decline with age of the mechanical properties of male human femoral bone. Young's modulus and ultimate stress decreased by 2.3% and 3.7% per decade, respectively.

2.2.3.2 Disease

Joint diseases such as rheumatoid arthritis and osteoarthritis (see Chapter 3) can affect the material properties of bone as a result of changes in bone structure and composition. Patients with rheumatoid arthritis (RA) have shown lower cancellous bone apparent density, strength and stiffness than normal cancellous bone, as well as cortical thinning. Different findings have been reported in osteoarthritic (OA) patients. Hvid [64] reported lower *in vivo* compressive strength for tibial and femoral cancellous bone in RA patients than in OA patients, as measured during total knee arthroplasties by using a

penetration-based technique. At two millimetres underneath the tibial resection surface, median values of 13.8 MPa and 12.2 MPa were reported for the OA and RA groups respectively. For the femur, the median values were 12.0 MPa for the OA group and 8.0 MPa for the RA group. They suggested that tibial bone strength values in RA and OA were lower than the values reported in studies of normal cadaver knees. Yang et al.[172] measured the stiffness of cancellous bone *in vitro* from rheumatoid arthritic proximal tibiae and concluded that RA affected bone had significantly lower stiffness than normal and osteoarthritic bone, after comparing their results with those reported by Finlay et al.[45]. They both used an indentation technique to measure the stiffness of tibial plateaus obtained during total knee arthroplasties. The average stiffness for the RA group in Yang et al.'s [172] study was 675 N/mm, whereas Finlay et al.[45] reported 1287 N/mm and 1116 N/mm for the normal and OA groups, respectively. This shows a decrease of 13% in the OA group and of 48% in the RA cases, relative to the normal group. On the contrary to the findings just mentioned, Li & Aspden [90] found, in their study of the composition and mechanical properties of cancellous bone from OA and normal femoral heads, that OA bone presented statistically significant higher apparent density (51% increase) and stiffness (15% increase) than normal bone. However, the material density from the OA group was found to be 8% lower than the material density of normal bone.

Metabolic diseases can modify normal bone composition, leading to changes in its mechanical integrity and material properties. In osteoporosis, normal age-related bone changes, such as the decrease in trabecular bone density and cortical thickness and the change in bone architecture, become more acute [108], increasing the risk of bone fracture. In the study mentioned above, Li & Aspden [90] also assessed osteoporotic (OP) femoral heads. OP bone apparent density, stiffness and yield stress showed statistically significant differences, with values 19%, 20% and 24% lower than normal bone, respectively. Bone material density was not significantly different. Several other pathologies, such as infectious diseases, can also affect bone structure and composition and, therefore, its mechanical behaviour. However, not much is known about the changes in the material properties of the affected bone in such cases.

2.3 STRUCTURE AND MATERIAL PROPERTIES OF THE ANKLE BONES

Despite the numerous experimental studies on bone material properties available in the literature, those referring to the ankle bones are sparse. No data have been found about material properties of cortical bone in the ankle joint. Only a few studies reported on the mechanical properties of the trabecular bone of the talus and the distal tibia. All of them showed a marked variability between individuals. In general, the cancellous bone in the distal tibial seemed to be weaker than the cancellous bone of the talus (40% on average [66]).

2.3.1 Tibia and fibula

As all long bones, the tibia and fibula show strong cortical bone along their tubular diaphyses. At their epiphyses, a much thinner layer of cortical bone on the outside covers the cancellous bone. The density of the cancellous bone in the distal tibia decreases from the periphery to the centre. An area of dense cancellous bone (subchondral bone) is present underneath the articular surface on the tibial plafond.

Regarding the cancellous bone in the distal tibia, all the studies considered the subchondral bone layer as the strongest region, with a significant reduction in bone strength with depth (from distal to proximal), especially within the central region. Hvid et al.[66] studied the bone strength in amputation specimens by means of penetration tests, stating that their results were comparable to those from conventional compression tests. They found an area of maximum strength located posteriorly and medially in the distal tibia. Mean penetration strength values ranged from around 5 MPa to approximately 43 MPa at the closest level to the subchondral bone. Figure 2.4 A shows the variation of average strength with depth, with a considerable decrease between the first levels, followed by a slight decrease thereafter. A mean decrease of 2.12 MPa was found between the first two levels, and 1.24 MPa, 0.34 MPa and 0.45 MPa between the subsequent levels. Jensen et al.[68] found the maximum strength at the antero-lateral area, crossing the central part to the postero-medial part, at the closest level to the subchondral bone studied. They used both compression and penetration tests on autopsy specimens. In the compression test, they observed a significant reduction of bone strength at the central and antero-lateral areas between the first two levels. The mean decrease ranged from 24 % to 36%. Mean peak strength values from the compression test were: 18 MPa for yield stress and 24 MPa for ultimate stress. They suggested that ankle specimens from below knee amputations are generally weaker and differ in their bone strength profile from ankle specimens obtained at autopsies. This could explain the differences between their results

and those by Hvid et al.[66]. Jensen et al.[68] did not find uniform strain profiles. Yield strain showed only slight inter-individual and intra-individual variability and typical values for an individual varied between 1.5% and 6.5%. Ultimate strain had a large variability, with typical values between 4% and 15%. It is not clear if these strain data included data from the talus as well. Nevertheless, these strain values are much larger than the values reported for other bones. Average yield strain values between 0.61 and 0.85% have been measured for human vertebra, proximal tibia and femoral neck (Table 2.3, page 23). End artefacts make experimental determination of strains in trabecular bone difficult, leading to substantial errors if appropriate techniques are not used [27]. This might explain the large differences between Jensen et al.[68]'s values and other studies.

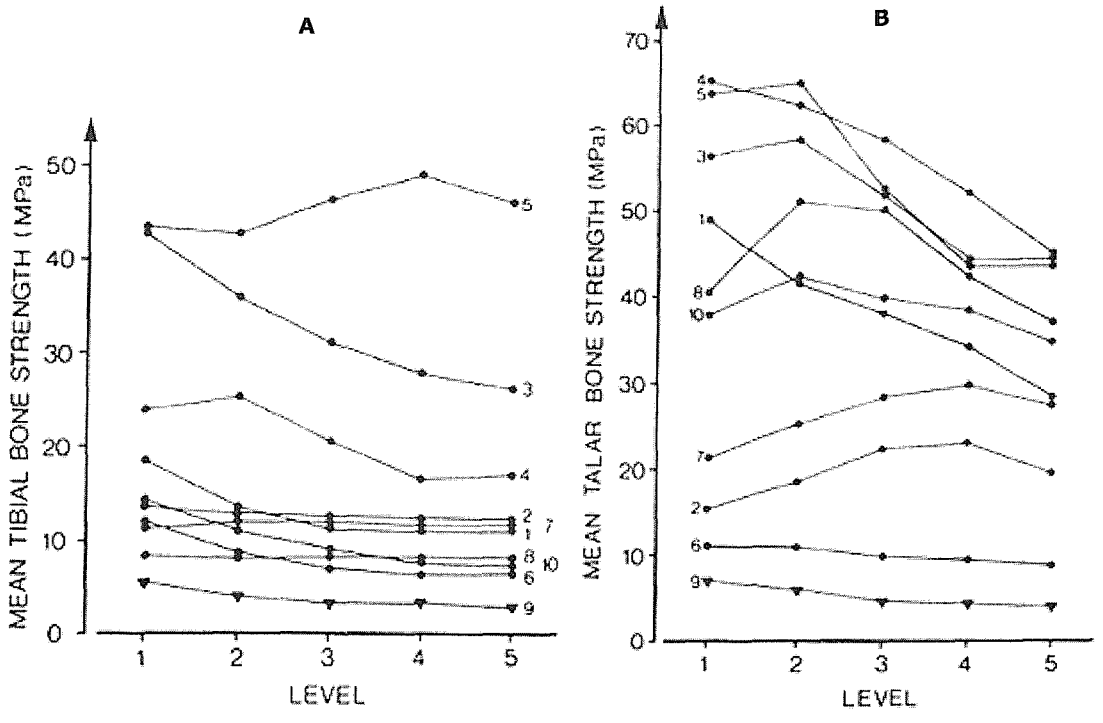

Figure 2.4 Cancellous bone strength profiles at the ankle joint (10 specimens). **A** Tibial strength. Levels 1 to 5 go from distal to proximal in 2 mm intervals, starting just above the subchondral bone plate. **B** Talar dome strength. Levels 1 to 5 go from proximal to distal in 2 mm intervals, starting just beneath the subchondral plate *(From Hvid et al.[66])*.

With regard to the Young's modulus of distal tibial bone, Destresse et al.[37], using an ultrasound technique, reported a median value for the Young's modulus of the cancellous bone of E_{median}= 1210 MPa (ranging from 718 to 2057 MPa) at a level adjacent to the subchondral bone (Figure 2.5). Measurements were performed along the direction of the longitudinal axis of the tibia. Jensen et al.[68] found a maximum value of E_{max}=827 MPa.

Aitken et al.[2], using an indentation technique on amputee specimens, obtained even lower values for the Young's modulus, ranging from 150 to 300 MPa for the subchondral level, and from 60 to 120 MPa just 1-2 cm above it. A maximum value of 427 MPa was reported. To be able to compute the Young's modulus, they assumed the bone to be an isotropic linear elastic material with a Poisson's ratio of 0.2. Differences in testing techniques and specimens may explain some of the differences observed between all these results. No data was found about the Young's modulus of distal tibial cortical bone. Typical values from the tibial mid-diaphysis ranged from 10 to 22 GPa [134,152].

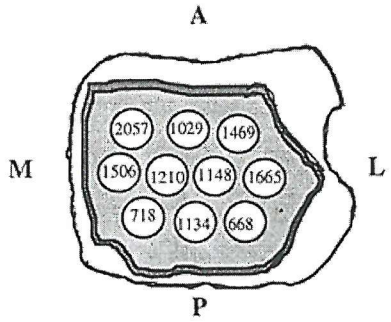

Figure 2.5 Mean Young's moduli (MPa) measured on a transversal slice of the distal tibia (just above the subchondral plate) (*From Destresse et al.[37]*).

Only Jensen et al.[68] have reported data about the mechanical properties of the distal fibula. They performed compression tests in cylinders obtained proximal and distally from the lateral malleoli, at right angles with the articular surface. Mean ultimate stress was 6.5 MPa (range 2.8-32.0 MPa) for the proximal cylinder and 5.7 MPa (range 1.2-24.2 MPa) for the distal one.

2.3.2 Talus

A thin layer of cortical bone forms the outer shell of the talus. This shell is thicker at the lateral aspects of the neck and the head. The core of the talus consists of cancellous bone of varying densities. An area of subchondral bone lies underneath the articular surface at the top of the talar dome.

No data have been reported in the literature about the mechanical properties of the cortical bone of the talus. In fact, no study of the mechanical properties of the cortical shell that covers the small bones of the foot has been found.

With regard to trabecular bone, Hvid et al.[66] reported a bone strength increase from the subchondral plate into the first level and a posterior decrease towards the deeper levels (see Figure 2.4 B). A mean increase of 1.47 MPa was found between the first two levels and mean decrease values of 2.50 MPa, 3.38 MPa and 4.30 MPa between the subsequent levels. They found the strongest area situated posteriorly and medially, at roughly corresponding locations with the strongest area found in the distal tibia. Jensen et al.[68] located the strongest area anteriorly and laterally and observed a highly significant reduction in bone strength from the subchondral level to deeper areas. The mean decrease between levels 1 and 2 ranged from 19% to 59%, and from 25% to 46% between levels 2 and 3. They reported maximum values of ultimate stress and yield stress of 30 MPa and 23 MPa respectively, as well as a maximum Young's modulus of E_{max}=1224 MPa.

The only experimental relationship found between apparent density and Young's modulus for trabecular bone at the ankle joint is the one provided by Destresse et al.[37] in their ultrasound study of the mechanical properties of proximal and distal tibia:

$$E = 0.2\ \rho^{1.52}$$

where E represents the Young's modulus (MPa) and ρ the apparent density (kg m^{-3}). No relationships between bone density and other mechanical properties have been found for the trabecular and cortical bone at the ankle.

Chapter 3

THE DISEASED ANKLE AND ANKLE ARTHRODESIS

3.1 THE DISEASED ANKLE

Ankle joint diseases, such as ankle arthritis, can lead to chronic pain, deformation and functional disability, particularly when severe. *Arthritis* is an inflammatory disease affecting the cartilage and lining of the joints, which has multiple causes, on occasions with undetermined origin. One of the most common types of arthritis is *rheumatoid arthritis*. It is a complex chronic disorder that often affects several joints and may even involve other systems of the body. The initial inflamation and swelling of the soft tissues of the joints can later produce pain, cartilage destruction, bone erosion, malalignment, subluxation, joint stiffness and even fusion of the joint at the end stages of the disease [156]. Despite many theories proposed, the precise etiology remains unclear. Another common form of arthritis is *osteoarthritis*, a gradual degenerative disease. Wear and tear of the articular cartilage leads to exposure of subchondral bone, which then acts as the articular surface. Subsequent events of the degenerative process are bone spurs (osteophytes) along the margin of the articular cartilage, increased density of the subchondral bone and bone atrophy in areas of decreased or no stress. The incidence of osteoarthritis increases dramatically with age but traumatic injuries, deformity and metabolic disorders can also cause it [156].

The incidence of arthritis in the ankle is lower than in other joints such as the hip and the knee, but it still affects many people, causing severe pain and disability [84]. About 6% of the rheumatoid arthritic patients have the ankle joint initially damaged, though multiarticular rheumatoid arthritis involves the ankle in 15 to 52% of the patients. In the case of juvenile onset of rheumatoid arthritis, 68% of the patients have the ankle affected [84]. Primary osteoarthritis of the ankle joint is very rare, but osteoarthritis of the ankle secondary to trauma and to septic arthritis is more common [34,70]. An important increase in the incidence of posttraumatic osteoarthritis in the ankle has occurred during the last decades mainly due to safety improvements in the car industry, which have led to a decrease in fatalities but an increase in trauma injuries affecting the lower limbs [5,141].

Several options are available to treat ankle arthritis and other causes of ankle disease such as fractures, infection or osteonecrosis. They include conservative nonoperative means, bone debridement, ligamentous reconstruction, corrective osteotomy, arthrodesis and arthroplasty [1,19]. As with any problem of the musculoskeletal system, the treatment must be individualized for each patient [34]. *Ankle arthrodesis* (ankle fusion) is one of the

most popular choices to relieve pain and provide stability, restoring the patients to their daily activities. It is a surgical procedure to eliminate motion in a joint by promoting bony fusion. It has been widely and successfully used especially in severely affected patients, despite the obvious loss of mobility at the ankle and several complications associated with it. Some specialists consider all the problems associated with ankle arthrodesis (see section 3.2.3) as unacceptably high. *Ankle arthroplasty* (ankle joint replacement) appears as a logical alternative to ankle arthrodesis, trying to emulate the success of the hip and knee joint replacements, providing pain relief while preserving joint function. The first designs of total ankle replacements produced poor results, with significant and frequent complications such as subsidence and loosening of implant components, ankle instability, wound healing problems and infection. Second generation prostheses are becoming increasingly popular. They are showing a better short-term performance, especially with a good patient selection and a good surgical technique. However, long-term results are not known yet [24,114,141].

3.2 ANKLE ARTHRODESIS

Numerous orthopaedic surgeons have recommended and still recommend ankle arthrodesis as the treatment of choice for end-stage ankle arthritis, regardless of its pathological cause. It presents complications and disadvantages, and unsatisfactory results have been reported. Modern surgical techniques have significantly improved ankle arthrodesis results and reduced the complication rates associated with it. Nevertheless, fusion failures are still reported, showing that there is still scope for further improvements.

3.2.1 Indications

The general indications for ankle fusion are severe pain, joint destruction and arthritis. Post-traumatic ankle joint destruction is one of the main indications [78,157]. A normal subtalar joint will help the hindfoot to compensate for the loss of mobility at the fused ankle. There are certain preoperative factors that could increase the risk of nonunion, infection and further complications when undergoing an ankle fusion. They include a massive loss of bone from a previous problem, osteonecrosis of the talus and previous failed ankle arthrodesis [18,39]. Infection, deformity, sensory deficit and bony defects can complicate the fusion and result in pseudoarthrosis or even amputation [146]. Ankle arthrodesis is the preferred method of salvage of failed total ankle arthroplasty [77]. Patient selection for ankle arthrodesis is somewhat controversial. For instance, while being considered an excellent choice for young, active patients diagnosed with posttraumatic

arthritis of one foot [34,101], high risk of ankle fusion failure has been related with arthritis caused by open trauma [1,123].

Despite its limitations, numerous authors continue to consider ankle fusion as the gold standard for the treatment of rheumatoid arthritis and osteoarthritis, especially when the joint does not respond to conservative treatments [34,36,44,70,78].

3.2.2 Surgical techniques

Numerous ankle arthrodesis techniques have been described, varying in their surgical approach, articular surface preparation, type of fixation and method of postoperative care [1,34,70,146]. The technique selection is usually based on the underlying disorder. The two main surgical approaches are open surgery and closed surgery. Open surgery is used for any kind of patient, whereas closed surgery (percutaneous techniques), although much less invasive, is limited to ankles without severe deformity.

The shape of the articular surfaces can be preserved (with or without cartilage removal) or resected, normally with two parallel cuts on the tibia and the talus; there is also a wide range of methods of onlay grafts (Figure 3.1). In terms of methods of fixation, both external and internal types have been described, usually trying to apply a certain level of compression through the fusion site. External fixation uses devices externally fixed to the shank and talus with pins and screws (Figure 3.1 g). These devices allow a change of the compression across the joint postoperatively. Staples, pins, screws and plates are used in various configurations and combinations in internal fixation (Figure 3.2). The use of the fibula as strut graft is also possible, being fixed to the tibia and talus with additional screws. Whatever the fixation means, bone graft can be added to improve the stability of the construct, especially in patients with poor bone quality.

Regardless of the surgical procedure, the recommended fusion position for the ankle is in neutral dorsiflexion/plantar flexion, slight valgus (5º) and 5º to 10º of external rotation. A slightly posterior translation of the talus relative to the tibia is also advised, in order to improve the mechanical level arm of the calcaneus during ambulation [1,34,70,146]. Ankle arthrodesis increases the stresses on the surrounding joints of the foot and leg, often leading to secondary degenerative changes. Accurate positioning of the ankle will minimise the increase of stress, as well as avoid further alteration of the patient's gait.

The postoperative management varies depending upon the surgical technique. Usually, a minimum non weight-bearing period of between 4 and 6 weeks in a low leg cast

is followed by a partial and progressive weight-bearing period, until joint fusion is complete and the patient is able to walk pain-free.

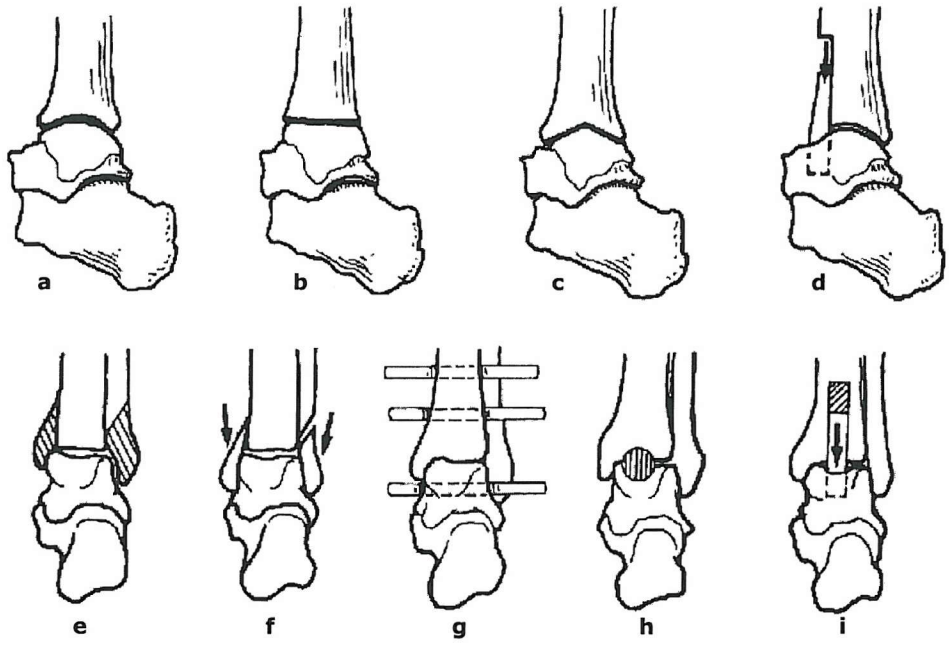

Figure 3.1 Examples of ankle arthrodesis techniques. **a** Removal of articular cartilage. **b** Flat cut arthrodesis. **c** Chevron type cut. **d** & **i** Anterior tibial sliding graft. **e** Malleolar excision. **f** Malleolar onlay graft. **g** External fixation. **h** In situ dowel graft. *(Modified from Katcherian [70]).*

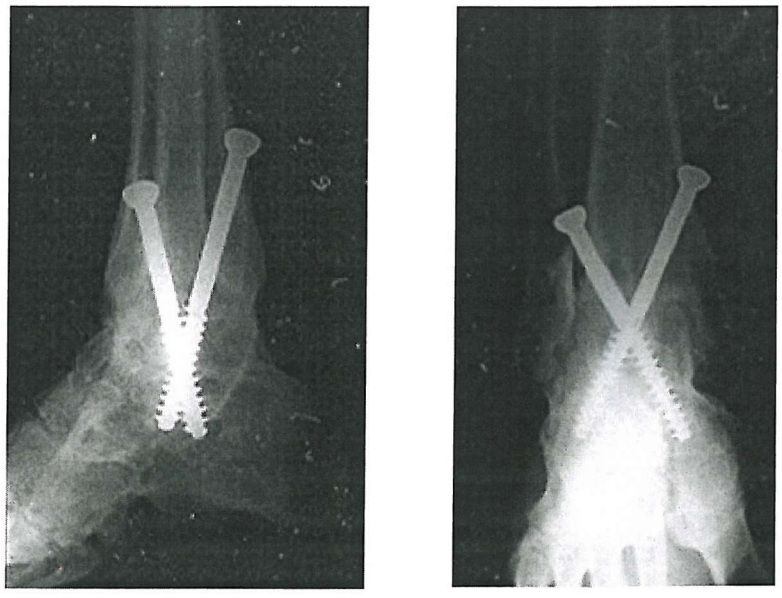

Figure 3.2 Lateral (left) and frontal (right) radiographs of a fused ankle with internal fixation. Two crossed screws were placed from proximal to distal using a percutaneous technique *(Source: Lund University Hospital, Sweden).*

3.2.3 Complications and disadvantages

The wide spectrum of post-operative complications associated with ankle arthrodesis includes nonunion, delayed union, malunion, infection, wound healing problems, neurovascular injury, tibial fracture and pseudoarthrosis. The most frequent complication associated with ankle arthrodesis is nonunion [1,25], which represents the failure of the fusion procedure. The incidence of ankle fusion failure and the factors affecting its outcome will be addressed in the following section and in Chapter 4. Subsequent surgery and/or non-surgical treatments can be attempted to deal with the above-mentioned complications and, in the worst cases, below-knee amputation is the recommended alternative [25]. Longer-term problems after ankle fusion include arthrosis of adjacent joints, possibly related with the increase of stress on these joints, especially the subtalar and talonavicular joints [125,157]. Other disadvantages associated with ankle arthrodesis are the loss of function and the time needed for the fusion to occur (usually between 12 and 16 weeks) [34,89].

3.3 CLINICAL RESULTS OF ANKLE ARTHRODESIS

Rates of primary union (when secondary surgery is not needed to achieve union) and clinical evaluations provide objective information about the results of ankle arthrodesis, whereas the level of patient satisfaction offers a subjective assessment. An overwhelming number of studies reporting on the clinical results of ankle arthrodesis can be found in the literature [18,19,23,35,36,39,44,61,96,97,101,105,117,123,125,151,157]. A summary of clinical results of ankle arthrodesis is shown in Table 3.1. Comparisons are certainly difficult due to the different means of assessment, the wide range of techniques used and the differences within the patient populations. Published scoring systems help to evaluate the clinical results of ankle arthrodesis. They typically gather information about function, patient's subjective evaluation, radiographic assessment or clinical findings (e.g. Mazur grading system [35,151], HMS Score [157], McGuire System for Ankle Study Evaluation [101,125]). There is no standard scoring system being routinely used to assess the performance of ankle fusion in large series of patients [1], though several recent studies have applied the AOFAS Ankle and Hindfoot Rating Scale to evaluate their results [79,96,105].

Failure rates (primary nonunion) vary widely from around 0% to 40% (see Table 3.1). Dereymaeker et al.[36] and Dohm et al.[39] reported failure rates close to 40%. In the first study, pooled results of external (70%) and internal fixation procedures on rheumatoid arthritic patients were presented. In contrast, Felix & Kitaoka [44] reported a low 4% failure rate in rheumatoid arthritic patients, using either external or internal fixation. Dohm et

al.[39] presented pooled results of six different fixation techniques in a mixed patient population. Although the overall failure rate was 35%, it ranged between 71% for fibular strut fixation to 0% for T-plate fixation. McGuire et al.[101] reported 33% of nonunions within a patient population with osteoarthritis or failed ankle arthroplasty. Bone graft or external fixation was used. Also using external fixation, but in rheumatoid ankles, Smith & Wood [151] obtained 27% of failed fusions. 26% of failed fusions were reported by Holt et al.[61] in their study of internally fixed arthrodeses in a mixture of traumatic osteoarthritic (80%) and rheumatoid arthritic patients. The failure rate decreased to 7% when high-risk patients were excluded. Maurer et al.[97] obtained 18% and 0% failure rates for external and internal fixation techniques respectively, in a patient population with majority of traumatic osteoarthritis. In a similar patient population, Colgrove & Bruffey [23] reported no failures using external fixation and internal screws simultaneously. Low failure rates, around 5%, were mostly reported for internal fixation techniques (Dennis et al.[35], Chen et al.[18], Monroe et al.[105]).

The mean time to fusion normally ranged from 11 to 18 weeks (see Table 3.1), though sometimes it is not clear if the times to union after secondary procedures were being considered. Dennis et al.[35] and Monroe et al.[105] reported very short fusion times (around 9 weeks). In both cases ankle arthrodesis was performed with internal fixation with screws, in similar patient populations (majority of posttraumatic osteoarthritis). Pfahler et al.[125] presented shorter mean times to fusion for arthrodeses with internal fixation (11 weeks) than for those with external fixation (17 weeks). A high 28-week time to fusion was reported by McGuire et al.[101], in a series of 18 ankles fixed either externally or with bone graft only. They included those ankles that initially failed to fuse but eventually did after second a arthrodesis. Dohm et al.[39] and Cooper [25] pointed out the importance of primary union, as achieving union in the presence of a previous nonunion becomes a very challenging task. The time to fusion after secondary procedures increased significantly and so did the period of disability of the patients. In addition, reported rates of failure went up considerably. In Mann & Rongstad's study [96], only 10% of primary arthrodesis failed, while 25% of patients with previous nonunion did not achieve fusion after secondary surgery.

Although, in general, patient satisfaction and good clinical evaluation agrees with low primary nonunion rates (e.g. Dennis et al.[35], Chen et al.[18], Pfahler et al.[125], Monroe et al.[105]), some have reported patient satisfaction despite high nonunion rates [36]. After short and mid-term follow-ups, highly positive rates of clinical evaluation and patient satisfaction (see Table 3.1) show the ability of ankle arthrodesis to improve the main patients' concerns prior to surgery, such as pain and ambulatory skills. However, long-term complications after ankle fusion could have a negative impact in these rates if longer follow-ups were performed.

Table 3.1 Clinical results of ankle arthrodesis.

Source of data	Arthrodesis fixation	Number of ankles	Nonunion rate (%)	Mean time to fusion (weeks)	Mean follow-up (months)	Clinical evaluation (%)*
McGuire et al (1988)[101]	External & bone graft (pooled results)	18	33	28	40	94[a]
Dennis et al (1990)[35]	Internal	16	6	9.2	15.1	80[a]
Smith & Wood (1990)[151]	External	11	27	-	58	62[b]
Maurer et al (1991)[97]	Internal	35	0	-	24	-
	External	8	18	-	24	-
Holt et al (1991)[61]	Internal	23	26[c]	16	26	-
Dohm et al (1994)[39]	Various	37	35	11-20	-	-
Chen et al (1996)[18]	Internal	40	5	13	48	90
Pfahler et al (1996)[125]	Internal	14	5	11	40	80
	External	7		17	40	
Dereymaeker et al (1998)[36]	Ext. & internal (pooled results)	14	36	18.4	41.2	86[d]
Felix & Kitaoka (1998)[44]	Ext. & internal (pooled results)	24	4	-	60	-
Monroe et al (1999)[105]	Internal	29	7	9	24	81[e]
O'Brien et al (1999)[117]	Internal	36	17	-	-	-
Thermann et al (1999)[157]	Internal	28	-	-	89	70
	External	22	-	-	89	46-64
Colgrove & Bruffey (2001)[23]	Combined ext. & internal	26	0	11.3	13	-

* Excellent and good results. [a] Including data after secondary surgical procedures. [b] Points in the Mazur grading system (total 100 points). [c] 7% if high-risk patients are excluded. [d] Only rate of patient's satisfaction. [e] Points in the AOFAS scale (maximum 96 after ankle arthrodesis), obtained only from 25 of the 29 cases.

As mentioned before, the performance of all the existing methods to achieve ankle fusion is difficult to compare and, thus, there is little agreement on which method provides the best results. Nevertheless, in the last years, internal fixation techniques have been especially recommended for their higher union rates, shorter fusion times, fewer complications and better improvement according to scoring systems than external fixation techniques [1,19,35,39,61,78,97,125,157]. This is especially true when the patients are not considered at high risk for failure of fusion, i.e. patients with infection or neurological problems. The use of screws is one of the most popular means of rigid internal fixation in ankle arthrodesis, and may be considered as standard procedure [1,78]. Screws are easy to insert, cause lower levels of disruption of the surrounding soft tissues and vessels, and provide good stability. Moreover, they are the only choice when closed surgery is attempted. The best screw configuration is not known. Some authors have considered two crossed screws as the best choice [1,78], though a third screw and fibular graft have been recommended to increase the stability when bone quality is compromised [44].

Chapter 4
MECHANICAL FACTORS AFFECTING ANKLE ARTHRODESIS

4.1 BONE HEALING: MECHANICAL ENVIRONMENT

In the musculoskeletal system, the mechanical environment plays a key role in maintaining, repairing and regenerating connective tissues such as bone. In bone fracture healing, bone fusion or implant fixation, bone repair or regeneration occurs as a result of the combination of biological and mechanical factors.

The role of the mechanical factors can be assessed at different levels, from the organ level down to the molecular level [12]. An enormous amount of research has been done in this multidisciplinary field in the last decades, but, nevertheless, further research is needed to clearly understand the overall process of bone healing. Information about how forces, displacements, loading rates or stiffness (at an organ level) and stresses or strains (at a tissue level) correlate with the results of bone healing processes is being complemented with the expanding knowledge of how the cells sense and react to these stimuli and the molecular changes associated with them. It is necessary to know what happens at the different levels as well as understand the relations between them, as can be clearly understood from the following statement by Carter et al.[12]:

> *"... it can be observed at the organ level that fracture instability leads to delayed fracture healing. At the tissue level, fracture instability relates to increased stress and strain in the differentiating tissue and different forces lead to different spatial distribution of stress and strain in the tissues. At the cellular level, local tissue stress and strain may cause changes in cell pressure or shape. At the molecular level, cell shape changes may cause a disruption of the actin cytoskeleton. This may be a molecular signal for the initiation of a certain pattern of protein synthesis that on the organ level results in delayed fracture healing."*

Two types of bone healing can take place during the process of bone regeneration: direct (primary) bone healing and indirect (secondary) bone healing. During primary bone healing, bone tissue forms between contacting bone fragments under conditions of rigid

stabilization, via osteonal remodelling. When stabilization of the bone fragments is less rigid, secondary bone healing occurs, with the formation of a callus that bridges across the fracture gap. This callus undergoes various stages of tissue differentiation, where cartilage is formed, then calcified and finally replaced by bone tissue (endochondral ossification) [51,130].

Research on bone healing has been mostly done on diaphysial fractures of long bones, i.e. on cortical bone healing. In this case, secondary bone healing is the most likely to occur. Periosteal and endosteal callus is formed bridging the bone fragments. During this process, tissue differentiation is strongly affected by the mechanical environment. For instance, a high degree of instability at the fracture site may hinder endochondral ossification of the callus, leading to an unstable fibrous union. On the other hand, over rigid fixation can prevent callus formation, leading to an atrophic nonunion. Different concepts and theories have been introduced to explain the mechanical influence on tissue differentiation during bone healing. Goodship and Cunningham [51] summarised them as follows:

- Primary bone formation is favoured by low values of strain and hydrostatic pressure.
- Cartilage formation is favoured by high values of compressive hydrostatic stress, if strain is low. Secondary bone formation will then occur via endochondral ossification under conditions of relative stability.
- Connective tissue (fibro-cartilage) is formed in areas of high strain and high hydrostatic pressure.

The ideal mechanical environment for bone healing of different types of fracture still needs to be determined, bringing together the effect of the rigidity of the fixation device, the geometry of the fracture and the loading of the limb. Although it seems clear that some degree of instability is beneficial for healing of long bone fractures, the optimal magnitude, pattern and timing of the loads acting at the fracture site remains to be found. For more details on the current knowledge of bone healing and the related mechanical and biologic factors, refer to Bone Mechanics Handbook [27] (section V), Carter et al.[12] and Mandracchia et al.[95].

The management of fractures and osteotomies on small bones and at the epiphysis/metaphysis of long bones seems to differ from that of diaphysial fractures. The cortical shell that surrounds the cancellous bone represents only a small portion of the cross-sectional area, and thus, most of the repairing process involves healing of cancellous bone. Cortical and cancellous bone healing seem to be somewhat different [42,165]. Cancellous bone healing is characterised by endosteal trabecular activity and union

generally occurs by direct formation of bone at the sites of contact between the cancellous fracture surfaces. Periosteal bone formation only occurs in the presence of instability or gross displacements at the fracture site. Schatzker et al.[144] studied the effects of motion on the healing of cancellous bone in dog's olecranon osteotomies. At the site of the osteotomy, the olecranon was mostly cancellous bone with an extremely thin cortex. Due to the type of fixation, a gradient of stability was present along the osteotomy interface. They observed primary bone formation where stability was absolute, secondary bone formation (via endochondral ossification of the internal cartilaginous callus) where stability was not absolute and strain did not exceed the strain tolerance of cartilage, and fibrous tissue formation where strain exceeded this tolerance. Under conditions of good blood supply with large contact areas and inter-fragmental stability, a solid union is likely to occur rapidly. Therefore, in the management of such fractures or osteotomies, bone healing is usually sought via good bone apposition and rigid fixation [32].

4.1.1 Bone fusion in arthrodesis

The aim of an arthrodesis is certainly different from the treatment of a bone fracture. Rather than trying to restore the structure and function of the fractured bone, joint arthrodesis seeks a change in the normal function of the bones involved, by joining them together to form one solid body. A solid osseous union will ensure long-term stability of the fused joint. As the bony parts involved in arthrodesis are the epiphyses of long bones and/or small bones, bone fusion follows a similar pathway to that described above for cancellous bone healing. Therefore, a good neurovascular condition in the area of the arthrodesis, bone coaptation between large surfaces of cancellous bone and interfragmental stability would be expected to increase the likelihood of a successful fusion. Although the ideal level of stability at the fusion site or the ideal rigidity provided by the fixation construct has not been determined for any type of arthrodesis, it is generally accepted in the literature that rigid fixation enhances bone fusion [43,78,81].

The concept that compression between the bone fragments enhances fusion remains controversial. Generally, compression at the fusion site is considered advantageous to facilitate early fusion, increase fusion rates and decrease complications [17,35,47,178]. Some even consider it as a requirement for a successful fusion, together with bone coaptation and rigid fixation [97]. It could be speculated that compression improves bone coaptation and, therefore, enhances cancellous bone healing; increases the rigidity of the fixation device and, therefore, the likelihood of rapid healing; or has some beneficial effect on the biologic events occurring during bone formation. However, it is not clear what the merits of compression are in itself. Neither it is known what the optimal level of initial compression is, nor how long that initial compression effectively lasts. Cunningham et al.[28] assessed

compression and healing in 10 knee arthrodeses with joint surfaces flat cut and fixed with an external fixator. The arthrodesis bending stiffness was measured several times during the healing period, whilst the external fixator was in place. An initial 500 N compression was applied across the arthrodesis. They found a negligible effect of compression on the bending stiffness of the arthrodesis. Compression across the arthrodesis decreased rapidly and daily adjustments were required to restore the initial level of compression. This produced a progressive loss of length across the arthrodesis. Lowering the compression load to 200 N resulted in a decrease of the rate of loss of length. They concluded that a level of compression that does not decrease rapidly and does not produce a significant loss of length should be applied across the arthrodesis. In a different study, Hart et al.[58] compared the effects of compression on the maturity and pattern of bone healing in canine mid-tibial osteotomies. An external fixation device was used to treat the osteotomy and apply compression. They concluded that compression increased the rigidity of fixation, but did not provide any benefit for bone healing in itself. It is not clear whether this result can be extrapolated to ankle arthrodesis; if so, compression could be beneficial when the fixation device is not stable enough, but would not enhance healing when the fixation device provides adequate rigidity.

The use of internal fixation in bone fractures, osteotomies or arthrodeses does not allow compression between the bones to be readjusted after the initial tightening. Compression can be achieved with screws placed to cross the fracture or fusion site, directly producing compression between the bone fragments (lag screw). Alternatively, the screws can be used to fix a plate to the bone, by compressing the plate against the bone (plate screw). With correct design and placement of the plate, compression across the fracture site is indirectly achieved when tightening the screws [110]. Little information is available about the change over time of the initial interfragmental compression generated by orthopaedic screws. Compression can be assessed by measuring the axial tension generated in the screw when it is tightened. Two *in vivo* studies measured the change in the axial force developed when fixing cortical screws† to long bone diaphyses. Cordey et al.[26] and Blümlein et al.[8] measured the screw axial force during several weeks after the screws were inserted in intact tibial shafts of sheep, with and without the use of plates. They observed a fast initial drop during the first day/days (loss of around 20% of the initial force) and a much slower decrease thereafter. The fast initial drop was attributed to the viscoelasticity of bone (following screw tightening, the stress initially placed by the screw upon the bone relaxes with time), whereas the later slow decrease was attributed to the remodelling of cortical bone under pressure. The effect of possible interfragmentary displacement on the change of the compression was not accounted for, as intact tibiae were used in both experiments; therefore, they represent ideal cases of bone stability.

† A cortical screw is a type of orthopaedic screw designed with a shallow thread to bite cortical bone.

4.2 ASSESSMENT OF INITIAL STABILITY IN ANKLE ARTHRODESIS

From what has been discussed in the previous sections and from the numerous clinical studies carried out to evaluate the results of ankle arthrodesis, it seems clear that stability of the arthrodesis achieved at the time of surgery is one of the factors in determining its final outcome. A large number of ankle arthrodesis techniques and different means of fixation have been described in the literature (Chapter 3), but direct comparisons of the level of stability of the arthrodesis constructs are limited. Intra-operatively, surgeons can assess the stability of the arthrodesis by manually checking the rigidity of the fixed joint. Screw insertion torques may also give an indication of the level of purchase of the screw threads. However an objective measure and comparison of the mechanical behaviour of the arthrodesis constructs could help the surgeon to choose the most stable construct *a priori*.

4.2.1 *In vitro* biomechanical studies

Assuming that more stable fixation leads to a higher chance of fusion due to the minimisation of the motion between the tibiotalar interfaces, some biomechanical experiments have tested the ability of different arthrodesis constructs to bear the loads more likely to affect the fused ankle in the immediate postoperative period.

Several studies have compared the rigidity of external and internal means of fixation. Pilette et al.[126] recommended internal fixation whenever the bone quality made it possible, after testing the Charnley external fixator and two types of internal fixation, crossed cancellous-bone screws and T-plate compression. Tibiotalar joint contours were flat cut. Talar rotation, plantar flexion/dorsiflexion and posterior-anterior shear force were considered the most important loading modes to assess from a clinical point of view. They found the T-plate the stiffest construct and the external device the least stiff. Thordarson et al.[160] tested the stability of a Calandruccio external compression device and of two crossed cancellous-bone screws, preserving the joint contours. The constructs were subjected to tibial torque, plantar flexion-dorsiflexion moment and medial-lateral bending moment (in this order, the most likely modes of loading expected to affect the ankle postoperatively, when placed in a short leg cast). Loads were applied manually on the proximal end of the tibia (tibiae resected at mid-diaphysis), while the talus was fixed. The gross motions between the talus and the tibia were recorded. Two screws had an equal or superior behaviour when bone quality was good and purchase of the screws was secure. Although the external fixation had a lower control of plantar flexion-dorsiflexion, it was recommended for cases of poor quality bone.

Comparisons of the stability of different methods of internal fixation or variations of the same technique have been performed. Dohm et al.[40] compared the relative stiffness of fixation with two crossed screws, fibular strut arthrodesis and compression T-plate constructs, resecting the joint surfaces with parallel cuts. Equal length of tibia were used and kept fixed in each case, while the talus was loaded to simulate dorsiflexion. The T-plate provided a stiffer construct than the screws and was far stiffer than the fibular strut. Thordarson et al.[161] tested the stability of ankle fusion with two screws and the effect of adding fibular strut graft. The methodology was the same as in their work described above. Tibial torque always produced the largest relative tibiotalar motions, followed by plantar flexion-dorsiflexion and medial-lateral bending moments. Quality of the bone was found to be the major determinant of the amount of tibiotalar motion. For good quality bone, the strut graft did not add very much stability to the construct, especially in tibial torsion. However, a significant improvement was observed in specimens with poor quality bone. Friedman et al.[46] compared the stiffness of two crossed screws and two parallel screws in ankle arthrodesis performed with flat resections of the joint surfaces. Tibial torsion and bending tests (plantar flexion-dorsiflexion and eversion-inversion) were the loading modes considered. Although they obtained mixed results in the bending tests, the better torsional stability offered by the crossed configuration made them suggest that this choice may increase the possibility of fusion success. Ogilvie-Harris et al.[119] assessed the stability of ankle arthrodesis when adding a third screw to a two-crossed screw configuration. Joint surfaces were resected and the construct subjected to tibial torsion. Significant greater resistance to tibial torque, as well as greater compression through the fusion site were observed when placing the third screw.

Only one study has compared the effect on stability of the method of surface preparation. Miller et al.[103] compared the stability of two crossed screws when preserving the joint contours and when resecting them with parallel cuts. Cyclic loading was applied in internal-external torsion and plantar flexion-dorsiflexion bending and the relative tibiotalar motion measured. Although slightly higher amounts of torsional motion were observed in the flat-cut arthrodeses, no significant differences were found between the two techniques.

All the studies mentioned above were performed using cadaver ankles with no evidence of bone or joint pathologies. Others have used bone substitutes to carry out similar studies, mainly to minimise inter-specimen variability. Nasson et al.[111] compared the stability provided by two crossed screws and a blade plate inserted in foam tibial and talar specimens. Joint contours were flat cut. Rotation and bending forces (plantar flexion-dorsiflexion and eversion-inversion) were applied on the talus, while the tibia was fixed. Two crossed screws were more stable in dorsiflexion and inversion, whereas no differences were found in the other load cases. Lauge-Pedersen et al.[86] tested the strength and stiffness of simplified ankle arthrodeses using foam blocks, comparing the same two

surface preparation techniques as tested by Miller et al.[103]. They wanted to investigate the benefits of preserving the subchondral bone and of producing interlocking geometries. Low-density foam was used to simulate rheumatoid cancellous bone. Four-point bending (plantar flexion) and torque (external rotation) tests were performed. The construct with curved joint contours and a layer of subchondral bone was found to be the most stable.

Comparisons between the results of all these studies are difficult due to the differences in study design, specimens used and arthrodesis techniques tested. Apart from differences in the surgical procedures, different portions of the tibia and talus were embedded or fixed to supports in different ways and mounted in different materials testing systems (Figure 4.1). Relative degrees of rotation and/or relative linear displacements produced by various torques and loads of different magnitudes were measured (Table 4.1). Moreover, their findings referred either to the stiffness of the entire construct or to the gross relative movements between the tibia and the talus. The experimental set-ups made it impossible to determine what level of stability was due to the elastic deformation of the entire constructs and what was due to the amount of motion at the fusion site. Therefore, only limited information can be obtained from these biomechanical studies, especially considering that the relevance of the bone interface motions in the fusion process has not been addressed.

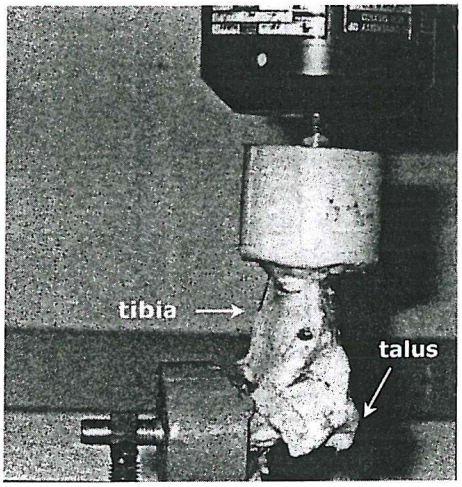

Figure 4.1 Ankle arthrodesis construct mounted in a materials testing machine (*from Miller et al.[103]*).

The experimental measurement of relative motion at contact interfaces is certainly challenging. Different techniques have been used to estimate the initial stability of joint prostheses, measuring relative motions between the implant and the host bone. For instance, Claes et al.[21] and Monti et al.[106] used displacement transducers (LVDT) attached to the bone and the implant and measured the relative motion between points that were close to the interface. Still, since neither the implant nor the bone are rigid, some of that motion might have resulted from the deformation of the materials. No such techniques have been used so far to try and estimate relative motions at the interface between two fragments of cancellous bone, as would be necessary to assess the stability of ankle arthrodesis constructs.

Table 4.1 Load cases used in biomechanical studies of ankle arthrodesis stability.

Study	Torsion (N·m)	Bending (N·m)	P-A force (N)
Pillete et al[126]	15 *(talus IR)*	150 *(DF)* *	500
Thordarson et al[161]	8 *(tibial IR-ER)*	8 *(PF-DF)* 8 *(M-L)*	-
Thordarson et al[160]	4 *(tibial IR-ER)*	4 *(PF-DF)* 4 *(M-L)*	-
Ogilvie-Harris et al[119]	10	-	-
Friedman et al[46]	5 *(tibial IR-ER)*	3.49 *(PF-DF)* † 3.49 *(M-L)* †	-
Miller et al[103]	2.8 *(IR-ER)* ‡	1.40 *(PF-DF)*	-

IR=internal rotation, ER=external rotation, PF=plantar flexion, DF=dorsiflexion, M-L=medial-lateral bending, P-A= posterior-anterior force. * Linear force applied to simulate ankle dorsiflexion. † mm of displacement applied to simulate plantar flexion-dorsiflexion and medial-lateral bending. ‡ Cyclic loading: 2Hz, 5000 cycles.

4.2.2 Computational methods

Mathematical models are a complementary option to *in vitro* experimental models studied in orthopaedic biomechanics. Variables of interest that are difficult or impossible to measure experimentally can be predicted from adequate models. The improvement of numerical simulation techniques and the latest available hardware and software packages allow refined numerical models of sufficient detail and complexity so as to be an acceptable approach to different orthopaedic issues and a complement to both clinical and biomechanical data. This is the case of the Finite Element (FE) method, briefly described below.

4.2.2.1 Finite element method: brief description

The mathematical formulation of a physical process leads to a set of differential equations and boundary conditions relating the quantities that characterise it. This mathematical model can be evaluated using computed-assisted numerical methods in

order to estimate these characteristics of the physical process. As the exact solution of the governing equations is often an enormous task and not always possible, approximate methods of analysis are an alternative way to estimate solutions. This is the case of the *finite element method* (FEM).

In the FEM, the original complex domain of the physical problem being analysed is represented as a collection of simple discrete parts, the finite elements. The finite elements are connected to each other at points, called nodes. The method approximates the solution over each element, using approximation functions (often algebraic polynomials) in terms of the values of the solution at the nodes of the element. The approximation functions are usually derived using interpolating concepts, their degree depending upon the number of nodes in the element and the order of the differential equation being solved. Based on the idea that the solution is continuous at the element boundaries, the method assembles all the element equations imposing the interelement continuity and balance of the interelement forces. It then applies the boundary and initial conditions and solves the resulting algebraic equations for the values of the solution at the nodes.

In the case of mechanical analysis, the forces and displacements at the nodes of an element are related by the local stiffness matrix of the element. A global stiffness matrix ([K]) is assembled considering the continuity at the nodes connecting the elements, so that all the nodal forces ({F}) and nodal displacements ({u}) are related: $\{F\} = [K]\{u\}$. Once the balance of the forces at the nodes has been considered and the boundary conditions applied to the previous equation, it can be solved for the unknown nodal displacements. Strain values can be derived from the nodal displacements and so can stresses, by using the material constitutive equations.

4.2.2.2 Finite element method in orthopaedic biomechanics

Since the early 1970s, FE models have been used in orthopaedic biomechanics to assess the mechanical behaviour of different human tissues and structures. Areas investigated with the FE method include musculoskeletal structures; tissue growth, adaptation and degeneration; and design, testing and optimisation of orthopaedic devices [62,129].

A necessary balance has to be met between the level of complexity required to replicate the real physical structure or process, and the simplicity required for the models to be solved. With the continuous improvement of modelling and computational capabilities, more and more sophisticated models can be built, eliminating some

simplifications once considered necessary. As part of the inherent complexity of analysing living structures, determination of realistic boundary conditions is one of the main problems of using FE models in orthopaedic biomechanics. Although more complex load cases have been introduced since the early models, accurate data of *in vivo* loads are still scarce. Also, more precise geometric representations and improved definitions of the material and interface properties are being constantly researched. Direct validation of the predictions of FE models against experiments is not always possible in orthopaedic biomechanics. Indirect validation against clinical and experimental studies is accepted when they produce the same conclusions. For all this, the quantitative accuracy of FE results remains limited and, therefore, for the moment, FE analysis is mostly used in orthopaedic biomechanics as a qualitative tool in all sorts of comparative and parametric studies.

4.2.2.3 Finite element method and stability of arthrodesis

FE models have been used to predict the initial stability of total joint replacements [153,162,167], measuring the micromotions at the bone/implant interfaces. Others have used FE models to study the stability of fracture fixation with different orthopaedic devices [48,137]. However, FE analyses of arthrodesis are not common. Only spinal fusion studies have used FE models to predict the initial stability of spinal arthrodesis constructs [76,113,127]. The models presented different levels of complexity, usually representing a section of the spine (two or more vertebrae) and including some soft tissues, such as articular cartilage, intervertebral discs and ligaments. Plates, screws, interbody cages and bone graft were some of the complex fusion techniques simulated; usual load cases included spine flexion-extension, axial torsion and lateral bending. In most of the cases, either variations of the stiffness of the spinal functional unit (vertebrae plus soft tissues) or the relative motions between the vertebrae were reported. Fusion interface stability was only addressed by Kim [76], in their FE study of the bone/interbody cage interfaces in fusion of a lumbar segment. They predicted the relative micromotions between the bone and the cage and reported the effects on them of friction coefficients, loading conditions and age-related material properties.

4.2.2.4 Objective of the thesis

In the search for the ankle arthrodesis technique that would best minimise the motion between the bone surfaces, thus increasing the chances of fusion, information regarding the mechanical benefits of different techniques and their variations would help the orthopaedic surgeon during the preoperative stage. As a complement to clinical and experimental approaches, the FE method has proved to be a successful qualitative tool in the assessment of similar issues in the areas of joint replacements, bone fracture fixation and spinal fusion.

The aim of this thesis is to compare the effect of variations in the arthrodesis technique on the initial stability at the fusion site. Following a well-known procedure in orthopaedics biomechanics, the FE method is used to assess the initial stability of ankle arthrodeses internally fixed with screws, which has been recommended as a standard method of fixation [1,78]. The specific objectives of this work can be summarised as follows:

- Determine the effect on the stability of the ankle arthrodesis construct of the joint surface preparation technique. To do so, two common techniques are compared: intact joint contours and flat resected surfaces.
- Assess the effect on the stability of the ankle arthrodesis construct of the screw configuration. Two and three screws are investigated in a number of clinically relevant positions and orientations.
- Assess the effect on the stability of the ankle arthrodesis constructs of the bone quality. Aged and pathological bone qualities are simulated as compared to normal bone.

Chapter 5

FINITE ELEMENT ANALYSIS OF ANKLE ARTHRODESIS: ASSESSMENT OF MODELLING PARAMETERS

A basic model of an ankle arthrodesis construct was initially defined and used to carry out mesh refinement tests and sensitivity analyses for different modelling parameters. The model was based on an ankle arthrodesis performed with two parallel cuts to the articular surfaces and fixed with two crossed cancellous screws[†]. Variations of this construct will be described in subsequent chapters, although the same modelling procedure was followed.

5.1 FE ANALYSIS PROCEDURE

A detailed description of the steps followed during the FE analysis of the basic ankle arthrodesis construct follows, from the model definition to the processing of the results. Figure 5.1 displays a diagram of the general procedure used in all the FE analyses presented in chapters 6 to 8.

5.1.1 Extraction of bone geometries

Musculoskeletal structures generally have complex geometries. As a result, it is common practice for FE models to be constructed from computed tomography (CT) images of the bones or joints of interest. This approach is known as digital image-based finite element modelling. Appendix A provides some information about CT. The intact lower leg and foot of a healthy male was scanned, with the ankle in neutral position (source: Orthopaedic Department, Lund University, Sweden). The voxel size was 0.468x0.468 mm and the slice thickness was 1 mm. The slices were obtained every millimetre except at the proximal end of the tibia were the distance was gradually increased up to 5 mm (see Figure 5.2). Despite the ankle joint being formed by talus, tibia and fibula (Chapter 1, page 3), the fibula was not included in the model. The fact that several biomechanical studies of ankle arthrodesis stability did not include the fibula in the arthrodesis constructs tested (Chapter 4, page 47)[46,86,103,111] shows that the fibula is somewhat less important for the stability of the construct than the tibia and the talus. Dohm et al.[40] found that fixing the ankle joint only by using the fibula as strut graft provided 25% of the stability

[†] Cancellous screw is a type of orthopaedic screw designed with a deep thread to bite cancellous bone.

achieved using only two crossed screws through the ankle joint. Although the fibula used as a strut graft has been shown to add stability to fixation with two screws, especially when bone quality is poor [161], the small stability added in the case of good bone quality, raised the question of whether the use of the strut graft was justified. Therefore, given that adding the fibula, as well as the screws needed to fix it, to the FE model would increase the computational costs of the model and this is not likely to affect the comparative studies performed in this thesis, the fibula was not included in the model.

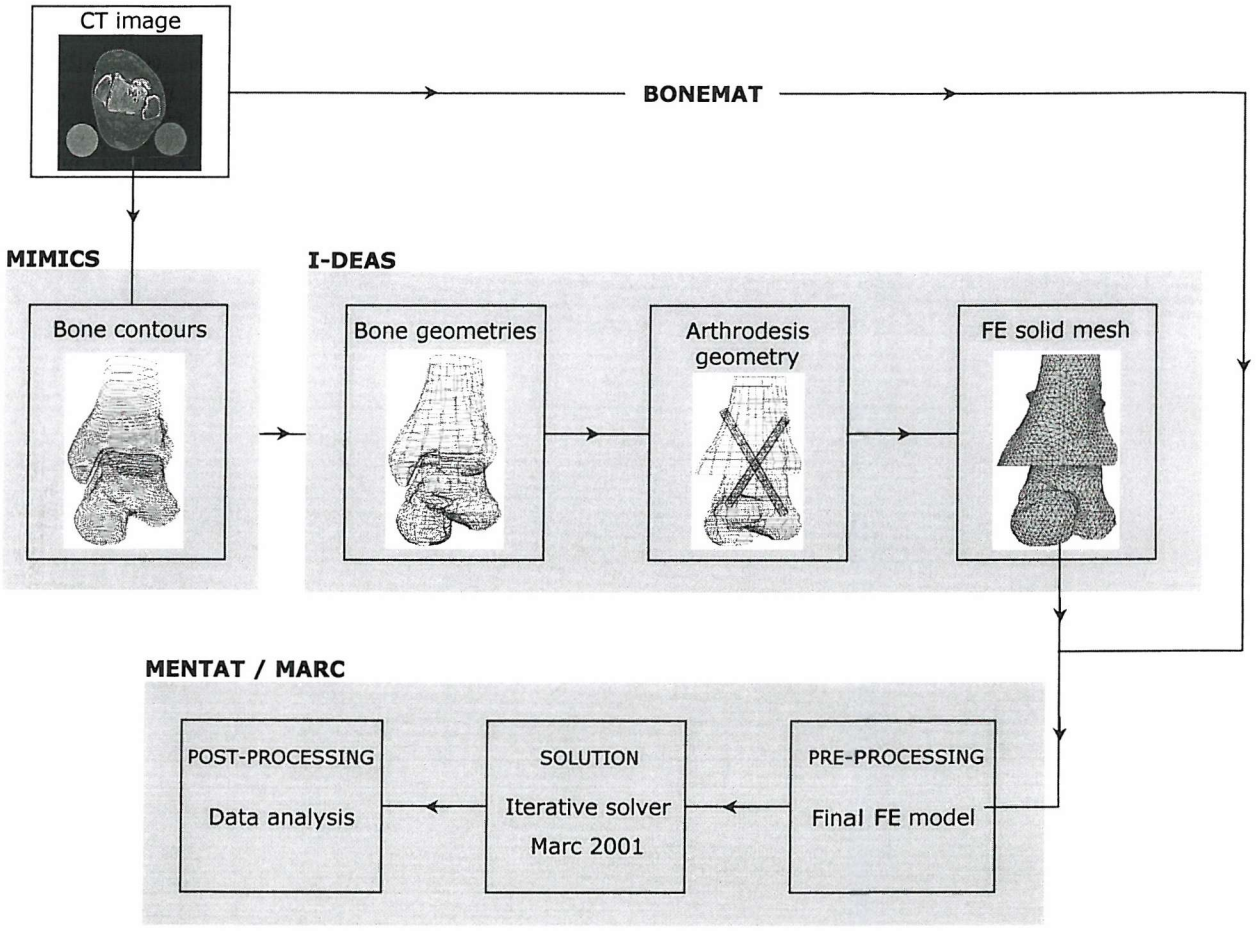

Figure 5.1 Stages of the FE analysis procedure followed to assess ankle arthrodesis with internal fixation.

Therefore, only the contours of the talus and the tibia were extracted from each CT slice in a software system for the visualisation and segmentation of medical images (MIMICS 6.1 -Materialise Software, Leuven, Belgium). The stacked set of curves representing the whole talus and approximately 7 cm of the distal tibia was used to generate three-dimensional (3D) representations of the two bones within I-DEAS (I-deas Master Series 7.0 -SDRC, Hitchin, UK), where subsequent geometric manipulations were carried out (Figure 5.2).

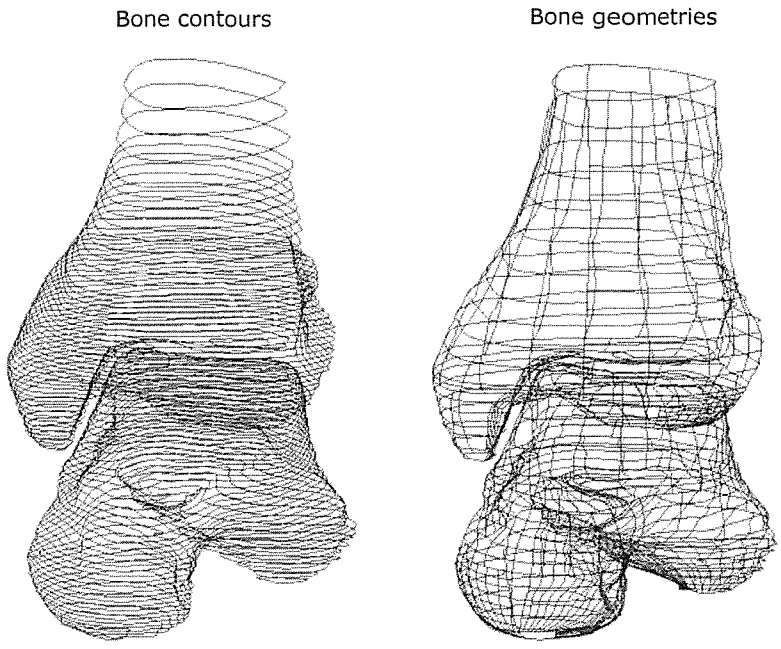

Figure 5.2 Frontal view of the stacked set of 2D bone contours obtained from the CT scan images (left) and the 3D solids generated from them (right).

Following common clinical procedures, two flat parallel cuts were made to remove the tibial plafond and the dome of the talus (Figure 5.3). The medial malleolus was also resected. The cut in the tibia was performed at about 1 mm above the articular surface and 4 mm of bone were resected from the top of the talar dome. Although the exact amount of bone resected differs in each patient, the values for this subject were considered clinically reasonable. The talus was then displaced upwards in the frontal plane until the two resected planes were coincident and, therefore, bone-on-bone contact was achieved.

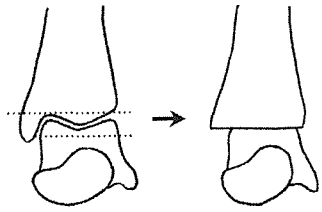

Figure 5.3 Flat parallel cuts performed on the tibia and the talus. Anterior view.

Two solid cylinders (diameter 4.5 mm) were created and crossed through the joint, from both sides of the tibia into the body of the talus, simulating 7.0 mm cancellous screws with a partial thread. The medial screw had a slightly postero-medial to antero-lateral direction. The lateral screw was placed anterior to the lateral malleolus, crossing behind the medial screw, in an antero-lateral to postero-medial direction. In the frontal plane, each screw formed a 30-degree angle with the longitudinal axis of the tibia (called the *insertion angle* henceforth). Also in the frontal plane, the two screws crossed each other approximately 5 mm beneath the flat bone-to-bone interface (fusion site). The final arthrodesis construct, including the resected bones and the screws (Figure 5.4), was assessed by an orthopaedic surgeon (Dr. Lauge-Pedersen, Orthopaedic Department, Lund University, Sweden) and deemed to be clinically satisfactory. Given the complex geometry of cancellous bone screws, they were modelled as simple cylinders and the head and thread were not explicitly modelled; however, their actions were considered. See section 5.1.4 (page 62) for a full description of the screw modelling.

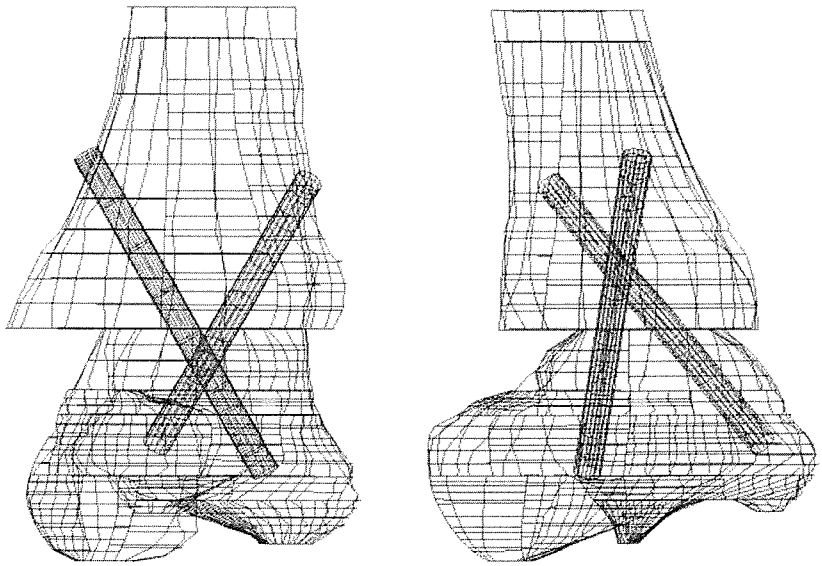

Figure 5.4 Anterior (left) and lateral (right) views of the final arthrodesis construct.

5.1.2 Meshing

The arthrodesis construct was meshed in I-DEAS. Initially, a surface mesh was defined using linear triangular elements. Solid meshes of linear tetrahedral elements were generated from the surface mesh for all the enclosed volumes (tibia, talus, medial screw and lateral screw) (Figure 5.5). The resulting tetrahedral elements on the model's surfaces shared the same nodes with the surface elements, which were later deleted. The size of the elements was determined by fixing an element edge length of 1.5 mm for all the contact interfaces and 2.5 mm for the rest of the surfaces. These values were chosen after a mesh refinement study was performed to assess the mesh (see section 5.2, page 68). The total number of tetrahedral elements was 48638. The arthrodesis construct mesh was then exported to Mentat, the pre- and post-processor of the FE software Marc 2001 (MSC Software, Camberley, U.K.), where the rest of the pre-processing was performed.

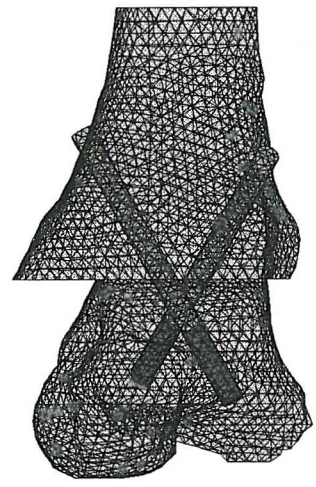

Figure 5.5 Anterior view of the FE solid mesh. The section of the cylinders equivalent to the screw thread is shown in black.

5.1.3 Material properties

The apparent density-dependent characterisation of bone material properties seems to be the most suitable way to consider their local variations and general distribution when building FE models of bony structures [170], despite the fact that it does not account for the effect of bone architecture and thus anisotropy (Chapter 2, page 24). The vast majority of the FE simulations present in the literature have assumed isotropic bone mechanical properties. Still, further research is needed to have a comprehensive apparent density-dependent characterisation of bone, as so far most of the data only concerns Young's modulus and compressive strength of cancellous and cortical bone.

Linear elastic material properties were used throughout the model. The Poisson's ratio for the bones and screws was assumed to be 0.3 [71]. The Young's modulus of the screws was assumed to be 200 GPa (stainless steel). A modified version of the freeware program Bonemat [173] was used to assign non-homogeneous Young's moduli to the bones.

Bonemat reads a CT data set and a FE mesh generated from it and assigns to each finite element the Young's modulus derived from the CT numbers at the element location. For each element of the mesh, the algorithm builds the smallest parallelepiped containing the element, with its faces parallel to the coordinate system of the CT data set. It considers all the voxels included in the parallelepiped to calculate an average CT number for the element. The input of a calibration relationship between the CT numbers and apparent density is needed to convert the mean CT number into the average bone apparent density for each element. An experimental relationship between apparent density and Young's modulus must be chosen and input to the program, so that for each element the mean apparent density value is converted into the mean Young's modulus. The original version of Bonemat, obtained from the authors at Laboratorio di Tecnologia Medica, Istituti Ortopedici Rizzoli (Bologna, Italy), was modified to read the mesh data in Marc's data file format and write a text file with the Young's modulus assigned to each element. This file was read by Marc at the beginning of each model solution to assign the bone material properties to the model.

5.1.3.1 Conversion from CT values to Young's moduli

As high correlation coefficients have been found for linear relationships between mineral-equivalent density measured using CT and bone apparent density [31,74], calibrated CT numbers are commonly used to obtain information about the apparent density of bone. Generally, different solutions of a bone mineral-equivalent substance (such as K_2HPO_4 or different calcium compounds) are scanned along with the patient so that a linear calibration equation between CT numbers and mineral-equivalent density can be established [74,152]. The lack of experimental data related to material properties of ankle bones, as well as the calibration information available for this work, led to the election of two calibration rods as phantoms, as previously done elsewhere [122]. The CT scan images used to generate the bone geometries contained two calibration rods of Plexiglas (118 kg m^{-3}) and acetal (331 kg m^{-3}). A calibration equation (Equation 1) was obtained taking into account the apparent density of the two rods; the average CT numbers measured for them; the null apparent density of air; and its correspondent average CT number obtained from various locations of the CT images:

$$\begin{aligned} \rho_{app} &= 1036 \cdot 10^{-4} \, (HU-126) + 118 \qquad \text{for } HU < 126 \\ \rho_{app} &= 977 \cdot 10^{-3} \, (HU-126) + 118 \qquad \text{for } HU \geq 126 \end{aligned} \qquad \text{(Equation 1)}$$

where ρ_{app} is the apparent density in kg m^{-3} and HU is the CT number in Hounsfield Units.

To convert apparent density into Young's modulus, two equations were taken from the literature and combined to obtain a continuous relationship:

$$E = 0.2\ \rho_{app}^{1.52} \quad \text{for } \rho_{app} < 476.7 \text{ kg m}^{-3} \quad \text{(Equation 2)}$$

$$E = -3842 + 13\ \rho_{app} \quad \text{for } \rho_{app} \geq 476.7 \text{ kg m}^{-3} \quad \text{(Equation 3)}$$

where ρ_{app} is the apparent density in kg m^{-3} and E is the Young's modulus in MPa. Equation 2, obtained by Destresse et al.[37] in their study of the material properties of the proximal and distal tibia (Chapter 2, page 33), was used for cancellous bone. It is the only experimental relationship of this type found describing cancellous bone properties of the ankle bones. Equation 3 was chosen to convert higher bone density values. It was obtained by Rho et al.[135] for the cortical bone of tibial diaphysis. For cortical bone of apparent density between 1800-2000 kg m^{-3}, the corresponding Young's modulus would vary from 20-22 GPa. In the case of cancellous bone, apparent densities of 400 and 100 kg m^{-3} would give Young's moduli of 1800 and 220 MPa respectively.

5.1.3.2 Assigned bone Young's moduli *versus* experimental data

The calibration equation and the apparent density-Young's modulus relationship described above were input in the modified version of Bonemat and the Young's moduli assigned to the finite elements of the tibia and the talus (Figure 5.6).

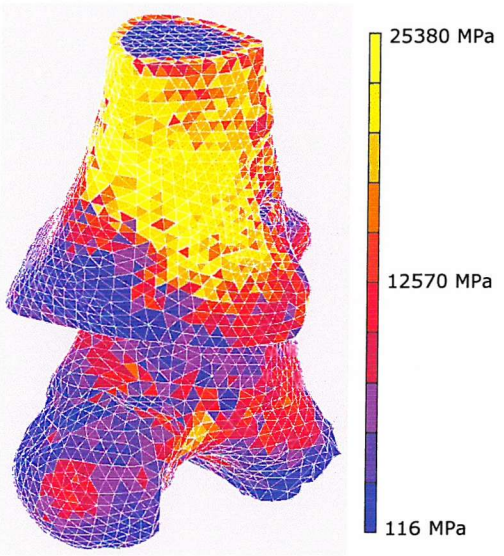

Figure 5.6 Young's modulus distribution in the tibia and the talus.

Checking the assigned values of bone apparent density, a distribution of higher values on the outer areas of the bones and much lower in the interior was obtained, as would be expected. Values ranged from approximately 80 to 2200 kg m^{-3} for the tibia and from 70 to 1800 kg m^{-3} for the talus.

Cattaneo et al.[14] compared the distribution of bone density values when applying two different calibration equations. One equation was obtained using density values from water, air and Plexiglas, and the corresponding HU values retrieved from the CT. This equation extrapolated the calibration for the higher density range. The second equation combined calibration information found in the literature for cancellous and cortical bone separately. Although for density values in the range of cancellous bone both methods produced very similar density values, an overestimation was observed on the higher density range when using the single equation. In the current model, the calibration equation (Equation 1) had been obtained from known densities in the region of cancellous bone, so that the calibration for higher density values had to be extrapolated. Although less than 1% of the elements of the modelled tibia had apparent density above 2000 kgm^{-3} (all of them on the outer shell of the bone), there may be an overestimation of the higher values due to the calibration equation used. For instance, Snyder and Schneider [152] reported apparent density values for the cortical bone of the tibial diaphysis ranging from 1748 to 1952 kg m^{-3}. No data have been found regarding density values of the cortical shell of the talus. Although they may have also been overestimated, the maximum values assigned within the talus are in the range of density values reported for dense cortical bone (Chapter 2, page 18). No published apparent density values were available for the cancellous bone in the distal tibia or the talus to compare the assigned values to. However, the values assigned to the inner elements of both bones are in the range of reported values of cancellous bone density for other anatomical sites.

Concerning the Young's modulus, Snyder and Schneider [152] obtained values from 14.3 to 21.1 GPa for the tibial diaphysis cortical bone, and Rho et al.[134], for the same bone, reported average values of 18.6 GPa and 20.7 GPa, from mechanical and ultrasound tests respectively. In the current model, about 12% of the elements of the tibia had Young's modulus between 10 and 25.4 GPa, all of them on the outer shell and almost all in the diaphysis. Less then 1% had values above 22GPa. These peak values seemed considerably high, probably due to an overestimation of the apparent density. About 30% of the elements had values between 2 and 10 GPa, mainly located on the outer shell of the tibial epiphysis and towards the inside close to the resected articular surface. Again, this distribution agrees with the idea of a thin shell of less dense cortical bone around the diaphysis and dense trabecular bone near the articular surface (subchondral bone). The rest of the elements (about 60%) had values below 2 GPa, located in the inner areas of the tibia. These values are also in agreement with Destresse et al.[37], whose equation was

used to convert density to Young's modulus. They reported a range of values for the cancellous bone in distal tibia from 718 to 2057 MPa.

Jensen et al.[68] reported a maximum Young's modulus of 1224 MPa for the trabecular bone just underneath the superior articular surface of the talar dome. No data have been found with regard to the material properties of talar cortical bone. About 2% of the elements of the talus had a Young's modulus between 10 and 20 GPa, and they were all distributed on the outer shell of the talus. More than 50% of the elements had values below 2.5 GPa, most of them being located in the core of the bone.

In general, the distribution of Young's moduli in the two bones agrees with that of cortical and cancellous bone in long and short bones. Despite the good agreement with the scarce experimental data available, there is possibly an overestimation on the higher Young's modulus range. However, the percentage of elements presenting this overestimation is very small. Therefore, and for the purpose of the comparative analyses to be performed with the model, the distribution of material properties seems to be a reasonable approximation.

5.1.4 Boundary conditions

Different levels of simplification have been assumed in the literature with regard to modelling screws in FE studies of orthopaedic problems. Spears et al.[153] simulated the effect of the screws in acetabular cups only by specifying zero relative displacement between paired nodes, one element deep, on either side of the interface. Tissakht et al.[162], in a micromotion analysis of the fixation of the tibial component of a total knee replacement, modelled the screws as cylinders and the effect of the threads was simulated by considering the bone-screw interface to be perfectly bonded. In the contact analysis of a cervical spine plate, Villarraga et al.[168] also modelled the screws as cylinders directly connected to the bone. To simulate the fully threaded cortices, they included a layer of interfacial elements between the cylinder and the bone, with material properties intermediate to those of the screw and the bone. Hashemi & Shirazi-Adl [59] used results from previous experimental studies to model the screws in their FE analysis of tibial implants. Screws were represented as posts with a friction coefficient of 2.0 and an initial interference of 0.025. In effect, this means that the very high coefficient of friction will prevent sliding and the interference fit will limit the amount of opening at the interface. At low loads, this can be approximated by bonding the thread/bone interface. Therefore, in the current model, the screws were represented as cylinders. To simulate the effect of the screw head, nodes on the screws close to the proximal holes of the tibia were linked to

opposite nodes on the tibia by tying their degrees of freedom together. Bonded contact was defined between the distal 16 mm of each screw and the talus, to simulate the effect of the 16 mm thread.

The screw-bone system can fail in different ways, depending on a number of variables, such as screw dimensions, number of screws, screw orientation, type of bone, bone size and geometry and loading mode. Screw failure can happen due to overloading, fatigue or corrosion [164]. Screw cutting through the bone and thread stripping are a result of bone failure. Screw holding power (fixation strength) has traditionally been measured in pull-out or push-out tests of single screw-bone systems [16,109,158]. These tests addressed the bone failure by thread stripping, which can occur when a screw is over tightened or a large enough force acts along the longitudinal axis of the screw. Reported values of pullout strength vary widely due to differences in the screws and bone (or bone substitute) tested. For instance, Muller et al.[109] reported pull-out strengths between 2550 and 3550 N for 6.5 mm cancellous screws (30-mm thread length) inserted 30 mm in the calcaneus. Values around 1000 N were reported for the same type of screws but with a 16-mm thread length and inserted 16 mm in the calcaneus. Thompson et al.[158] used foam as cancellous bone substitute (mean Young's modulus around 115 MPa) to measure pull-out forces of several types of screws. Cancellous screws with a 16 mm thread length yielded values between 426 and 589 N. However, uniaxial pull-out tests are not enough for testing the fixation strength of bone screws as the screws could additionally be subjected to shearing and bending loads [67,109]. In ankle arthrodesis with screw fixation, the orientation of the screws and the bones and the loads acting upon the system are likely to produce shearing strain and stresses between the bones and the screws, in addition to screw pull-out forces. Given the relatively low magnitude of the loads used in the current work, and the fact that bone quality was good, thread stripping was not expected. Thus, rigid screw fixation in the bone was assumed.

Except for the bonded contact between talus and screw threads, all the contact interfaces were initially considered as frictionless. See section 5.1.5.1 (page 64) and section 5.3.2 (page 76) for more details about contact definitions in the model. A static load case was defined to simulate tibial torsion (Figure 5.7), the loading mode most likely to compromise the initial stability of ankle arthrodesis during the early post-operative period in a low leg cast [160]. Low leg casts do not seem to completely constrain torsional motion about the long axis of the tibia, allowing internal and external rotation. Therefore, in the model, internal and external torques of 10 Nm were generated by applying two opposite medio-lateral forces to a pair of nodes at the top of the tibia. The magnitude of the load applied was similar to those used in most of the biomechanical studies examining ankle arthrodesis stability (Chapter 4, page 47). Although in the case of very poor bone quality the magnitude of the load applied could exceed the ultimate strength of the bone,

it was considered appropriate as the model was built from a healthy ankle. During the early post-operative period, the patient is asked to avoid weight bearing on the affected ankle. Therefore, like Miller et al.[103], Friedman et al.[46] and Thordarson et al.[160], joint axial loading was not considered. The nodes at the inferior face of the talus were fixed. The loads applied to the top of the tibia were somewhat idealised and produced some artificial localized deformations and stress/strain concentrations. However, they were located far enough away from the area of interest, i.e. the fusion site.

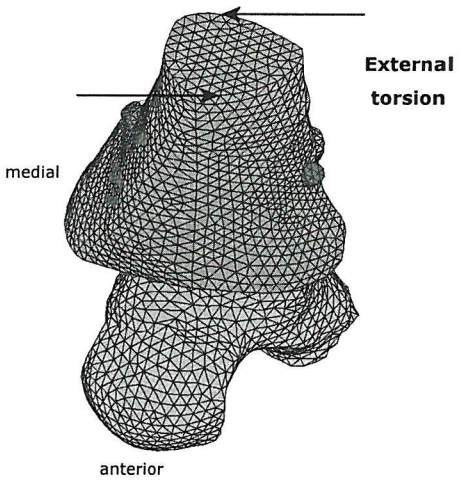

Figure 5.7 Load case considered in the analysis: torque to generate external tibial torsion (for internal tibial torsion, forces go in the opposite directions). Inferior face of talus fully constrained, not shown.

5.1.5 Solution

Marc 2001 (MSC Software, Camberley, U.K.) was used to solve the static non-linear FE problem described in the previous sections. Contact between the different bodies was the source of the non-linearity of the system. The solution was obtained using several increments: the external loads were applied in multiple steps, the results obtained in each step providing the initial conditions for the next step.

5.1.5.1 Contact in Marc 2001

A brief description of the way contact is simulated in Marc is given below. Please, refer to Marc's user Guide (MSC.Marc Volume A, Chapter 8) for more detailed information. Marc allows contact analysis to be performed automatically, without manually having to define

contact elements, by using the so-called direct constraint method. The motion of the bodies is tracked, a contact algorithm detects when contact occurs and, when it does, direct constraints are placed on their motion.

The tibia, the talus and the screws were defined as contact bodies. This meant that every node on an exterior surface was automatically treated as a potential contacting node; all element faces lying on the outer surface of the bodies were automatically considered as potential contact surfaces. A contact tolerance is associated with each potential contact surface, so that a node is considered to be in contact with a surface when it is within its contact tolerance. The size of the contact tolerance has a significant impact on the accuracy of the solution and the computational cost. An effective compromise between both is to bias the contact tolerance so that a smaller distance is considered towards the outside of the surface than towards the inside (Figure 5.8). The contact tolerance was set to 0.01 mm and the bias to 0.9. See section 5.3.2.1 (page 76) for details about the model sensitivity to these parameters.

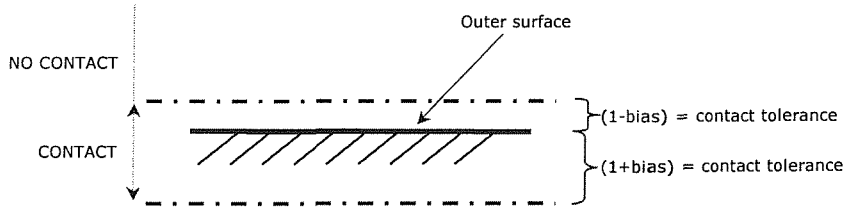

Figure 5.8 Contact tolerance associated with a potential contact surface.

If a tensile force occurs at a node that is in contact with a surface, the node separates from the surface. A threshold value for the separation force is needed to avoid unnecessary separations due to possible errors in equilibrium. A separation force of 0.01 N was chosen. See section 5.3.2.2 (page 77) for details about the model sensitivity to this parameter.

The constraint relationships placed between a contacting node and the nodes of the contacted element face use information regarding the normal to the surface. The normal is calculated based on the piecewise linear representation of the element face. This produces a discontinuity in the normal from one element face to another, leading to potential numerical problems. To improve this situation, a smooth surface (Coons surface) was automatically fitted through the outer elements of the contact bodies, giving a more accurate calculation of the normals.

5.1.6 Post-processing

5.1.6.1 Micromotions at the bone-to-bone interface

In order to assess the initial stability of the arthrodesis construct at the fusion site, the relative motion between the tibia and the talus at the contact interface was calculated. Pairs of nodes across the fusion site were identified, one node belonging to the tibia and the other to the talus. The relative displacements between these nodal pairs were calculated and the global magnitudes of these relative micromotions presented. The values from all the nodal pairs were bi-linearly interpolated to be displayed as contour bands over the contact interface of the talus. In addition, components of the global micromotions were calculated normal and tangential to the fusion site, in order to understand how the bone surfaces moved relative to each other. For this purpose, a local orthogonal coordinate system was defined, with the origin on the anterior edge of the resected plane of the talus, the x and y axes lying in this plane and the z axis perpendicular to it (Figure 5.9).

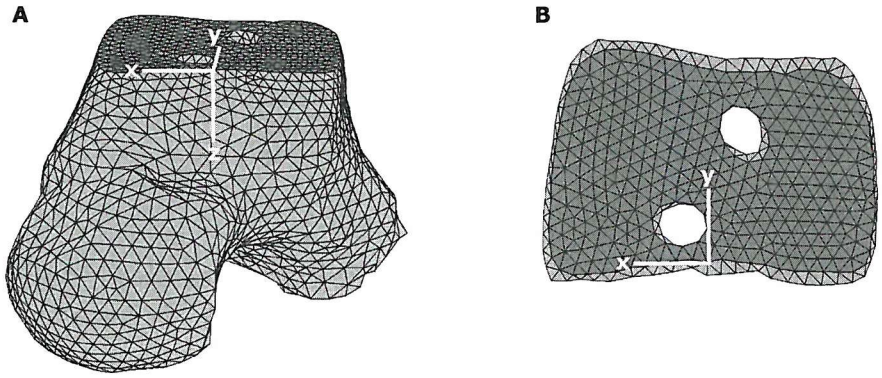

Figure 5.9 **A** Frontal view of the talus with the local coordinate system defined to calculate the micromotion components. Fusion site marked in dark grey. **B** Superior view of the fusion site, where micromotions will be displayed.

5.1.6.2 Strain

Because bone is a heterogeneous material, stress values are not enough to examine the possibility of bone failure. Due to the fact that cancellous bone strain can be considered to be isotropic and homogeneous, at least, at the same anatomical location, (Chapter 2, page 18), strain failure criteria have started to be used for assessing bone strength in FE models with heterogeneous material properties [150,159]. It has been shown

that strain contour plots provide better indicators of local bone fracture than do stress plots [150]. Therefore, strain values were examined in the tibia and the talus.

Equivalent elastic strain is a scalar value that represents an envelope of the normal and shear strain components:

$$\varepsilon_E = [\varepsilon_X^2 + \varepsilon_Y^2 + \varepsilon_Z^2 - \varepsilon_X\varepsilon_Y - \varepsilon_Y\varepsilon_Z - \varepsilon_Z\varepsilon_X + 0.75\,(\gamma_{XY}^2 + \gamma_{YZ}^2 + \gamma_{ZX}^2)]^{1/2}$$

where ε_X, ε_Y, ε_Z are the normal strains and γ_{XY}, γ_{YZ}, γ_{ZX} the shear strains. In the case of the linear tetrahedral element used in the model, strain is constant throughout the element. The strain values can be averaged between the elements at the nodes, so that continuous contour bands can be displayed and nodal strain values reported. The element equivalent elastic strain values will be reported here, unless otherwise stated. An assessment of the equivalent strain (ES) distributions and peak values was performed to, firstly, determine the areas of ES concentrations predicted in the different models studied and, secondly, determine where and in which models the risk of bone failure could be higher. Given the reported values of yield strain in human bone (Chapter 2, page 19), a value of 1% strain was chosen as a reference to compare to the predicted values of ES in the models. The peak equivalent strains produced at the top of the tibia as a result of the application of the loads were not considered in the ES assessment.

5.2 MESH ASSESSMENT

Mesh refinement was carried out to test the convergence of parameters of interest at the fusion site. Six FE models were generated from the model described in the previous section by varying the mesh density. Starting with an initial 2.5 mm element edge length in all the surfaces, consecutive refined meshes were created decreasing the element edge length at all the contact surfaces: interfaces between tibia and talus and between the bones and the screws. Table 5.1 shows the total number of tetrahedral elements and nodes in the models.

Table 5.1 Element size at the contact surfaces and total number of elements and nodes for the models included in the mesh refinement study.

Element size (mm)	Number of elements	Number of nodes
2.5	26497	6372
2.1	30944	7357
1.7	40294	9404
1.5	48638	11173
1.3	60849	13772
1.2	64583	14573

Material properties were assigned and boundary conditions defined as reported in the previous section. Only the external tibial torsion load case was studied. Micromotion at the fusion site is the main parameter of interest in this work. Therefore, convergence of the micromotion was examined. In order to compare the micromotions at the fusion site between the different mesh refinement levels, only the global magnitudes of the micromotions along the edge of the fusion site were analysed in each model. These micromotions, which were the maximum micromotions predicted at the fusion site, are displayed in Figure 5.10. Perillo-Marcone et al.[122] concluded that unless there is convergence in the Young's modulus distribution, convergence of the stress field or of other parameters of interest will not occur. In order to check this finding in the current study, convergence of the Young's modulus and convergence of the equivalent strain were also examined (Figure 5.11 and Figure 5.12). Nodal values of both parameters are examined along the edge of the fusion site in the talus (shown in Figure 5.10).

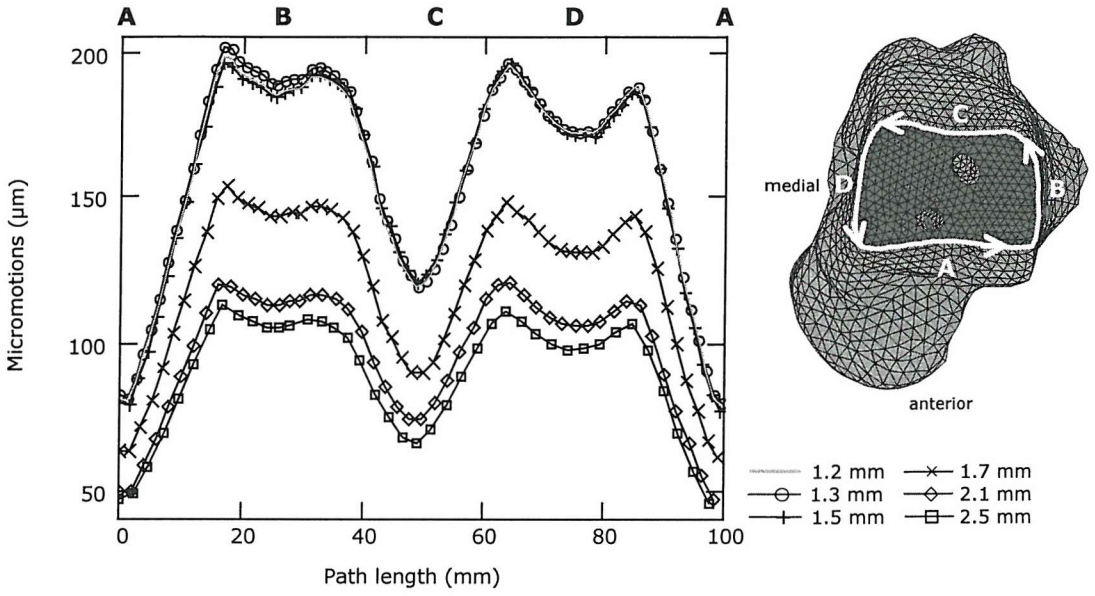

Figure 5.10 Micromotions predicted along the edge of the fusion site for each level of mesh refinement. The path and direction followed are shown on the right superimposed on the talus (superior view).

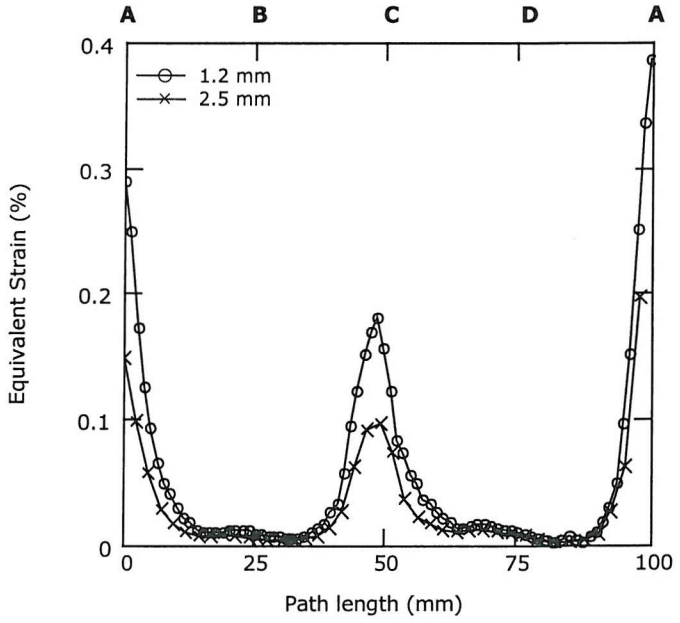

Figure 5.11 Nodal equivalent strain along the edge of the fusion site for the finest (1.2 mm) and the coarsest (2.5 mm) meshes.

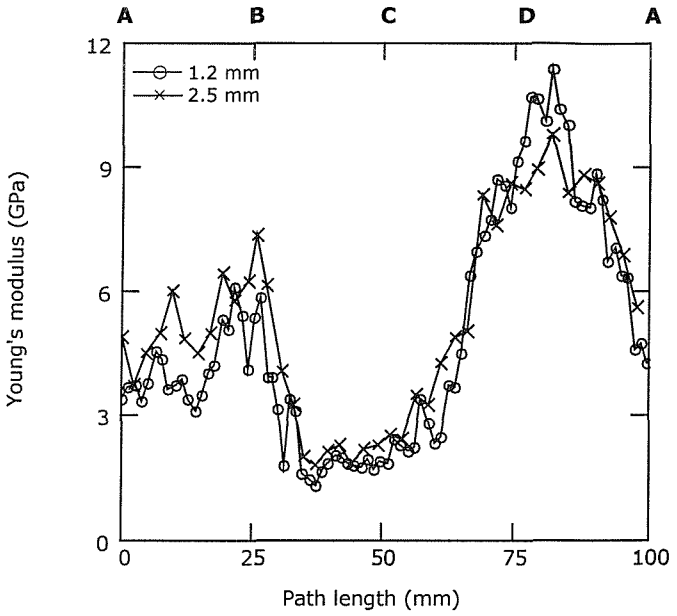

Figure 5.12 Nodal Young's modulus along the edge of the fusion site for the finest (1.2 mm) and the coarsest (2.5 mm) meshes.

The nodal pairs analysed varied in number and position along the edge of the fusion site between models. For each parameter examined, a cubic spline was generated based on the values predicted at the nodal pairs of the finest mesh (1.2 mm) and used as a reference. The differences between the values at each nodal pair and the value obtained from evaluating the spline at the same location were calculated for each of the other models. Linear regression analyses were used to evaluate these differences (Figure 5.13). Correlation coefficients, slope of the regression lines and mean errors were used to measure the degree of convergence in the three variables. Mean residual error (MRE) was calculated as the mean distance from the data points to the regression line, and mean percentage error (MPE) was calculated as the mean percentage of the distance from the data points to the regression line. The results are summarised in Table 5.2 (page 72).

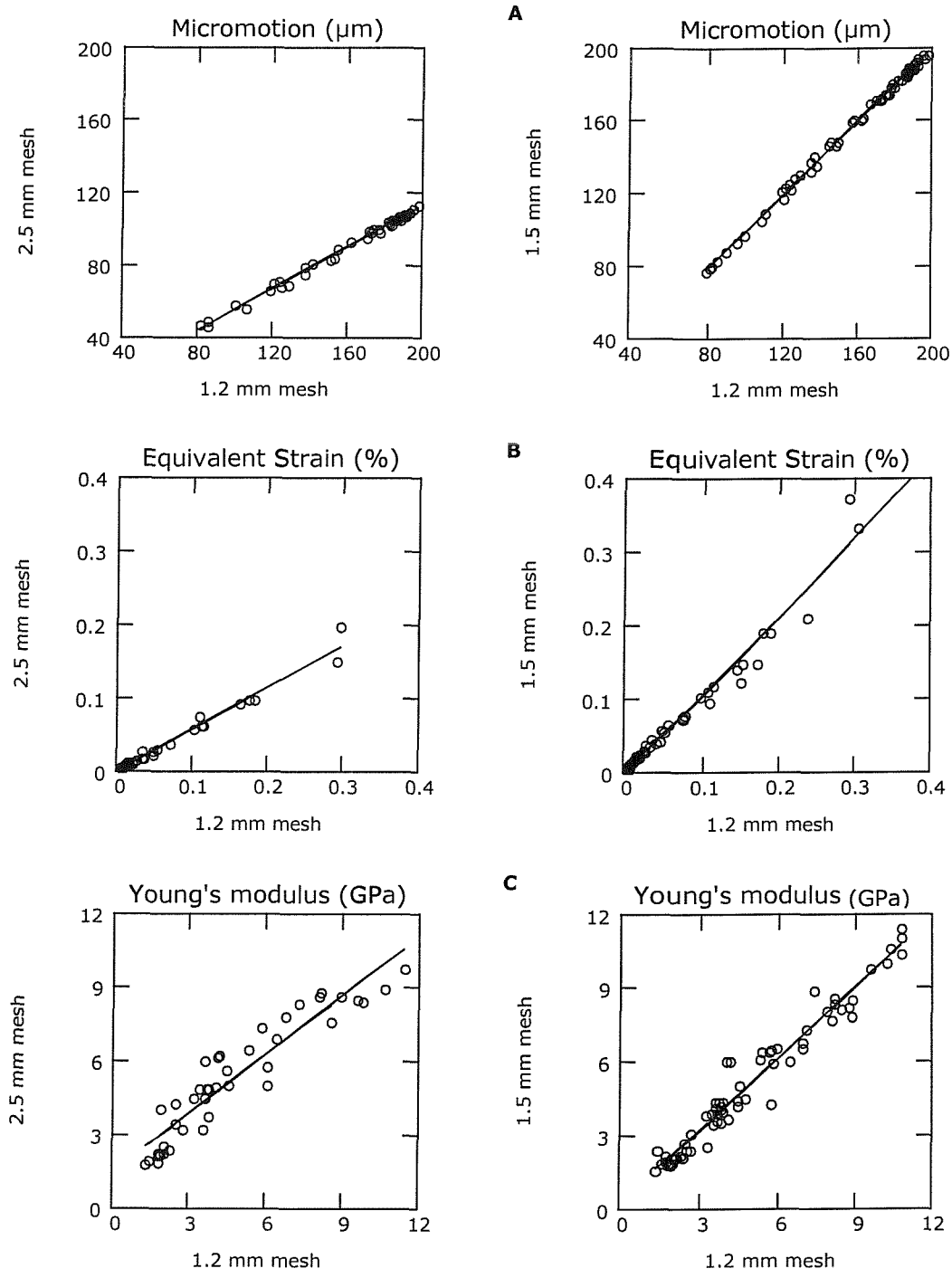

Figure 5.13 Regression lines for the 2.5 mm and the 1.5 mm meshes with respect to the 1.2 mm mesh. Differences along the edge of the fusion site in **A** Micromotion, **B** Equivalent strain and **C** Young's modulus.

Table 5.2 Correlation coefficient (r), slope of regression line, mean residual error (MRE) and mean percentage error (MPE) for each mesh compared with the 1.2 mm mesh. **A** Micromotion, **B** Equivalent strain and **C** Young's modulus. The plots represent the mean residual error as a function of the element size.

A

Element size (mm)	r	slope	MRE (μm)	MPE (%)
2.5	0.9974	0.575	69.5	43.7
2.1	0.9973	0.626	61.7	39.0
1.7	0.9989	0.767	37.6	23.8
1.5	0.9988	1.009	0.4	0.3
1.3	0.9994	1.012	1.4	0.9

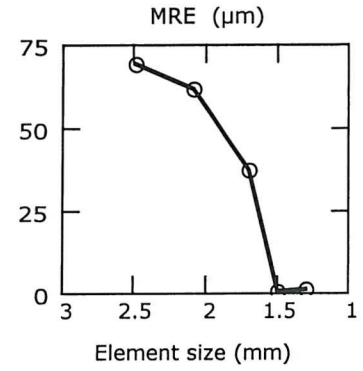

B

Element size (mm)	r	Slope	MRE (% strain)	MPE (%)
2.5	0.9898	0.575	0.0220	38.0
2.1	0.9847	0.774	0.0130	30.0
1.7	0.9821	0.805	0.0098	13.6
1.5	0.9903	1.073	0.0033	7.8
1.3	0.9911	1.065	0.0030	3.9

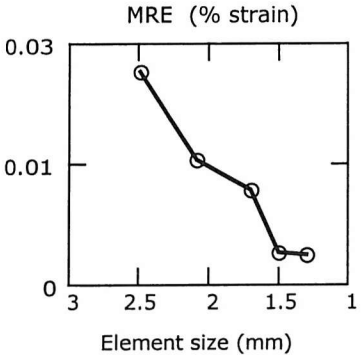

C

Element size (mm)	r	Slope	MRE (MPa)	MPE (%)
2.5	0.9364	0.796	694	26.01
2.1	0.9633	0.858	531	19.7
1.7	0.9822	0.944	336	11.9
1.5	0.9778	1.073	206	7.3
1.3	0.9797	1.005	208	5.8

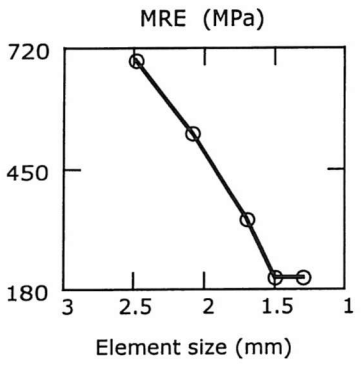

Very similar convergence behaviour was observed for the micromotions, the equivalent strain and the Young's modulus. High correlation coefficients (always higher than 0.93) showed a very good qualitative agreement between all the models, although in general, slightly higher values were obtained for the finer meshes. The degree of quantitative agreement between the models, measured by the slope of the regression line, showed a clear improvement for decreasing element sizes. For element sizes 1.5 mm and 1.3 mm, slopes were close to 1 in all the cases, whilst the coarsest mesh produced values around 0.6 for the micromotions and the equivalent strain. The Young's modulus showed slightly less variation in the slope, with values ranging from around 0.8 for the coarsest mesh to almost 1 for the finer meshes. The degree of uncertainty of the three parameters, assessed by both the MRE and the MPE, was also reduced for decreasing element sizes. Mean differences in micromotions were under 1% for the 1.5 mm mesh and below, whilst values reached over 40% for the coarsest mesh. Decreasing mesh density produced an increasing underestimation of the micromotions (Figure 5.10). Mean differences of less than 8% were predicted for both the equivalent strain and the Young's modulus for element sizes 1.5 mm and below. Maximum values of 38% and 26 % respectively were predicted for the coarsest mesh. Again, decreasing mesh density meant an increasing underestimation of the equivalent strain (Figure 5.11). In summary, a clear convergence of the micromotion, equivalent strain and Young's modulus was observed, with little sensitivity of these parameters to further mesh refinement below a 1.5 mm element size.

The mesh refinement was performed selectively rather than globally, by reducing the element size on the contact surfaces. In this way, a clear convergence was obtained whilst keeping manageable solution times. It has been shown in the literature that too coarse a mesh results in underestimations of strain and stresses, by failing to capture the material properties variations observed in bones [75,122]. The results obtained in the current study agreed with these findings. Figure 5.12 shows how the coarsest mesh did not manage to represent the Young's modulus variations that the finest mesh did account for. Given the degree of convergence shown by the tested meshes, further mesh refinement would seem unlikely to improve the results obtained when using the 1.5 mm mesh. In addition, much finer meshes could compromise the continuum assumption accepted in this FE model. Harrigan et al.[57] concluded that finite elements smaller than 3-5 times the micro-structural parameters would result in a break down of the continuum assumption. Therefore, considering the sizes of the trabeculae and trabecular spacing, elements should be at least 1-2 mm in size [122].

Given the results of this mesh refinement study, the FE model with the 1.5 mm mesh was chosen to carry out the following tests and any model generated henceforth will have a mesh density defined by choosing an element edge length of 1.5 mm on all the contact surfaces.

5.3 MODEL SENSITIVITY

The robustness of the model was checked by performing sensitivity analyses to certain modelling parameters. The FE model chosen in the mesh refinement study was used to perform the sensitivity analyses that follow, with the same material properties and boundary conditions.

5.3.1 Convergence tolerance

The convergence criterion determines when the current iteration predicts the state of equilibrium within a certain degree of approximation, and is defined by the convergence tolerance parameter. The convergence criterion used is based on the magnitude of the maximum residual load compared to the maximum reaction force:

$$\frac{|F_{residual}|_{max}}{|F_{reaction}|_{max}} < \text{tolerance}$$

where $|F_{residual}|_{max}$ and $|F_{reaction}|_{max}$ represent the highest absolute values of the residual and reaction forces respectively.

The values of the convergence tolerance were varied between 0.5 and 0.008. Differences in the micromotions measured along the edge of the fusion site were calculated, taking the case of the lowest convergence tolerance value as the reference. Mean and maximum errors are reported for relative and absolute values (Table 5.3 and Figure 5.14).

Decreasing the value of the convergence tolerance produced a general decrease in both the relative and absolute differences in micromotions with respect to the reference case. For a convergence tolerance of 0.015 and below, mean relative errors were close to 1%. A highest maximum error of 3% was measured for the highest value of the convergence tolerance. In terms of the absolute magnitude of these differences, all the models produced considerably small errors, with a highest of 5 μm for a 0.5 convergence tolerance. Mean absolute differences around 1.5 μm were found for convergence values from 0.015 and below. Several runs were attempted for convergence values lower than 0.008, but all failed to converge to a solution.

Table 5.3 Relative(*) and absolute changes in the micromotions along the edge of the fusion site for decreasing values of the convergence tolerance. The case with a convergence tolerance of 0.008 was taken as reference.

Convergence tolerance	Mean relative error (%)	[SD]	Max relative error (%)	Mean absolute error (μm)	[SD]	Max absolute error (μm)
0.5	2.1	[0.5]	3.0	3.0	[1.0]	5.0
0.1	1.9	[0.2]	2.3	3.1	[0.8]	4.1
0.05	1.8	[0.3]	2.4	2.9	[0.7]	3.8
0.015	1.0	[0.1]	1.3	1.6	[0.4]	2.1
0.01	0.9	[0.3]	1.5	1.5	[0.5]	2.1

* Relative errors are calculated as: 100 x |(Ref – Value)/Ref| , where "Ref" is the micromotion at a nodal pair in the model with the lowest convergence tolerance, and "Value" is the micromotion at the same nodal pair in any of the other models.

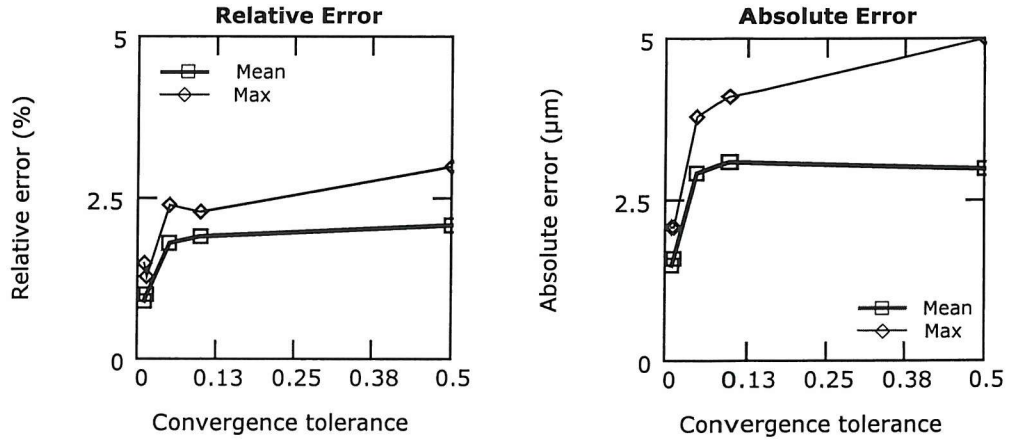

Figure 5.14 Mean and maximum errors as a function of the convergence tolerance.

In summary, the current model predictions of micromotions are quite stable for changes in the convergence tolerance. Nevertheless, and whenever possible, convergence tolerance values around 0.01 were used in the different models presented in the following chapters, in order to keep comparative analyses between them as consistent as possible.

5.3.2 Contact parameters

Most of the contact parameters are numerical parameters needed by the contact algorithm and do not have a physical meaning. In these cases, they cannot be measured experimentally and are therefore difficult to identify. Nevertheless, several exploratory runs were carried out, as has been recommended [7], to show the effect of these parameters in the most relevant variable being reported, i.e. micromotions at the fusion site.

5.3.2.1 Contact tolerance

For the contact tolerance, Marc recommends using a small number compared to the geometrical features of the model being analysed. As a guide, a value of 1/20 of the smallest element size is suggested. Considering the mesh in the current model, this recommendation would mean a contact tolerance just below 0.02 mm. As mentioned before, the size of the contact tolerance significantly affects the computational time and the accuracy of the solution. Too small a value could make detection of contact difficult and produce many cases of node penetration, therefore increasing the computational costs. Too big a value could cause premature contact, resulting in a loss of accuracy. The bias factor helps to find a good compromise. It must be a number between 0 and 1. A value of 0.9 was chosen and kept fixed while varying the contact tolerance between 0.02 and 0.0005 mm. Differences of micromotion between each model and that with the smallest contact tolerance were calculated along the edge of the fusion site. Table 5.4 and Figure 5.15 show the mean and maximum values of the relative and absolute errors.

A slight decrease of the relative errors was observed for decreasing values of the contact tolerance, except for the case of a 0.005 mm contact tolerance. In all the cases, the mean error values were under 1%. In fact, in terms of the absolute magnitudes of the errors when comparing all the cases with the reference, marginal differences were observed. This shows that little is achieved when decreasing the contact tolerance further from the value recommended by Marc. It should be noted that several attempts were made to check the sensitivity of the micromotions to higher values than 0.02 mm, but all failed. When decreasing the values of the contact tolerance below 0.01 mm, a progressive increase of the computational time was observed. Therefore, and to keep the number of changes to a minimum between models, a contact tolerance of 0.01 mm will be used in all the models presented henceforth.

Table 5.4 Relative and absolute changes in the micromotions along the edge of the fusion site for decreasing values of the contact tolerance. The case with a contact tolerance of 0.0005 mm was taken as reference.

Contact tolerance (mm)	Mean relative error (%) [SD]	Max relative error (%)	Mean absolute error (μm) [SD]	Max absolute error (μm)
0.02	0.7 [0.3]	1.2	0.4 [1.2]	2.3
0.01	0.4 [0.3]	0.9	-0.9 [0.9]	0.7
0.005	0.8 [0.2]	1.3	-1.3 [0.4]	-0.3
0.001	0.12 [0.05]	0.2	0.05 [0.2]	0.4

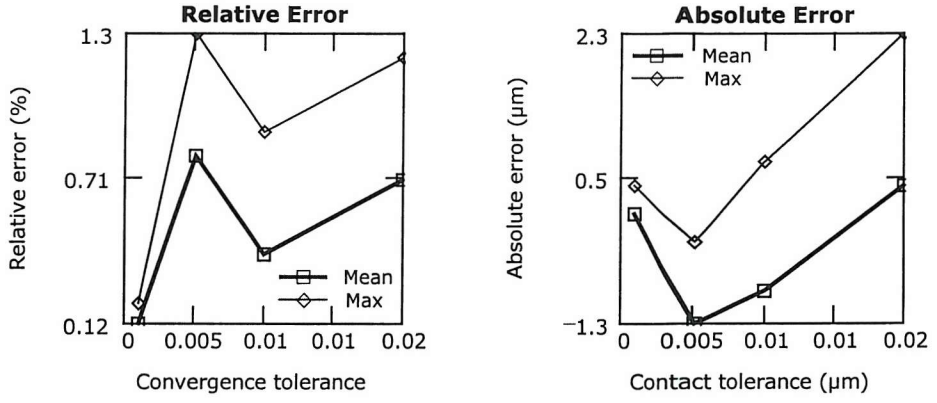

Figure 5.15 Mean and maximum errors as a function of the contact tolerance.

5.3.2.2 Separation force

On one hand, too small a value of the separation force parameter could result in many separations and contacts, increasing the computational costs. On the other hand, too large a value could result in unrealistic contact behaviour, despite reducing the computational time. The separation force values analysed ranged between 0.05 and 0.0001 N. The model with the lowest value was used as a reference to compare the micromotions along the edge of the fusion site. Table 5.5 and Figure 5.16 show the mean and maximum values of the relative and absolute errors.

Table 5.5 Relative and absolute changes in the micromotions along the edge of the fusion site for decreasing values of the separation force. The case with a 0.0001 N separation force was taken as reference.

Separation force (N)	Mean relative error (%) [SD]	Max relative error (%)	Mean absolute error (μm) [SD]	Max absolute error (μm)
0.05	2.4 [0.2]	2.8	3.8 [0.8]	4.9
0.01	1.3 [0.1]	1.6	2.0 [0.5]	2.7
0.005	0.3 [0.1]	0.5	0.5 [0.3]	1.0
0.001	0.6 [0.2]	0.8	0.9 [0.4]	1.5

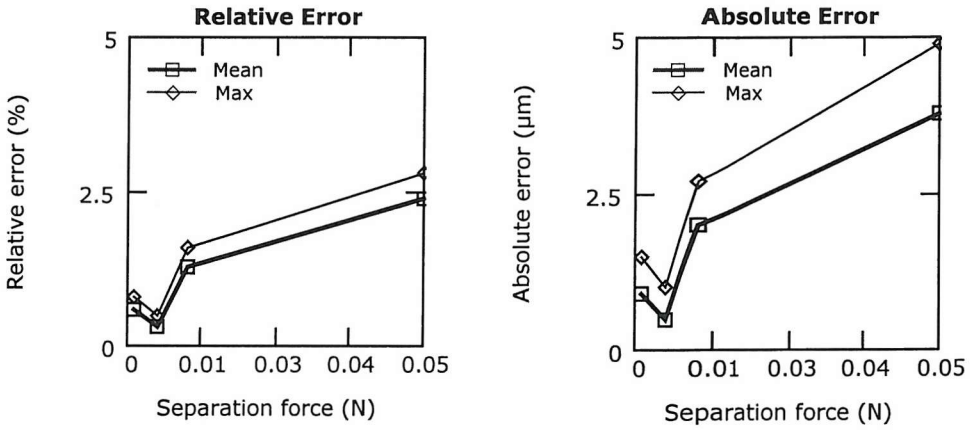

Figure 5.16 Mean and maximum errors as a function of the separation force.

Mean relative and absolute errors decreased when the separation force was between 0.05 and 0.005 N when compared to the reference case. This trend was somewhat broken by the 0.005 N separation force. However, the differences between cases were always relatively small; except for the case of 0.05 N of separation force, the rest of the cases showed mean relative errors close to 1% and below. For the absolute differences, the mean values ranged between 3.8 and 0.5 μm, whereas the highest maximum error was under 5 μm. These results also show the stability of the micromotions predicted by the current model for changes in the separation force. In order to keep the computational cost as low as possible, a value of 0.01 N was chosen for the separation force and will be used in all the models presented henceforth.

5.3.2.3 Friction coefficients

Unlike the previous contact parameters, the friction coefficients defined at contact interfaces have a physical meaning. Research has been carried out to experimentally determine friction coefficients relevant for FE modelling in orthopaedics [148,175]. In the current model, there are two types of contact interfaces to consider: cancellous bone-to-cancellous bone contact and cancellous bone-to-smooth stainless steel contact. No direct information about friction coefficients for tibia-talus and stainless steel-tibia or talus interfaces has been found. Zhang et al.[175] reported an average friction coefficient of bovine cancellous bone against bovine cortical bone of 0.61 ± 0.07. Shirazi-Adl et al.[148] obtained friction coefficients between 0.39 and 0.44 for human tibial cancellous bone against a smooth-surfaced stainless steel plate.

Three different contact situations were defined: a worst case of frictionless contact for the tibia-talus, tibia-screw shaft and talus-screw shaft interfaces (Case 1); and two friction contact cases using the Coulomb model implemented in Marc 2001. Given the value for cortical against cancellous bone reported by Zhang et al.[175], a friction coefficient of 0.7 was chosen for the tibia-talus contact (cancellous bone against cancellous bone). Considering the values reported by Shirazi-Adl et al.[148], a value of 0.4 was chosen for the friction coefficient between tibia or talus cancellous bone and the smooth surface of the screw shaft (stainless steel). These two values represent the Case 3. In order to check the sensitivity of the micromotions to the friction coefficients, a third case (Case 2) was defined by halving the values chosen for Case 3. Therefore, this intermediate case had friction coefficients of 0.35 and 0.2 for the tibia-talus and bone-screw contacts respectively. The frictionless case was taken as reference to compare the micromotions along the edge of the fusion site. Mean and absolute values of the relative and absolute errors were calculated and are shown in Table 5.6 and Figure 5.17.

As expected, including friction in the model produced a decrease of the micromotions at the fusion site. The higher the friction coefficients, the larger the decrease in the predicted micromotions. A mean relative difference in the predicted micromotions along the edge of the fusion site of 10% (with a maximum of 15%) was observed for the intermediate case, whereas 17% (with a maximum of 28%) was obtained for Case 3. In terms of absolute magnitude of the differences in the micromotions, the intermediate case produced mean and peak values of 15 and 19 μm respectively. These values increased up to 26 and 34 μm for the highest friction coefficients.

Table 5.6 Relative and absolute changes in the micromotions along the edge of the fusion site for decreasing values of the friction coefficients. The frictionless case was taken as reference.

Friction coefficients	Mean relative change (%) [SD]	Max relative change (%)	Mean absolute change (μm) [SD]	Max absolute change (μm)
Case 3	17 [3]	28	26 [5]	34
Case 2	10 [2]	15	15 [3]	19

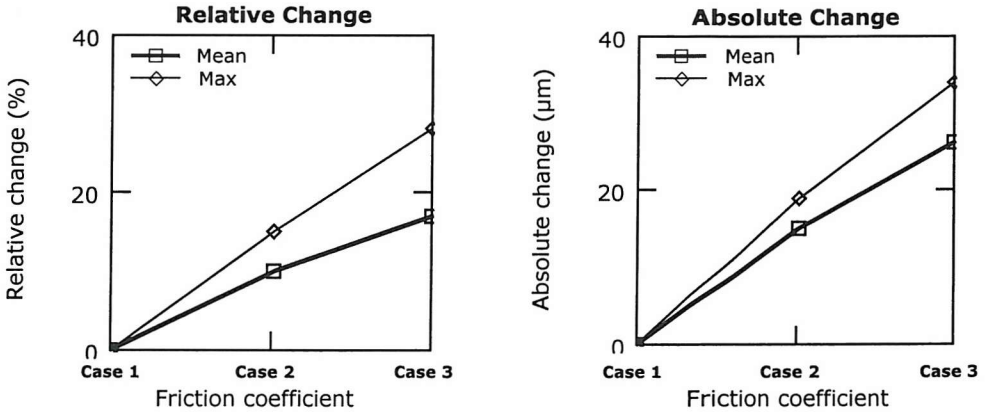

Figure 5.17 Mean and maximum changes in the micromotions as a function of the friction coefficient. Case 1 is the frictionless case taken as reference; Case 2 is the case with friction coefficients of 0.35 and 0.2; and Case 3 is the case with friction coefficients of 0.7 and 0.4 for the tibia-talus and bone-screw shaft interfaces, respectively.

Frictionless contact will be used in the models included in the comparative studies to be presented in the following chapters. Friction contact as defined in Case 3 will be used in some representative models, in order to check its effects on the results presented.

5.4 SUMMARY

A FE model of an ankle arthrodesis has been built and its robustness tested for different modelling parameters. A final mesh density has been chosen after a convergence of the relevant result variables was achieved. Convergence tolerance, contact tolerance and separation force values have been chosen, taking into account the results of the sensitivity analyses performed and the computational costs involved. These values will be kept constant in the models to be presented in the following chapters in order to minimise the effect of modelling changes between different cases, making the comparative analyses more consistent. Whenever any change was needed to achieve convergence to a solution, it will be mentioned, although given the stability of the reference model to these parameters, the changes are not likely to affect the results of the comparisons.

The FE method is used in this work as a comparative tool and, therefore, relative changes in the micromotions between cases will be reported and analysed. Given the results of the sensitivity analyses presented above, absolute differences in micromotions between cases below 5 μm will probably be not significant as they will be within the error of the model.

Chapter 6
COMPARISON OF TWO METHODS OF JOINT SURFACE PREPARATION

6.1 INTRODUCTION

Two crossed screws have been recommended as a standard method of fixation for ankle arthrodesis [1,78], at least when bone quality is not very poor. Usually, the two screws are inserted on either side of the distal tibia aimed towards the talus. A number of different screw orientations are found in the literature. However, no comparative analysis, either clinical or biomechanical, has been performed to check the effect of the location and orientation of the two screws on the initial stability of the arthrodesis construct.

In addition to the method of fixation, the geometry of the bone surfaces to be fused may also play a role in the initial stability of the arthrodesis construct. Open surgery and bone resections are necessary when high levels of bone and joint deformation are present in the ankle joint, although they are also used in less severe cases. A relatively easy way of obtaining a good area of contact between the tibia and the talus is by resecting the articular surfaces with two parallel cuts (see Figure 5.3, page 56), but this technique requires open surgery. There are other types of bone resections (see Figure 3.1, page 38), but they are more technically demanding. Bone resections involve removal of portions of bone that include the cortical and the subchondral bone, i.e. the stiffest bone. This may weaken the whole bone and affect the initial stability of the arthrodesis construct. However, trying to preserve the shape of the joint surfaces using open surgery and bone debridement is highly demanding. When deformation is not high, preserving joint contours through percutaneous techniques offers a less invasive alternative.

Two experimental studies have assessed the initial stability of ankle arthrodesis comparing the effect of the joint surface preparation. Miller et al.[103] studied cadaver ankle arthrodesis preserving the joint contours and resecting them with two parallel cuts (see Figure 4.1, page 49). Ankles with no apparent pathology were used and, therefore, normal bone quality was expected. Two crossed screws were used in all the cases, medial and laterally inserted at a 30-degree angle relative to the long axis of the tibia. They tested four pairs of constructs in internal/external torsion and dorsiflexion/plantar flexion with cyclic loading. They measured the gross motion between the tibia and the talus. The preserved joint contours produced slightly better stability than the flat cut. For instance, the mean torsional movement after cyclic loading increased 28% when the joint contours were flat cut compared to when left intact; the mean stiffness in dorsiflexion/plantar

flexion after the cyclic tests was 8% lower in the flat cut joint contours than in the preserved ones. However, no statistically significant differences were found between the two techniques. Lauge-Pedersen et al.[86] simulated ankle arthrodeses fixed with two crossed screws using blocks of a synthetic bone substitute (Sawbones, Malmö, Sweden). Twenty-four flat end constructs and twenty-four arch-shaped constructs were prepared, with and without a simulated layer of subchondral bone. They were tested to failure in four-point bending (simulating plantar flexion) and in external torsion. In the case of the torsion test, an axial pre-load of 300 N was also applied to the model, this being half body weight in a light rheumatoid patient. Poor bone quality was accounted for by using low-density sawbones. They measured the gross motion between the blocks and stiffness and strength of the constructs were determined. The most stable construct was that equivalent to an ankle arthrodesis with preserved joint contours. This construct was 1.1 and 1.5 times stiffer and 1.6 and 1.3 times stronger than the construct equivalent to the flat cut technique, in torsion and bending respectively.

A number of questions arise related to the screw configuration and the joint surface preparation technique. How does the screw orientation and location affect the initial stability at the arthrodesis site? How does the joint surface preparation technique affect it? Answers to these questions would provide the surgeon with useful pre-operative information to achieve the most stable ankle arthrodesis. In this chapter, FE analyses were performed to compare the initial stability at the fusion site of two methods of joint surface preparation: resecting the articular surfaces to produce flat mating surfaces and preserving the natural contours of the joint surfaces. In both cases, two screws were inserted medial and laterally in the tibia at different locations and orientations.

6.2 METHOD

The modelling procedure presented in Chapter 5 was followed to build the models in this study. The reference model initially built represented the ankle arthrodesis with the joint contours resected with two parallel cuts. An additional model was created by preserving the joint contours. Once the bone geometries were obtained, the two intact bones were put in contact by moving the talus upwards in the frontal plane. To obtain good bone apposition, the talus was then rotated into a slightly valgus position (2.7 degrees), still leaving the ankle within the limits of the recommended fusion position [1] (Figure 6.1).

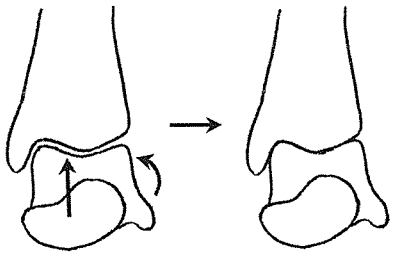

Figure 6.1 Displacement and rotation of the talus in the frontal plane to get good bone contact when preserving joint contours.

The two screws were inserted medial and laterally, as explained in Chapter 5 (page 57). The locations and lengths of these screws were varied to create different models for each type of joint surface preparation, keeping a constant thread length of 16 mm. Henceforth, the models will be referred to as members either of the "flat cut " group or the "intact" group. Two parameters were examined to account for different screw locations and orientations: the level the screws crossed relative to the fusion site and the insertion angle. Both parameters were measured in the frontal plane. The level of screw crossing was set at approximately +5, 0 and -5 mm relative to the fusion site, by moving the screws vertically in the frontal plane (Figure 6.2). The angle between each screw and the longitudinal axis of the tibia was set to 30, 45 and 60 degrees, by rotating the screws around an axis perpendicular to the frontal plane (Figure 6.2). Only those models considered as clinically viable were included in this study (see Table 6.1, page 86). The model with the screws at 45 degrees with the long axis of the tibia and crossed 5 mm above the level of the fusion site, as well as the models with the screws at 60 degrees and crossed approximately +5 and 0 mm relative to the fusion site, were rejected either because the screws crossed outside the fusion site or because they only achieved a very superficial purchase at the top of the body of the talus.

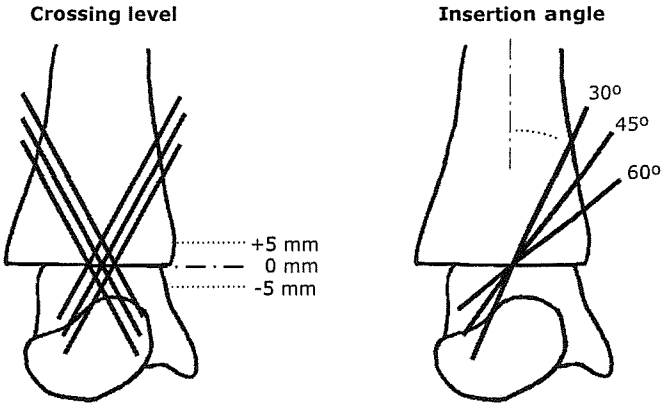

Figure 6.2 Screw configurations (frontal view).

First order tetrahedral meshes were defined as in Chapter 5. Figure 6.3 shows the FE meshes of the models included in each group. The total number of elements in each model ranged from 43102 to 50189 (Table 6.1). Two load cases were defined to compare the stability of the constructs: torsion and dorsiflexion (Figure 6.4, page 86). After torsion, plantar flexion-dorsiflexion motion is considered the next most likely to affect the ankle in the cast, due to compression of soft tissues or involuntary weight bearing [160]. The two load cases considered are equivalent to the rotational and dorsiflexion torque tested in some of the published biomechanical studies (Chapter 4, page 47). External and internal torsion were simulated by applying a 10 Nm torque at the top of the tibia. Posterior-anterior (PA) forces were applied to the nodes at the top of the tibia for a total of 200 N, equivalent to a dorsiflexion moment of approximately 10 Nm at the fusion site (Figure 6.4 B). As in the torsion case, the nodes at the inferior face of the talus were fixed.

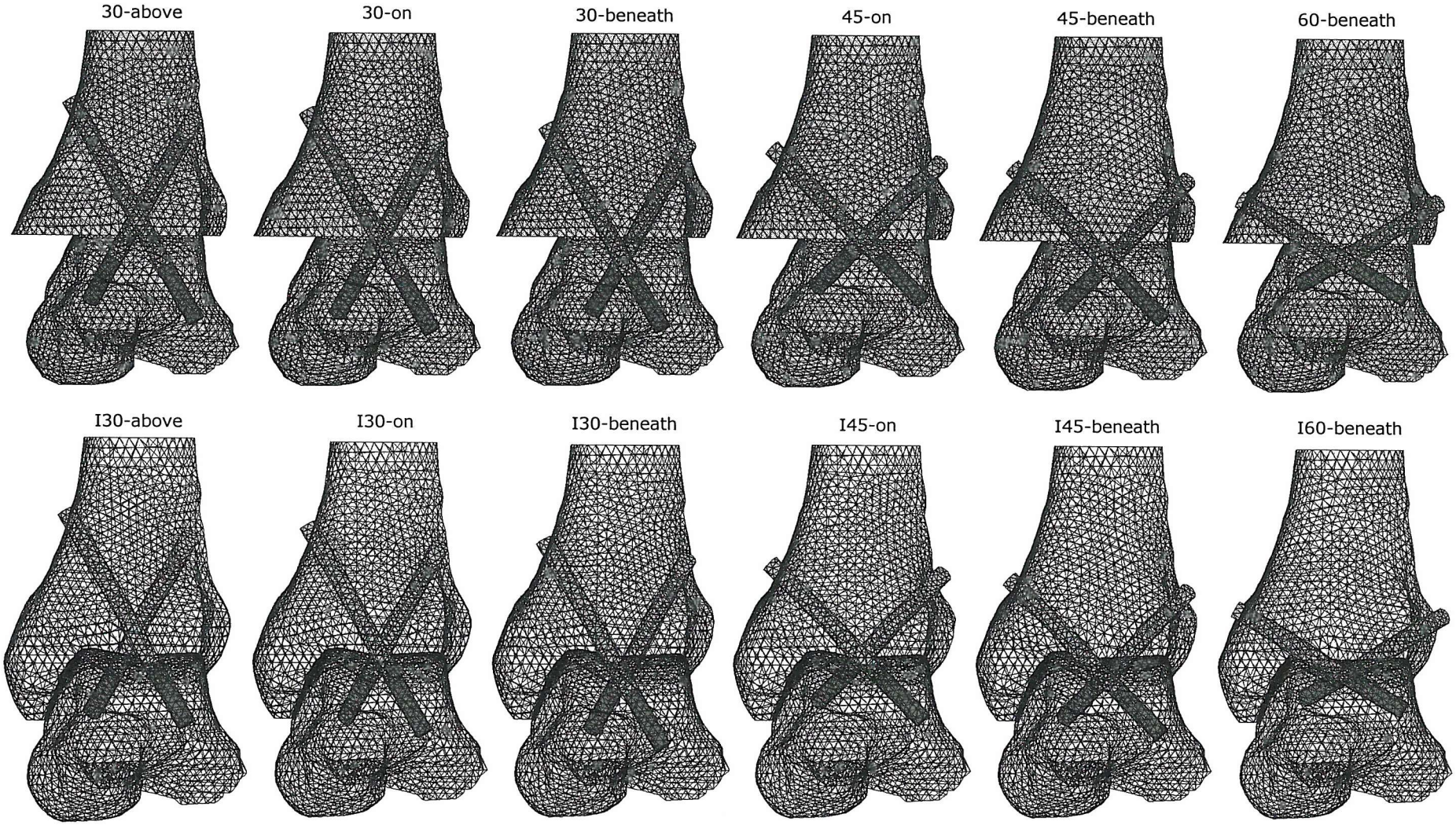

Figure 6.3 FE meshes of the arthrodesis constructs included in the flat cut group (above) and the intact group (below). Frontal view.

Table 6.1 Models included in the study. Screw configuration and number of finite elements.

Model	Screw length (mm)	Crossing level (mm)	Insertion angle (°)	Number of elements
Flat cut group				
30-above	65	+5	30	46005
30-on	65	0	30	47598
30-beneath	60	-5	30	48638
45-on	55	0	45	46209
45-beneath	55	-5	45	45095
60-beneath	50	-5	60	43102
Intact group				
I30-above	60	+5	30	47709
I30-on	60	0	30	48630
I30-beneath	60	-5	30	50189
I45-on	55	0	45	47867
I45-beneath	55	-5	45	47433
I60-beneath	50	-5	60	44733

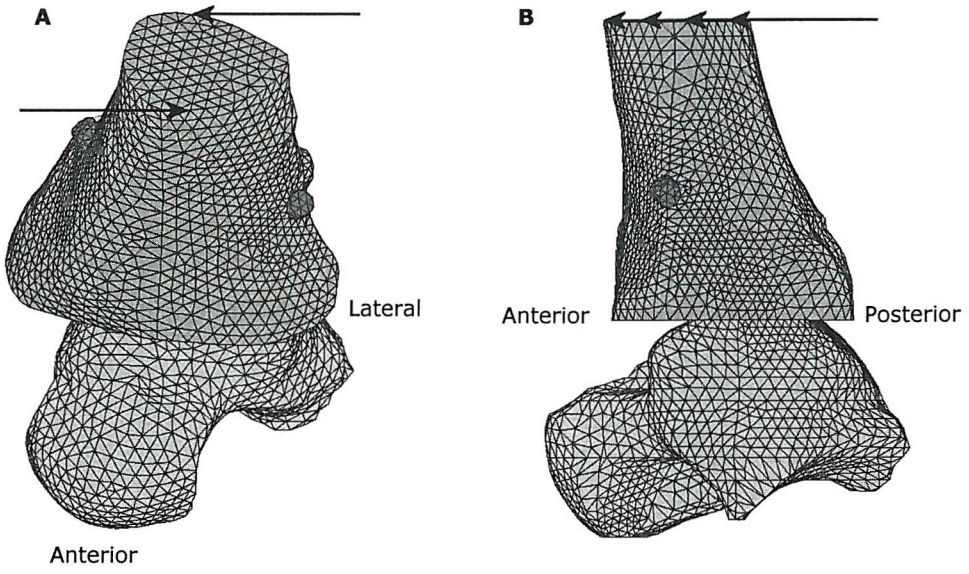

Figure 6.4 Load cases considered in the FE analysis (inferior face of talus fully constrained, not shown). **A** 10 Nm external tibial torsion; for internal tibial torsion, forces go in the opposite directions. **B** Posterior-anterior force equivalent to a 10 Nm dorsiflexion torque.

Initially, frictionless contact was considered in all the models. For a selection of models, the analyses were also performed including friction. A Coulomb friction model was used, assuming a friction coefficient of 0.7 for the bone-to-bone interface and a friction coefficient of 0.4 for the bone-screw interface (Chapter 5, page 79).

All models were run in Marc 2001, with the contact parameters and convergence tolerance values chosen in Chapter 5. In some cases, the convergence tolerance initially considered (0.01) had to be varied in order to reach a solution. The modified values ranged from 0.015 to 0.05, except for two cases where the value was 0.1 (see Table 6.2).

Table 6.2 Convergence tolerance values used in the models of the flat cut and intact groups, when different from 0.01.

Model	External torsion	Internal torsion	Dorsiflexion
30-above (F)	-	0.05	0.05
30-beneath	0.015	0.015	-
30-beneath (F)	0.02	-	0.05
45-on	-	-	0.1
45-on (F)	-	-	0.05
I30-above (F)	-	-	0.1
I30-on	-	0.015	-

F refers to the friction case.

The resultant micromotions at the fusion site were measured (Chapter 5, page 66) and compared between the models. In addition, components of the micromotions were calculated normal and tangential to the fusion interface, in order to observe how the bone surfaces were moving relatively to each other. For the flat cut group, a single orthogonal coordinate system was defined (Figure 5.9, page 66). For the intact group, various local orthogonal coordinate systems were defined across the fusion interface, with x and y axes tangential to the contact surface and z axes perpendicular to it at each location. Equivalent strains predicted by each model were also compared.

6.3 RESULTS

The micromotions at the fusion site are displayed over the contact interface of the talus for each model and for each load case. The peak micromotions at the fusion site and the equivalent strain are compared between the models.

6.3.1 Frictionless contact

6.3.1.1 Torsion test

Table 6.3 shows the peak micromotions predicted at the fusion site in external and internal torsion. Figure 6.5 and Figure 6.6 display the predicted micromotions over the contact interface of the talus. The majority of the models in the intact group produced lower peak micromotions than the equivalent models in the flat cut group. Resecting the articular surfaces resulted in peak micromotions between 18 and 77 % higher than those observed in the intact group. Two models, those with the screws crossed 5 mm beneath the fusion site, at 45 and 60 degrees, produced slightly lower peak micromotions for the flat cut technique, but only in the external torsion case. All the constructs in both groups were more stable in internal torsion, with peak micromotions from 1.2 to 1.9 times higher in external torsion. In all the cases, the peak micromotions were located at the periphery of the fusion site.

Table 6.3 Peak micromotions (μm) at the fusion site in external and internal torsion, for the intact and flat cut groups.

Screw configuration	External torsion			Internal torsion		
	Intact group	Flat cut group	%*	Intact group	Flat cut group	%*
30°/5 mm	87	146	**68**	70	104	**49**
30°/0 mm	115	177	**54**	74	131	**77**
30°/-5 mm	161	194	**21**	92	137	**49**
45°/0 mm	169	200	**18**	102	137	**34**
45°/-5 mm	179	159	**-11**	94	113	**20**
60°/-5 mm	168	150	**-11**	**	97	**

*Percentage of change relative to the intact group. ** Results not available.

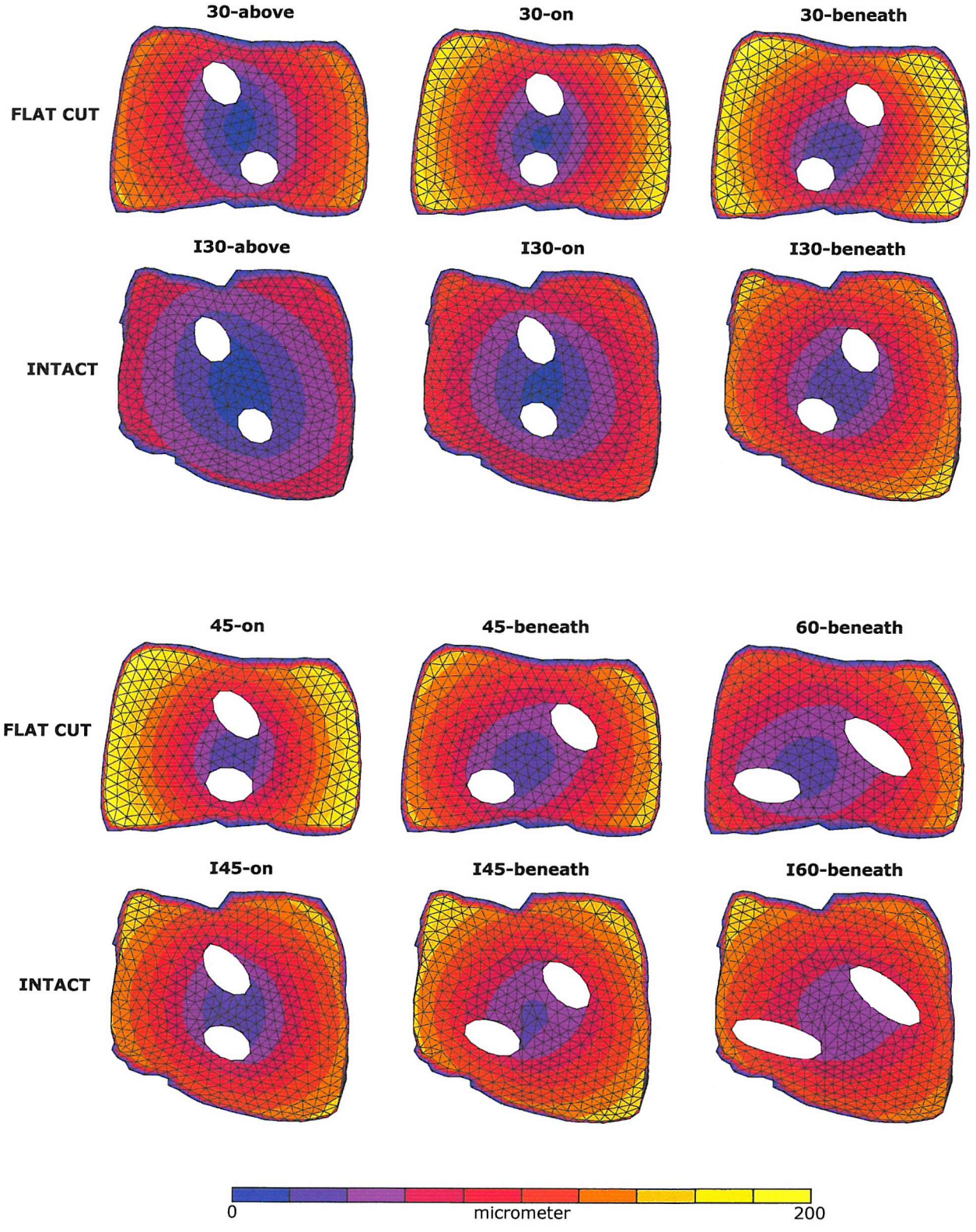

Figure 6.5 Micromotions at the fusion site in external torsion, displayed over the contact interface of the talus.

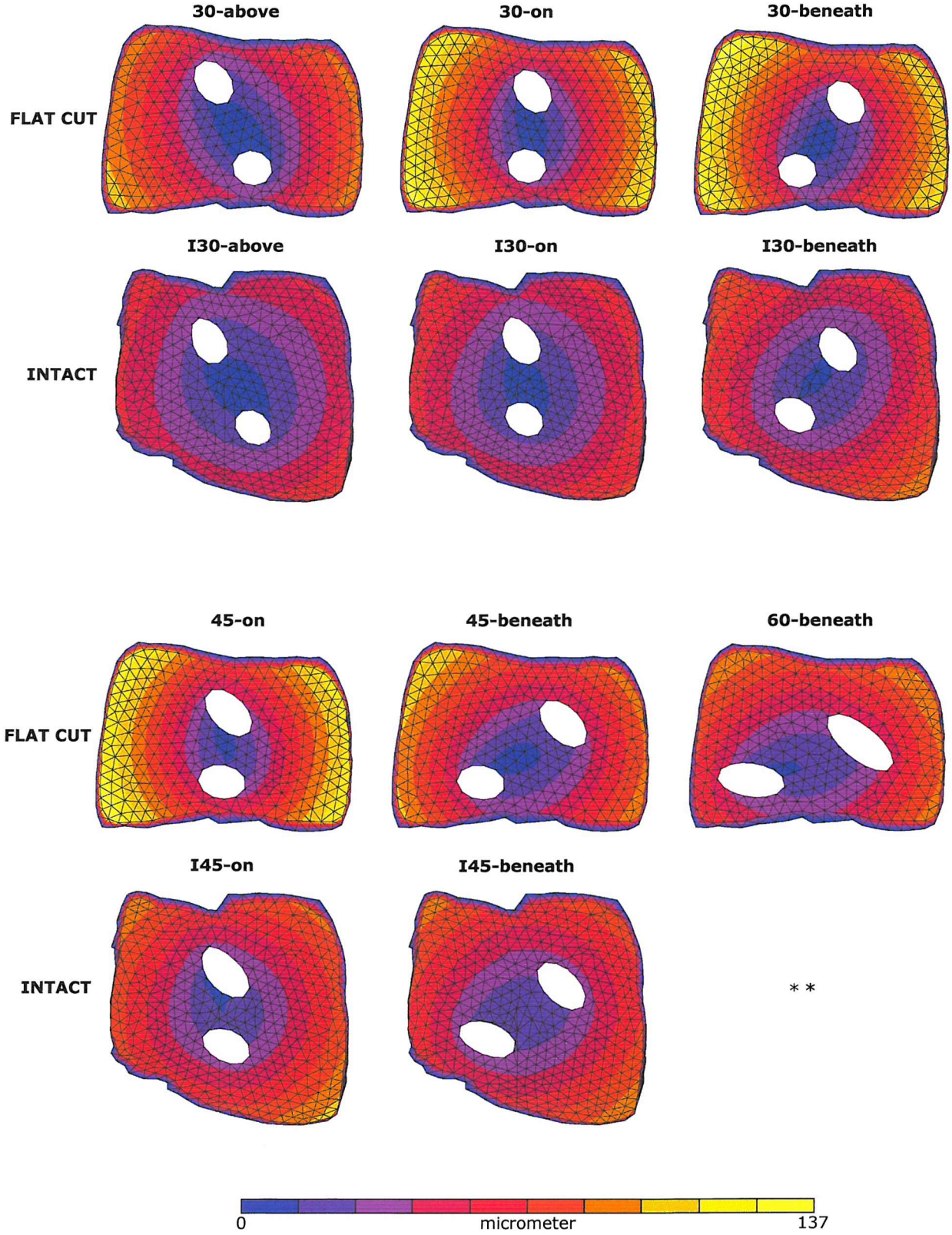

Figure 6.6 Micromotions at the fusion site in internal torsion, displayed over the contact interface of the talus. (* No results available).

Mixed results were noted when the screw configurations were compared. For all the constructs with the screws inserted at a 30-degree angle, it was found that the higher the screw crossing level, the lower the peak micromotions. This trend was reversed for all the constructs with a 45-degree insertion angle, except for the intact group in external torsion. In the intact group, the most stable constructs were I30-above and I30-on, with peak micromotions between 90-110 μm in external torsion and around 70 μm in internal torsion. In the flat cut group, the most stable constructs were 30-above and 60-beneath, with peak micromotions around 150 and 100 μm in external and internal torsion, respectively. The least stable constructs were those with the screws crossed at the level of the fusion site and inserted at 45 degrees (45-on and I45-on), except for the intact group in external torsion, where I45-beneath presented the highest peak micromotions. Maximum differences within the groups ranged from 1.3 to 2 times the peak micromotions predicted for the most stable constructs, with values reaching up to 200 and 140 μm in external and internal torsion, respectively.

With regard to the micromotion components (normal and tangential to the bone-to-bone interface) in the flat cut group in external torsion, most of the motion was due to sliding (tangential component). A small gap (normal component) developed at the interface, leaving small areas of contact between the two bones, mainly around the screws. The gap tended to be slightly smaller towards the antero-medial area of the fusion site, as can be seen in Figure 6.7. Along the edge of the fusion site, the normal component was, on average, between 15 and 39% of the tangential component. In internal torsion, the contact zones covered larger areas, especially along the lateral part of the fusion site, reducing to almost marginal the size of the gap in the rest of the interface (Figure 6.7). In this case, both micromotion components along the periphery were lower, but especially the normal component, with mean values ranging from 1 to 13% of the tangential component.

In the intact group, contact areas were observed in posterior-medial and anterior-lateral areas in external torsion, and in posterior-lateral and anterior-medial areas in internal torsion, with small gaps developing towards the opposite areas. Tangential components were also smaller in internal torsion than in external torsion. Normal components in the non-contact areas were similar to those in external torsion, with maximum values for the normal component along the periphery reaching over 60% of the peak tangential component.

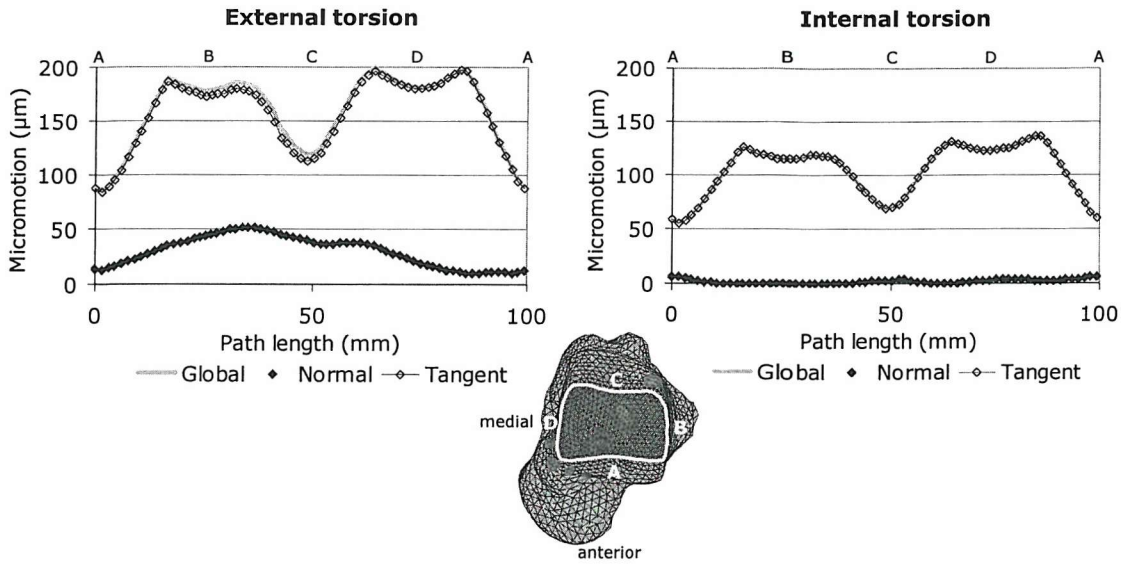

Figure 6.7 Micromotions, normal and tangent components, along the edge of the fusion site in a model from the flat cut group (45-on).

The patterns of equivalent strain (ES) distribution in the bones were similar for the models within each group, both in external and internal torsion. In all cases, areas of strain concentration were located around the screw holes at the fusion site in the talus and, in the tibia, around the screw holes at the fusion site and around the proximal holes. Additional areas were found depending on the group and the load case. In external torsion, areas of ES concentration were also found, in the intact group, in postero-medial and antero-lateral areas at the fusion site, both in the talus and the tibia. Figure 6.8 (page 94) shows the ES distributions predicted in one model of the intact group and the equivalent model in the flat cut group. In internal torsion, ES concentrations in the flat cut group were also found in antero-lateral areas at the fusion site in both bones. In the intact group, additional patches of ES concentration were found in antero-medial and postero-lateral areas, both in the talus and the tibia; and along the postero-medial edge of the fusion site in the talus.

Peak ES values are summarised in Table 6.4 and Table 6.5 (page 95) for the external and internal torsion, respectively. In the vast majority of the models, the tibia presented higher peak values than the talus. Peak ES values were located either around the proximal holes of the tibia or around the holes at the fusion site, except in the intact group in internal torsion, where they were located at the contact areas of the fusion site. Comparing the intact and flat cut groups, lower peak ES were generally predicted in the intact models than in the corresponding flat cut models in external torsion, following the same trend as the peak micromotions. Mixed results were observed in internal torsion, despite the clear

trend in the peak micromotions. Comparing the different screw configurations, peak values in the talus increased for decreasing levels of screw crossing and increasing insertion angles in both groups and load cases. Peak values in the tibia followed the same trend only in the models with the screws inserted at a 30-degree angle.

Taking a value of 1% as the yield strain for bone (Chapter 5, page 66) and comparing it with the values predicted in external and internal torsion, showed that in a number of models areas around the proximal holes of the tibia or around the screw holes at the fusion site would be failing. However a close examination of each model showed that the number of elements with ES above 1% was very small (up to seven elements in the worst case, accounting for less than 0.005% of the total bone volume), whereas the rest were below it. Isolated badly shaped elements may have produced the highest peak values predicted in some of these models.

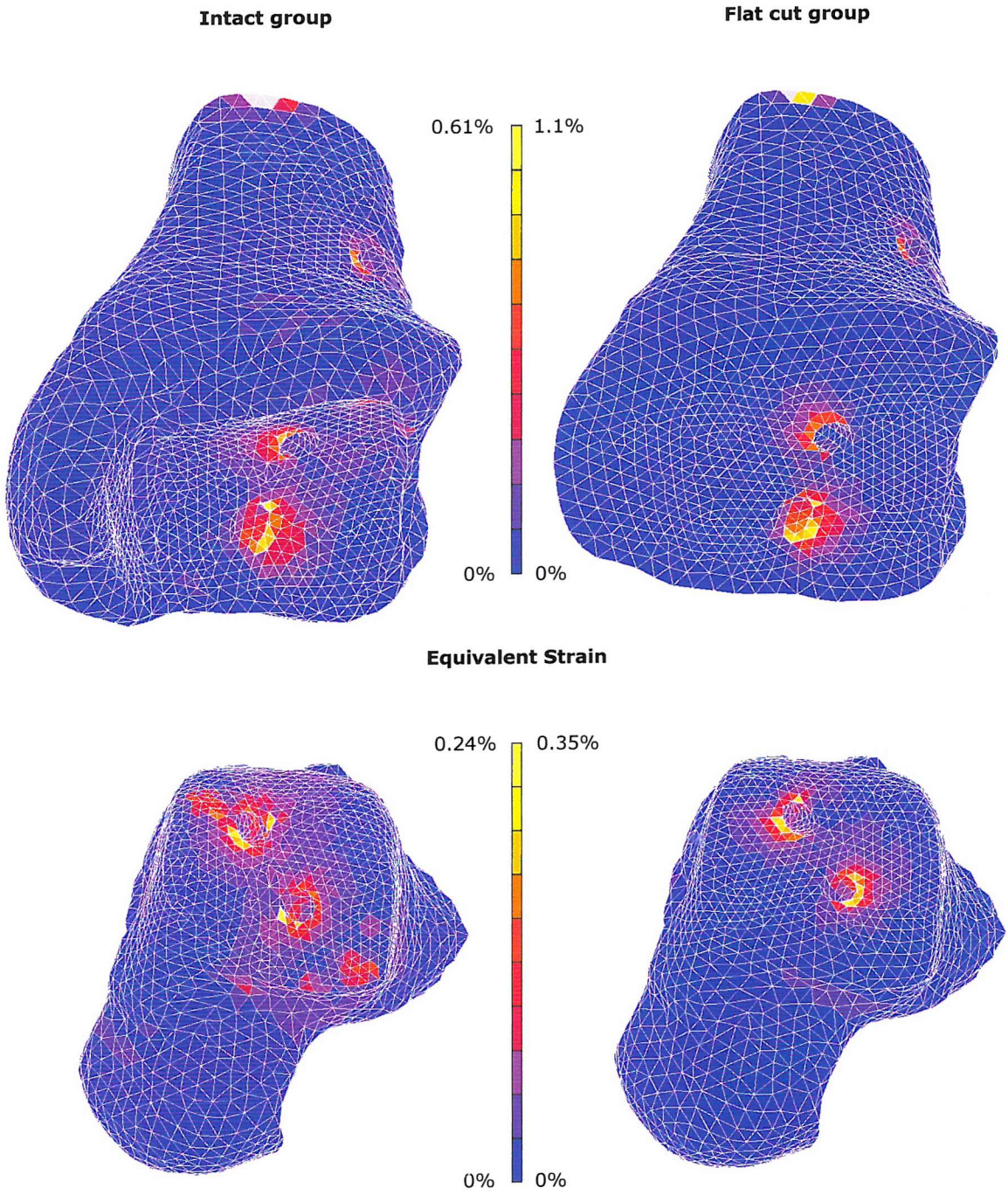

Figure 6.8 Distribution of the equivalent strain predicted in external torsion, in models of the intact group (I30-above) and the flat cut group (30-above). Antero-inferior view of the tibia (top); antero-superior view of the talus (bottom).

Table 6.4 Equivalent strain peak values (%) in the talus and the tibia. External torsion.

Flat cut group	Talus[a]	Tibia[a]	Intact group	Talus[a]	Tibia[a]
30-above	0.35	1.10	I30-above	0.24	0.61
30-on	0.41	1.25	I30-on	0.76 (0.33)[c]	0.79
30-beneath	0.79	1.35 (1.00)[b]	I30-beneath	0.75	0.84 (0.71)[b]
45-on	0.58	1.27	I45-on	0.46	1.1
45-beneath	0.77	1.20 (0.65)[b]	I45-beneath	1.32	0.71 (0.56)[b]
60-beneath	0.86	1.20 (0.55)[b]	I60-benetah	1.15	0.85

[a] Peak values located around screw holes at the fusion site unless stated otherwise.
[b] Peak value located around the proximal screw hole (next peak value: around screw holes at the fusion site).
[c] Isolated peak value, maybe due to a badly shaped element (next peak value: around screw holes at the fusion site)

Table 6.5 Equivalent strain peak values (%) in the talus and the tibia. Internal torsion.

Flat cut group	Talus[a]	Tibia[a]	Intact group	Talus[a]	Tibia
30-above	0.40	0.79	I30-above	0.26	1.31 (1.10)[c]
30-on	0.51	0.79	I30-on	0.27	1.20 (0.66)[d]
30-beneath	0.93	1.20 (1.00)[b]	I30-beneath	0.63	0.77[e]
45-on	0.52	2.70 (0.93)[b]	I45-on	0.59	1.61[e]
45-beneath	0.80	1.77(0.76)[b]	I45-beneath	2.04 (0.62)[f]	1.85[e]
60-beneath	0.81	1.80 (0.61)[b]	I60-beneath	*	*

[a] Peak values located around screw holes at the fusion site unless stated otherwise.
[b] Peak value located around the proximal screw hole (next peak value: around screw holes at the fusion site).
[c] Isolated peak value, maybe due to a badly shaped element (next peak value: postero-lateral area at fusion site)
[d] Isolated peak value, maybe due to a badly shaped element (next peak value: antero-lateral area at fusion site)
[e] Peak value located in posterior-lateral area at fusion site.
[f] Isolated peak value, maybe due to a badly shaped element (next peak value: around screw holes at fusion site).
* No results available.

6.3.1.2 Dorsiflexion test

Table 6.6 summarises the peak micromotions predicted at the fusion site in dorsiflexion. Figure 6.9 displays the predicted micromotions over the contact interface of the talus. All the models in the intact group produced lower peak micromotions than the equivalent ones in the flat cut group when tested in dorsiflexion. For this load case, resecting the articular surfaces meant increasing the peak micromotions between 12 and 49%. In all the cases, the peak micromotions were located towards the posterior edge of the fusion site.

Comparing the different screw configurations, it was found that the larger the insertion angle and the deeper the screw crossing level, the larger the peak micromotions were for both surface preparation techniques. Thus, the most stable constructs were those with the screws inserted at 30 degrees, crossing 5 mm above the fusion site (30-above and I30-above). These models predicted peak micromotions around 50 μm. The least stable constructs were those with the screws inserted at 60 degrees, crossing 5 mm beneath the fusion site (60-beneath and I60-beneath). The peak micromotions in the latter were 4 and 5 times larger than in the former, for the intact and flat cut groups respectively, with magnitudes around 200 and 270 μm.

Table 6.6 Peak relative micromotions (μm) at the fusion site for the intact and flat cut groups in dorsiflexion.

Screw configuration	Dorsiflexion		
	Intact group	Flat cut group	%*
30°/5 mm	49	55	**12**
30°/0 mm	58	73	**26**
30°/-5 mm	69	103	**49**
45°/0 mm	105	122	**16**
45°/-5 mm	122	165	**35**
60°/-5 mm	198	274	**38**

*Percentage of change from intact to flat cut group.

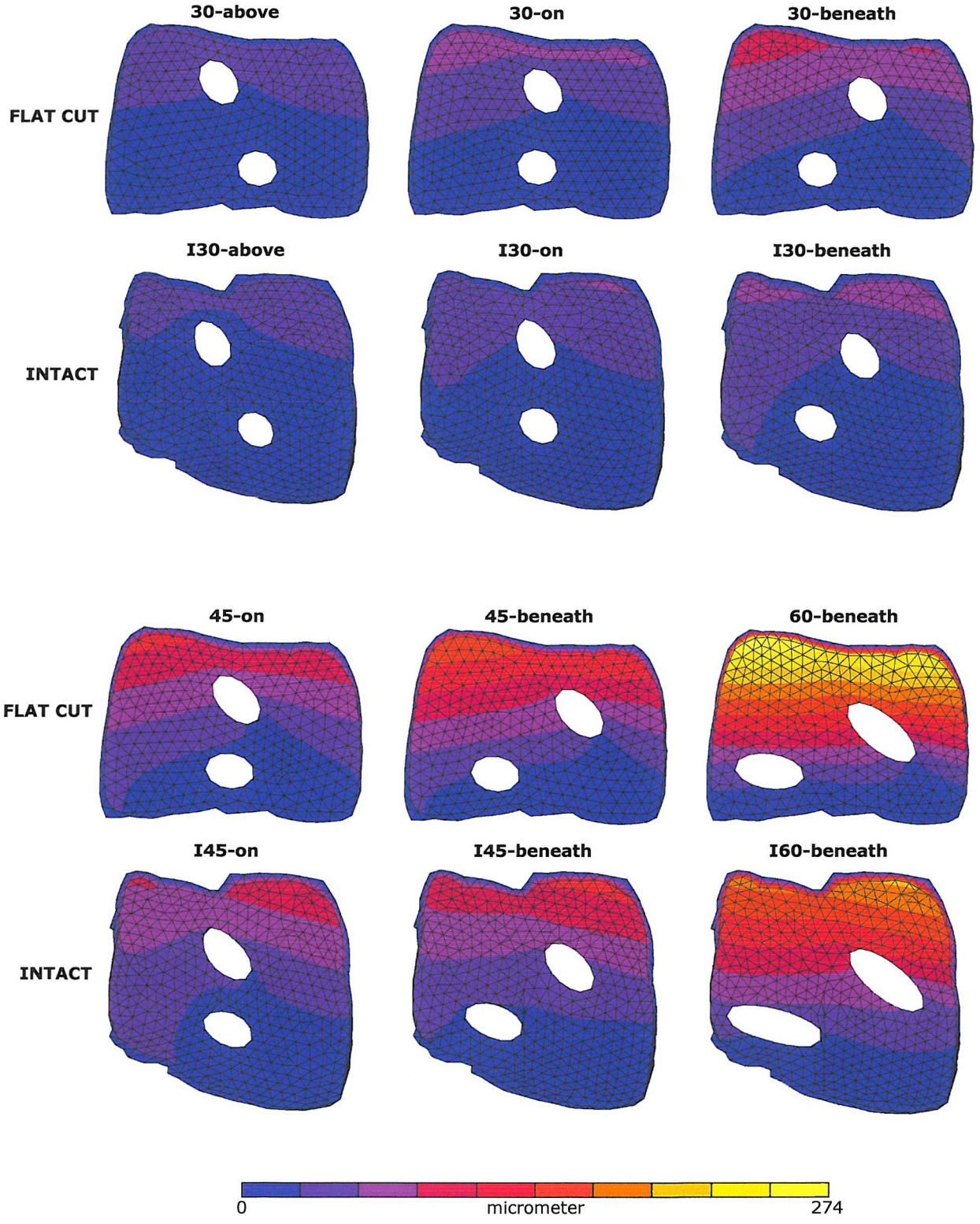

Figure 6.9 Micromotions at the fusion site in dorsiflexion, displayed over the contact interface of the talus.

In all the models, the postero-anterior force applied at the top of the tibia produced a gap at the fusion site, leaving bone contact areas only towards the anterior part of the fusion site. Some sliding (tangential component) was observed in these contact areas, as shown in Figure 6.10. Tangential components on the posterior area of the fusion sites were approximately 10 to 40% of the normal components in the flat cut group and approximately 50 to 100% in the intact group.

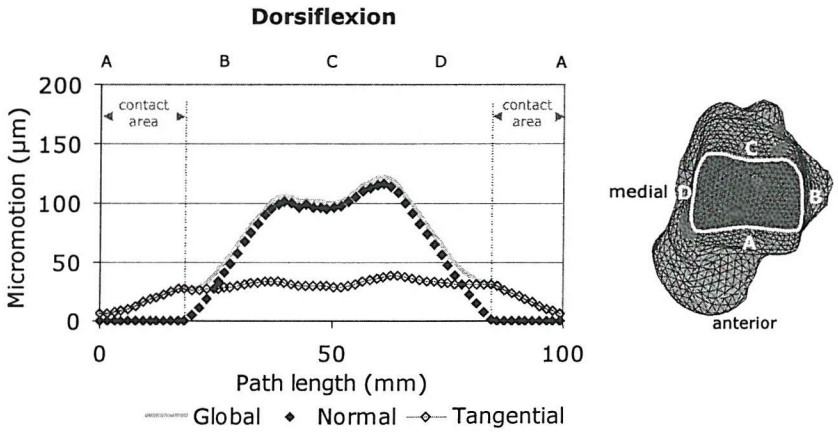

Figure 6.10 Micromotions, normal and tangential components along the edge of the fusion site in a model from the flat cut group (45-on). Dorsiflexion.

The equivalent strain distribution in the bones was similar in both groups. In the talus, patches of ES concentration were found towards the anterior areas of the fusion site, around the holes at the fusion site and along parts of the walls of the holes glued to the screws. In the tibia, ES concentrations were located around the screw holes and in anterior areas at the fusion site and, again, around the proximal screw holes as seen with the torsion tests. Table 6.7 summarises the peak ES predicted in each model. The tibia presented higher peak values than the talus in the majority of the models. In general, resecting the joint surfaces meant a decrease in the peak values in the talus, following the opposite trend to the peak micromotions, though mixed results were predicted for the tibia. Whereas the peak values in the talus were always found around the screw holes at the fusion site in the intact group, in the flat cut group half of the models presented the peak values towards the anterior areas of the fusion site. For the tibia, while the majority of the models in the intact group presented the highest values towards the anterior areas of the fusion site, most of the models in the flat cut group presented the highest values around the proximal screw holes. Comparing the different screw configurations, the larger the insertion angle and the lower the crossing level, the higher the peak ES predicted in both bones, following the same trend as the peak micromotions. The lower peak ES values

were predicted for the models with the screws inserted at 30° and crossing above the fusion site, i.e. the most stable models. Some peak ES values in the tibia were above the yield limit, being located around the proximal holes in the flat cut group and at the fusion site in the intact group. However, the number of elements above this limit was again very small (up to 7 elements in the worst case). 60-beneath was the only model with a substantial number of elements above 1% of strain: 21 elements, which accounted for around 0.008% of the total bone volume in the model. Some badly shaped elements may have caused some of the peak values obtained.

Table 6.7 Equivalent strain peak values (%) in the talus and the tibia. Dorsiflexion.

Flat cut group	Talus[a]	Tibia	Intact group	Talus[b]	Tibia[a]
30-above	0.24	0.52[b]	I30-above	0.25	0.55
30-on	0.28	0.58 (0.55)[d]	I30-on	0.37	0.67 (0.33)[c]
30-beneath	0.31[b]	0.79 (0.66)[d]	I30-beneath	0.42	0.92
45-on	0.36	1.25 (0.95)[d]	I45-on	0.60	1.16
45-beneath	0.55[b]	1.49 (1.10)[d]	I45-beneath	0.60	1.02
60-beneath	0.62[b]	1.84 (1.78)[d]	I60-beneath	0.67	1.56[b]

[a] Peak values located on the anterior area of the fusion site unless stated otherwise.
[b] Peak values located around screw holes at fusion site unless stated otherwise.
[c] Isolated peak value, maybe due to a badly shaped element (next peak value: around screw holes at the fusion site).
[d] Peak value located around proximal screw holes (next peak value: around lateral screw hole at the fusion site).

6.3.2 Friction contact

In order to check the effect of friction on the results reported above, three models were chosen from each group: the least and most stable models and one intermediate model. They were tested under the load cases that produced the largest micromotions in the frictionless case: external torsion and dorsiflexion.

6.3.2.1 Torsion test

Table 6.8 compares the peak micromotions predicted at the fusion site in external torsion for the frictionless and the Coulomb friction cases. Figure 6.11 shows the predicted micromotions over the contact interface of the talus. Considering friction decreased the peak micromotions between 12 and 14% in the flat cut group, whereas in the intact group, the reduction ranged from 28 to 32%.

Table 6.8 Comparison of peak micromotions predicted for the frictionless and friction cases in external torsion.

Model	No friction	Friction	%*
Flat cut group			
30-above	146	128	**-12**
30-beneath	194	167	**-14**
45-on	200	175	**-13**
Intact group			
I30-above	87	59	**-32**
I30-beneath	161	109	**-32**
I45-beneath	179	129	**-28**

*Percentage of change relative to the frictionless case.

Both tangential and normal components along the periphery of fusion site showed similar decreasing levels in torsion. Median values ranged from 9 to 14 % in the flat cut group and from 30 to 36% in the intact group.

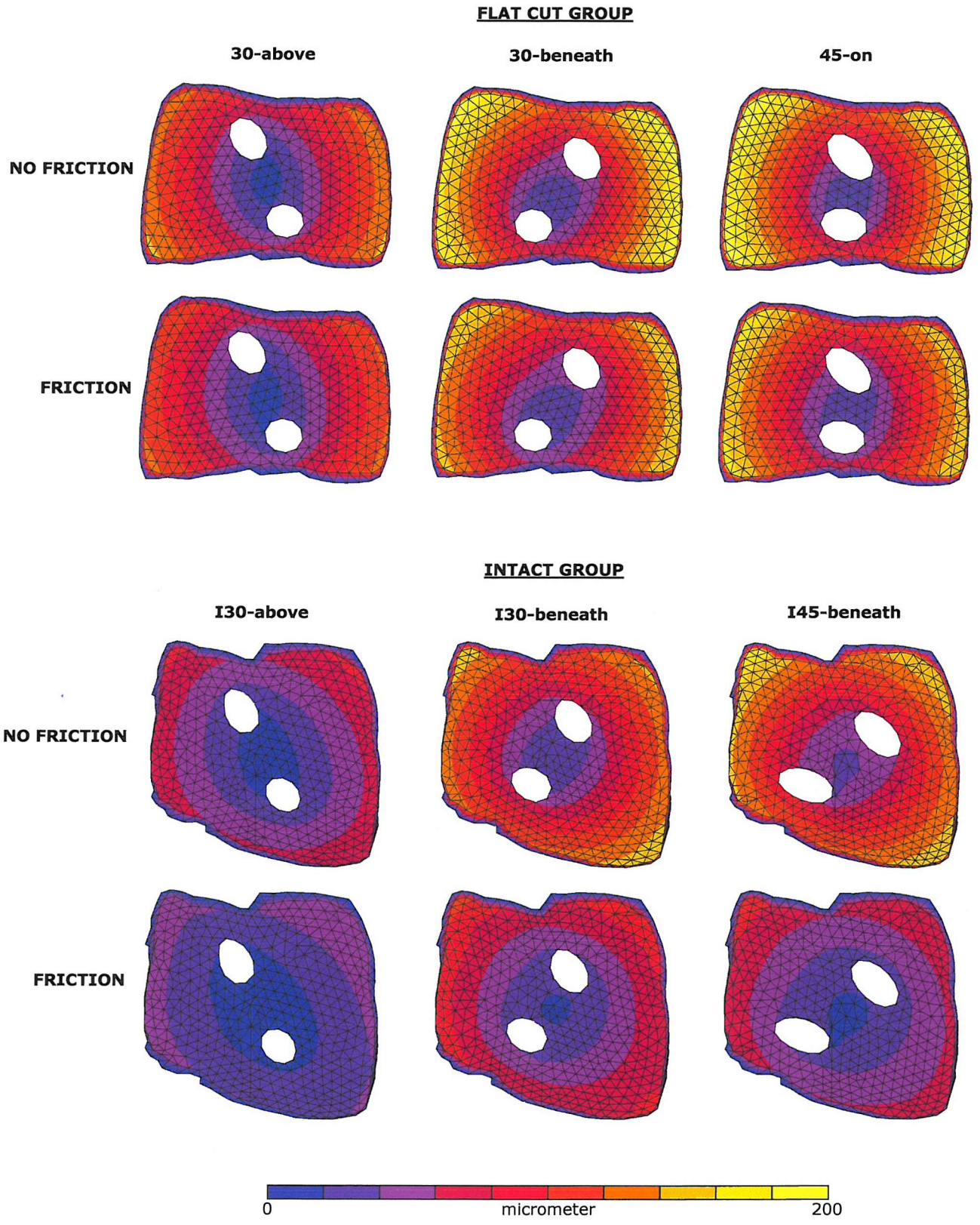

Figure 6.11 Comparison of the micromotions at the fusion site in external torsion for the frictionless and friction contact models.

The equivalent strain distribution in the bones followed the same pattern as in the frictionless external torsion. Peak ES values are displayed in Table 6.9. Overall, the peak values in both bones and both groups were lower than in the frictionless case, following the same trend as the peak micromotions, which also decreased when friction contact was considered. Also, the reduction in the peak ES was larger in the intact group than in the flat cut group. The only exception was the model I45-beneath, which presented a higher peak ES than in the frictionless case. In three models, the tibia produced higher peak ES than the yield limit, which was assumed to be 1%. However, the number of elements with ES above 1% was extremely low (up to 8 elements in the worst case). Again, some badly shaped elements are likely to have caused some of the peak ES predicted.

Table 6.9 Equivalent strain peak values (%) in the talus and the tibia when friction was considered. External torsion.

Flat cut group	Talus[a]	Tibia[a]	Intact group	Talus[a]	Tibia[a]
30-above	0.35	0.96	I30-above	0.19	0.50
30-beneath	0.58	1.20 (0.83)[b]	I30-beneath	0.42	0.65 (0.59)[b]
45-on	0.53	1.25	I45-beneath	0.80	1.65 (0.47)[b]

[a] Peak values located around screw holes at the fusion site unless stated otherwise.
[b] Peak values located around proximal screw holes (next peak value: around screw holes at the fusion site).

6.3.2.2 Dorsiflexion test

Table 6.10 compares the peak micromotions predicted at the fusion site in dorsiflexion. Figure 6.12 (page 105) displays the predicted micromotions over the contact interface of the talus. In the flat cut group, the peak micromotions decreased between 5 and 7% when friction contact was considered, whereas in the intact group, the reduction ranged from approximately 0 to 7%.

Table 6.10 Comparison of peak micromotions predicted for the frictionless and friction cases in dorsiflexion.

Model	No friction	Friction	%*
Flat cut group			
30-above	55	52	**-5**
45-on	122	114	**-7**
60-beneath	274	256	**-7**
Intact group			
I30-above	49	49	**0**
I30-beneath	69	64	**-7**
I60-beneath	198	189	**-5**

*Percentage of change relative to the frictionless case.

In the intact group, the tangential and normal components along the periphery of the fusion site showed similar reductions in the predicted micromotions: median decreases between 5 and 18%. A large difference between the tangential and the normal components was observed in the flat cut group: whilst median decreases ranged from 8 to 10% for the normal components, median decreases ranged from 31 to 40 % for the tangential components.

The equivalent strain distribution in the bones also followed the same pattern as in the frictionless dorsiflexion. Peak ES values are summarised in Table 6.11. Peak values in the flat cut group were very similar to those in the frictionless dorsiflexion case, whereas those in the intact group were lower, both in the tibia and the talus. Some models presented peak values above the yield limit. But, except for the model 60-beneath (as

happened in the frictionless case), only a few elements showed ES above 1%. Again, some of these peak values may have been caused by badly shaped elements.

Table 6.11 Equivalent strain peak values (%) in the talus and the tibia when friction was considered. Dorsiflexion.

Flat cut group	Talus	Tibia	Intact group	Talus[c]	Tibia[c]
30-above	0.28[a]	0.51[a]	I30-above	0.23	0.33
45-on	0.46[b]	1.24 (0.85)[d]	I30-beneath	0.68 (0.33)[e]	0.71[a]
60-beneath	0.55[c]	1.86 (1.50)[d]	I60-beneath	0.66	1.37

[a] Peak value located in the anterior area of the fusion site.
[b] Peak value located along the glued portion of the lateral screw hole.
[c] Peak value located around screw holes at the fusion site.
[d] Peak value located around the screw proximal holes (next peak value: around screw holes at the fusion site).
[e] Isolated peak value, maybe due to a badly shaped element (next peak value: around screw holes at the fusion site).

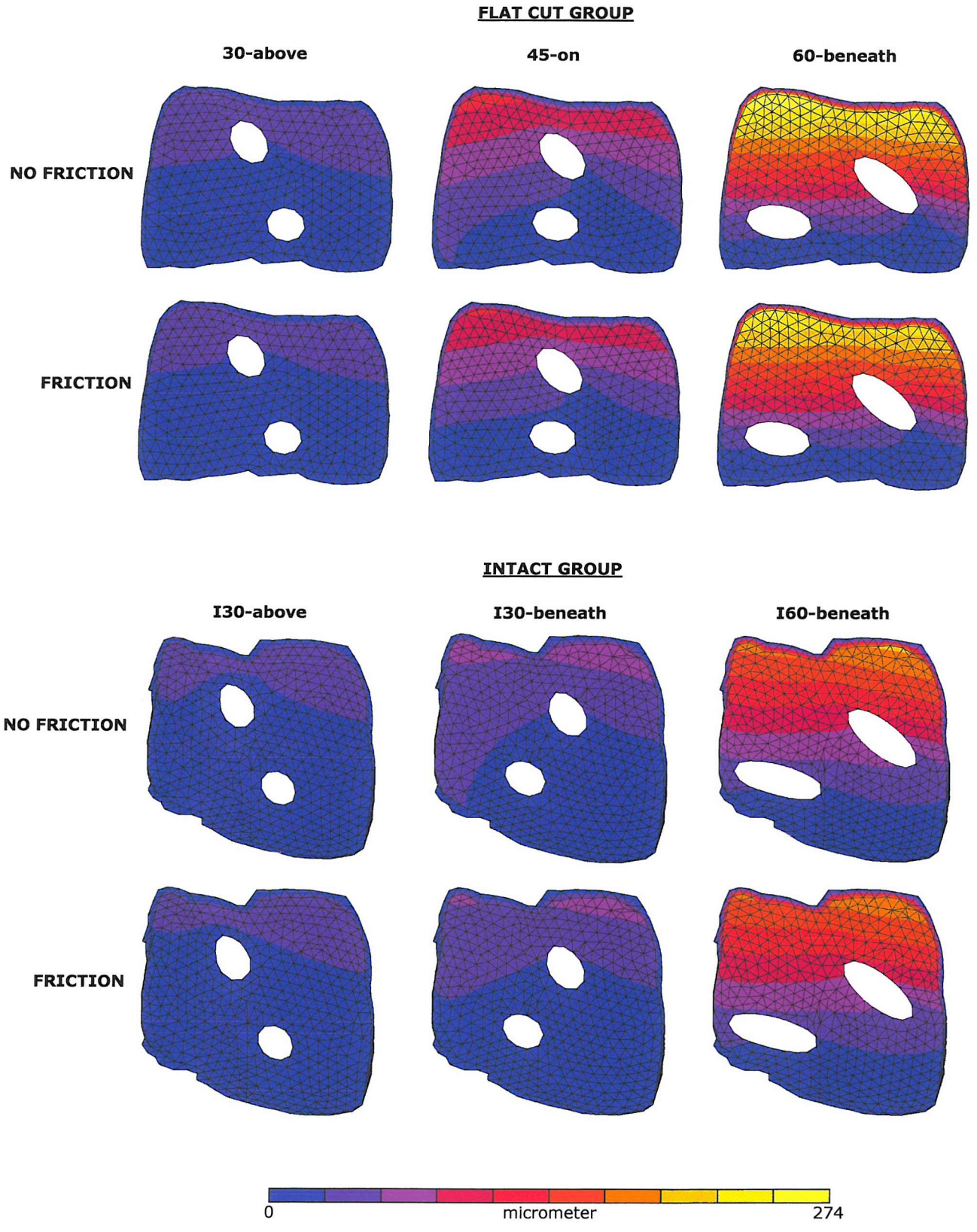

Figure 6.12 Comparison of the micromotions at the fusion site in dorsiflexion for the frictionless and friction contact models.

6.4 DISCUSSION

Overall, the results of this study showed an improved initial stability of the arthrodesis constructs when the joint surfaces were preserved. Only in external torsion, two models predicted lower peak micromotions with resected joint surfaces, although this represented about a 10% decrease relative to the corresponding intact models. In the rest of the models, peak micromotions in the flat cut group were from 1.2 to 1.8 times higher in torsion and from 1.1 to 1.5 times higher in dorsiflexion than in the intact group. These predictions support the conclusions presented by Lauge-Pedersen et al.[86]. They reported the strength and stiffness of the whole arthrodesis construct analogues and concluded that the most stable construct was that equivalent to an ankle arthrodesis that preserved the joint contours. The fact that preserved joint contours may offer better initial stability could partially explain the good results obtained with percutaneous ankle arthrodesis [87,178]. The arthrodesis constructs and load cases analysed in the current study are similar to those examined by Miller et al.[103]. However no direct comparison with their results can be performed as they measured the gross motion between the tibia and the talus. Despite finding a slightly increased stability when preserving the joint contours, the differences were not statistically significant. However, the low number of pairs of specimens tested (four pairs) might not be enough to rule out the possibility of relevant differences between both techniques.

Regarding the different screw configurations, a clinical range of insertion angles and crossing levels was examined. Although some mixed results were obtained in torsion, especially in the flat cut group, overall, inserting the screws at 30 degrees with respect to the long axis of the tibia and crossing them above the fusion site, seemed to offer the most stable arthrodesis construct both in torsion and dorsiflexion. The 2 to 5-fold differences in peak micromotions between the most and least stable models could well affect the success of the ankle arthrodesis.

The differences in contact areas between both groups affected the way the bones moved relative to each other. In the torsion test, the curved surfaces in the intact group models seemed to pivot on the contact areas, lifting off and sliding on the rest, indicating some surface interlocking as would be expected. The resected surfaces in the flat cut group seemed to separate slightly in external torsion but not in internal torsion, although sliding prevailed in both. In the dorsiflexion test, only anterior portions of the surfaces remained in contact, with slightly larger contact areas in the intact group. This fact, together with the smaller tangential/normal component ratios in the flat cut group and the large decrease in sliding in the flat cut group when friction was considered, may indicate a higher degree of rocking motion at the fusion site in the flat cut group than in the intact group.

As expected, a decrease in the magnitude of the micromotions was predicted when friction was considered, although the ranking of the models was not affected. If anything, the better initial stability predicted when preserving the joint contours became more significant. In dorsiflexion, the decrease in the peak micromotions in the intact and flat cut groups was similar (around 6%). In external torsion, the decrease in the peak micromotions in the intact models was considerably higher than in the flat cut models.

As mentioned in Chapter 5 (page 63), shear and bending strains between the screws and the bones were expected, in addition to pulling forces acting along the long axis of the screws. The equivalent strain distributions showed that, in all the load cases, strain concentrations occurred towards the ends of the screw holes in the tibia (proximal and distal ends) and around the screw holes at and near the fusion site in the talus. The ES concentrations around the screw holes at the fusion site showed the tendency of the screws to cut through the bone as a result of the loads applied. Although strain concentrations were expected around the proximal holes in the tibia, it is not clear to what extent the high values obtained were due to the boundary conditions defined to simulate the effect of the screw head. In the frictionless case, the majority of the peak ES predicted in the flat cut group models was located in this area, both in torsion and in dorsiflexion. In the intact group in torsion, strain concentrations also occurred in the contact areas between the bones as a result of the surfaces interlocking. The peak values in the talus were found around the screw holes by the fusion site and the peak values in the tibia tended to occur at the fusion site (contact areas or around screw holes) rather than around the proximal holes, showing the differences in the load transfer between the flat cut and the intact arthrodesis. In both groups in dorsiflexion, strain concentrations were also found towards the anterior region of the fusion site, where the bones stayed in contact. The peak values in the talus were found at the fusion site in the flat cut group (around the screw holes or the anterior region), and only around the screw holes at the fusion site in the intact group. In the tibia, the peak values occurred around the proximal holes in the flat cut group and mostly in the anterior areas of the fusion site in the intact group.

Some of the ES values reported may have been caused by distorted elements. The complex geometry of the bones required automatic meshing of the models, making it difficult to completely avoid some badly shaped elements. Nevertheless, the fact that, in general, higher equivalent strain peak values were predicted in the tibia than in the talus could indicate a higher risk of bone failure in the tibia. No clinical evidence of this fact has been found in the literature. When the ES peak values were compared with a yield strain of 1%, a number of models predicted possible bone failure, although, in the vast majority, the number of elements affected was very small, typically less than 10 elements. Only the 60-beneath model showed higher number of elements with strains above the yield level, both in the frictionless and friction cases.

When comparing the intact and flat cut arthrodeses, peak micromotions and peak ES followed a similar trend in the external torsion. In general, the intact models presented lower peak micromotions and lower peak ES than the corresponding flat cut models. The two intact models that predicted larger peak micromotions than the flat cut models (I45-beneath and I60-beneath) also presented higher peak ES. Results were mixed in internal torsion. In dorsiflexion, peak ES followed the same trend as the peak micromotions (lower values in the intact models) in the least stable models, whereas the trend was reversed in the more stable models, those with a 30-degree insertion angle. When comparing different screw configurations, the peak ES followed the same trend as the peak micromotions in dorsiflexion, with values increasing for increasing insertion angles and lowering levels of crossing. In external torsion, the peak ES and peak micromotions also seemed to follow similar patterns of change, but not in internal torsion. Overall, the more stable models, those with the screws inserted at 30 degrees and crossing above the fusion site (30-above and I30-above), were also the models with the lower peak ES.

Adding friction did not change the equivalent strain distribution of the models studied and, again, the highest peak values were always found in the tibia. In general, peak values occurred in the same areas of the bones as found in the frictionless cases, both in external torsion and dorsiflexion. In the flat cut group, the peak values were similar or slightly lower than in the frictionless case, whilst in the intact group, the decrease was in general larger.

The convergence tolerance value was kept constant in about 80% of the total number of models run in this study. In the rest of the models (10 out of 47), it was increased from the reference value 0.01 in order to reach a solution (Table 6.2, page 87). Given the results of the sensitivity analysis performed on the reference model (Chapter 5, page 74), a slight overestimation (up to 2%) of the micromotions predicted in these models would be expected when comparing the results with those models with the reference convergence tolerance. However, this overestimation is not likely to significantly affect the results of the analyses and the ranking of the models.

Bone quality affects the stability of arthrodesis constructs [46,161], so that additional means are needed to achieve rigid fixation. In the current models, normal bone quality was assumed. If bone quality is poorer, as happens in some patients undergoing ankle arthrodesis, screw fixation can be a problem and larger micromotions are expected [76], which could compromise the success of the fusion. In these cases, joint geometry could have an even greater influence on the initial stability of the arthrodesis [86]. The effect of bone quality on the initial stability of ankle arthrodesis constructs is analysed in Chapter 8.

Summary of results

- Preservation of the joint contours produced better initial stability at the fusion site than resection of the joint surfaces.

- Overall, inserting the two screws at a 30-degree angle with respect to the long axis of the tibia and crossing them above the fusion site improved the initial stability and lowered the bone strain values, in both joint preparation techniques.

- Lowering the crossing level produced a decrease in the initial stability at the fusion site and, in general, an increase in the strain values in the bones. Increasing the insertion angle did not improve the initial stability and the levels of bone strain in torsion, but produced a substantial decrease in the initial stability and an increase in the bone strains in dorsiflexion.

- Two-fold and five-fold differences in the initial stability were predicted between the most and least stable models in torsion and dorsiflexion, respectively.

Chapter 7

TWO *VERSUS* THREE-SCREW FIXATION

7.1 INTRODUCTION

In ankle arthrodesis fixed with screws, at least two screws are needed to achieve good stability at the fusion site. Although the ideal number of screws has not been determined, it seems that in the case of normal bone quality, two crossed screws should be enough to ensure a rigid fixation [1,78]. Sometimes the decision on the number of screws is left to the surgeon's preference [123]. In general, intraoperative manipulation of the arthrodesis construct is used to assess the rigidity provided by the two screws. If the surgeon considers it unsatisfactory, a third screw is usually inserted. Thermann et al.[157] recommended a four-screw technique even in the cases of good bone stock. However, increasing the number of screws is not always possible due to the small size of the talus and the dimensions of the screws. In addition, adding screws means increasing the operative time and increasing the damage to the bone, possibly weakening its structure. More research is needed to find the optimal compromise between bone integrity, number of screws and the initial stability achieved.

Ogilvie-Harris et al.[119] carried out a cadaver study comparing a two *versus* a three-screw ankle fixation in a crossed configuration. In several human cadaver ankles, the tibial plafond and the talar dome were flat cut, without detaching the fibula. Two 6.5 mm cancellous screws were crossed through each joint at 45 degrees with the horizontal plane (Figure 7.1 A). Although it was not explicitly mentioned, it seems as if the screws were crossed below the joint line. The length of the screws varied between 50 and 60 mm, keeping a constant 16 mm thread length. A third screw was placed anterior to the tibia, at 30 degrees relative to the long axis of the tibia, aiming towards the postero-inferior portion of the talar body (Figure 7.1 B). Nine specimens were tested in a materials testing system by applying ramped torques to a maximum of 10 Nm and measuring the resultant rotation between the tibia and the talus. The displacement at the midpoint of the hysteresis curve produced by the applied torque was used to compare the degree of rotation between the two and three-screw fixation in each specimen. They found a highly significant difference between both screw configurations, with the three-screw fixation having a greater resistance to torque. On average, adding the third screw meant a 16% reduction of the displacement between the bones (range 9-31%, median 14%). In seven specimens, they also measured the compression at the fusion site by placing pressure sensitive film between the tibia and the talus before screw insertion. Screws were inserted

at a 4 Nm torque. Greater compressive forces were measured with three screws than with two and the differences were highly significant. Despite considerable variability in the results, they considered the difference between groups sufficient to prove the superiority of the three-screw configuration. In summary, they recommended the use of three screws on a routine basis.

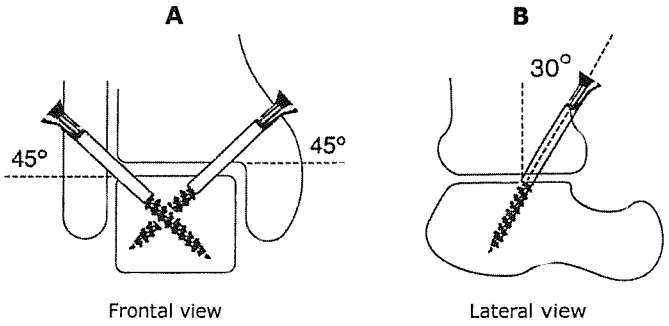

Figure 7.1 Screw configuration in Ogilvie-Harris et al.[119]. **A** Lateral and medial screws inserted at 45° relative to the horizontal plane. **B** Third screw inserted at 30° relative to the long axis of the tibia.

This is the only study found comparing the mechanical behaviour of two *versus* three crossed screws in ankle arthrodesis. No clear description was given of how the torsion was applied to the construct or how the resulting degree of rotation was measured. It is assumed the reported results reflected the gross motion between tibia and talus. But, how much of the added stability happened at the fusion site?

In order to assess the change in the initial stability at the fusion site when adding a third screw to a two-crossed-screw configuration, further FE models of ankle arthrodesis were built by adding a third screw to the models studied in Chapter 6. When adding a third screw to a two-screw configuration such as the one used in the current work, there are two options. Either the third screw is inserted postero-laterally on the tibia, pointing anteriorly and slightly medially towards the neck of the talus [61,87], or it is inserted anteriorly on the tibia, pointing towards the postero-inferior portion of the body of the talus, as done in Ogilvie-Harris et al.[119]. Both configurations were considered here in order to compare the degree of initial stability they provided at the fusion site.

7.2 MODELLING

Two groups of FE models were built by adding a third screw to the two-screw models that predicted the maximum and the minimum peak micromotions at the fusion site in Chapter 6, both in the flat cut and intact arthrodeses (see Table 6.3 and Table 6.6). The "anterior" group included models with a third screw inserted through the anterior face of the tibia, pointing down towards the body of the talus in the posterior direction. The "posterior" group comprised models with a third screw inserted through the postero-lateral part of the tibia, pointing down towards the neck of the talus, in an antero-medial direction. A model representative of each group is displayed in Figure 7.2. Table 7.1 and Table 7.2 show the length and the location of the third screw in each model.

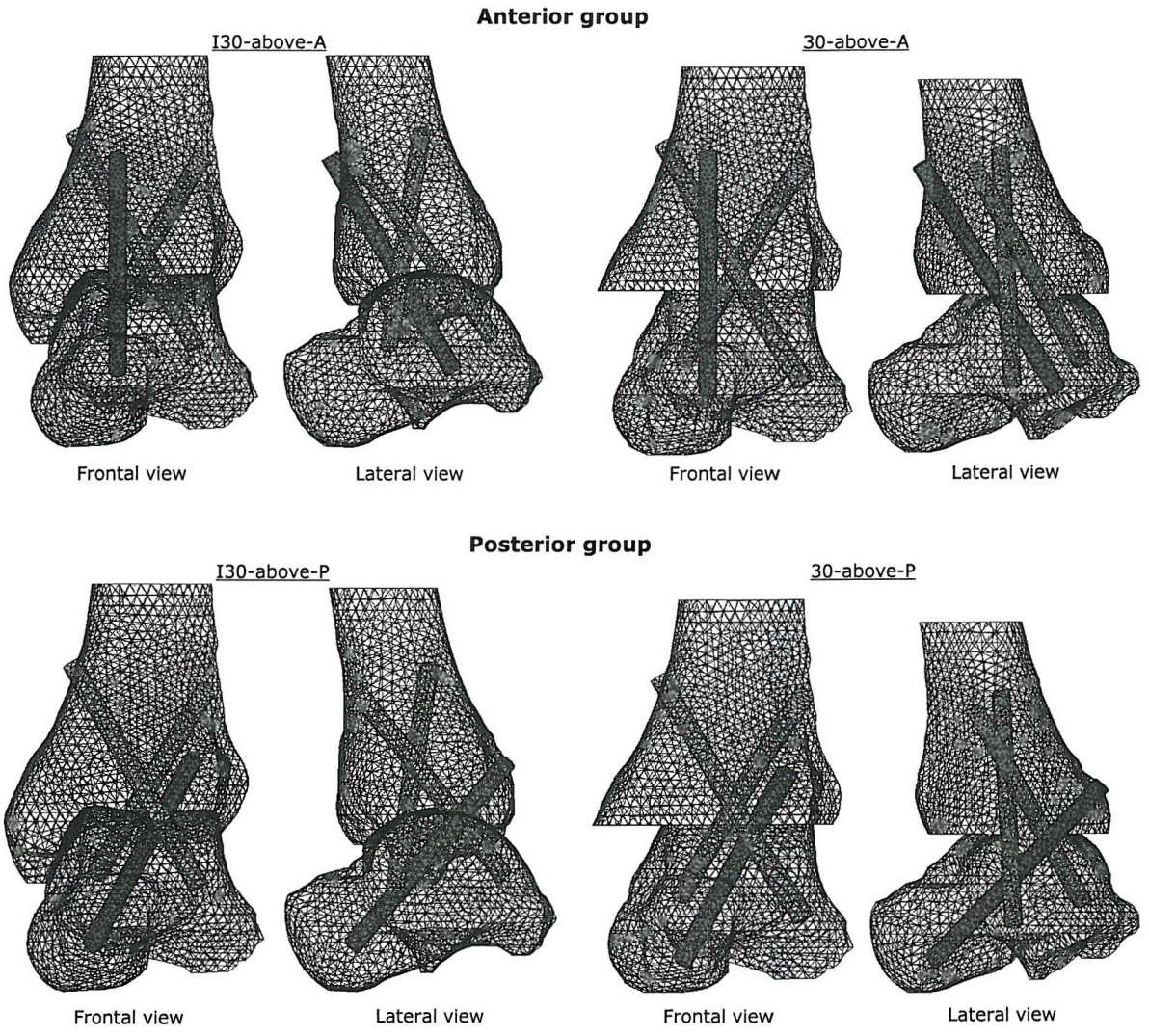

Figure 7.2 FE meshes of an intact and flat cut model in the anterior group and an intact and flat cut model in the posterior group, displayed in frontal and lateral views. The third screw is shown in black.

Table 7.1 Models in the anterior group. Description of the third screw location and load cases studied.

	Model	Screw length (mm)	Angle 1[a]	Angle 2[b]	Height[c] (mm)	Load case tested[d]	
Flat cut	30-above-A	65	33°	1°	27	T	DF
	45-on-A	60	36°	5°	22	T	DF
Intact	I30-above-A	60	31°	1°	24	T	DF
	I45-on-A	60	31°	1°	22	T	-
	I60-beneath-A	50	38°	3°	7	-	DF

[a] Angle between the anterior screw and the long axis of the tibia in the sagittal plane.
[b] Angle between the anterior screw and the postero-anterior direction in the transverse plane.
[c] Distance from the screw insertion point to the fusion site.
[d] T=external torsion, DF=dorsiflexion.

Table 7.2 Models in the posterior group. Description of the third screw location and load cases studied.

	Model	Screw length (mm)	Angle 1[a]	Angle 2[b]	Height[c] (mm)	Load case tested[d]	
Flat cut	30-above-P	60	40°	32°	10	T	DF
	45-on-P	60	40	32	11	T	DF
	60-beneath-P	60	34°	43°	11	-	DF
Intact	I30-above-P	60	40°	32°	10	T	DF
	I45-on-P	60	40°	32°	10	T	-
	I60-beneath-P	60	40°	33°	7	-	DF

Symbols as in Table 7.1.

The load cases tested were those that produced the largest micromotions in the two-screw arthrodesis: external torsion and dorsiflexion. The third screw was added to the most and least stable models in external torsion and dorsiflexion (Table 7.1 and Table 7.2). The orientation of the third screw was kept constant whenever possible, although in some models they had to be slightly modified to avoid conflict with the other two screws. In one case (60-beneath), it was impossible to add the anterior screw crossing the fusion

site without interfering with the other two screws. For completeness of the study, the 45-on models with an anterior and a posterior screw were also tested in dorsiflexion. Mesh and boundary conditions were defined in all the models as explain in Chapter 5.

All models were run in Marc 2001, with the contact parameters and convergence tolerance values chosen in Chapter 5. In some cases, the convergence tolerance initially considered (0.01) had to be varied to reach a solution. The modified values ranged from 0.015 to 0.04 (Table 7.3).

Table 7.3 Convergence tolerance values used in the models of the anterior and posterior groups, when different from 0.01.

Model	External torsion	Dorsiflexion
30-above-A	0.04	0.02
45-on-A	0.02	-
60-beneath-P	-	0.04
I30-above-A	0.02	-
I45-on-P	0.015	-
I60-beneath-P	-	0.02

7.3 RESULTS

7.3.1 External torsion

Table 7.4 compares the peak micromotions predicted at the fusion site for the anterior and posterior groups with those predicted for the corresponding two-screw configuration models in external torsion. Figure 7.3 (page 117) shows the distribution of micromotions over the fusion site of the talus and how adding a third screw produced a decrease of the micromotions at the fusion site. In both the anterior and posterior groups, the peak micromotions were located along the periphery of the fusion site. As the anterior screw crossed the fusion site antero-medially, the peak micromotions in the anterior group occurred along the lateral region. The peak micromotions in the posterior group were located along the medial region of the fusion site, as the posterior screw was located postero-laterally (Figure 7.4, page 118). The decrease of the peak micromotions ranged from 31 to 53% in the anterior group and between 24 and 37% in the posterior group. In all the cases, the anterior screw decreased the peak micromotions more than the posterior screw, producing differences between the models above 20 µm. However, in the case of the model I30-above, the peak micromotions predicted for both three-screw configurations only differed by 5 µm. All the models with the third screw inserted anteriorly predicted peak micromotions below 100 µm.

Table 7.4 Peak micromotions (µm) predicted at the fusion site for the two and three-screw models in external torsion.

	Model	2 screws	Anterior*		Posterior*	
Flat cut	30-above	146	91	**-38%**	111	**-24%**
	45-on	200	95	**-53%**	131	**-35%**
Intact	I30-above	87	60	**-31%**	65	**-25%**
	I45-on	169	81	**-52%**	107	**-37%**

* Percentage of change in the micromotions when the third screw was added.

In the two-screw configuration, the most stable model was that with the screws inserted at 30 degrees, crossing above the fusion site, both in the intact and flat cut groups (30-above and I30-above). The least stable was the model with the screws inserted at 45 degrees, crossing at the level of the fusion site (45-on and I45-on). This result did

not change when a third screw was added, although the differences between the most and least stable configurations were lower. The decrease in the peak micromotions predicted when adding the third screw was larger in the case of the least stable two-screw configurations in all the groups. Thus, in the flat cut arthrodesis, whilst the peak micromotion predicted in the 45on model was 1.4 times larger than in the 30-above model, it was 1.2 times larger in the posterior group; in the anterior group the differences were almost nil (less than 5 μm). In the intact group, the peak micromotion predicted in the I45-on model was 1.9 times larger than in the I-30above model, and 1.4 and 1.6 times larger in the anterior and posterior groups, respectively.

When comparing the two surface preparation techniques, all the models with three-screw fixation and intact arthrodesis were more stable than their corresponding models with flat cut arthrodesis, as found with the two-screw configuration. Resecting the joint contours meant an increase of the peak micromotions ranging from 17 to 71%. In both the anterior and posterior groups, this increase was much higher when adding the third screw to the most stable 2-screw configurations (30-above and I30-above) than to the least stable ones (45-on and I45-on).

As shown with the two-screw configuration in the flat cut arthrodesis (Chapter 6), most of the motion at the fusion site was due to sliding, although a small gap still developed at the interface. In both the anterior and the posterior groups, the normal component of the micromotions along the edge of the fusion site was, on average, between 13 and 23% of the tangential component. Figure 7.4 (page 118) compares the micromotions and its components along the edge of the fusion site for a two-screw configuration and the corresponding models in the anterior and posterior group. Adding the third screw posteriorly tended to reduce the gap opening slightly more than adding the screw anteriorly, as expected given the fact that in the two-screw configuration the gap was larger towards the lateral and posterior areas of the fusion site; however it also produced a slight increase of the gap in the antero-medial area of the fusion site. In the intact arthrodesis, the same contact areas predicted in the two-screw configuration were observed when the third screw was added (antero-lateral and postero-medial areas of the fusion site). The gaps opening in the opposite areas also predicted in the two-screw configuration were reduced when adding the third screw. In the anterior group, only the postero-lateral gap was observed, with maximum values of the normal component along the edge of the fusion site about 60% of the tangential component. In the posterior group, the postero-lateral gap was reduced more than 50%, with maximum values of the normal component around 30% of the tangential component.

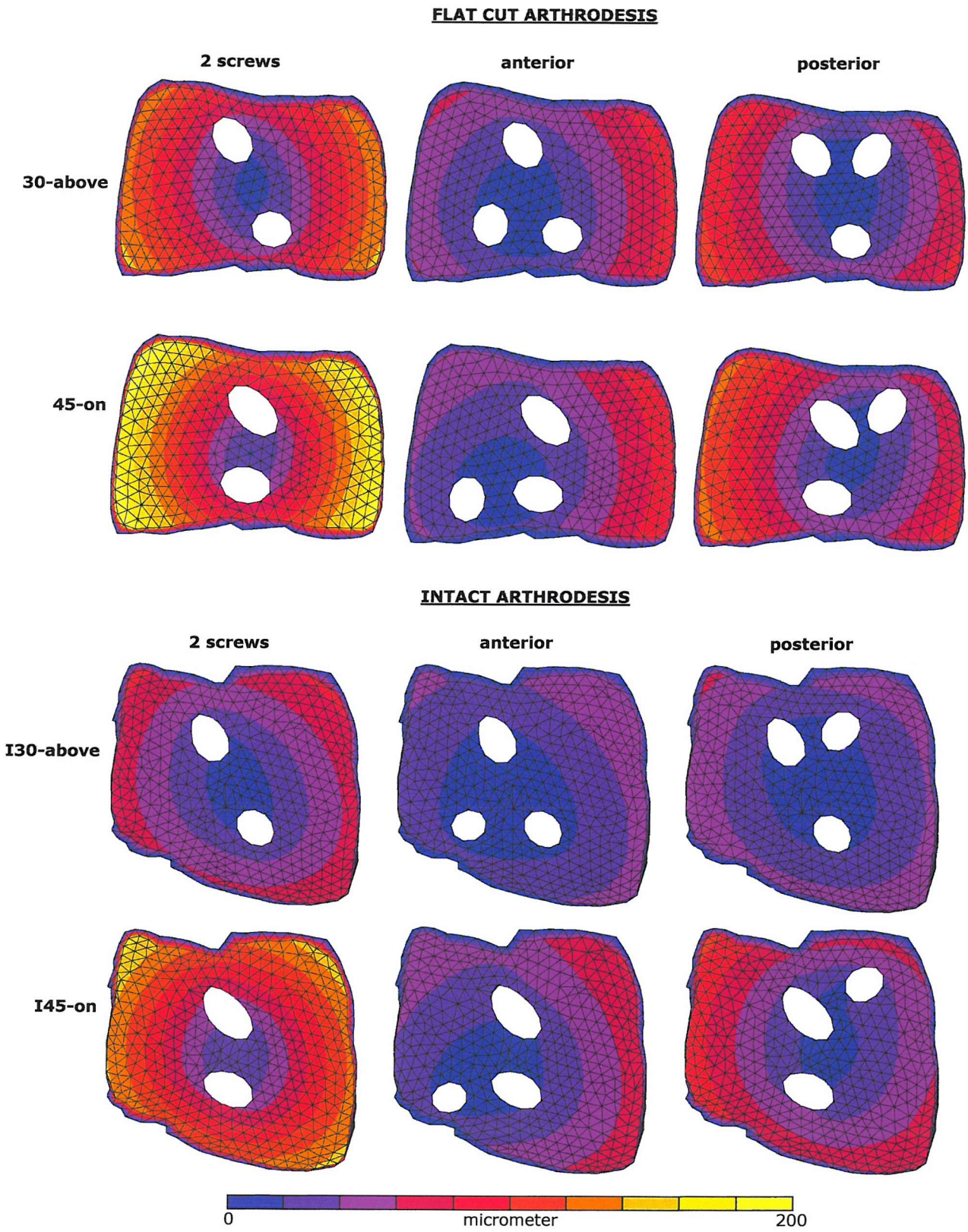

Figure 7.3 Micromotions at the fusion site in external torsion for the models with two and three-screw fixation.

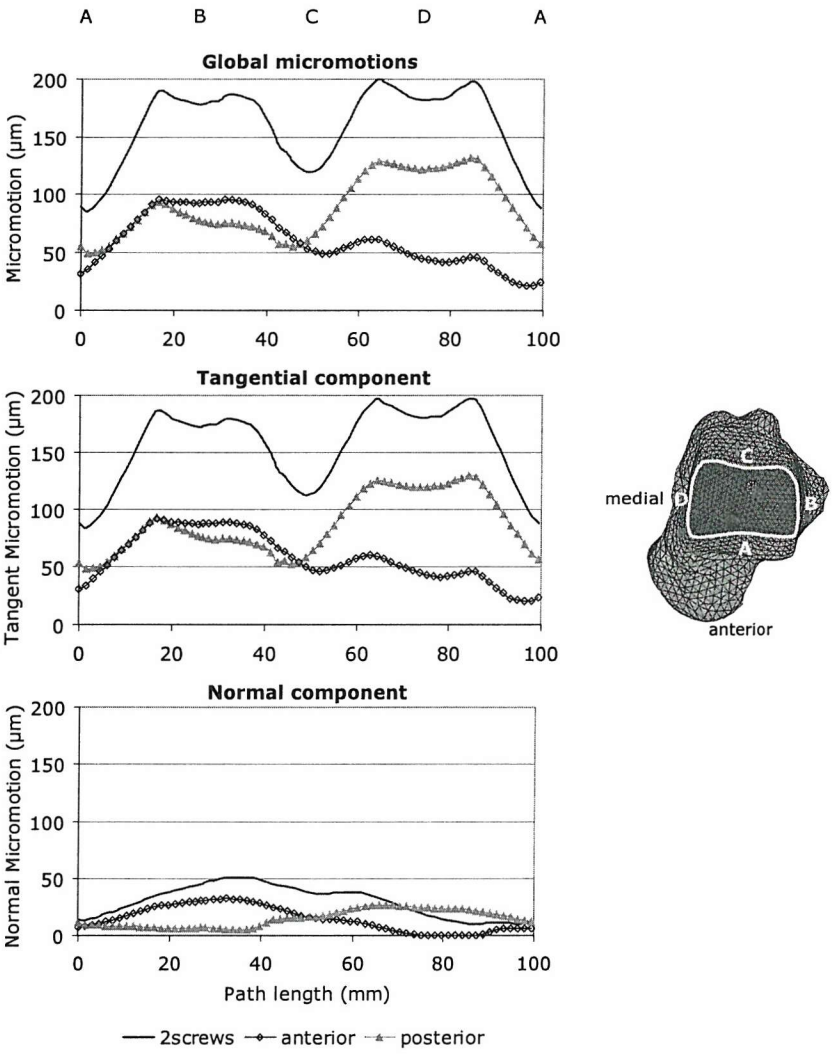

Figure 7.4 Micromotions, tangential and normal components predicted along the edge of the fusion site for a 2-screw configuration (45-on) and the corresponding models in the anterior and posterior group. External torsion.

The patterns of equivalent strain (ES) distribution were very similar to the two-screw configuration when the third screw was added. In general, the areas of ES concentration were located around the screw holes at the fusion site in the talus and the tibia and around the proximal screw holes in the tibia. Also, in the anterior group in the intact arthrodesis, areas of ES concentration were found in antero-lateral areas of the fusion site in the tibia. Figure 7.5 shows the ES distributions predicted in one model of the anterior group and the equivalent model in the posterior group. Peak values for all the models are summarised in Table 7.5. Peak values were nearly always higher in the tibia than in the talus, as happened with the two-screw configuration (Table 6.4, page 95). In all the cases, inserting the third screw anteriorly produced lower peak values in both the tibia and the talus than

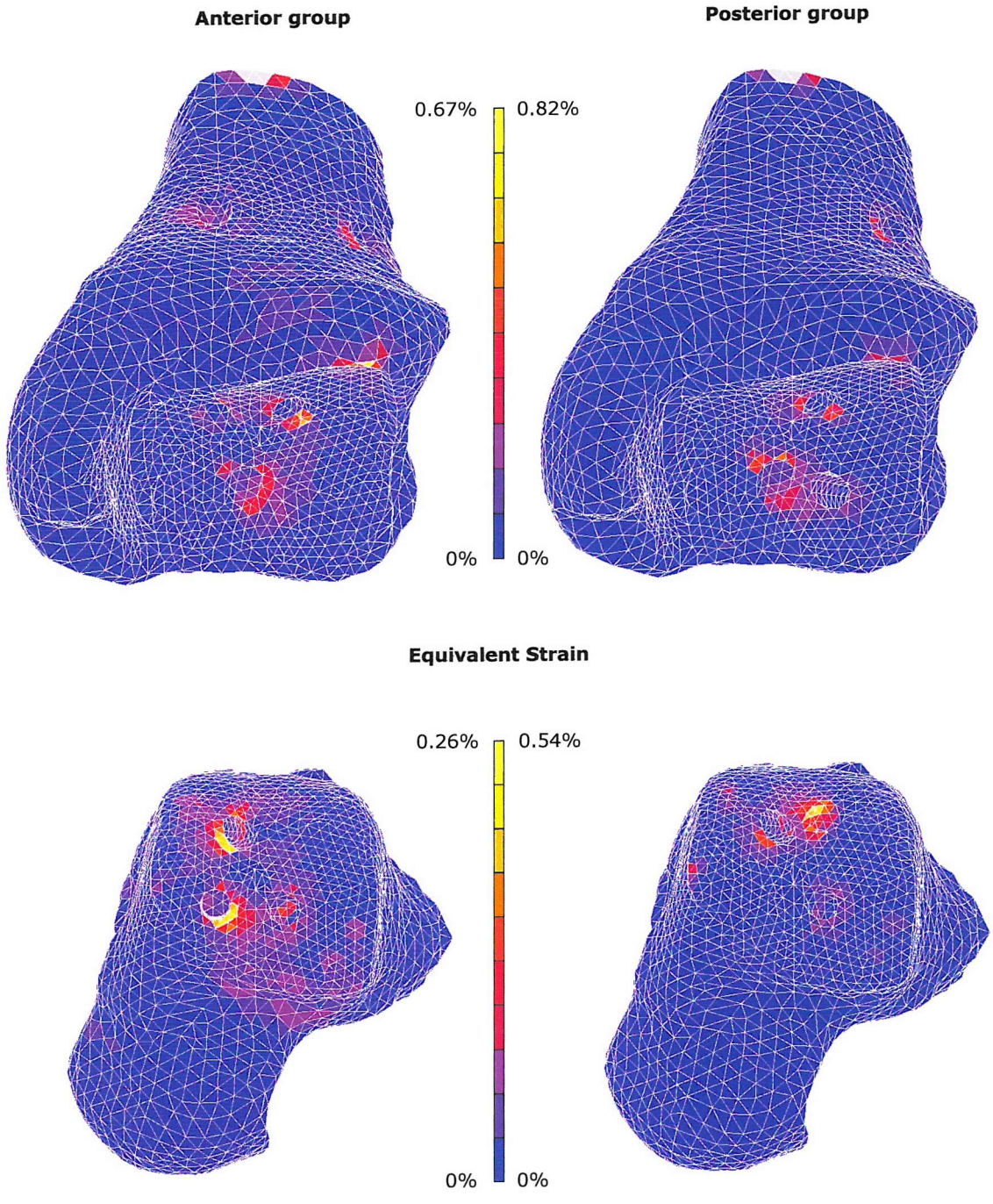

Figure 7.5 Distribution of the equivalent strain predicted in external torsion in models of the anterior group (I30-above-A) and the posterior group (I30-above-P). Antero-inferior view of the tibia (top); antero-superior view of the talus (bottom).

when inserting the screw posteriorly. In fact, peak values in both bones tended to be lower in the anterior group than in the two-screw configuration. In the posterior group, peak values in the talus were considerably higher than in the two-screw models, whereas mixed results were observed in the tibia. In the anterior group, peak values in the talus were located around the hole of the anterior screw at the fusion site. In the tibia, peak values were found around the screw holes at the fusion site, except in the model I30-above-A where they were located along the antero-lateral edge of the fusion site. In the posterior group, the talus presented peak ES around the hole of the medial screw at the fusion site; the tibia presented peak values around the proximal hole of the posterior screw in the models 30above-P and I30-above-P and around the hole of the lateral screw at the fusion site in the models 45-on-P and I45-on-P. In the two-screw configuration, resecting the joint surfaces meant an increase of the ES peak values. This finding is also true in the posterior group, for both the tibia and the talus, whereas in the anterior group is only true for the tibia, i.e. for the absolute peak values. When comparing the different screw configurations, in the two-screw models, 45-on and I45-on presented higher peak values than 30-above and I30-above in both bones. In the anterior group this trend only held for the talus and it was reversed for the tibia. This opposite trend was also observed in most of the cases in the posterior group. Overall, the models with lower peak ES values were I45-on-A and I30-above-A. All the models in the anterior group presented ES well below the yield strain (1%). Three models in the posterior group presented peak ES above the yield limit. However, in all the cases the number of elements with larger ES than 1% was low (two elements in each case).

Table 7.5 Equivalent strain peak values (%) in the talus and the tibia for the anterior and posterior groups. External torsion.

	Anterior group	Talus[a]	Tibia[b]	Posterior group	Talus[d]	Tibia[f]
Flat cut	30-above-A	0.31	0.77	30-above-P	0.88	1.76 (0.95)[g]
	45-on-A	0.33	0.72	45-on-P	0.77	1.15
Intact	I30-above-A	0.26	0.67[c]	I30-above-P	0.54	0.82 (0.55)[g]
	I45-on-A	0.46	0.46	I45-on-P	1.02 (0.72)[e]	0.56

[a] Peak values located around the hole of the anterior screw at the fusion site.
[b] Peak values located around screw holes at the fusion site.
[c] Peak value located by the antero-lateral edge of the fusion site.
[d] Peak values located around the hole of the medial screw at the fusion site.
[e] Isolated peak value, maybe due to a badly shaped element (next peak value: as [d]).
[f] Peak values located around the hole of the lateral screw at the fusion site.
[g] Peak value located around the proximal hole of the posterior screw (next peak value: as [f]).

7.3.2 Dorsiflexion

Table 7.6 summarises the peak micromotions predicted at the fusion site for the models in the anterior and posterior groups and compares them with the corresponding two-screw configurations in dorsiflexion. Figure 7.6 shows the distribution of the micromotions over the contact surface of the talus, with peak micromotions located along the posterior region of the fusion site in the anterior group and towards the postero-medial region in the posterior group. In all the models studied, the added third screw produced a decrease of the micromotions at the fusion site, with peak micromotions decreasing between 4 and 39% in the anterior group and between 16 and 59% in the posterior group. In the intact arthrodesis, adding the screw posteriorly decreased the peak micromotions considerably more than adding the screw anteriorly.

Table 7.6 Peak micromotions (μm) predicted at the fusion site for the two and three-screw models in dorsiflexion.

	Model	2 screws	Anterior*		Posterior*	
Flat cut	30-above	55	44	**-20%**	46	**-16%**
	45-on	122	75	**-39%**	80	**-34%**
	60-beneath	274	-	-	121	**-56%**
Intact	I30-above	49	47	**-4%**	34	**-31%**
	I60-beneath	198	166	**-16%**	81	**-59%**

* Percentage of change in the micromotions when the third screw was added.

In the two-screw configuration, the higher the crossing level and the smaller the insertion angle, the lower were the peak micromotions predicted in both the flat cut and intact arthrodeses. This trend was not affected after the addition of the third screw. In the flat cut arthrodesis, the 5-fold difference between the most and least stable models in the two-screw configuration (30above and 60beneath) was reduced to 2.6 times in the posterior group. No comparison was possible with the anterior group, as the anterior screw could not be inserted in the model 60beneath without interfering with the other screws. For completeness of this comparison, a third screw was added to the model 45on. In this case, the 2.2-fold difference with the most stable model was reduced to 1.7-fold difference both in the anterior and posterior groups. In the intact group, the 4-fold difference between the most and least stable models (I-30above and I-60beneath) was reduced to 3.5 and 2.4-fold differences when adding the screw anterior and posteriorly, respectively.

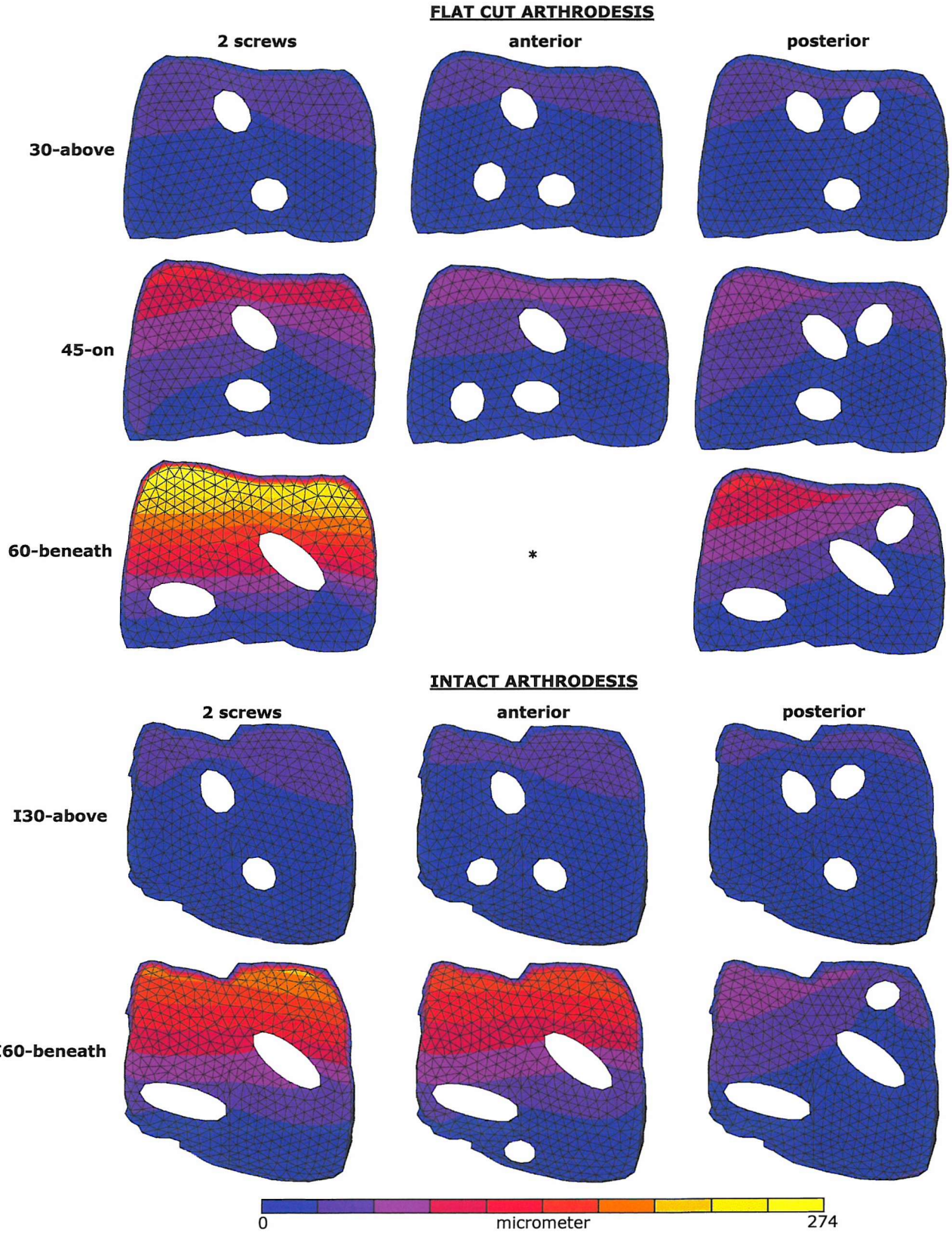

Figure 7.6 Micromotions at the fusion site for the models with two and three-screw fixation in dorsiflexion (* Not possible to add the anterior screw without interfering with the other two screws. For completeness of the comparison model 45-on was included in this load case).

Comparing the two surface preparation techniques, the intact arthrodesis produced lower peak micromotions than flat cut arthrodesis in the posterior group, whilst no difference was found in the anterior group.

In the flat cut arthrodesis, as predicted in the two-screw configuration, most of the relative motion between the tibia and the talus was due to the increasing opening gap towards the posterior region, although some degree of sliding was also observed. Figure 7.7 shows an example of the change in the micromotion and its components along the edge of the fusion site. The addition of the third screw produced the same decrease in the peak normal micromotions in both groups, with an expected higher decrease around postero-lateral areas in the posterior group. The anterior screw tended to generally reduce the sliding at the fusion site, whereas the posterior screw almost only decreased the sliding in the lateral region. Thus, in the anterior group the tangential component along the posterior edge of the fusion site was, on average, between 14 and 17% of the normal components, whereas in the posterior group it was between 27 and 41%. In the intact group, both components were reduced more when the posterior screw was added, especially in the model I60-beneath. Tangential components were over 70% of the normal components along the posterior edge of the fusion site. The sliding was slightly reduced when adding the anterior screw, except for the antero-lateral area, were it increased. Tangential components in the anterior group were over 60% of the normal components along the posterior edge of the fusion site.

The equivalent strain concentrations generated in the bones in dorsiflexion were similar to those in the two-screw configuration. They were located anteriorly and around the screw holes at the fusion site in both the tibia and the talus; and around the proximal screw holes in the tibia. In the flat cut arthrodesis, some areas of ES concentration were also found in the talus along the walls glued to the lateral screw. Table 7.7 (page 125) summarises the peak values predicted in each model. In the anterior and the posterior groups, the peak ES tended to be lower than in the two-screw configuration, especially in the tibia. In general, the tibia presented higher peak values than the talus, as happened in the two-screw configuration. Inserting the third screw anteriorly tended to produce lower peak values in both bones than inserting the screw posteriorly, in the models with the two screws inserted at 30 degrees. The opposite was true for the models with the screws inserted at 60 degrees. Mixed results were observed in the model with the two screws inserted at 45 degrees, although the overall peak value was lower in the anterior group. In the anterior group, peak values in the talus were located around the different screw holes at the fusion site, while in the tibia they were found around the hole of the lateral screw at the fusion site. In the posterior group, peak values in the talus were located around the hole of the posterior screw at the fusion site and, in the tibia, around the proximal hole of the posterior screw.

When comparing the flat cut and intact arthrodeses, no clear trend was found for the peak equivalent strains in the two-screw configuration. When adding the third screw, slightly lower peak values were predicted in the intact arthrodesis in the anterior group, and mixed results were found in the posterior group. When comparing the screw configurations, the higher the crossing level and the smaller the insertion angle, the lower the peak ES in the two-screw configuration. This finding was also true in both the anterior and the posterior groups. Only in two models (60-beneath-P and I60-beneath-A), did the peak ES exceed the chosen yield limit, although this happened only in one element in each model. The rest of the models presented ES well below this limit.

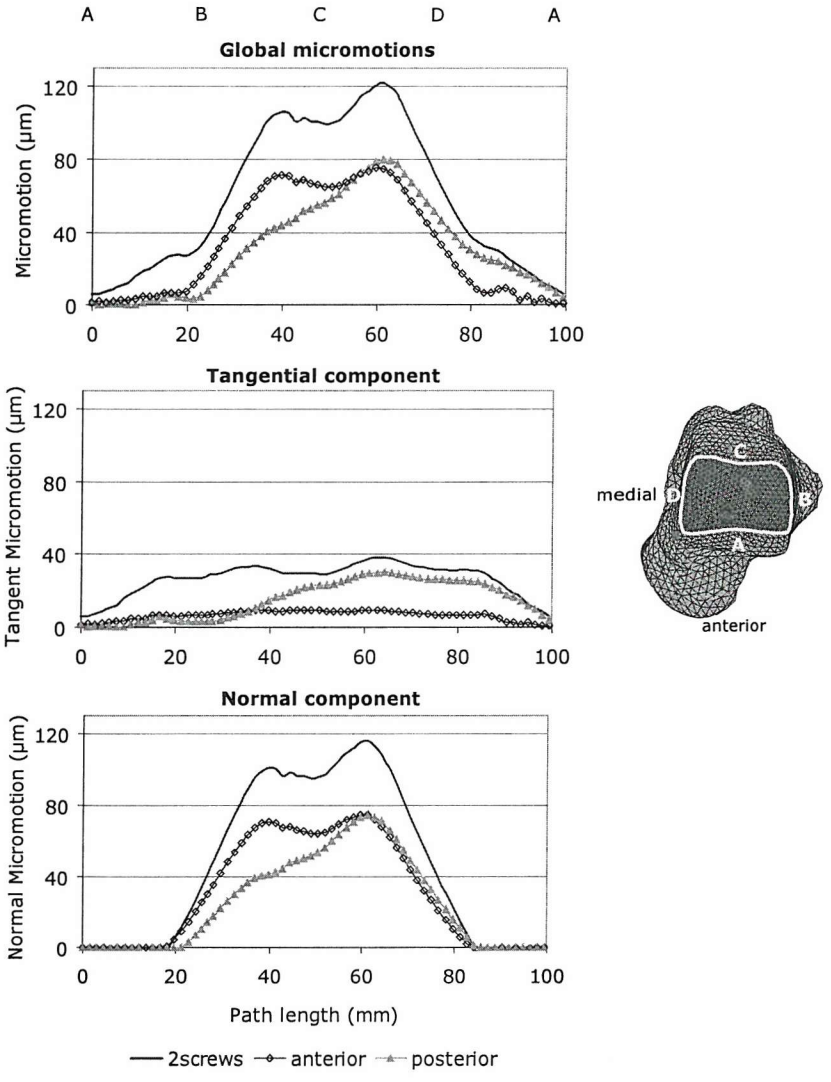

Figure 7.7 Global micromotions, tangential and normal components predicted along the edge of the fusion site for a two-screw configuration (45-on) and the corresponding models in the anterior and posterior groups (I45-on-A and I45-on-P). Dorsiflexion.

Table 7.7 Equivalent strain peak values (%) in the talus and the tibia for the anterior and posterior groups. Dorsiflexion.

	Anterior group	Talus	Tibia[d]	Posterior group	Talus[e]	Tibia[f]
Flat cut	30-above-A	0.17[a]	0.37	30-above-P	0.31	0.39
	45-on-A	0.30[b]	0.64	45-on-P	0.86	0.55
				60-beneath-P	0.64	1.05
Intact	I30-above-A	0.40 (0.24)[c]	0.27	I30-above-P	0.30	0.55[g]
	I60-beneath-A	0.69[b]	1.3	I60-beneath-P	0.65	0.95

[a] Peak value located around the hole of the anterior screw at the fusion site.
[b] Peak value located around the hole of the medial screw at the fusion site.
[c] Isolated peak value, maybe due to a badly shaped element (next peak value: as [a]).
[d] Peak values located around the hole of the lateral screw at the fusion site.
[e] Peak values located around the hole of the posterior screw at the fusion site.
[f] Peak values located around the proximal hole of the posterior screw.
[g] Peak values located by the antero-lateral edge of the fusion site.

7.4 DISCUSSION

Ogilvie-Harris et al.[119] had observed a greater resistance to torque in a 3-screw ankle arthrodesis as compared to a 2-screw configuration, measuring the gross motion between the tibia and the talus in several cadaver arthrodesis constructs. The objective of the current study was to compare the initial stability at the fusion site provided by 2 and 3-screw configurations. For a wider comparison than that performed by Ogilvie-Harris et al.[119], two different locations for the third screw were tested, in addition to the two surface preparation techniques. Only the most and least stable two-screw configurations in external torsion and dorsiflexion were included in this study.

The results obtained showed an overall better initial stability at the fusion site when a third screw was added, either anteriorly or posteriorly. In external torsion, the anterior screw produced lower peak micromotions than the posterior screw, except in the case of the most stable model (I30-above), where no significant differences were found. Also, the anterior screw reduced the differences in peak micromotions between the most and least stable models more than the posterior screw did, especially in the flat cut arthrodesis. When comparing the two surface preparation techniques, intact arthrodeses with three screws were more stable than flat cut arthrodeses with the same three-screw configuration.

In dorsiflexion, the posterior screw was expected to increase the initial stability more than the anterior screw, due to the gap developing towards the posterior area of the fusion site as a result of the postero-anterior force applied at the top of the tibia. Thus, in the intact arthrodesis, significantly lower peak micromotions were predicted in the posterior group than in the anterior group. However, similar levels of stability were observed in the flat cut arthrodesis, whether the third screw was inserted anteriorly or posteriorly. This behaviour was explained by the fact that although the peak normal micromotions were much lower around the postero-lateral area of the fusion site in the posterior group than in the anterior group, similar higher values were observed around the postero-medial area of the fusion site in both groups. In addition, the posterior screw increased the sliding on the same postero-medial area (see Figure 7.7, page 124). For the different screw configurations, and as happened with the two-screw fixation, the higher the crossing level and the smaller the insertion angle, the more stable the models both in the anterior and posterior groups. Although, as predicted in the torsion case, the differences between the most and least stable models were lower, especially in the posterior group, they were still substantial.

The patterns of equivalent strain distribution in the bones predicted in the three-screw models were similar to those observed in the two-screw configurations, i.e. ES concentrations were located around the screw holes at the fusion site in both bones, and around the proximal screw holes in the tibia. In dorsiflexion, some areas of ES concentration were also found along the anterior portion of the fusion site. In both load cases studied, the tibia could be at higher risk of bone failure as it generally presented the highest peak ES values. However, in most of the cases, the ES predicted were below the considered yield level. Some distorted elements may have caused some of the peak values predicted; however, as mentioned in Chapter 6, the automatic meshing of the bones made it difficult to avoid some badly shaped elements. The decrease in the peak micromotions when a third screw was added was generally coupled with a decrease in the peak ES in both load cases, showing a more uniform distribution of the load in the bones. The only exception were the models in the posterior group with a 30-degree insertion angle (30-above-P and I30-above-P) in external torsion, where higher values than in the corresponding two-screw models were predicted. However, these peak values occurred in two isolated elements around the proximal hole of the posterior screw in the tibia, and could have been caused by the boundary conditions defined to model the effect of the screw head. As was also observed in the peak micromotions, adding a third screw to the least stable models in the two-screw configuration reduced the peak ES more than adding it to the most stable models.

In most of the cases in external torsion, the peak values were located around the screw holes by the fusion site in both bones, as predicted in the two-screw configuration. However the load transfer was considerably different in the anterior and posterior groups, which could explain the differences in the predicted stability. Adding the third screw anteriorly produced the peak ES in the talus to occur around its hole, while adding it posteriorly, made the peak values occur around the hole of the medial screw. In the tibia, only adding the screw posteriorly produced a clear trend in the location of the peak ES, which tended to occur around the hole of the lateral screw. In dorsiflexion, adding the screw anteriorly produced peak ES located at the fusion site in the tibia, around the hole of the lateral screw, which is the screw situated most posteriorly. Adding the screw posteriorly produced most of the peak values located around its proximal hole in the tibia. It is worth noting that the part of the tibia where the posterior screw was inserted was close to the distal end of the bone and represented a lower Young's modulus than more proximal areas. The head of a screw inserted in such a position could put the bone at higher risk of failure. In the talus, only adding the screw posteriorly produced a clear trend in the location of the peak ES, which tended to occur around the hole of the posterior screw at the fusion site.

The convergence tolerance value was the only modelling parameter that had to be modified in order to reach a solution in some of the models included in this study (see Table 7.3, page 114). However, due to the low sensitivity shown by the micromotions to changes in the convergence tolerance (Chapter 5, page 74), this variation would account for less than a 2% difference. Therefore, it is unlikely to significantly affect the comparative results presented.

Summary of results

- Three-screw fixation predicted higher initial stability at the fusion site than two-screw fixation.
- Three-screw fixation also predicted better initial stability in the intact arthrodesis than in the flat cut arthrodesis.
- The third screw inserted anteriorly increased the initial stability more than inserted posteriorly in torsion, also producing lower strain values in the bones, possibly reducing the risk of bone failure. Only in the intact arthrodesis in dorsiflexion, did the posterior screw improve the stability more than the anterior screw.
- In a flat cut arthrodesis, the anterior screw seemed to offer overall better performance than the posterior screw as it produced more stable constructs with lower risk of bone failure.
- In an intact arthrodesis where the main concern was the torsional stability of the construct, an anterior screw seemed to be a better option, especially if the initial two-screw configuration presented screw insertion angles larger than 30 degrees. However, if the main concern was the stability in dorsiflexion, a posterior screw seemed to produce the most stable construct.

Chapter 8
INFLUENCE OF BONE QUALITY

8.1 INTRODUCTION

It has been shown that both age and disease affect bone quality (Chapter 2, page 27). Changes in the structure and composition of bone result in changes in its mechanical properties. Therefore, achieving a good clinical performance of orthopaedic devices used under such circumstances becomes more challenging.

Screw fixation in ankle arthrodesis can be compromised by poor bone quality, so that additional screws or alternative means of fixation may be needed to improve the rigidity of the arthrodesis construct. Screw fixation in poor quality bone is more likely to fail than in healthy bone. High correlations between different measures of screw fixation strength and bone mineral density have been reported as well as significant drops in the fixation strength when aged or diseased bone was considered. For instance, Okuyama et al.[120] obtained significant correlations between pull-out forces and tilting moments with bone mineral density, when studying the mechanical stability of transpedicle screws in the osteoporotic lumbar spine. They reported a 60 N decrease in the pull-out force of the screws when bone mineral density decreased by 10 kg m^{-3}. Halvorson et al.[55] reported averaged pull-out forces of 1540 ± 361 N and 206 ± 159 N in normal and osteoporotic vertebrae, respectively. No such data have been found in the literature regarding lower limb bones. Nevertheless, bone failure in the screw-bone system in ankle arthrodesis is also expected to follow a similar trend. Thordarson et al.[160,161] and Friedman et al.[46] found quality of bone to be a determinant of the rigidity of the in vitro ankle arthrodesis constructs they studied (Chapter 4, page 47). In cases of poor bone quality, Thordarson et al.[161] observed a slight enlargement of the screw holes in the cortex of the tibia during loading of the arthrodesis construct and screws becoming loose in some holes. As a result, larger gross motions between the tibia and the talus were recorded than in specimens with good bone quality. The use of the fibula as a strut graft, despite the poor purchase of the added screws in the cancellous bone, produced a substantial improvement in the rigidity of the arthrodesis construct.

In the analyses of the initial stability of ankle arthrodesis presented in Chapter 6 and Chapter 7, normal bone quality was assumed as the bone geometries and material properties were derived from the CT scan of a healthy ankle. Given the wide use of ankle arthrodesis in patient populations suffering from diseases such as rheumatoid arthritis,

osteoarthritis or osteoporosis (Chapter 3), and the changes in bone material properties that these diseases produce (Chapter 2, page 27), the following questions arise. How does bone quality affect the initial stability of ankle arthrodesis at the fusion site? What is the effect of poor bone quality on the differences in initial stability provided by different number of screws and different screw configurations? Does the relative importance of joint surface geometry on the initial stability increase when bone quality is poor?

In order to offer some insight in these issues, a parametric variation of the Young's moduli assigned to the bone elements was performed, following changes of Young's modulus with age and disease reported in the literature. The reduction of Young's modulus was applied to representative models of both the two and three-screw configurations of ankle arthrodesis constructs studied in the previous chapters.

8.2 MODELLING

Generally, FE analyses of orthopaedic problems are performed using models obtained from non-pathologic bones or built assuming material properties derived from experimental tests on non-pathological bone samples. In the relatively small number of FE analyses found in the literature involving poor bone quality, different approaches were taken. The most common approach [83,104,113,128] was to build FE meshes from non-pathologic bones, assigning homogeneous material properties obtained from experimental tests on healthy bone samples to the elements in the cortical and cancellous bone regions. Reductions in Young's modulus were later applied to simulate the pathologic cases, based on either data from mechanical tests of pathological bone samples or calculations relating bone density measurements in healthy and pathologic bone to Young's moduli. A second approach was to build FE meshes and assign heterogeneous material properties directly from non-pathologic bones, and later decrease by a certain amount the Young's modulus assigned to each element, based on experimental data of changes in bone density with disease [30,85]. Finally, FE models have also been built from pathologic bones, assigning heterogeneous material properties derived from the bone density of the actual bones [10].

Given the FE modelling process followed in this thesis, a similar procedure to the second approach described above was followed. Three patterns of Young's modulus (E) decrease were applied to the normal quality bone values originally assigned from the CT scan images (Chapter 5, page 58). A different variation was applied to cortical and cancellous Young's moduli in each case. A cut-off value of 7858 MPa, corresponding to a bone apparent density of 900 kg m^{-3}, was chosen to distinguish cortical from cancellous bone. Table 8.1 shows the percentage of decrease of the Young's modulus in each case and the source of the value. Case 1 represents the change in modulus due to age. Zioupos

and Currey [177] reported 2.3% decay per decade (from 35 years) for the Young's modulus of cortical bone from the femoral diaphysis. A value of 10% was chosen to represent the decay after 75 years. Ding et al.[38] reported around 26% decay in the Young's modulus of cancellous bone from proximal tibias between a middle age group (40 to 59 years) and an old age group (60 to 83 years). Case 2 represents the reduction of modulus due to osteoporosis. Polikeit et al.[128] and Natarajan et al.[113] simulated the material properties of osteoporotic human vertebrae decreasing by one third and two thirds the normal modulus for cortical and cancellous vertebral bone, respectively. These values were based on calculations relating bone mineral density values obtained in healthy and osteoporotic vertebrae to Young's moduli. The most extreme case of modulus reduction (Case 3) represents that of rheumatoid arthritic bone. Dalstra et al.[30] simulated rheumatoid arthritic glenoids (part of the shoulder joint) by reducing normal modulus values by 50 and 90% for cortical and cancellous bone, respectively. These values were based on experimental measures of bone density in normal and rheumatoid arthritic glenoids.

Table 8.1 Percentages of Young's modulus decrease for cortical and cancellous bone used to define the three cases of poor bone quality studied. Literature source, cause of the poor bone quality and anatomical location are provided for each value.

Name	Cortical bone	Source Cause* / Location	Cancellous bone	Source Cause* / Location
Case 1	**10** %	Zioupos & Currey [177] Age / femoral diaphysis	**26** %	Ding et al.[38] Age / proximal tibia
Case 2	**33** %	Polikeit et al.[128] OP / vertebra	**66** %	Polikeit et al.[128] and Natarajan et al.[113] OP /vertebra
Case 3	**50** %	Dalstra et al.[30] and Lacroix et al.[85] RA / glenoid	**90** %	Dalstra et al.[30] and Lacroix et al.[85] RA / glenoid

* OP = osteoporotic bone, RA = rheumatoid arthritic bone.

In the first part of this parametric study, the three cases of poor bone quality were applied to a selection of the two-screw ankle arthrodesis models studied in Chapter 6. The most and least stable models in the flat cut and intact groups were chosen in the external torsion and dorsiflexion load cases. External torsion and dorsiflexion were simulated as done in the previous chapters; internal torsion was not included as it predicted lower micromotions than external torsion. In the second part of this study, one case of poor bone quality (Case 2) was applied to a selection of the three-screw ankle arthrodesis

models studied in Chapter 7. These models were the most and least stable models in the anterior and posterior groups, also in the external torsion and dorsiflexion load cases. Table 8.2 lists all the models included in the study.

Table 8.2 Models included in the parametric study of bone quality*.

2-screw fixation		3-screw fixation	
External torsion	**Dorsiflexion**	**External torsion**	**Dorsiflexion**
	Flat-cut		
30-above	30-above	30-above-A	30-above-A
		30-above-P	30-above-P
45-on	60-beneath	45-on-A	†
		45-on-P	60-beneath-P
	Intact		
I30-above	I30-above	I30-above-A	I30-above-A
		I30-above-P	I30-above-P
I45-on	I60-beneath	I45-on-A	I60-beneath-A
		I45-on-P	I60-beneath-P

* See Chapter 6 and Chapter 7 for a description of each model.
† Model not built. Not possible to add the anterior screw without interfering with the other two screws.

All the models were run in Marc 2001, with the same boundary conditions and contact parameters as described in Chapter 5. In some cases, the convergence tolerance initially considered (0.01) had to be varied to reach a solution. Values ranged from 0.015 to 0.05 (Table 8.3). Given the low sensitivity of the models to the variation of this parameter shown in Chapter 5 (page 74), the effect of the increase of the convergence tolerance is unlikely to affect the comparative results between the models, as it would account for less than 2% difference in the micromotions at the fusion site.

Table 8.3 Convergence tolerance values used when different from 0.01.

Model	Case 1	Case 2	Case 3
2-screw			
30above	-	0.04 (T)	0.05 (T)
I-30above	0.015 (T)	-	-
I-45on	-	0.015 (T)	-
3-screw			
45on-A	-	0.02 (T, D)	-
45on-P	-	0.02 (D)	-

T = External torsion, D = Dorsiflexion.

8.3 RESULTS

8.3.1 Two-screw fixation

8.3.1.1 External torsion

Decreasing the Young's modulus produced a uniform increase in the micromotions predicted at the fusion site in each model. The distribution of the micromotions at the fusion site was very similar to that predicted with normal quality bone, with peak values located along the periphery of the fusion site (see Figure 6.5, page 89), and, therefore, they are not shown. Table 8.4 compares the changes in the peak micromotions predicted at the fusion site between normal bone quality and the three cases of reduced Young's moduli. Aged bone (Case 1) produced increases in the peak micromotions between 13 and 18%, with values ranging from around 100 to 225 μm; osteoporotic bone (Case 2) produced increases between 59 and 80%, with values ranging from around 150 to 300 μm; and rheumatoid arthritic bone produced much larger increases, ranging from 157 to 215%, with very large peak micromotions, even above 500 μm.

Table 8.4 Peak micromotions (μm) predicted at the fusion site in two-screw fixation models, for different decreased levels of bone Young's moduli. External torsion.

	Model	Normal	Case 1*	Case 2*	Case 3*
Flat cut	30-above	146	166 **14%**	238 **63%**	375 **157%**
	45-on	200	225 **13%**	317 **59%**	524 **162%**
Intact	I30-above	87	103 **18%**	157 **80%**	274 **215%**
	I45-on	169	197 **17%**	294 **74%**	512 **203%**

* Percentage of change in the micromotions relative to the normal bone quality.

Intact arthrodesis always predicted lower peak micromotions than flat cut arthrodesis, although the worse the bone quality the lower the differences between both surface preparation techniques. With normal quality bone, resecting the joint surfaces meant increases in the peak micromotions of 68 and 18% in the most and least stable models, respectively; in the worst case of bone quality, these increases were reduced to 37% and

2% respectively. When comparing between the screw configurations, the differences predicted with normal quality bone did not change in any of the cases of poor bone quality. The peak micromotions predicted in the least stable models (45-on and I45-on) were around 1.4 and 1.9 times those predicted in the most stable models (30-above and I30-above), in the flat cut and intact group respectively. In all the levels of bone quality, the model I30-above predicted the lowest peak micromotions.

The motion between the bones at the fusion site followed similar patters as predicted with normal quality bone (Chapter 6, page 91). Most of the motion at the fusion site in all the cases of poor bone quality was due to sliding (tangential component), both in the intact and flat cut arthrodeses, although a small gap (normal component) also developed at the fusion site (Figure 8.1). In the flat cut models, the gap tended to be smaller towards the antero-medial area of the fusion site and only small areas between the two bones remained in contact. In the intact models, postero-medial and antero-lateral areas of the fusion site remained in contact, with gaps opening towards the opposite areas, as happened with normal quality bone. The more the Young's modulus decreased, the larger the sliding and the gap. However, the ratio between both micromotion components along the edge of the fusion site remained almost constant within each model, in both intact and flat cut arthrodeses.

The patterns of equivalent strain (ES) distribution in the bones were similar to those in the normal bone quality, with areas of ES concentration located around the holes of the screws at the fusion site in both bones and around the proximal holes in the tibia (see Figure 6.8, page 94). In the intact arthrodesis, additional patches of ES concentration were found in the contact areas (antero-lateral and postero-medial areas of the fusion site). As bone quality worsened, higher ES values were predicted. The areas around the ends of the screw holes became larger, expanding along the inside of the holes. In case 3, areas of strain concentration were also found along the parts of the talus glued to the screws. Table 8.5 (page 137) shows the comparison of the peak ES predicted when decreasing the Young's moduli. Peak values followed similar trends to those predicted in the peak micromotions. In each model, the more the Young's modulus decreased, the larger the peak ES in both bones and the larger the increases relative to the normal quality bone. Tibial peak values were always larger than talar peak values. Resecting the joint surfaces meant an increase of the peak ES in all the levels of bone quality. Regarding the screw configurations, the most stable models (30-above and I30-above) always predicted lower peak ES than the corresponding least stable models (45-on and I45-on), in both bones. In general, higher peak ES in both bones always corresponded with higher peak micromotions at the fusion site; only in the worst case of bone quality, the model 45-on predicted a lower peak ES than the model I45-on, despite predicting slightly higher peak micromotions.

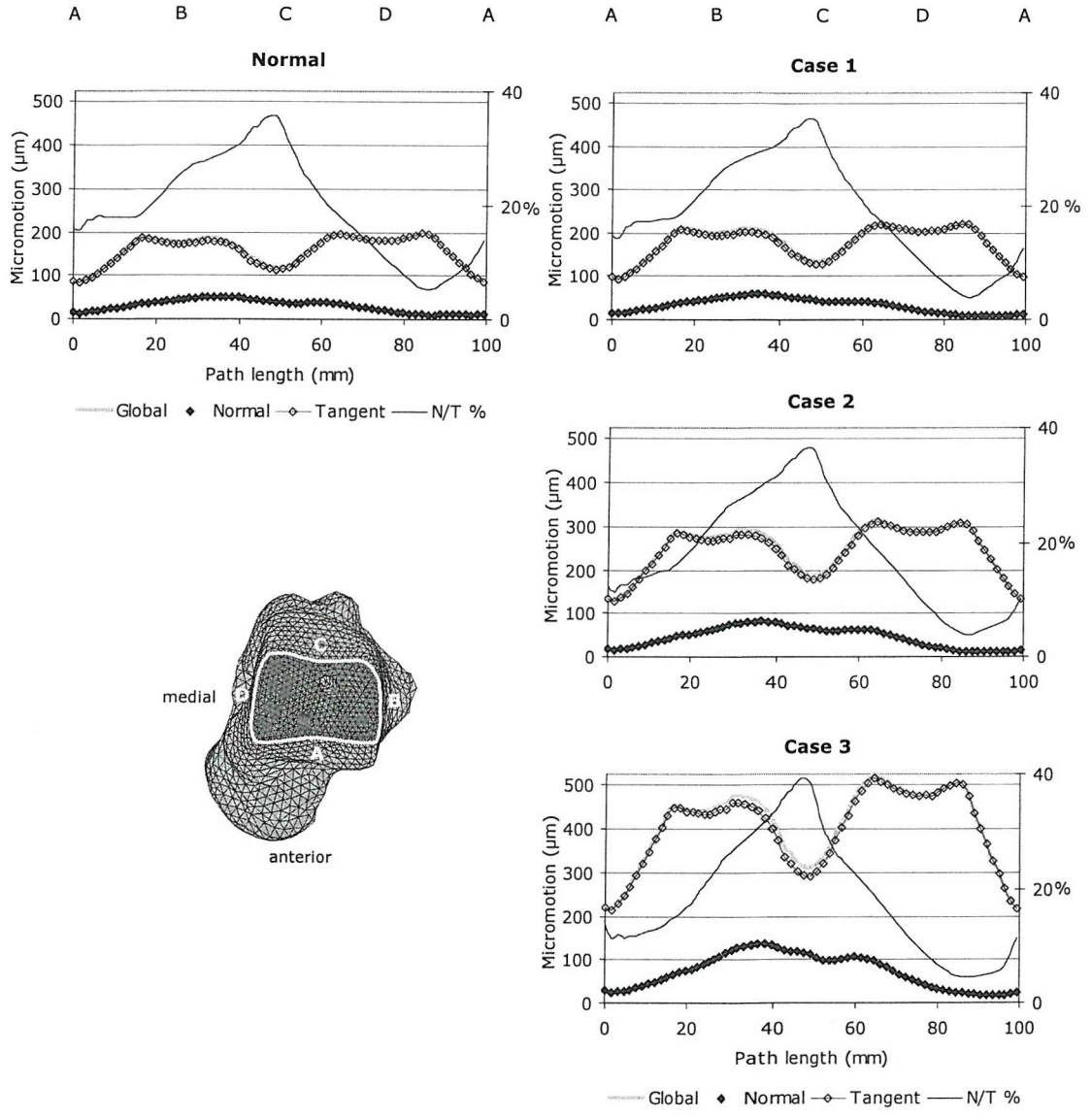

Figure 8.1 Micromotions, normal and tangential components along the edge of the fusion site in the normal and poor bone quality cases. Values predicted in external torsion in a model from the flat cut group (45-on). N/T% is the percentage ratio between the normal and tangent components.

Almost all the models predicted peak ES above the considered yield level (1%). As explained in Chapter 6, the number of elements with ES above 1% in the normal quality bone was extremely reduced. However, as the bone quality worsened, the number of elements gradually increased and the peak values reached values well beyond the yield and ultimate strain values reported for human bones (Table 2.3, page 23). The volume of elements with ES above 1% was calculated in each model and it is displayed in Figure 8.2

(page 138) as a percentage of the total bone volume. The percentage volumes of failed elements below 0.001% were not considered relevant, as it always involved a very low number of elements (less than 5 elements) and could have been caused by isolated distorted elements. Figure 8.2 also shows the areas of the failed volumes in each case. Only the model 45-on predicted substantial failed volumes in all the cases of normal and poor bone quality studied; this model was also the least stable in all the cases. The other model in the flat cut arthrodesis (30-above) predicted failed volumes in the three cases of poor bone quality. Although the failed volumes were larger than those predicted in the model I45-on, the peak micromotions in the former were always lower than in the latter. The model I30-above predicted substantial failed volume only in the worst case of bone quality; this model was the most stable model in all the cases studied.

Table 8.5 Comparison of peak equivalent strains predicted in the tibia and the talus for different cases of bone quality in two-screw arthrodesis. Peak ES (%) in the bones and percentage increase relative to the normal quality bone (shown in italics) in external torsion.

	Model	Talus[a]						Tibia[b]					
		Normal	Case1		Case2		Case3	Normal	Case1		Case2		Case3	
Flat cut	30-above	0.35	0.39	*11%*	0.53	*51%*	1.05[c] *200%*	1.10	1.35	*23%*	2.10	*91%*	3.78	*244%*
	45-on	0.58	0.71	*22%*	1.25	*116%*	3.00 *417%*	1.27	1.60	*26%*	2.27	*79%*	4.57	*260%*
Intact	I30-above	0.24	0.36	*50%*	0.41	*71%*	0.83 *246%*	0.61	0.84	*38%*	1.40	*130%*	2.90	*375%*
	I45-on	0.46	0.55	*20%*	0.89	*93%*	1.90 *313%*	1.10	1.40	*27%*	2.27	*106%*	5.12	*365%*

[a] Peak values located around the hole of the medial screw at the fusion site unless stated otherwise.
[b] Peak values located around the hole of the lateral screw at the fusion site unless stated otherwise.
[c] Peak value located along the area of the hole of the lateral screw glued to the screw.

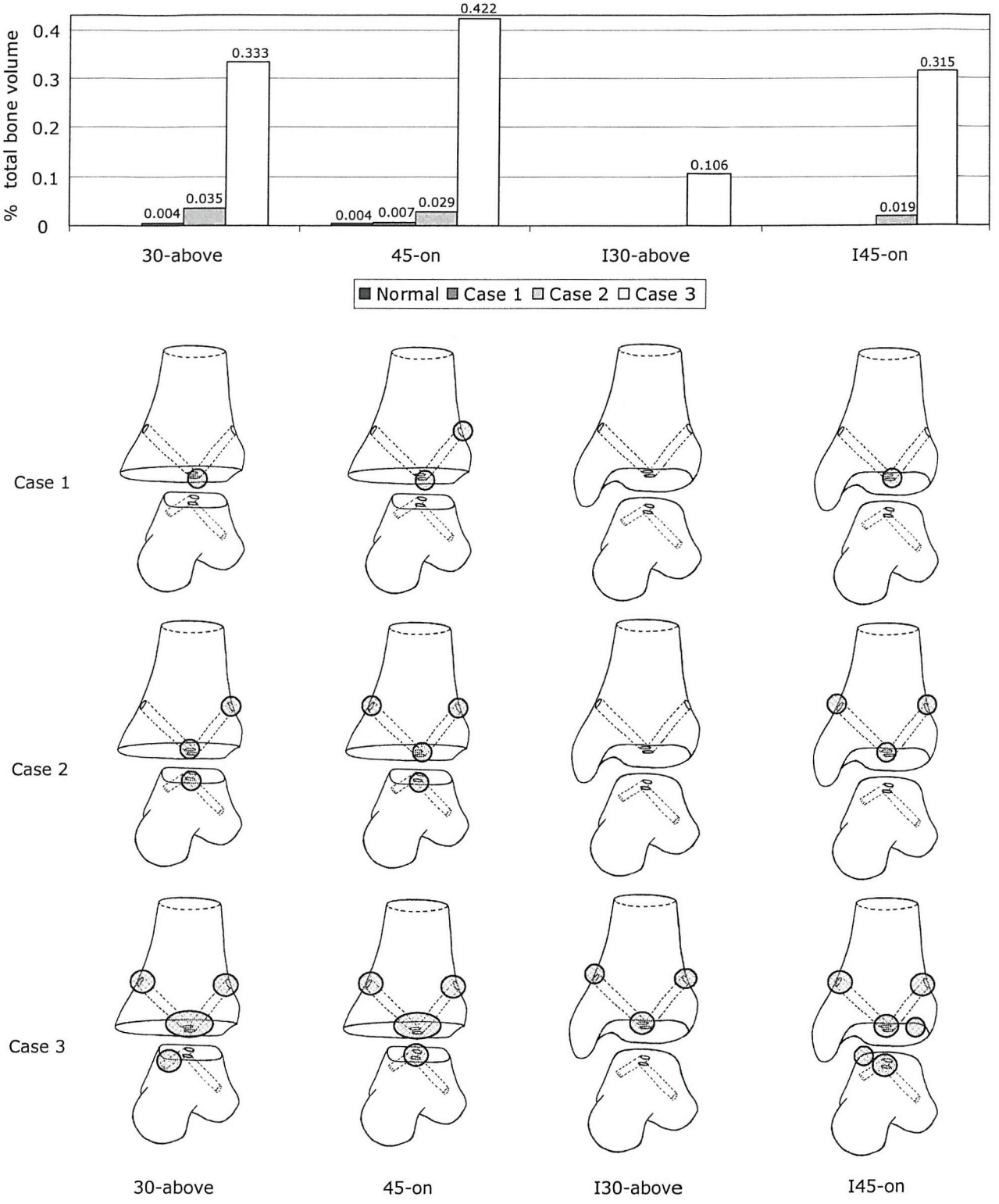

Figure 8.2 Graph representing the % of the total bone volume above yield strain (1%) in each model and case of bone quality, in external torsion. Below, schematic representation of the areas of bone failure in each model (frontal view of the bones, separated for clarity).

8.3.1.2 Dorsiflexion

Table 8.6 compares the peak micromotions predicted at the fusion site between the normal and poor bone quality models. The distribution of the micromotions at the fusion site followed the same pattern as with normal quality bone, with the peak micromotions located towards the posterior edge of the fusion site (see Figure 6.9, page 97). Aged bone produced increases in the peak micromotions between 16 and 27%; osteoporotic bone increased the peak micromotions between 65 and 112%; and much larger increases were predicted for the rheumatoid bone, ranging from 167 to 399%. Differences in the peak micromotions between the intact and the flat cut arthrodeses rapidly decreased for decreasing values of the Young's modulus. No substantial differences were predicted between the most stable models (30-above and I30-above), as the peak micromotions differed in the same or less amount than the estimated model error (5 μm). In the case of the least stable models (60-beneath and I60-beneath), resecting the joint surfaces produced a 38% increase in the micromotions in the normal bone quality and 33, 20 and 3% decreases as quality bone worsened. The worse the bone quality, the larger the differences between the screw configurations. With normal quality bone, the least stable models had produced peak micromotions 4 and 5 times those predicted by the most stable models, in the intact and flat cut arthrodeses. For the poorest bone quality, the peak micromotions were 7 times larger in both surface preparation techniques, reaching values as high as 1000 μm in the least stable models.

Table 8.6 Peak micromotions (μm) predicted at the fusion site in two-screw fixation models, for different decreased levels of bone Young's moduli. Dorsiflexion.

	Model	Normal	Case 1*		Case 2*		Case 3*	
Flat cut	30-above	55	64	**16%**	91	**65%**	147	**167%**
	60-beneath	274	325	**19%**	502	**83%**	1017	**271%**
Intact	I30-above	49	62	**27%**	89	**82%**	146	**198%**
	I60-beneath	198	244	**23%**	420	**112%**	989	**399%**

* Percentage of change in the micromotions relative to the normal bone quality.

The pattern of motion between the bones at the fusion site did not change much from the normal quality bone (Chapter 6, page 98), with most of the motion due to the opening gap towards the back of the fusion site, leaving contact areas towards the anterior part of the fusion site. Some sliding (tangential component) was observed in the contact areas. Nevertheless, some variations were observed as the bone quality worsens. In the flat cut

arthrodesis, the more the Young's modulus decreased, the larger the normal components along the posterior edge of the fusion site. The tangential component along the edge of the fusion site, also increased as the Young's modulus decreased in the model 30-above; in the model 60-beneath, the tangential component in the non-contact areas did not change from the normal quality bone except in the worst bone quality, while in the contact areas followed the same trend as in 30-above. In the non-contact areas, the median tangential/normal component ratio gradually increased from 29% in the normal bone quality up to 56% in case 3 in model 30-above, but decreased from 12% in the normal case to 5% in case 3 in model 60-beneath. In the intact arthrodesis, the more the Young's modulus decreased, the larger both micromotion components along the edge of the fusion site. The tangential/normal ratio along the non-contact areas gradually increased in the model I30-above, and slightly decreased in the model I60-beneath. Figure 8.3 shows an example of the change in the micromotion components along the edge of the fusion site.

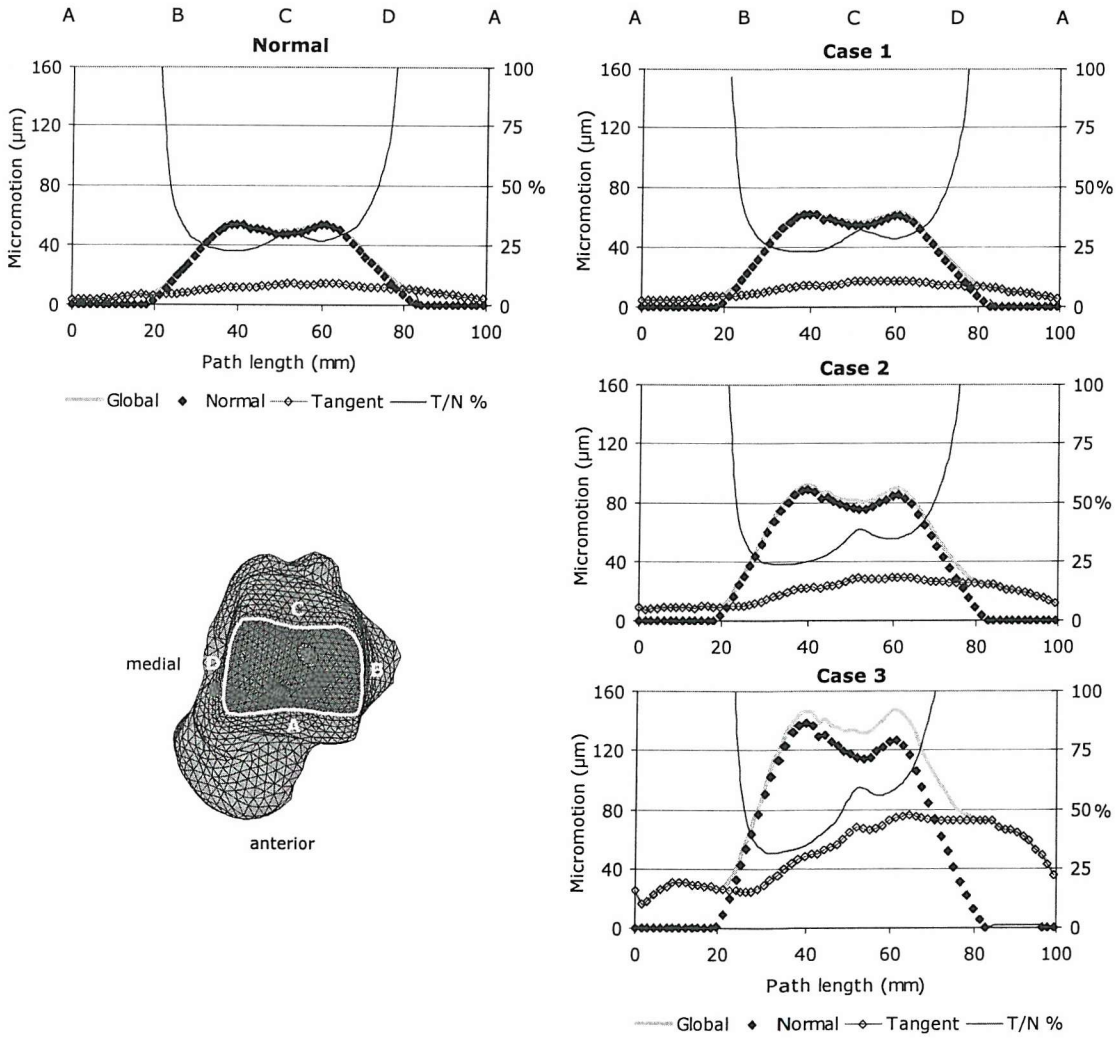

Figure 8.3 Micromotions, normal and tangential components along the edge of the fusion site in normal and poor bone quality, in dorsiflexion. Data from a model in the flat cut group (30-above). T/N% is the ratio between the tangent and normal components.

The patterns of equivalent strain (ES) distribution in the bones were similar to those predicted in the normal quality bone (Chapter 6, page 98). The talus presented areas of ES concentration along the anterior parts of the fusion site, around the screw holes at the fusion site and along the areas glued to the screws, especially the lateral one. The tibia presented areas of ES concentration around the proximal and distal ends of the screw holes and along the anterior parts of the fusion site. As bone quality worsened, these areas became larger and higher ES values were predicted. Table 8.7 compares the peak ES predicted in both bones for the different levels of bone quality. In each model, the poorer the bone quality, the larger the peak ES in both bones and the larger the increases relative to the normal case. Tibial peak values were always larger than talar peak values, in all the models, especially in those with 60-degrees insertion angles. Unlike in the torsion load case, mixed results were observed when comparing the surface preparation techniques. Between the most stable models (30-above and I30-above), differences in peak ES were very small in the normal quality bone and case 1; the intact model predicted lower peak values in the talus but larger peak values in the tibia than the flat cut model, in cases 2 and 3. Between the least stable models (60-beneath and I60-beneath), the intact model predicted larger peak ES in the talus but lower peak ES in the tibia than the flat cut model in all cases of bone quality; except in case 3, where the tibia presented higher peak ES in the intact model than in the flat cut model. When comparing the screw configurations, the peak ES predicted in the most stable models was always lower than in the corresponding least stable models, following the same trend as the peak micromotions; the differences increased as bone quality worsened, with peak values in the least stable models being much larger than the reported values of yield and ultimate strain.

Figure 8.4 (page 143) displays the volume of bone above the yield level of 1% relative to the total bone volume. Schematic figures also show the location of the failed volumes. In the case of normal bone quality, only the model 60-beneath predicted a substantial, though still small, number of elements with ES above the yield level (Chapter 6, page 99), located around the proximal and distal ends of the lateral screw in the tibia. As the bone quality worsened, the volumes of failed elements and the regions affected increased, especially in the least stable models, those with the screws inserted at 60 degrees. The most stable models only presented failed volumes with the poorest bone quality; the volumes were much smaller than in the corresponding least stable models. The model 60-beneath presented the larger volumes of failed elements with all the levels of bone quality, being always the least stable model.

Table 8.7 Comparison of peak equivalent strains predicted in the tibia and the talus for different cases of bone quality in 2-screw arthrodesis. Peak ES (%) in the bones and percentage increase relative to the normal quality bone (shown in italics) in dorsiflexion.

	Model	Talus[a]						Tibia[a]					
		Normal	Case1		Case2		Case3	Normal	Case1		Case2		Case3
Flat cut	30-above	0.24[b]	0.31[b]	*29%*	0.60[c]	*150%*	1.77[c] *638%*	0.52	0.64	*23%*	0.99	*90%*	1.92 *269%*
	60-beneath	0.62[d]	0.76[d]	*23%*	1.27[d]	*105%*	3.01[d] *385%*	1.84	2.29	*24%*	4.03	*119%*	10.81 *488%*
Intact	I30-above	0.25	0.29	*16%*	0.55	*120%*	1.19 *376%*	0.55[b]	0.69[b]	*25%*	1.18[b]	*115%*	2.59[b] *371%*
	I60-beneath	0.67	0.88	*31%*	1.77	*164%*	4.50 *572%*	1.56	2.14	*37%*	3.81	*144%*	11.36 *628%*

[a] Peak values located around the hole of the lateral screw at the fusion site unless stated otherwise.
[b] Peak values located at the anterior area of the fusion site.
[c] Peak values located along the area of the hole of the lateral screw glued to the screw.
[d] Peak values located around the hole of the medial screw at the fusion site.

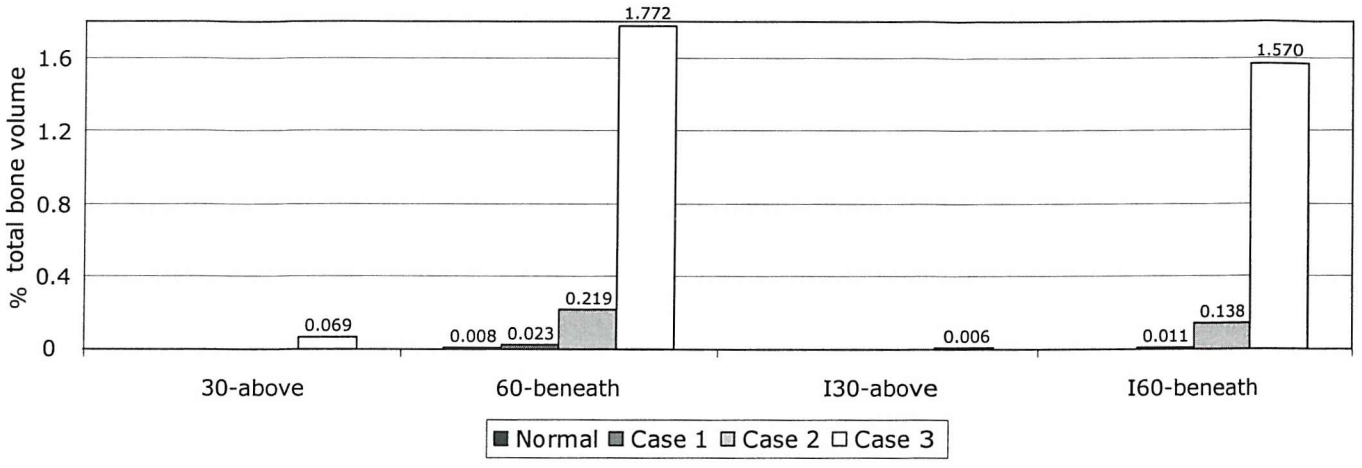

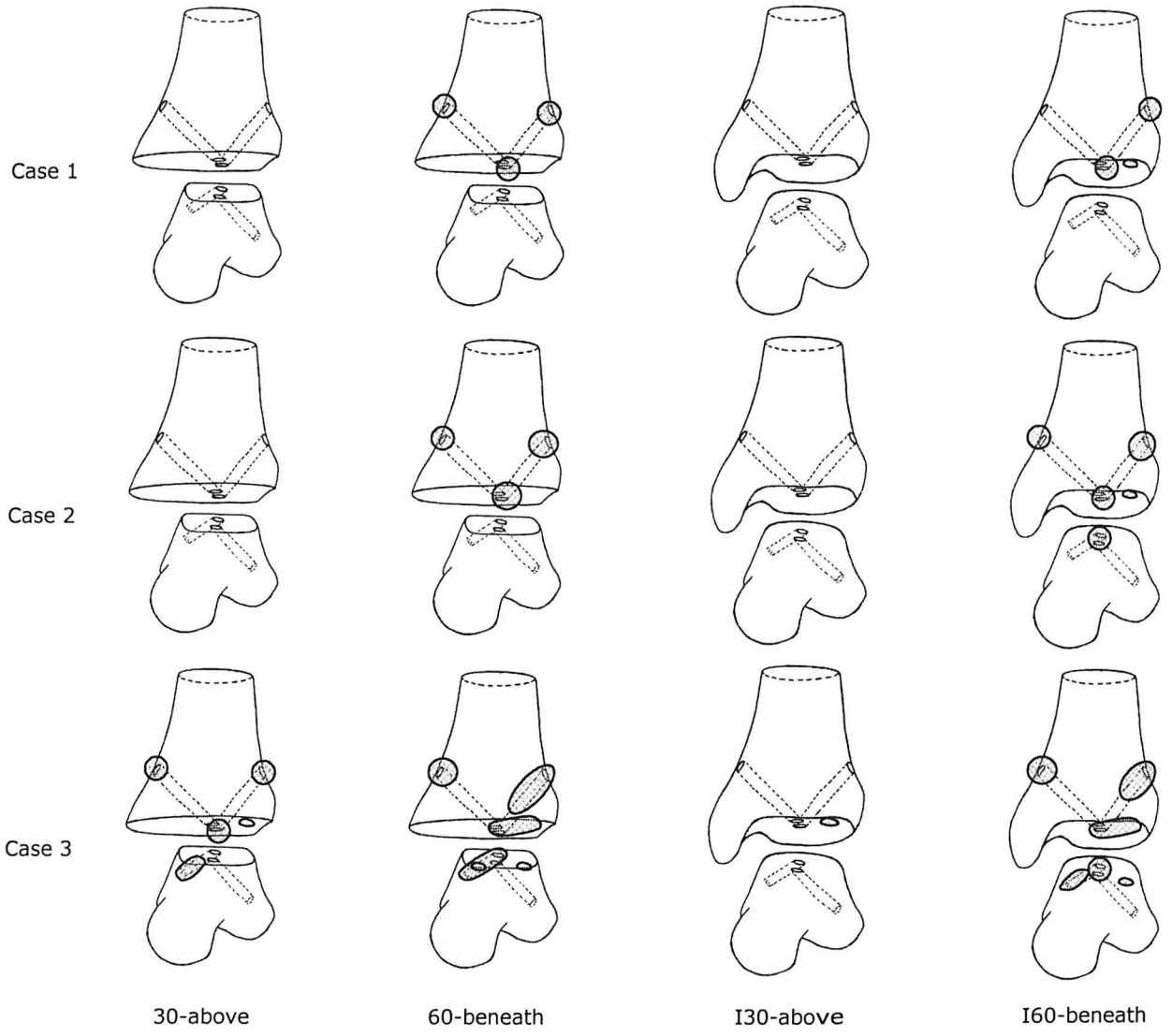

Figure 8.4 Graph representing the % of the total bone volume above yield strain (1%) in each model and case of bone quality, in dorsiflexion. Below, schematic representation of the areas of bone failure in each model (frontal view of the bones, separated for clarity).

8.3.2 Three-screw fixation

The results obtained in the two-screw configuration, presented in the previous section, showed a substantial deterioration of the initial stability predicted at the fusion site as bone quality worsened. This was especially true for the cases 2 and 3, simulating osteoporotic and rheumatoid arthritic bone quality, where substantial areas of the bones were likely to have failed. Given the number of models to be checked (Table 8.2, page 132), only one case of poor bone quality was used to assess its effect on the three-screw fixation. Case 2 was chosen as an intermediate level of poor bone quality, but having predicted considerable decreases in stability (above 50%).

8.3.2.1 External torsion

Table 8.8 compares the peak micromotions predicted at the fusion site between the normal and osteoporotic bone quality in the models with three-screw fixation. The distribution of the micromotions at the fusion site followed the same patterns as in the normal bone quality (Figure 7.3, page 117). Reducing the Young's modulus produced a uniform increase of the micromotions throughout the fusion site, with increases in the peak micromotions ranging from 66 to 89%. All the models in the anterior group predicted lower peak micromotions than the corresponding models in the posterior group when bone quality was poor. Peak micromotions in the posterior group were between 1.2 and 1.3 times those in the anterior group. The same trend had been predicted with normal quality bone, except for the comparison between the most stable models (I30-above-A and I30-above-P).

Comparing the surface preparation techniques, flat cut arthrodesis with three screws always predicted larger peak micromotions than intact arthrodesis in the case of poor bone quality, as predicted with normal quality bone. Resecting the joint surfaces produced larger increases in peak micromotions in the posterior than in the anterior group with normal quality bone; these differences decreased when bone quality was poor. As predicted with normal quality bone, the differences between both techniques were larger in the models with a 30-degree insertion angle for the two crossed screws than in those with a 45-degree insertion angle. Poor bone quality did not affect the stability provided by the three screws when comparing the two-screw configurations. Thus, in both anterior and posterior groups, models with the two screws inserted at 45 degrees always predicted larger peak micromotions than the corresponding models with the screws inserted at 30 degrees; the differences were larger in the posterior group.

Table 8.8 Peak micromotions (μm) predicted at the fusion site in three-screw fixation models, for the normal and one case of decreased levels of bone Young's moduli. External torsion.

	Model	Normal	Case 2*	
Flat cut	30-above-A	91	154	**69**%
	30-above-P	111	184	**66**%
	45-on-A	95	166	**75**%
	45-on-P	131	221	**69**%
Intact	I30-above-A	60	105	**75**%
	I30-above-P	65	123	**89**%
	I45-on-A	81	146	**80**%
	I45-on-P	107	194	**81**%

* Percentage of change in the micromotions relative to the normal bone quality.

Worsening the bone quality did not substantially change the pattern of motion between the two bones in the models with three-screw fixation (Chapter 7, page 116). The reduction of the Young's moduli resulted in an increase of the sliding (tangential component) throughout the fusion site and an increase of the gap (normal component) at the non-contact areas, both in the anterior and posterior groups and the intact and flat cut arthrodeses. However, the ratio between both micromotion components along the edge of the fusion site did not change much relative to the normal quality bone. Figure 8.5 shows an example of the change in the micromotion components along the edge of the fusion site.

The distribution of the equivalent strain in the bones in the case of poor bone quality was similar to that predicted in the normal case (Figure 7.5, page 119) and an expected increase in the values was observed. Table 8.9 (page 147) displays the change in the ES peak values. The location of the peak values in both bones was the same than with normal bone quality. Again, as predicted with normal bone quality, peak values in the tibia were higher than in the talus and anterior insertion of the third screw produced lower peak values than posterior insertion, in both bones. The only exception was the model I45-on-P which predicted higher peak ES in the tibia than the model I45-on-A. Resecting the joint surfaces also produced an increase in the peak ES, except in the comparison between I45-on-A and 45-on-A.

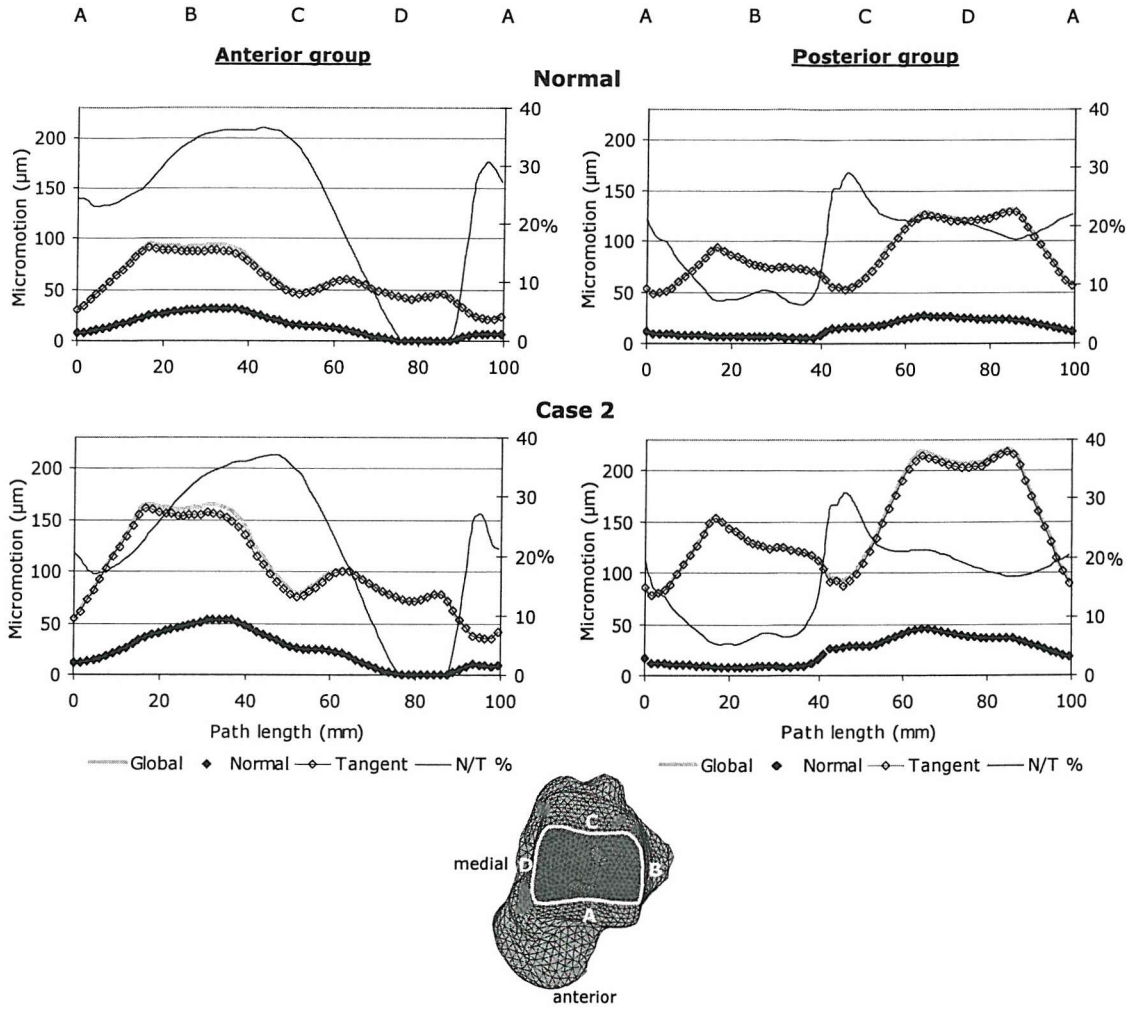

Figure 8.5 Micromotions, normal and tangential components along the edge of the fusion site in the normal and poor bone quality cases, in external torsion. Data from models in the anterior group (45-on-A) and posterior group (45-on-P). N/T% is the percentage ratio between the normal and tangent components.

Figure 8.6 (page 148) displays the volume of elements with ES above the yield limit relative to the total bone volume, as well as the location of the failed bone. Models in the posterior group always presented larger volumes of failed bone than the corresponding models in the anterior group. Only in the posterior group, did the talus show failed bone volumes, which were always located around the hole of the posterior screw at the fusion site. It is worth noting that the three models that did not show volumes of failed elements (I30-above-A, I30-above-P and I45-on-A) predicted, in this order, the lowest peak micromotions at the fusion site.

Table 8.9 Comparison of peak equivalent strains predicted in the tibia and the talus for two cases of bone quality in three-screw arthrodesis. Peak ES (%) in the bones and percentage increase relative to the normal quality bone (shown in italics) in external torsion.

Anterior group	Talus[a]			Tibia[b]				Posterior group	Talus[c]			Tibia[d]		
	Normal	Case 2		Normal	Case 2				Normal	Case 2		Normal	Case 2	
30-above-A	0.31	0.57	*84%*	0.77	1.40	*82%*	*Flat cut*	30-above-P	0.88	1.49	*69%*	1.76[f]	3.04[f]	*72%*
45-on-A	0.33	0.53	*61%*	0.72	1.20	*67%*		45-on-P	0.77	1.76	*129%*	1.15	2.17	*89%*
I30-above-A	0.26	0.73[d]	*181%*	0.67[e]	1.25[e]	*87%*	*Intact*	I30-above-P	0.54	1.04	*93%*	0.82[f]	1.89[f]	*130%*
I45-on-A	0.46	0.65	*41%*	0.46[d]	1.45[e]	*215%*		I45-on-P	0.72	1.34	*86%*	0.56	1.25	*123%*

[a] Peak values located around the hole of the anterior screw at the fusion site unless stated otherwise.
[b] Peak values located around the hole of the medial screw at the fusion site unless stated otherwise.
[c] Peak values located around the hole of the posterior screw at the fusion site.
[d] Peak values located around the hole of the lateral screw at the fusion site unless stated otherwise.
[e] Peak values located at the anterior area of the fusion site.
[f] Peak values located around the proximal end of the posterior hole.

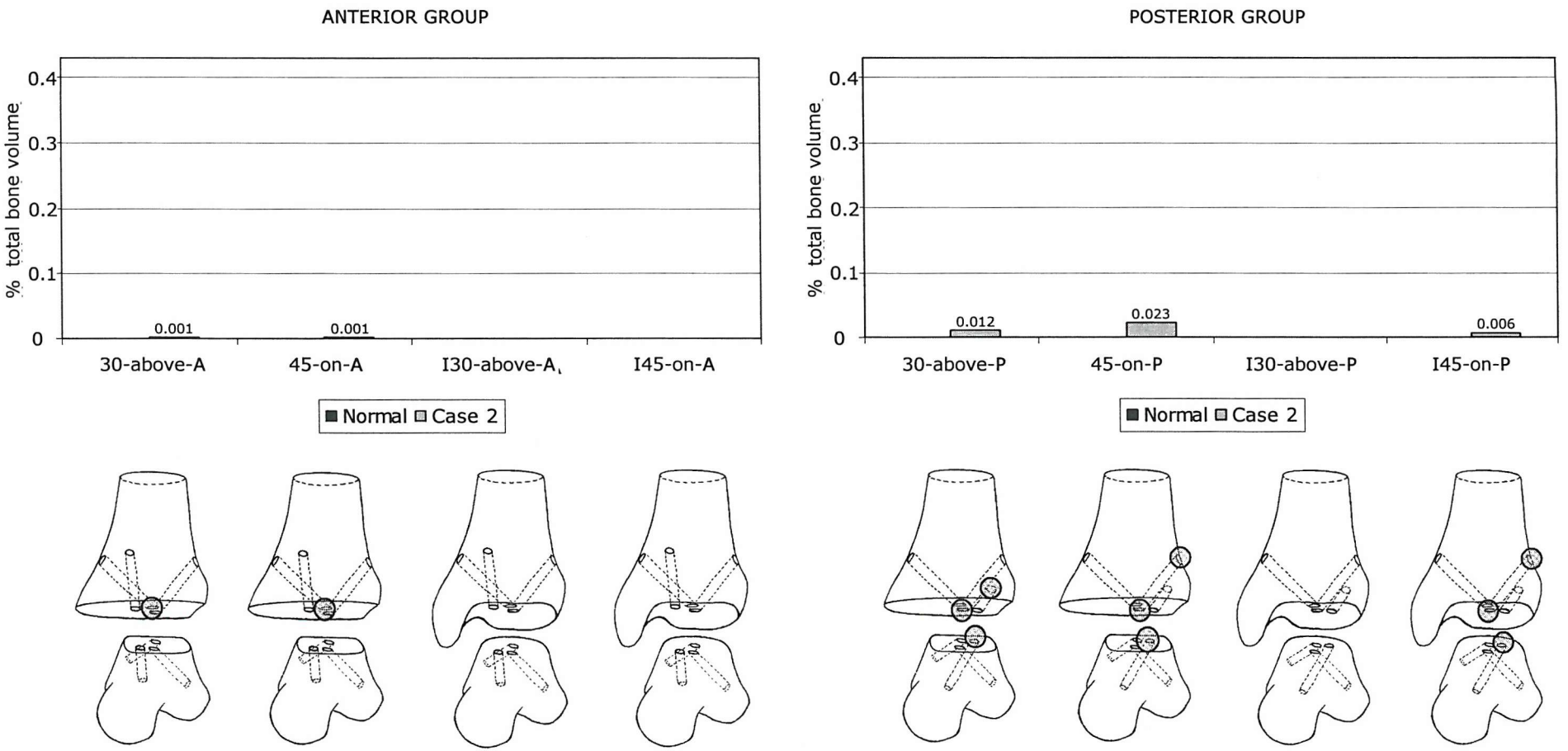

Figure 8.6 Graph representing the % of the total bone volume above yield strain (1%) in each model in external torsion. Below, schematic representation of the areas of bone failure in each model (frontal view of the bones, separated for clarity). Note: for comparative purposes, the scale of the graph was kept the same as in Figure 8.2.

Comparing these results with those obtained in the two-screw fixation for the same case of poor bone quality (section 8.3.1.1, page 133) showed that the addition of the third screw always reduced the peak micromotions, as happened with normal bone quality. And similar percentages of reduction were observed in both anterior and posterior groups. As for the equivalent strain, it was found that adding a third screw anteriorly reduced the volumes of failed bone and the number of areas affected as compared to the 2-screw configuration (see Figure 8.2, page 138). This was also reflected in the lower peak ES predicted in the models of the anterior group. Adding the third screw posteriorly also produced a reduction of the failed volumes, although lower than in the anterior group. This reduction was only reflected in the lower peak ES predicted in the models 45-on-P and I45-on-P; higher peak ES was predicted in the models 30-above-P and I30-above-P than in the corresponding two-screw models, although the number of elements affected was lower.

8.3.2.2 Dorsiflexion

Table 8.10 shows the changes in the peak micromotions at the fusion site when bone quality was reduced in the models with three-screw fixation. The distribution of the micromotions at the fusion site followed the same patterns as with normal quality bone (Figure 7.6, page 122), with peak values located along the posterior part of the fusion site in the anterior group and in the postero-medial part in the posterior group. The poorer bone quality produced a uniform increase of the micromotions at the fusion site, with median percentages of increase relative to the normal bone quality very similar to those reported for the peak micromotions. These increases were larger in the models in the posterior group. With normal quality bone, no differences were predicted between the models 30-above-A and 30-above-P; when the bone quality was poor, 30-above-A predicted lower peak micromotions than 30-above-P. On the contrary, in the intact arthrodesis, the models with the third screw added posteriorly predicted lower peak micromotions than those with the screw added anteriorly, as in the normal bone quality, although the differences were slightly lower, again with the largest differences between the models I60-beneath-A and I60-beneath-P.

Table 8.10 Peak micromotions (μm) predicted at the fusion site in three-screw fixation models, for the normal and one case of decreased levels of bone Young's moduli. Dorsiflexion.

	Model	Normal	Case 2*	
Flat cut	30-above-A	44	70	**59%**
	30-above-P	46	82	**78%**
	60-beneath-P	121	228	**88%**
Intact	I30-above-A	47	77	**64%**
	I30-above-P	34	61	**79%**
	I60-beneath-A	166	328	**98%**
	I60-beneath-P	81	175	**116%**

* Percentage of change in the micromotions relative to the normal bone quality.

Both in the anterior and posterior groups, the models with the two screws inserted at 30 degrees to the long axis of the tibia also predicted lower peak micromotions than those with the screws at 60 degrees with poor bone quality. The differences increased as compared to the normal quality bone: peak micromotions in the 60-degree models were almost 3 times and more than four times those in the 30-degree models, in the posterior and anterior groups respectively. Peak values were well above 150 μm in all the 60-degree models. Comparing the surface preparation techniques, the intact arthrodesis produced lower peak micromotions in the posterior group, as predicted with normal quality bone. The difference was similar between the most stable models (30-above-P and I30-above-P), but reduced from 49 to 30% between the least stable models (60-beneath-P and I60-beneath-P). Very small differences were found between intact and flat cut models in the anterior group (between 30-above-A and I30-above-A).

Poor bone quality did not substantially change the pattern of motion between the tibia and the talus as compared to the normal bone quality (Chapter 7, page 123), despite the increase of both normal and tangential components in all the models. In the flat cut group, most of the motion was still due to the gap opening at the posterior areas of the fusion site; the ratio tangential/normal component along the edge of the fusion site in the non-contact areas did not change with poor bone quality in the posterior group and slightly increased in the anterior group. The anterior screw predicted lower sliding than the posterior screw, especially along the postero-medial and medial parts of the edge of the fusion site. The higher peak micromotions predicted in the posterior group were also due to the large increase of the gap along the postero-medial area of the fusion site. In the intact group, both micromotion components were lower in the posterior group, as observed in the normal bone quality. With poor bone quality, sliding increased at the contact areas (along the anterior edge of the fusion site), both in the anterior and posterior groups. In the non-contact areas, the ratios tangential/normal components along the edge of the fusion site did not change with the change in bone quality in either the anterior or the posterior groups.

Despite the increase in the ES values observed in all the models, poor bone quality did not affect the pattern of equivalent strain distribution in the bones as compared with normal quality bone (Chapter 7, page 123). Table 8.11 (page 153) shows the changes in the peak ES in the models with three-screw fixation when bone quality was worsened. The location of the peak values in both bones was generally the same as with normal quality bone. In the anterior group, tibial peak values were larger than talar peak values, except in the model I30-above-A; in the posterior group, almost no difference was found between the peak values in both bones in the most stable models (30-above-P and I30-above-P), whereas larger peak values were predicted in the tibia in the least stable models (60-beneath-P and I60-beneath-P). Similar peak ES were predicted between the corresponding

models in the anterior and posterior groups, except in the case of the models I60-beneath-A and I60-beneath-P. As found with normal quality bone, the most stable models predicted lower peak ES than the corresponding least stable models.

Figure 8.7 (page 154) shows the bone volumes with ES above yield strain (1%), as well as the location of these failed areas, in the case of poor bone quality studied. Only those three-screw models with the two screws inserted at 60 degrees presented volumes of failed elements. These cases were also by far the least stable models, with larger failed volumes corresponding with larger peak micromotions. A larger failed volume was predicted in the model I60-beneath-A than in the corresponding model in the posterior group.

Comparing these results with those obtained in the two-screw fixation for the same case of poor bone quality (section 8.3.1.2, page 139) showed that the addition of the third screw always reduced the peak micromotions, as happened with normal quality bone. In general, the reduction when adding the screw anteriorly slightly increased, as compared to the normal bone quality, and did not change when adding the screw posteriorly. With regards to the predicted ES and volumes of elements above the yield limit, it was found that in all the models, the volumes predicted were lower than in the corresponding two-screw models (Figure 8.4, page 143). Adding the screw anteriorly (I60-beneath-A), did not change the location of the failed bone in the tibia; in the talus, the volume affected was much lower than in the tibia and was located around the hole of the anterior screw at the fusion site. Adding the screw posteriorly (60-beneath-P and I60-beneath-P) changed the location of the failed bone in both bones; areas of bone failure in the tibia were predicted around the proximal holes of the posterior and lateral screws and, in the talus, around the hole of the posterior screw at the fusion site.

Table 8.11 Comparison of peak equivalent strains predicted in the tibia and the talus for two cases of bone quality in three-screw arthrodesis. Peak ES (%) in the bones and percentage increase relative to the normal case (shown in italics) in dorsiflexion.

Anterior group	Talus[a]			Tibia[b]				Posterior group	Talus[c]			Tibia[d]		
	Normal	Case 2		Normal	Case 2				Normal	Case 2		Normal	Case 2	
30-above-A	0.17	0.44	*159%*	0.37	0.67	*81%*	*Flat cut*	30-above-P	0.31	0.62	*100%*	0.39	0.67	*72%*
								60-beneath-P	0.64	1.72	*168%*	1.05	2.15	*105%*
I30-above-A	0.24	0.58	*142%*	0.27	0.50	*85%*	*Intact*	I30-above-P	0.30	0.56	*87%*	0.55[e]	0.57[f]	*4%*
I60-beneath-A	0.69	1.41	*104%*	1.30	3.42	*163%*		I60-beneath-P	0.65	1.48	*128%*	0.95	2.19	*131%*

[a] Peak values located around the hole of the anterior screw at the fusion site unless stated otherwise.
[b] Peak values located around the hole of the lateral screw at the fusion site unless stated otherwise.
[c] Peak values located around the hole of the posterior screw at the fusion site.
[d] Peak values located around the proximal hole of the posterior screw unless stated otherwise.
[e] Peak values located at the anterior area of the fusion site.
[f] Peak values located around the proximal hole of the lateral screw.

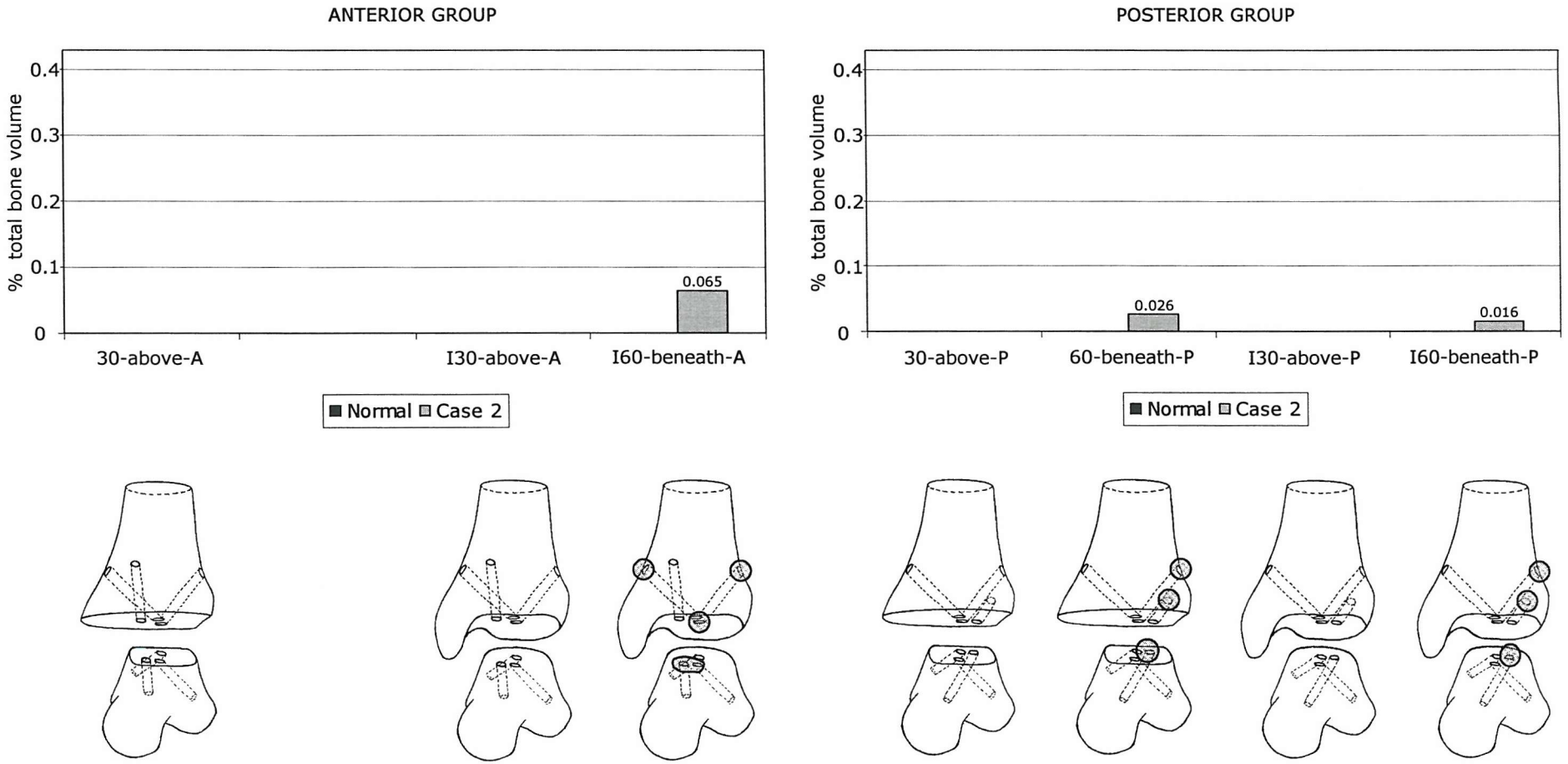

Figure 8.7 Graph representing the % of the total bone volume above yield strain (1%) predicted in dorsiflexion. Below, schematic representation of the areas of bone failure in each model (frontal view of the bones, separated for clarity).

8.4 DISCUSSION

Poor bone quality is common within the patient population that undergo ankle arthrodesis. Thordarson et al.[160,161] and Friedman et al.[46] found bone quality to be a major determinant of the rigidity of ankle arthrodesis constructs. In the FE analyses presented in this chapter, bone quality has shown to substantially affect the initial stability at the fusion site. In the case of ankle arthrodesis with two-screw fixation, the poorer the bone quality, the larger the micromotions at the fusion site and the larger the differences as compared to the normal quality bone. Bone quality of aged bone was simulated by decreasing the Young's moduli of cortical and cancellous bone by 10 and 26%, respectively; it produced peak micromotions around 1.2 times higher than those predicted in the healthy bone. Osteoporotic bone, simulated by decreasing the cortical and cancellous bone Young's moduli by 33 and 66% respectively, produced peak micromotions between 1.6 and 2.1 times those observed in the healthy bone. The most extreme case of poor bone quality, rheumatoid arthritic bone, was simulated by decreasing the cortical and cancellous bone Young's moduli by 66 and 90%, respectively; it produced very large peak micromotions, up to 5 times those predicted with normal quality bone. Peak micromotions as high as 500 and 1000 μm were predicted in torsion and dorsiflexion, respectively. Although a safe level of motion that will ensure bone fusion has not been described, this low level of initial stability provided by two screws, especially in the cases of osteoporotic and rheumatoid arthritic bone, may be insufficient for a successful outcome of the arthrodesis. The addition of a third screw substantially reduced the peak micromotions when tested in the case of the osteoporotic bone. Peak micromotions in the two-screw arthrodeses were up to 2.4 times higher than those predicted when a third screw was added.

The effect of bone quality on the initial stability provided by the different two-screw configurations studied presented mixed results. In external torsion, the same differences in peak micromotions between the most and least stable models were predicted in the normal and poor quality bone cases. As happened with normal quality bone, larger differences were predicted in the intact arthrodesis than the flat cut arthrodesis. In dorsiflexion, the poorer the bone quality, the larger the differences between the most and least stable models. Very large differences were predicted with all the levels of bone quality, reaching up to 7-fold differences in the case of rheumatoid arthritic bone. In both load cases, the most stable models were always those with the two screws inserted at 30 degrees relative to the long axis of the tibia. These models predicted peak micromotions below 150 μm in dorsiflexion, even in the poorest quality bone; however the fact that they predicted peak micromotions above 150 μm in all the cases of poor quality bone in

external torsion, may reflect the need to use a third screw to obtain enough initial stability in such cases. The only exception was the model I30-above with aged bone, as it predicted peak micromotions not larger than 100 μm in both load cases.

Within the two-screw configurations, intact arthrodesis predicted better stability than flat cut arthrodesis in all the levels of bone quality. The only exception was the case of the most stable models in dorsiflexion (those with a 30-degree insertion angle): the differences in peak micromotions were not significant as they were of the same order or smaller than the model error. In torsion, the differences in peak micromotions between the two techniques were considerably higher between the most stable models (those with a 30-degree insertion angle) than between the least stable models (those with a 45-degree insertion angle). Despite these differences, the relative importance of the joint surface geometry did not increase but, rather, decrease as bone quality worsened. Thus, in the poorest quality bone, considerable differences in stability between the two techniques were only predicted in the models with the screws inserted at 30 degrees in torsion (peak micromotion in the model 30-above was 1.3 times higher than that in the model I30-above).

As well as increasing the micromotions at the fusion site, poorer bone quality also produced larger strains in the bones, as expected. The patterns of strain distribution were similar to those observed with normal quality bone, although the regions enlarged as the bone quality worsened. Initial stability, strain values and volume of failed elements (those with equivalent strain above the yield level) seemed to follow similar trends; however, in the comparison between all the different models, higher peak strain values did not always imply larger peak micromotions at the fusion site or larger volumes of failed elements. Within each model, the poorer the bone quality, the larger the peak strains and the larger the increases as compared to the healthy bone; in those models with volumes of failed elements, the poorer the bone quality the larger the failed volumes and the higher the number of regions affected. Peak strains in the tibia were always higher than in the talus and, in general, failed volumes were larger in the tibia than in the talus. In both load cases, the most stable two-screw configurations always predicted lower peak strains than the corresponding least stable ones; as observed in the peak micromotions, the differences were marginally affected by bone quality in external torsion but increased in dorsiflexion as bone quality worsened. The very large peak micromotions predicted with rheumatoid arthritic bone were linked with large volumes of failed elements and high number of regions affected, especially in the least stable models in dorsiflexion (60-beneath and I60-beneath). In the torsion load case, the most stable model (I30-above) also seemed to be the best option to avoid bone failure, although some regions of the tibia could fail with the worst bone quality. In dorsiflexion, the models with the two screws inserted at 30 degrees offered similar high levels of stability, even with rheumatoid arthritic bone; none of them

predicted failed volumes with aged or osteoporotic bone but, with rheumatoid arthritic bone, the intact arthrodesis (I30-above) seemed to be a better option as predicted a lower failed volume concentrated in only one small region.

The addition of a third screw in the case of poor bone quality (studied in the osteoporotic bone) substantially increased the initial stability at the fusion site, as happened with normal quality bone (Chapter 7). This increase was generally larger when adding the third screw to the least stable two-screw models in both load cases. The addition of an anterior screw always produced better stability than that of a posterior screw in external torsion. This was also true in the flat cut arthrodesis in dorsiflexion, but the opposite happened in the intact arthrodeses, as the posterior screw provided better stability. The most stable two-screw models remained the most stable with the addition of a third screw, irrespective of being anterior or posteriorly inserted; the only exception was the flat cut arthrodesis in torsion, as adding the screw anteriorly always produced better stability, regardless of the two-screw configuration. Three-screw fixation with the intact arthrodesis always predicted better stability than the corresponding flat cut arthrodesis, except for the models 30-above-A and I30-above-A in dorsiflexion, which predicted similar results.

The strain values predicted in the bones were markedly reduced by the addition of the third screw. Peak values decreased by up to 60%, although, in two cases in torsion, the addition of the posterior screw produced an increase of the peak strains relative to the two-screw models (30-above-P and I30-above-P). But even in these two cases, the volumes of failed elements decreased significantly. In torsion, failed volumes decreased between 20 and 100%, with larger decreases when adding the screw anteriorly; those models that predicted failed volumes corresponded with the least stable models and, in general, the larger the failed volume and the number of regions affected, the less stable the model. In dorsiflexion, failed volumes decreased from around 50 to 90%; those models with failed volumes were, by far, the least stable (those with the two screws inserted at 60 degrees) and also, the larger the failed volume, the less stable the model.

Poor bone quality was simulated by uniformly decreasing the Young's modulus assigned to the bone elements, following one of the approaches reported in the literature [30,85]. Local changes in bone density or bone structure produced by age or disease were, therefore, not considered. Modelling the bones directly from a diseased ankle would have possibly reflected these local changes. However, it is difficult to reconstruct the three-dimensional bone geometry from two-dimensional CT scan images of diseased ankles. In the earlier stages of this thesis, an attempt was made to reconstruct the tibia and talus geometries from the CT scan images of a rheumatoid arthritic ankle. Large deformations at the joint surfaces, as well as irregular cysts inside the bones made the reconstruction

process certainly unreliable and a healthy ankle was used instead. The three levels of poor bone quality were defined using values of reduction of the Young's moduli reported in the literature, for aged or diseased cortical and cancellous bone (page 130). Although none of these values had been obtained from the tibia or the talus, they were chosen given the lack of data in the literature with regard to Young's modulus variation in the talus and distal tibia due to age or disease. The levels of bone quality described as aged bone, osteoporotic bone and rheumatoid arthritic bone may not represent exactly the values found at the ankle, but they were treated as generic cases to assess and compare the effect of poor bone quality in the different ankle arthrodesis constructs studied.

Rigid fixation of the screw threads in the talus was assumed in all the models and bone qualities studied, even in the case of largest modulus decreases. A priori, and without enough clinical or experimental information in the issue, it was not clear which mode of bone failure would first occur in the arthrodesis constructs. As mentioned in Chapter 5 (page 63), due to the orientation of the screws in the bones and the loads applied, screw cutting through the bone as well as thread stripping could be expected in the cases of poorer bone quality. Given the location of the regions of failed elements and the location of the peak strain values predicted in both load cases and levels of bone quality, several comments can be made. The tibia seemed more likely to fail before the talus, by screw cutting around the proximal and distal ends of the screw holes. This agrees with Thordarson et al.'s[161] observations of bone deformation (hole enlargement) around the head of the screws in ankle arthrodesis constructs with poor bone quality. In two-screw fixation, strain values in the talus were in general higher around the screw holes at the fusion site, so that, as bone quality worsened, bone failure would be more likely to occur due to screw cutting in those regions. In some models in both load cases, but only in the worst case of bone quality studied, additional regions of bone failure in the talus were also observed at the interface with the screw thread of the lateral screw, indicating possible bone failure also by thread stripping. The addition of the third screw somewhat changed the location of the regions of failed elements and of the peak strain values in general. No model presented peak strains or failed volumes in the talus by the interface with the screw thread; peak values were generally located around the hole of the anterior screw at the fusion site in the anterior group, and around the hole of the posterior screw in the posterior group. Thus, as bone quality worsened, screw cutting was expected at those areas, as shown by the failed volumes that appeared there. The fact that the distal end of the screws was kept glued to the talus may have, therefore, produced a conservative estimate of the micromotions at the fusion site only in the case of two-screw fixation with very poor bone quality.

Clinical studies of ankle arthrodesis fixed with screws in patients with rheumatoid arthritis have shown substantial differences in the rates of fusion (Chapter 3, page 39). On one hand, some have reported high failure rates and suggested the lack of purchase of the screws in the poor quality bone as a possible cause [36]. On the other hand, high fusion rates have been achieved [44,87,163], despite the poor bone quality and the presence of bone cysts and talar necrosis. In these cases, three screws and resected joint surfaces (Felix and Kitaoka [44]) and two or three screws with intact joint contours (Turan et al.[163], Lauge-Pedersen et al.[87]) were the techniques employed. These good results may indicate that the overall rigidity achieved by the combined effects of the screws and the bone interface geometry was good enough to allow for bone fusion. Looking at the results of the FE comparisons presented in this chapter, the peak micromotions predicted by the most stable model in the intact arthrodesis fixed with two screws (I-30above) were of similar magnitude to those predicted in the corresponding models of flat cut arthrodesis fixed with three screws (30above-A and 30above-P) in the case of poor bone quality, both in external torsion and dorsiflexion.

Summary of results

- Bone quality had a marked effect on the initial stability of ankle arthrodesis at the fusion site.
- For the stability provided and the lower risk of bone failure, inserting two screws at 30 degrees in an intact arthrodesis seemed the best option, especially as bone quality worsened. However, in the cases of worst bone quality, even this option may not be good enough to ensure fusion.
- The addition of a third screw increased the stability at the fusion site and decreased the risk of bone failure.
- A third screw inserted anteriorly seemed the best option as this provided better stability against torsion and a lower risk of bone failure in both load cases, especially when added to two-screw configurations with small insertion angles.
- Overall, intact joint surfaces and three-screw fixation, with the lateral and medial screws inserted at 30 degrees relative to the long axis of the tibia, produced the most stable ankle arthrodesis constructs with poor bone quality.

Chapter 9
DISCUSSION AND CONCLUSIONS

Ankle arthrodesis has been the gold standard treatment for painful and disabling ankle diseases. Although the knowledge drawn from decades of clinical use and the improvements and further development of ankle arthrodesis techniques have resulted in high levels of performance, there is scope for further improvement, as cases of failed fusion are still reported (Chapter 3). *In vitro* biomechanical studies have tried to establish the best way to achieve rigid fixation, as initial stability of the construct is believed to be one of the main mechanical factors affecting the outcome of ankle arthrodesis (Chapter 4). However, due to the difficulties to experimentally assess it, little is known about the mechanical response at the fusion site, i.e. at the interface between the tibia and the talus. Therefore, the main purpose of this research was to use the strength of the finite element method as a comparative tool to assess the initial stability at the fusion site of ankle arthrodesis constructs, internally fixed with cancellous bone screws. To the author's knowledge, three-dimensional finite element analyses of the mechanical behaviour of ankle arthrodesis have never been reported in the literature, nor have the micromotions taking place at the fusion site been assessed before.

A well-established procedure in the field of orthopaedic biomechanics was followed to build finite element models of ankle arthrodesis constructs. Chapter 5 contained a detailed description of the digital image-based FE modelling, as well as the tests performed to assure the robustness of the resulting model. A mesh density was chosen so that the convergence of the variables of interest (especially the micromotions at the fusion site) was achieved. Also, the sensitivity of the micromotions at the fusion site to changes in some modelling parameters was checked; the reference model proved to be stable against changes of the convergence tolerance and contact parameters, except for the friction coefficients. In a number of models, the convergence tolerance had to be increased from the reference value to reach a solution; the effect of this change in the comparisons performed between the different models was not considered relevant, as it would have produce maximum relative differences in the micromotions of around 2%. The rest of the modelling parameters were kept constant throughout the comparisons.

The type and magnitude of the forces most clinically relevant when assessing the stability of ankle arthrodesis have not been precisely determined. Nevertheless, ankle torsion and dorsiflexion/plantar flexion loads have been regarded, in this order, as the most likely to affect the ankle arthrodesis in the postoperative period when the leg is in a

short-leg cast and weight-bearing is not allowed [160]. These load cases have been used to test the rigidity of ankle arthrodesis constructs *in vitro* (Table 4.1, page 50); different magnitudes have been applied in each case and, in general, they seem to have been chosen so that a majority of the constructs did not show signs of failure under such loads. The values used in this research (Chapter 5, page 63 and Chapter 6, page 84) are within the range of those reported in the literature (Chapter 4, page 50); they were considered reasonable as, in the case of normal quality bone, the majority of the models predicted strain values unlikely to produce bone failure. Although initially both internal and external tibial torsion were tested, given the lower micromotions always predicted at the fusion site in internal torsion in the two-screw configuration, only external torsion was used thereafter, together with dorsiflexion.

Surface preparation technique

Results from Chapter 6 and Chapter 7 show that ankle arthrodesis fixed with two or three screws provided higher stability at the fusion site when the joint surface contours were preserved than when resected with flat cuts, regardless of the precise screw location and orientation. The only exceptions occurred in dorsiflexion, for the models with the two screws inserted at 30 degrees and crossing above the fusion site (30-above and I30-above) and when the third screw was added to them anteriorly (30-above-A and I30-above-A). In these cases, the differences in peak micromotions between the intact and flat cut models cannot be considered relevant as they were within the estimated error of the modelling technique (5 μm). The same behaviour was predicted when poor bone quality was simulated (Chapter 8), although the poorer the bone quality, the smaller the differences between both surface preparation techniques. The better stability predicted for the preserved joint contours in the two-screw configuration further improved when friction was modelled. Also, in both the two and three-screw configurations, although preserving the joint contours generally predicted lower peak strains in the bones in torsion, no clear trends were observed in dorsiflexion. This result was also observed in the simulated cases of poor bone quality; in addition, lower percentages of failed bone volume were generally predicted in the models with preserved joint contours (the only exception being the three-screw models in dorsiflexion). When friction was considered, a larger decrease in the peak strain was predicted for the preserved joint contours.

A number of factors may have contributed to the improved stability when preserving the joint contours. One of them is the surface interlocking in the preserved joint contour case, as shown by the contact areas and the patterns of motion observed at the fusion site and the areas of strain concentration predicted in the bones. Another factor may have been the preservation of areas of relatively stiff cancellous bone (subchondral bone) near

the joint surfaces. Areas of strain concentration, frequently containing peak strain values, were consistently predicted around the screw holes at the fusion site, both in the tibia and the talus. Thus, the removal of the subchondral bone was expected to cause an increase in the levels of deformation around those regions. This was confirmed when, in general, higher strains were predicted in the flat cut arthrodesis than in the intact arthrodesis in torsion.

The findings of this research are not directly comparable with any clinical or experimental results available in the literature. However, good agreement was observed with the results reported in two biomechanical studies (Chapter 6, page 82). Miller et al.[103] presented the first *in vitro* study to compare the effect of the shape of the joint contours on the stability of ankle arthrodesis. They tested four pairs of cadaveric ankles with preserved and flat cut joint contours, fixed with two crossed screws (30-degree insertion angle), in torsion and dorsiflexion/plantar flexion. Although they measured the gross motion between the tibia and talus and, thus, direct comparisons with the predictions of the FE models are not possible, similar trends were observed: the preservation of the joint contours yielded slightly better stability in torsion and only marginal differences were measured in dorsiflexion. However, as the differences were not statistically significant in any case, they concluded that both techniques were biomechanically sound. There is also agreement with the conclusions of the study by Lauge-Pedersen et al.[86]. They measured the stiffness and strength of blocks of a bone substitute, fixed with two cancellous screws, when loaded in torsion and bending. The most stable constructs were those equivalent to an ankle arthrodesis with preserved joint surface contours. Some clinical studies on ankle arthrodesis have specified the type of surface preparation technique used. But a comparison of the results based on the shape of the arthrodesis surfaces was not attempted due to the lack of control upon other variables that could have been responsible for any difference found.

Two-screw fixation

Abidi et al.[1] and Kitaoka et al.[78] recommended two crossed screws as a standard fixation technique in ankle arthrodesis, at least when bone quality was not compromised. As shown by some good fusion rates reported [18,47,97,117], such fixation has proved stable enough to allow for ankle fusion. The location and orientation of the two screws varies depending on the surgical approach; parameters such as insertion angles or crossing levels are not usually specified in the reported clinical studies. No clinical or biomechanical study has analysed the influence of the location and orientation of the two screws on either the clinical or the mechanical performance of the ankle arthrodesis constructs. A clinical range of insertion angles and crossing levels was examined in Chapter 6, initially assuming

normal quality bone. Overall, inserting the two screws at a 30-degrees angle relative to the long axis of the tibia and crossing them above the fusion site (30-above and I30-above) predicted the best stability and lowest strain values. Lowering the crossing level produced a decrease in the stability and, in general, an increase in the strain values. Increasing the insertion angle produced a substantial decrease in the stability in dorsiflexion and an increase in the strains; in torsion, despite some mixed results, stability and levels of strain did not improve for insertion angles larger than 30 degrees. The differences in stability between the most and least stable models were much larger in dorsiflexion than in torsion. When friction was considered, the differences in stability between the configurations did not substantially change, thus, not affecting the ranking predicted in the frictionless case.

The effect of poor bone quality on the initial stability provided by two-screw fixation was tested upon the most and least stable models in external torsion and dorsiflexion (Chapter 8). Within each model, the poorer the bone quality, the lower the stability, the higher the peak strains and the larger the differences as compared to the normal quality bone. In those models that predicted volumes of failed elements, the poorer the bone quality, the larger these volumes and the higher the number of regions affected. The least stable models predicted very large peak micromotions (between 200 and 525 μm in torsion and between 240 and 1000 μm in dorsiflexion) and volumes of failed bone occurred in all the cases of poor quality bone. The most stable models predicted considerably lower peak micromotions, especially in dorsiflexion, and smaller volumes of failed bone, if any. As compared to the normal quality bone, the differences in stability and strain between the most and least stable models hardly changed in torsion when bone quality worsened, but increased in dorsiflexion, where up to 7-fold differences in stability between the most and least stable constructs were predicted in the worst quality bone.

These findings, both in normal and poor quality bone, highlight the importance of the location and orientation of the two screws in order to increase the likelihood of bone fusion. Although a safe level of motion at the fusion site that will ensure ankle fusion is not known, the differences in stability predicted between the screw configurations may be the difference between a failed and a successful fusion. Although inserting the screws at 30 degrees relative to the long axis of the tibia, crossing them above the fusion site provided the best results, the substantial decrease in stability predicted in the cases of osteoporotic and rheumatoid arthritic bone may reflect the need to use a third screw to obtain enough initial stability in such cases.

Three-screw fixation

A third screw is often added to a two-screw configuration when intraoperative manual tests of the rigidity of the construct show apparent relative motion at the arthrodesis site. Clinical studies reporting on the results of ankle arthrodesis with two crossed screws frequently include cases were an extra screw was needed to ensure rigid fixation [18,87,117,123]. In an *in vitro* biomechanical study, Ogilvie-Harris et al.[119] concluded that 3-screw fixation was more effective in controlling torsion than two-screw fixation. They compared the gross motion between the talus and tibia in flat cut arthrodesis constructs fixed with two crossed screws, before and after the addition of an extra anterior screw. They obtained a reduction in the motion between 9 and 31% (median 14%) when the anterior screw was added. Chapter 7 and Chapter 8 compared the initial stability at the fusion site predicted by two types of three-screw fixation, obtained by adding a third screw, either anteriorly or posteriorly, to the most and least stable two-screw constructs studied in Chapter 6. In the comparison between two and three-screw fixation, the latter showed better stability at the fusion site and a more uniform distribution of the loads in the bones, as it predicted lower peak micromotions at the fusion site and, in general, lower strains, both in normal and poor quality bone. Adding a third screw reduced the peak micromotions at the fusion site between 22 and 53% (median 35%) in external torsion and between 4 and 59% (median 23%) in dorsiflexion, pooling all the results from both cases of bone quality. This increase in the stability was, in most of the cases, coupled with a marked decrease in the peak strains. In normal quality bone none of the three-screw models predicted relevant volumes of failed bone and, in most of the models, peak strains were well below the yield limit; in poor quality bone, adding the third screw always decreased the volumes of failed bone predicted in the corresponding 2-screw configurations (between 20 and 100% decrease in torsion and between 50 and 90% in dorsiflexion). In both cases of bone quality, adding a third screw to the least stable two-screw models improved the stability more than when added to the most stable models. Thus, the addition of a third screw reduced the differences between the best and worst two-screw configurations. Nevertheless, these differences were still substantial, especially in the dorsiflexion test, where up to above 3-fold and 4-fold differences in the normal and poor quality bone, respectively, were seen between the most and least stable constructs. This emphasises the importance of the orientation of the first two screws, even when a third screw is added.

The addition of an anterior screw predicted better stability at the fusion site and lower strains in the bones than the addition of a posterior screw in external torsion. Median differences between both configurations, in normal and poor quality bone, were about 27%. In addition, in poor quality bone, the insertion of an anterior screw yielded lower volumes of failed bone and a lower number of regions affected. Intuitively, inserting a third

screw from the posterior part of the tibia down towards the neck of the talus would be the best option to increase resistance to dorsiflexion/plantarflexion forces. This was confirmed in the dorsiflexion test in the intact arthrodesis, where the addition of an anterior screw predicted peak micromotions between 1.3 and 2 times higher than when the screw was added posteriorly. Also, when volumes of failed bone were predicted (only in the least stable two-screw configurations in poor quality bone), lower volumes were predicted when adding the screw posteriorly. In flat cut arthrodesis, the posterior screw predicted similar results to the anterior screw in normal quality bone, but worse results in poor quality bone. Assuming the most stable two-screw configurations (30-above and I-30above) and given the fact that the addition of a third screw always produced larger peak micromotions in external torsion than in dorsiflexion (between 1.3 and 2.4 times larger), inserting the extra screw anteriorly seemed to offer the best performance, regardless of the bone quality. Only in the case of an intact arthrodesis performed in normal quality bone, the addition of an anterior screw may not be advantageous over the posterior screw.

Practicalities and limitations of the FE analyses

The strain assessment included in the comparisons between the different models was intended to determine where in the bones and in which models the likelihood of bone failure could be higher. The digital image-based finite element modelling used in this research implied a semi-automatic meshing of the different parts of the arthrodesis constructs. As a result, the presence of some badly shaped elements could not be avoided. They may have caused some peak strains predicted in the bones of a number of the studied models. Nevertheless, they were always isolated elements whose peak strains were generally much higher than in the rest of the bone and, thus, are unlikely to affect the results of the comparative analyses carried out. Consistently, concentration of high strain values was predicted in the same regions in the bones. One of these regions was around the proximal end of the screw holes in the tibia. It is not clear to what extent these high strain values were due to the way the screw head had been modelled (Chapter 5, page 62). Nevertheless, high strains were expected in these regions as deformations around the screw heads have been previously observed in *in vitro* studies [161]. Overall, the results of the strain assessment provide useful information about the areas in the bones most likely to fail in the different screw configurations, which could help the surgeon when planning the screw location in specific patients.

Frictionless contact was used throughout this research. Including friction produced an expected decrease in the micromotions at the fusion site, as shown by the results of the sensitivity analysis to changes in the friction coefficients performed upon a reference model (Chapter 5, page 79). As a result of the substantial increase in the computational

cost of the analyses when friction was considered, only a selection of the two-screw models assessed in Chapter 6 was also run including friction. Peak micromotions at the fusion site decreased in both external torsion and dorsiflexion, with larger decreases predicted in torsion (between 12 and 32%) than in dorsiflexion (between 0 and 7%). In fact, in most of the cases in dorsiflexion, the absolute difference in peak micromotions was within the model error (5 μm). In general, peak strains in the bones also decreased with friction. Friction affected intact and flat cut arthrodeses differently. The stability predicted in the frictionless case in torsion increased, on average, 31 and 13% in the intact and flat cut models, respectively. Thus, the better stability predicted in the frictionless case when preserving the joint contours was emphasised with friction. Friction did not change the pattern of motion at the fusion site in intact arthrodeses, in both load cases, and in the flat cut arthrodeses in torsion; however, in dorsiflexion, a larger reduction of the tangential component of the micromotions than of the normal component in the flat cut arthrodesis indicated a higher degree of rocking motion than in the frictionless case. Despite these results, the differences in stability between the different two-screw configurations hardly changed with friction, thus not changing the ranking of the models obtained in the frictionless case. For this reason, the effect of bone quality on the initial stability of two-screw ankle arthrodesis was only studied in the frictionless case (Chapter 8), assuming the likely overestimation of the micromotions and the strains reported as compared to a friction case.

Attempts to run friction analyses with the three-screw models failed due to unexpected convergence problems. They were attributed to the higher complexity of the models as compared to the two-screw models, regarding the number of contact bodies and, thus, contact interfaces. Therefore, only frictionless results were compared in Chapter 7. Given the effects of friction on the initial stability predicted in the two-screw models, one could speculate that friction is likely to reduce the micromotions and the strains predicted in the frictionless case, in both the anterior and the posterior groups. Nevertheless, it is unlikely to change the results regarding the better performance of intact arthrodesis as compared to flat cut arthrodesis, nor the ranking of the models considering the two-screw configuration, always within each group. It is not that clear what the effect would be in the comparison between the stability provided by a third screw inserted anteriorly or posteriorly; however, the previous experience would suggest that the ranking of the models would not change.

The optimal level of compression between the bones to fuse is not known and, in general, the issue of the benefits of compression through the arthrodesis site remains controversial (Chapter 4, page 45). Cunningham et al.[28] observed a fast drop of the initial compression achieved with an external fixator in knee arthrodeses. Daily adjustments were needed to restore the same level of compression. As they stated, although compression

increases bone coaptation and, thus, the stability at the fusion site, high levels of compression could lead to lower stability, as a result of bone compactation or even bone resorption at the fusion site (specially in poor quality bone). They finally suggested the application of a reduced level of compression. In internal fixation, the initial compression through the arthrodesis site is achieved by the screw tightening at the time of surgery and cannot be readjusted postoperatively. In the 70's, Cordey et al.[26] and Blümlein et al.[8] observed a rapid drop in the axial force in cortical screws fixed to bovine intact tibial diaphysis (with and without plates). This drop, which took place during the first day or days after the operation, was followed by a slower reduction during the following weeks. The former was attributed to the bone viscoelasticity and the latter to the remodelling of cortical bone under pressure. No data has been found in the literature regarding the change with time of the initial compression achieved through the ankle arthrodesis site with cancellous screws. In an ongoing *in vitro* study, the change of the compression through the arthrodesis site is being assessed by measuring the change of the axial strain developed on a cancellous screw used to fixed a flat osteotomy in femoral heads. This study and the initial results are summarised in Appendix B. The initial results have shown a rapid drop in the compression during the first minutes, as compared to the maximum value achieved with the screw tightening; the average drop was around 40%, ranging between 20 and 70%. However, these results are not conclusive due to the so far unexplained longer-term behaviour of the decreasing compression.

An initial compression across the arthrodesis site was not included in the models presented in this work. If a substantial level of the maximum compression achieved with the screw tightening was still present at the fusion site after a few hours, it would probably be relevant for the mechanical performance of the fixation technique, regarding the stability at the fusion site. The addition of compression in the models would be expected to decrease the micromotions predicted at the fusion site. Although somewhat speculative, some thoughts about its effects on the comparative results obtained without modelling the compression can be offered. In principle, a lag screw would achieve the maximum compression when it is perpendicular to the fusion site [124]. In the flat cut arthrodesis, the fusion plane was cut perpendicular to the long axis of the tibia and, therefore, the larger the insertion angle, the lower the degree of compression achieved. In the intact arthrodesis, the shape of the surfaces is, as described in Chapter 1 (page 3), convex in the sagittal plane and slightly concave in the frontal plane. In this case, the level of compression would vary depending on the location and orientation of each screw relatively to these planes. In Chapter 6, the best initial stability was predicted for the models with the two screws inserted at 30 degrees and crossing above the fusion site. Thus, in the flat cut arthrodesis, larger insertion angles would be likely to remain less stable if compression was considered. The same would be expected in the intact arthrodesis as the change in the insertion angle took place in the frontal plane, where the arthrodesis site is almost

perpendicular to the long axis of the tibia. In the case of the models with three screws, the added anterior screw was inserted at a smaller angle relative to the long axis of the tibia in the sagittal plane than the posterior screw (see Tables 7.1 and Table 7.2, page 113). Thus, in the flat cut arthrodesis, the anterior screw would be expected to produce larger compression through the fusion site than the posterior screw and, therefore, further increase the better stability predicted when adding an anterior screw (Chapter 7). In the intact arthrodesis, the arthrodesis site presents marked convexity in the sagittal plane; a close examination of the angles in the sagittal plane between each screw and the normal to the articular surface revealed lower values for the anterior than for the posterior screw (mean difference 11 degrees); therefore, the anterior screw would also be expected to produce a greater degree of compression and, hence, better stability than the posterior screw. In the case of the stability in poor quality bone, the compression is likely to play a minor role as the worse the bone quality, the higher the risk of thread stripping when the screws are tightened; hence, lower the degree of compression through the arthrodesis site, if any.

Other limitations of the FE models, such as the absence of the fibula in the arthrodesis constructs or the simplified screw geometry, have been mentioned and discussed in Chapter 5. Difficulties to determine standard values for the mechanical characterisation of the bone are evident when dealing with human tissues. As a result of the current knowledge in this field, bone was considered isotropic and elastic. Moreover, experimental studies providing ankle joint characteristics to implement in FE models are scarce. The main concern of this research was with the relative differences between the models studied rather than with a quantitative assessment of the initial stability in each specific case. Any inaccuracies introduced will be present in all the models, with little effect on the comparative results presented.

Conclusions

This work has shown that the FE method can be used as an effective qualitative tool in assessing the initial stability of ankle arthrodesis at the fusion site, overcoming the difficulties of measuring interfacial micromotions experimentally. Measuring micromotions at the bone interfaces provides better knowledge of the mechanical conditions likely to affect the outcome of the arthrodesis. The FE analyses performed to compare the initial stability of ankle arthrodesis with internal fixation have produced the following results:

(a) Preserved joint contours predicted better initial stability at the fusion site and a more uniform distribution of loads in bones than resected joint surfaces.

(b) In two-screw fixation, inserting the screw at 30 degrees relative to the long axis of the tibia and crossing above the fusion site produced the best performance.

(c) Three-screw fixation predicted better initial stability, a more uniform distribution of loads in bones and lower risk of bone failure than two-screw fixation. Adding a third screw anteriorly produced overall better results than adding the screw posteriorly. Regardless of the configuration of the third screw, inserting the first two screws at 30 degrees relative to the long axis of the tibia and crossing above the fusion site always predicted the best performance.

(d) Large increases in instability at the fusion site were predicted when bone quality was severely diminished. Even the most stable two-screw configuration showed low levels of stability and regions at risk of bone failure, suggesting the need of a third screw.

(e) In poor bone quality, the differences in the initial stability between screw configurations became more pronounced, emphasising the need for an optimum screw placement.

The limitations of the models discussed above must be borne in mind when considering a direct transfer of the results into the clinical situation. Clinical and experimental studies are affected by the intrinsic inter and intra-subject variability of the numerous clinical and biomechanical parameters being analysed. For this reason, obtaining objective information about the benefits or drawbacks of variations of the arthrodesis techniques, in terms of the initial stability that each one is likely to achieve, is certainly difficult. FE analysis allows for a direct comparison of the results of such variations, as

tests can be performed several times without affecting the experimental conditions. This research should be seen as a step towards the use of FE modelling as a tool to provide additional information to the orthopaedic surgeon for the preoperative planning of ankle arthrodesis. It is hoped that future improvements of the current FE models together with foreseeable advances in areas such as bone mechanical characterisation, friction parameters or the multilevel relationships between mechanical and biological factors affecting bone fusion, will allow this ultimate goal to be reached.

RECOMMENDATIONS FOR FUTURE WORK

The improvement of the FE models studied is the natural extension of the present research. The current modelling has been a compromise between the FE software capabilities, the current knowledge on the material properties of bone and the complexity of the ankle arthrodesis constructs. A number of possible improvements are listed below.

- Friction: Limitations in the FE code are likely to have caused the difficulties which arose when running friction analyses with the three-screw configuration models and will need further investigation. Future releases of the FE software may allow friction analyses to converge to a solution. The addition of friction contact will provide a better estimate of the level of motion at the fusion site and the load transfer within the bones.

- Screw geometry: The simplified screw geometry would be improved by modelling the screw head and thread. A physical representation of the screw head is likely to provide a clearer picture regarding the bone deformation and possible bone failure around the heads. Modelling of screw threads leads to a wide field of research. Given the assumption of bone as a continuum material and the results obtained regarding the areas of strain concentration in the bones, explicitly modelling of the thread may not add much to the current research. Nevertheless, experimental data regarding the magnitude of the loads that would produce thread stripping could be implemented in the current models; this would allow for a better estimate of the micromotions in the cases when thread stripping is more likely to occur, i.e. two-screw fixation with very poor bone quality.

- Load cases: Conventional load cases were used in this work. Future clinical and experimental studies should produce information about more physiological and clinically relevant load cases. One approach to better model them would be to add representations of other bones and soft tissues related to the ankle, so that loads and constraints are not directly applied to the tibia and talus.

- Bone anisotropy: In order to consider the anisotropy of bone, two approaches could be taken. Micro-computed tomography is being used at the moment to represent the trabecular structure and, therefore, account for bone anisotropy. The number of elements increases dramatically and so does the computational time. Nevertheless, there are no reasons to doubt that future increases of computing power will allow the analysis of FE models of ankle arthrodesis

constructs built from micro-CT. Another approach could be to obtain anisotropic data to implement in the type of FE models presented in this research, assuming the bone as a continuum material.

- Poor quality bone: For a better representation of poor quality bone as a result of age or disease, further attempts to build the FE models from affected ankles are recommended. However, in the case of pathologic ankles with very deformed joint surfaces it may not be possible to obtain an accurate representation of the bone interfaces. Another approach would be to develop some kind of technique to implement bone density or Young's modulus data obtained from aged or diseased ankle bones into bone geometries obtained from healthy ankles.

- Compression across the arthrodesis site: It is hoped that the pilot study presented in Appendix B will eventually produce clear information about the level of compression to input in the models; this will allow the verification of the possible effects of compression on the results of this research, as discussed above.

For the progress towards the use of this type of FE analysis as a preoperative planning tool, further developments of the followed procedure would be needed. The models studied represent only a small number of possible variations on the surgical technique and type of fixation. Nevertheless, the number of models built, solved and post-processed was already considerable, as was the total time of the process. The different stages of the modelling procedure (bone geometry extraction, geometry manipulation to simulate the arthrodesis method, meshing, material properties assignment and boundary conditions) should be automated so that much less manual input is required. In addition, new ways to speed-up the solution time and analysis of the results would allow for an increase on the number of models studied. It may be that existing technology not yet used in the field of orthopaedic biomechanics can, in the near future, be applied to optimise these processes. Once this has been achieved, many other ankle arthrodesis techniques could be tested upon the same ankle model and, ultimately, allow for a patient-specific approach.

LIST OF REFERENCES

1. Abidi NA, Gruen GS and Conti SF. Ankle arthrodesis: indications and techniques. *J Am Acad Orthop Surg* 8 (3): 200-9, 2000.
2. Aitken GK, Bourne RB, Finlay JB, Rorabeck CH and Andreae PR. Indentation stiffness of the cancellous bone in the distal human tibia. *Clin Orthop* 201: 264-70, 1985.
3. Ashman RB, Cowin SC, Van Buskirk WC and Rice JC. A continuous wave technique for the measurement of the elastic properties of cortical bone. *J Biomech* 17 (5): 349-61, 1984.
4. Basmajian JV. Primary anatomy. 5th ed. Baltimore, Williams & Wilkins, 1964.
5. Beaugonin M, Haug E, Munck G and Cesari D. A preliminary numerical model of the human ankle under impact loading. In: International Conference on Pelvic and Lower Extremity Injuries (PLEI), Washington (USA), 1995.
6. Bentzen SM, Hvid I and Jorgensen J. Mechanical strength of tibial trabecular bone evaluated by X-ray computed tomography. *J Biomech* 20 (8): 743-52, 1987.
7. Bernakiewicz M and Viceconti M. The role of parameter identification in finite element contact analyses with reference to orthopaedic biomechanics applications. *J Biomech* 35: 61-7, 2002.
8. Blümlein H, Cordey J, Schneider UA, Rahn BA and Perren SM. [Long term measurements of the axial force of bone screws in vivo]. *Med Orthop Technik* 97: 17-9, 1977.
9. Brown GA, McCarthy T, Bourgeault CA and Callahan DJ. Mechanical performance of standard and cannulated 4.0-mm cancellous bone screws. *J Orthop Res* 18 (2): 307-12, 2000.
10. Büchler P, Ramaniraka NA, Rakotomanana LR, Iannotti JP and Farron A. A finite element model of the shoulder: application to the comparison of normal and osteoarthritic joints. *Clin Biomech* 17: 630-9, 2002.
11. Burstein AH, Reilly DT and Martens M. Aging of bone tissue: mechanical properties. *J Bone Joint Surg* 58-A (1): 82-6, 1976.
12. Carter DR, Beaupré GS, Giori NJ and Helms JA. Mechanobiology of skeletal regeneration. *Clin Orthop* 335 (Suppl): S41-S55, 1998.
13. Carter DR and Hayes WC. The compressive behavior of bone as a two-phase porous structure. *J Bone Joint Surg* 59 (7): 954-62, 1977.
14. Cattaneo PM, Dalstra M and Frich LH. A three-dimensional finite element model from computed tomography data: a semi-automated method. *Proc Inst Mech Eng [H]* 215 (2): 203-13, 2001.

15. Chang WC, Christensen TM, Pinilla TP and Keaveny TM. Uniaxial yield strains for bovine trabecular bone are isotropic and asymmetric. *J Orthop Res* 17 (4): 582-85, 1999.

16. Chapman JR, Harrington RM, Lee KM, Anderson PA, Tencer AF and Kowalski D. Factors affecting the pullout strength of cancellous bone screws. *J Biomech Eng* 118: 391-8, 1996.

17. Charnley J. Compression arthrodesis of the ankle and shoulder. *J Bone Joint Surg* 33 (2): 180-91, 1951.

18. Chen YJ, Huang TJ, Shih HN, Hsu KY and Hsu RW. Ankle arthrodesis with cross-screw fixation. Good results in 36/40 cases followed 3-7 years. *Acta Orthop Scand* 67 (5): 473-8, 1996.

19. Cheng YM, Huang PJ, Hung SH, Chen TB and Lin SY. The surgical treatment for degenerative disease of the ankle. *Int Orthop* 24: 36-9, 2000.

20. Ciarelli MJ, Goldstein SA, Kuhn JL, Cody DD and Brown MB. Evaluation of orthogonal mechanical properties and density of human trabecular bone from the major metaphyseal regions with materials testing and computed tomography. *J Orthop Res* 9: 674-82, 1991.

21. Claes L, Fiedler S, Ohnmacht M and Duda G. Initial stability of fully and partially cemented femoral stems. *Clin Biomech* 15: 750-5, 2000.

22. Cody DD, McCubbrey DA, Divine GW, Gross GJ and Goldstein SA. Predictive value of proximal femoral bone densitometry in determining local orthogonal material properties. *J Biomech* 29 (6): 753-61, 1996.

23. Colgrove RC and Bruffey JD. Ankle arthrodesis: combined internal-external fixation. *Foot Ankle Int* 22 (2): 92-7, 2001.

24. Conti SF and Wong YS. Complications of total ankle replacement. *Clin Orthop* 391: 105-14, 2001.

25. Cooper PS. Complications of ankle and tibiotalocalcaneal arthrodesis. *Clin Orthop* 391: 33-44, 2001.

26. Cordey J, Blümlein H, Ziegler W and Perren SM. [Study of the behaviour in the course of time of the holding power of cortical screws *in vivo*]. *Acta Orthop Belg* 42 (Suppl 1): 75-87, 1976.

27. Cowin SC. Bone mechanics handbook. 2nd ed. CRC Press, 2001.

28. Cunningham JL, Richardson JB, Soriano RM and Kenwright J. A mechanical assessment of applied compression and healing in knee arthrodesis. *Clin Orthop* (242): 256-64., 1989.

29. Czerniecki JM. Foot and ankle biomechanics in walking and running. A review. *Am J Phys Med Rehabil* 67 (6): 246-52, 1988.

30. Dalstra M, Frich LH and Sneppen O. The loss of load-bearing capability in rheumatoid glenoids. In: Proc. 10th Conference of the ESB, p. 178, 1996.

31. Dalstra M, Huiskes R, Odgaard A and van Erning L. Mechanical and textural properties of pelvic trabecular bone. *J Biomech* 26 (4/5): 523-35, 1993.

32. Dandy DJ and Edwards DJ. Essential orthopaedics and trauma. 3rd ed. Churchill Livingstone, 1998.

33. Deligianni DD, Maris A and Missirlis YF. Stress relaxation behaviour of trabecular bone specimens. *J Biomech* 27 (12): 1469-76, 1994.

34. Demetriades L, Strauss E and Gallina J. Osteoarthritis of the ankle. *Clin Orthop* 349: 28-42, 1998.

35. Dennis DA, Clayton ML, Wong DA, Mack RP and Susman MH. Internal fixation compression arthrodesis of the ankle. *Clin Orthop* 253: 212-20, 1990.

36. Dereymaeker GP, van Eygen P, Driesen R and De Ferm A. Tibiotalar arthrodesis in the rheumatoid foot. *Clin Orthop* 349: 43-7, 1998.

37. Destresse B, Hobatho MC and Darmana R. Etude des propriétés mécaniques de l'os spongieux du tibia humain par une méthode ultrasonore. *Innov Tech Biol Med* 16 (3): 288-99, 1995.

38. Ding M, Dalstra M, Danielsen CC, Kabel J, Hvid I and Linde F. Age variations in the properties of human tibial trabecular bone. *J Bone Joint Surg* 79-Br (6): 995-1002, 1997.

39. Dohm M, Purdy BA and Benjamin J. Primary union of ankle arthrodesis: review of a single institution/multiple surgeon experience. *Foot Ankle Int* 15 (6): 293-6, 1994.

40. Dohm MP, Benjamin JB, Harrison J and Szivek JA. A biomechanical evaluation of three forms of internal fixation used in ankle arthrodesis. *Foot Ankle Int* 15 (6): 297-300, 1994.

41. Draves DJ. Anatomy of the lower extremity. Baltimore, WIliams & Wilkins, 1986.

42. Elkouri ER. Review of cancellous and cortical bone healing after fracture or osteotomy. *J Am Podiatry Assoc* 72 (9): 464-6, 1982.

43. Feighan JE, Stevenson S and Emery SE. Biologic and biomechanical evaluation of posterior lumbar fusion in the rabbit. The effect of fixation rigidity. *Spine* 20 (14): 1561-7, 1995.

44. Felix NA and Kitaoka HB. Ankle arthrodesis in patients with rheumatoid arthritis. *Clin Orthop* 349: 58-64, 1998.

45. Finlay JB, Bourne RB, Kraemer WJ, Moroz TK and Rorabeck CH. Stiffness of bone underlying the tibial plateaus of osteoarthritic and normal knees. *Clin Orthop* 247: 193-201, 1989.

46. Friedman RL, Glisson RR and Nunley JA. A biomechanical comparative analysis of two techniques for tibiotalar arthrodesis. *Foot Ankle Int* 15 (6): 301-5, 1994.

47. Fu YC, Huang PJ, Tien YC, Hung SH, Cheng YM, Lin SY, Chen YC, Liu LL and Huang SH. Ankle arthrodesis: internal non-compression arthrodesis versus internal compression arthrodesis. *Kaohsiung J Med Sci* 15 (9): 550-5, 1999.

48. García JM, Doblaré M, Seral B, Seral F, Palanca D and Gracia L. Three-dimensional finite element analysis of several internal and external pelvis fixations. *J Biomech Eng* 122 (5): 516-22, 2000.

49. Genant HK, Wilson JS, Bovill EG, Brunelle FO, Murray WR and Rodrigo JJ. Computed tomography of the musculoskeletal system. *J Bone Joint Surg* 62-A (7): 1088-101, 1980.

50. Goldstein SA. The mechanical properties of trabecular bone: dependence on anatomic location and function. *J Biomech* 20 (11/12): 1055-61, 1987.

51. Goodship AE and Cunningham JL. Pathophysiology of functional adaptation of bone in remodeling and repair *in vivo*. In: *Bone mechanics handbook*, pp. 26/1-26/31. Edited by SC Cowin. 2nd ed. CRC Press, 2001.

52. Goulet RW, Goldstein SA, Ciarelli MJ, Kuhn JL, Brown MB and Feldkamp LA. The relationship between the structural and orthogonal compressive properties of trabecular bone. *J Biomech* 27 (4): 375-89, 1994.

53. Gray H. Anatomy of the human body. Lea & Febiger, 1918. www.bartleby.com, 2000.

54. Guo XE. Mechanical properties of cortical bone and cancellous bone tissue. In: *Bone mechanics handbook*, pp. 10/1-10/23. Edited by SC Cowin. 2nd ed. CRC Press, 2001.

55. Halvorson TL, Kelley LA, Thomas KA, Whitecloud III TS and Cook SD. Effects of bone mineral density on pedicle screw fixation. *Spine* 19 (21): 2415-20, 1994.

56. Hangartner TN and Gilsanz V. Evaluation of cortical bone by computed tomography. *J Bone Miner Res* 11 (10): 1518-25, 1996.

57. Harrigan TP, Jasty M, Mann RW and Harris WH. Limitations of the continuum assumption in cancellous bone. *J Biomech* 21 (4): 269-75, 1988.

58. Hart MB, Wu JJ, Chao EYS and Kelly PJ. External skeletal fixation of canine tibial osteotomies. *J Bone Joint Surg* 67-A (4): 598-605, 1985.

59. Hashemi A and Shirazi-Adl A. Finite element analysis of tibial implants - Effect of fixation design and friction model. *Comput Methods Biomech Biomed Engin* 3: 183-201, 2000.

60. Hayes WC. Biomechanics of cortical and trabecular bone: implications for assessment of fracture risk. In: *Basic orthopaedic biomechanics*. Edited by VC Mow and Hayes WC. New York, Raven Press Ltd., 1991.

61. Holt ES, Hansen ST, Mayo KA and Sangeorzan BJ. Ankle arthrodesis using internal screw fixation. *Clin Orthop* 268: 21-8, 1991.

62. Huiskes R and Chao EY. A survey of finite element analysis in orthopedic biomechanics: the first decade. *J Biomech* 16 (6): 385-409, 1983.

63. Hunt AE, Smith RM and Torode M. Extrinsic muscle activity, foot motion and ankle joint moments during the stance phase of walking. *Foot Ankle Int* 22 (1): 31-41, 2001.

64. Hvid I. Trabecular bone strength at the knee. *Clin Orthop* 227: 210-21, 1988.

65. Hvid I, Bentzen SM, Linde F, Mosekilde L and Pongsoipetch B. X-ray quantitative computed tomography: The relations to physical properties of proximal tibial trabecular bone specimens. *J Biomech* 22 (8/9): 837-44, 1989.

66. Hvid I, Rasmussen O, Jensen NC and Nielsen S. Trabecular bone strength profiles at the ankle joint. *Clin Orthop* 199: 306-12, 1985.

67. Jenny JY, Rapp E and Cordey J. Type of screw does not influence holding power in the femoral head. A cadaver study with shearing test. *Acta Orthop Scand* 70 (5): 435-8, 1999.

68. Jensen NC, Hvid I and Kroner K. Strength pattern of cancellous bone at the ankle joint. *Eng Med* 17 (2): 71-6, 1988.

69. Kabel J, Van Rietbergen B, Dalstra M, Odgaard A and Huiskes R. The role of an effective isotropic tissue modulus in the elastic properties of cancellous bone. *J Biomech* 32 (7): 673-80, 1999.

70. Katcherian DA. Treatment of ankle arthrosis. *Clin Orthop* 349: 48-57, 1998.

71. Keaveny TM and Hayes WC. A 20-year perspective on the mechanical properties of trabecular bone. *J Biomech Eng* 115 (4B): 534-42, 1993.

72. Keaveny TM, Morgan EF, Niebur GL and Yeh OC. Biomechanics of trabecular bone. *Annu Rev Biomed Eng* 3: 307-33, 2001.

73. Keller TS. Predicting the compressive mechanical behavior of bone. *J Biomech* 27 (9): 1159-68, 1994.

74. Keyak JH, Lee IY and Skinner HB. Correlations between orthogonal mechanical properties and density of trabecular bone: Use of different densitometric measures. *J Biomed Mater Res* 28: 1329-36, 1994.

75. Keyak JH and Skinner HB. Three-dimensional finite element modelling of bone: effects of element size. *J Biomed Eng* 14 (6): 483-9, 1992.

76. Kim Y. Prediction of mechanical behaviors at interfaces between bone and two interbody cages of lumbar spine segments. *Spine* 26 (13): 1437-42, 2001.

77. Kitaoka HB. Fusion techniques for failed total ankle arthroplasty. *Semin Arthroplasty* 3 (1): 51-7, 1992.

78. Kitaoka HB. Arthrodesis of the ankle: technique, complications, and salvage treatment. *Instr Course Lect* 48: 255-61, 1999.

79. Kitaoka HB, Alexander IJ, Adelaar RS, Nunley JA, Myerson MS and Sanders M. Clinical rating systems for the ankle-hindfoot, midfoot, hallux, and lesser toes. *Foot Ankle Int* 15 (7): 349-53, 1994.

80. Kitaoka HB, Luo ZP and An KN. Three-dimensional analysis of normal ankle and foot mobility. *Am J Sports Med* 25 (2): 238-42, 1997.

81. Komenda GA, Myerson MS and Biddinger KR. Results of arthrodesis of the tarsometatarsal joints after traumatic injury. *J Bone Joint Surg* 78-A (11): 1665-76, 1996.

82. Kopperdahl DL and Keaveny TM. Yield strain behaviour of trabecular bone. *J Biomech* 31: 601-8, 1998.

83. Kumaresan S, Yoganandan N and Pintar FA. Finite element analysis of the cervical spine: a material property sensitivity study. *Clin Biomech* 14: 41-53, 1999.

84. Lachiewicz PF. Rheumatoid arthritis of the ankle: the role of total ankle arthroplasty. *Semin Arthroplasty* 6 (3): 187-92, 1995.

85. Lacroix D, Murphy LA and Prendergast PJ. Three-dimensional finite element analysis of glenoid replacement prostheses: a comparison of keeled and pegged anchorage systems. *J Biomech Eng* 122: 430-6, 2000.

86. Lauge-Pedersen H, Aspenberg P, Ryd L and Tanner KE. Arch-shaped versus flat arthrodesis of the ankle joint: strength measurements using synthetic cancellous bone. *Proc Instn Mech Engrs Part H: J Engineering in Medicine* 216 (1): 43-9, 2002.

87. Lauge-Pedersen H, Knutson K and Rydholm U. Percutaneous ankle arthrodesis in the rheumatoid patient without débridement of the joint. *The Foot* 8: 226-9, 1998.

88. Leardini A, O'Connor JJ, Catani F and Giannini S. Kinematics of the human ankle complex in passive flexion: a single degree of freedom system. *J Biomech* 32: 111-8, 1999.

89. Lewis G. The ankle joint prosthetic replacement: Clinical performance and research challenges. *Foot Ankle Int* 15 (9): 471-6, 1994.

90. Li B and Aspden RM. Composition and mechanical properties of cancellous bone from the femoral head of patients with osteoporosis or osteoarthritis. *J Bone Miner Res* 12 (4): 641-51, 1997.

91. Linde F, Hvid I and Madsen F. The effect of specimen geometry on the mechanical behaviour of trabecular bone specimens. *J Biomech* 25 (4): 359-68, 1992.

92. Linde F, Norgaard P, Hvid I, Odgaard A and Soballe K. Mechanical properties of trabecular bone. Dependency on strain rate. *J Biomech* 24 (9): 803-9, 1991.

93. Lundberg A. Kinematics of the ankle and foot. In vivo roentgen stereophotogrammetry. *Acta Orthop Scand* 233 (Suppl): 1-24, 1989.

94. Lundberg A, Svensson OK, Nemeth G and Selvik G. The axis of rotation of the ankle joint. *J Bone Joint Surg* 71-B (1): 94-9, 1989.

95. Mandracchia VJ, Nelson SC and Barp EA. Current concepts of bone healing. *Clin Podiatr Med Surg* 18 (1): 55-77, 2001.

96. Mann RA and Rongstad KM. Arthrodesis of the ankle: a critical analysis. *Foot Ankle Int* 19 (1): 3-9, 1998.

97. Maurer RC, Cimino WR, Cox CV and Satow GK. Transarticular cross-screw fixation. A technique of ankle arthrodesis. *Clin Orthop* 268: 56-64, 1991.

98. McBroom RJ, Hayes WC, Edwards WT, Goldberg RP and White AA. Prediction of vertebral body compressive fracture using quantitative computed tomography. *J Bone Joint Surg* 67-A (8): 1206-13, 1985.

99. McCalden RW, McGeough JA, Barker MB and Court-Brown CM. Age-related changes in the tensile properties of cortical bone. The relative importance of changes in porosity, mineralization and microstructure. *J Bone Joint Surg* 75-A: 1193-1205, 1993.

100. McCalden RW, McGeough JA and Court-Brown CM. Age-related changes in the compressive strength of cancellous bone. The relative importance of changes in density and trabecular architecture. *J Bone Joint Surg* 79: 421-7, 1997.

101. McGuire MR, Kyle RF, Gustillo RB and Premer RF. Comparative analysis of ankle arthroplasty *versus* ankle arthrodesis. *Clin Orthop* 226: 174-81, 1988.

102. McMinn RMH, Hutchings RT and Logan BM. Color atlas of foot & ankle anatomy. 2nd ed. London, Mosby-Wolfe, 1996.

103. Miller RA, Firoozbakhsh K and Veitch AJ. A biomechanical evaluation of internal fixation for ankle arthrodesis comparing two methods of joint surface preparation. *Orthopedics* 23 (5): 457-60, 2000.

104. Mizrahi J, Silva MJ, Keaveny TM, Edwards WT and Hayes WC. Finite-element stress analysis of the normal and osteoporotic lumbar vertebral body. *Spine* 18 (14): 2088-96, 1993.

105. Monroe MT, Beals TC and Manoli 2nd A. Clinical outcome of arthrodesis of the ankle using rigid internal fixation with cancellous screws. *Foot Ankle Int* 20 (4): 227-31, 1999.

106. Monti L, Cristofolini L and Viceconti M. Methods for quantitative analysis of the primary stability in uncemented hip prostheses. *Artif Organs* 23 (9): 851-9, 1999.

107. Morgan EF and Keaveny TM. Dependence of yield strain of human trabecular bone on anatomic site. *J Biomech* 34 (5): 569-77, 2001.

108. Mosekilde L. Age-related changes in bone mass, structure and strength - effects of loading. *Z Rheumatol* 59 (Suppl 1): 1-9, 2000.

109. Muller M, Abel EW, McLeod G and Rowley DI. Pull-out strengths for a range of screws inserted into the calcaneus: a preliminary study. *Clin Biomech* 7: 125-8, 1992.

110. Müller ME, Allgöwer M, Schneider R and Willenegger H. Manual of internal fixation. Techniques recommended by the AO-ASIF Group. 3rd ed. Springer-Verlag, 1995.

111. Nasson S, Shuff C, Palmer D, Owen J, Wayne J, Carr J, Adelaar R and May D. Biomechanical comparison of ankle arthrodesis techniques: crossed screws vs. blade plate. *Foot Ankle Int* 22 (7): 575-80, 2001.

112. Natali AN and Meroi EA. A review of the biomechanical properties of bone as a material. *J Biomed Eng* 11: 266-76, 1989.

113. Natarajan RN, Chen BH, An HS and Andersson GBJ. Anterior cervical fusion. A finite element model study on motion segment stability including the effect of osteoporosis. *Spine* 25 (8): 955-61, 2000.

114. Neufeld SK and Lee TH. Total ankle arthroplasty: indications, results, and biomechanical rationale. *Am J Orthop* 29 (8): 593-602, 2000.

115. Niebur GL, Feldstein MJ, Yuen JC, Chen TJ and Keaveny TM. High-resolution finite element models with tissue strength asymmetry accurately predict failure of trabecular bone. *J Biomech* 33: 1575-83, 2000.

116. Norkin CC and Levangie PK. Joint structure and function. A comprehensive analysis. 2nd ed. Philadelphia, F.A. Davis Company, 1992.

117. O'Brien TS, Hart TS, Shereff MJ, Stone J and Johnson J. Open versus arthroscopic ankle arthrodesis: a comparative study. *Foot Ankle Int* 20 (6): 368-74, 1999.

118. Odgaard A and Linde F. The underestimation of Young's modulus in compressive testing of cancellous bone specimens. *J Biomech* 24 (8): 691-698, 1991.

119. Ogilvie-Harris DJ, Fitsialos D and Hedman TP. Arthrodesis of the ankle. A comparison of two versus three screw fixation in a crossed configuration. *Clin Orthop* 304: 195-9, 1994.

120. Okuyama K, Sato K, Abe E, Inaba H, Shimada Y and Murai H. Stability of transpedicle screwing for the osteoporotic spine. An *in vitro* study of the mechanical stability. *Spine* 18 (15): 2240-5, 1993.

121. Palastanga N, Field D and Soames R. Anatomy and human movement: structure and function. 2nd ed. Oxford, Butterworth-Heineman, 1994.

122. Perillo-Marcone A, Alonso Vázquez A and Taylor M. Assessment of the effect of mesh density on the material property discretisation within QCT based FE models: a practical example using the implanted proximal tibia. *Comput Methods Biomech Biomed Engin* 6 (1): 17-26, 2003.

123. Perlman MH and Thordarson DB. Ankle fusion in a high risk population: an assessment of nonunion risk factors. *Foot Ankle Int* 20 (8): 491-6, 1999.

124. Perren SM, Cordey J, Baumgart F, Rahn BA and Schatzker J. Technical and biomechanical aspects of screws used for bone surgery. *International Journal of Orthopaedic Trauma* 2: 31-48, 1992.

125. Pfahler M, Krodel A, Tritschler A and Zenta S. Role of internal and external fixation in ankle fusion. *Arch Orthop Trauma Surg* 115 (3-4): 146-8, 1996.

126. Pilette S, Huk OL, Yahia L and Fowles JV. Evaluation biomecanique comparative de la stabilite immediate de trois fixateurs dans l'arthrodese de la cheville. *Ann Chir* 47 (9): 905-11, 1993.

127. Pitzen TR, Matthis D, Barbier DD and Steudel WI. Initial stability of cervical spine fixation: predictive value of a finite element model. *J Neurosurg (Spine 1)* 97: 128-34, 2002.

128. Polikeit A, Nolte LP and Ferguson S. The effect of cement augmentation on the load transfer in an osteoporotic functional spinal unit: finite element analysis. *Spine* , in press.

129. Prendergast PJ. Finite element models in tissue mechanics and orthopaedic implant design. *Clin Biomech* 12 (6): 343-66, 1997.

130. Prendergast PJ and van der Meulen MCH. Mechanics of bone regeneration. In: *Bone mechanics handbook*, pp. 32/1-32/13. Edited by SC Cowin. 2nd ed. CRC Press, 2001.

131. Procter P. Ankle joint biomechanics. Bioengineering Unit, University of Strathclyde. Glasgow, 1980.

132. Procter P and Paul JP. Ankle joint biomechanics. *J Biomech* 15 (9): 627-34, 1982.

133. Reilly DT, Burstein AH and Frankel VH. The elastic modulus for bone. *J Biomech* 7: 271-5, 1974.

134. Rho JY, Ashman RB and Turner CH. Young's modulus of trabecular and cortical bone material: ultrasonic and microtensile measurements. *J Biomech* 26 (2): 111-9, 1993.

135. Rho JY, Hobatho MC and Ashman RB. Relations of mechanical properties to density and CT numbers in human bone. *Med Eng Phys* 17 (5): 347-55, 1995.

136. Roesler H. The history of some fundamental concepts in bone biomechanics. *J Biomech* 20 (11/12): 1025-34, 1987.

137. Rogge RD, Adams BD and Goel VK. An analysis of bone stresses and fixation stability using a finite element model of simulated distal radius fractures. *J Hand Surg* 27-A (1): 86-92, 2002.

138. Røhl L, Larsen E, Linde F, Odgaard A and Jorgensen J. Tensile and compressive properties of cancellous bone. *J Biomech* 24 (12): 1143-9, 1991.

139. Röhrle H, Scholten R, Sigolotto C and Sollbach W. Joint forces in the human pelvis-leg skeleton during walking. *J Biomech* 17 (6): 409-24, 1984.

140. Rüegsegger P. Imaging of bone structure. In: *Bone mechanics handbook*, pp. 9/1-9/24. Edited by SC Cowin. 2nd ed. CRC Press, 2001.

141. Saltzman CL, McIff TE, Buckwalter JA and Brown TD. Total ankle replacement revisited. *J Orthop Sports Phys Ther* 30 (2): 56-67, 2000.

142. Sarrafian SK. Anatomy of the foot and ankle: descriptive, topographic, functional. 2nd ed. Philadelphia, Lippincott, 1993.

143. Sasaki N, Nakayama Y, Yoshikawa M and Enyo A. Stress relaxation function of bone and bone collagen. *J Biomech* 26 (12): 1369-76, 1993.

144. Schatzker J, Waddell J and Stoll JE. The effects of motion on the healing of cancellous bone. *Clin Orthop* 245: 282-7, 1989.

145. Scott SH and Winter DA. Talocrural and talocalcaneal joint kinematics and kinetics during the stance phase of walking. *J Biomech* 24 (8): 743-52, 1991.

146. Scranton PE. An overview of ankle arthrodesis. *Clin Orthop* 268: 96-101, 1991.

147. Seireg A and Arkivar RJ. The prediction of muscular load sharing and joint forces in the lower extremities during walking. *J Biomech* 8: 89-102, 1975.

148. Shirazi-Adl A, Dammak M and Paiement G. Experimental determination of friction characteristics at the trabecular bone/porous-coated metal interface in cementless implants. *J Biomed Mater Res* 27: 167-75, 1993.

149. Siegler S, Chen J and Schneck CD. The three-dimensional kinematics and flexibility characteristics of the human ankle and subtalar joints. Part I: Kinematics. *J Biomech Eng* 110 (4): 364-73, 1988.

150. Silva MJ, Keaveny TM and Hayes WC. Computed tomography-based finite element analysis predicts failure loads and fracture patterns for vertebral sections. *J Orthop Res* 16 (3): 300-8, 1998.

151. Smith EJ and Wood PLR. Ankle arthrodesis in the rheumatoid patient. *Foot Ankle* 10 (5): 252-6, 1990.

152. Snyder SM and Schneider E. Estimation of mechanical properties of cortical bone by computed tomography. *J Orthop Res* 9: 422-31, 1991.

153. Spears IR, Pfleiderer M, Schneider E, Hille E and Morlock MM. The effect of interfacial parameters on cup-bone relative micromotions. A finite element investigation. *J Biomech* 34: 113-20, 2001.

154. Stauffer RN, Chao EYS and Brewster RC. Force and motion analysis of the normal, diseased, and prosthetic ankle joint. *Clin Orhtop* 127: 189-96, 1977.

155. Swindell W and Webb S. X-ray transmission computed tomography. In: *The physics of medical imaging*. Edited by S Webb. Bristol, IOP Publishing, 1988.

156. Taft TN, Burroughs PL and McDaniel WJ. Chronic arthritis. In: *The musculoskeletal system*, pp. 209-19. Edited by Wilson FC. JB Lippincott Company, 1975.

157. Thermann H, Huefner T, Schratt HE, von Glinski S, Roehler A and Tscherne H. Screw fixation for ankle arthrodeses. *Foot Ankle Surg* 5: 131-42, 1999.

158. Thompson JD, Benjamin JB and Szivek JA. Pullout strengths of cannulated and noncannulated cancellous bone screws. *Clin Orthop* 341: 241-9, 1997.

159. Thompson MS, Northmore-Ball MD and Tanner KE. Effects of acetabular resurfacing component material and fixation on the strain distribution in the pelvis. *Proc Instn Mech Engrs Part H: J Engineering in Medicine* 216: 237-45, 2002.

160. Thordarson DB, Markolf K and Cracchiolo A. Stability of an ankle arthrodesis fixed by cancellous-bone screws compared with that fixed by an external fixator. A biomechanical study. *J Bone Joint Surg* 74-A (7): 1050-5, 1992.

161. Thordarson DB, Markolf KL and Cracchiolo A. Arthrodesis of the ankle with cancellous-bone screws and fibular strut graft. *J Bone Joint Surg* 72-A (9): 1359-63, 1990.

162. Tissakht M, Eskandari H and Ahmed AM. Micromotion analysis of the fixation of total knee tibial component. *Computers & Structures* 56 (2/3): 365-75, 1995.

163. Turan I, Wredmark T and Felländer-Tsai L. Arthroscopic ankle arthrodesis in rheumatoid arthritis. *Clin Orthop* 320: 110-4, 1995.

164. Uhl RL. The biomechanics of screws. *Orthop Rev* 18 (12): 1302-7, 1989.

165. Uhthoff HK, Goto S and Cerckel PH. Influence of stable fixation on trabecular bone healing: a morphologic assessment in dogs. *J Orthop Res* 5: 14-22, 1987.

166. Van Rietbergen B, Odgaard A, Kabel J and Huiskes R. Relationships between bone morphology and bone elastic properties can be accurately quantified using high-resolution computer reconstructions. *J Orthop Res* 16 (1): 23-8, 1998.

167. Viceconti M, Monti L, Muccini R, Bernakiewicz M and Toni A. Even a thin layer of soft tissue may compromise the primary stability of cementless hip stems. *Clin Biomech* 16: 765-75, 2001.

168. Villarraga ML, Anderson RC, Hart RT and Dinh DH. Contact analysis of a posterior cervical spine plate using a three-dimensional canine finite element model. *J Biomech Eng* 121: 206-14, 1999.

169. Wheeler DL and McLoughlin SW. Biomechanical assessment of compression screws. *Clin Orthop* 350 (237-45), 1998.

170. Wirtz DC, Schiffers N, Pandorf T, Radermacher K, Weichert D and Forst R. Critical evaluation of known bone material properties to realize anisotropic FE-simulation of the proximal femur. *J Biomech* 33 (10): 1325-30, 2000.

171. Wu G, Siegler S, Allard P, Kirtley C, Leardini A, Rosenbaum D, Whittle M, D'Lima DD, Cristofolini L, Witte H, Schmid O and Stokes I. ISB recommendation on definitions of joint coordinate system of various joints for the reporting of human joint motion - part I: ankle, hip, and spine. *J Biomech* 35 (4): 543-8, 2002.

172. Yang JP, Bogoch ER, Woodside TD and Hearn TC. Stiffness of trabecular bone of the tibial plateau in patients with rheumatoid arthritis of the knee. *J Arthroplasty* 12 (7): 798-803, 1997.

173. Zannoni C, Mantovani R and Viceconti M. Material properties assignment to finite element models of bone structures: a new method. *Med Eng Phys* 20: 735-40, 1998.

174. Zernicke RF and Judex S. Adaptation of biological materials to exercise, disuse and aging. In: *Biomechanics of the musculo-skeletal system*. Edited by B Nigg and Herzog W. Wiley, 1995.

175. Zhang Y, Ahn PB, Fitzpatrick DC, Heiner AD, Poggie RA and Brown TD. Interfacial frictional behavior: cancellous bone, cortical bone, and a novel porous tantalum biomaterial. *Journal of Musculoskeletal Research* 3 (4): 245-51, 1999.

176. Zilch H, Rohlmann A, Bergmann G and Kölbel R. Material properties of femoral cancellous bone in axial loading. Part II: Time dependent properties. *Arch Orthop Traumat Surg* 97: 257-62, 1980.

177. Zioupos P and Currey JD. Changes in the stiffness, strength and toughness of human cortical bone with age. *Bone* 22 (1): 57-66, 1998.

178. Zvijac JE, Lemak L, Schurhoff MR, Hechtman KS and Uribe JW. Analysis of arthroscopically assisted ankle arthrodesis. *Arthroscopy* 18 (1): 70-5, 2002.

APPENDIX A

COMPUTED TOMOGRAPHY

Computed tomography (CT) allows the reproduction of series of cross-sectional digital images of the body. Unlike conventional radiography, X-ray transmission CT is able to distinguish structures along the direction of X-ray propagation. The commercial development of CT scanners is considered as one of the most important advances in medical technology [49,155]. Since the introduction of CT in the clinical environment in the early 70's, several generations of CT scanners have been developed; the evolution of the original technology has produced continuous improvements and increased its applicability. Amongst other uses, CT helps to: establish a correct diagnosis; show the extent of a disease process; or plan a medical or surgical treatment.

The main components of a CT system are: the gantry, which contains the scanning system with x-ray sources, detectors and data acquisition devices; the computer, which controls the hardware and processes and stores the data; and the operator's viewing console. A planar slice of the body is defined; X-ray beams are passed through the body in a number of different angles, all within the plane of the slice; and the transmitted beams are measured by the detectors. Reconstruction techniques are then used to obtain an image of the slice, that is, a two-dimensional distribution of the linear attenuation coefficient (μ). Linear attenuation coefficients are dependent on the energy of the X-rays, the atomic composition of the scanned material and its density. Series of slices are usually obtained by moving the body along the direction perpendicular to the plane of the beam, so that a three-dimensional data set containing the region of interest is created.

The reconstructed image is usually made on a rectangular array of picture elements (*pixels*). Each pixel has a value that corresponds to the linear attenuation coefficient in a volume element (*voxel*) of the scanned slice. The size of the voxels is determined by the source and detectors geometries, the number of detectors and the reconstruction algorithm. The voxel dimensions are usually called the nominal resolution. The two dimensions in the image plane coincide with the pixel size, while the third dimension is the *slice thickness*. The array of pixels is commonly displayed using varying shades of grey to represent the CT data (Figure A-1).

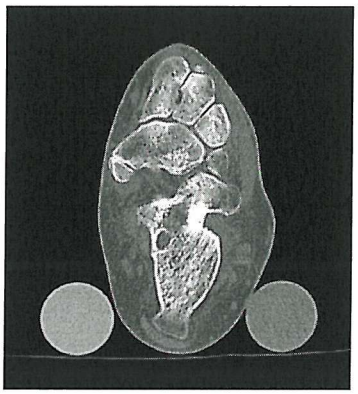

Figure A-1 CT image of a 1 mm cross-section of a foot; the image plane is perpendicular to the longitudinal axis of the leg.

It is conventional to rescale the CT data to the so-called CT numbers, defined as:

$$\text{CT number} = 1000\left(\frac{\mu}{\mu_0} - 1\right)$$

where μ_0 is the linear attenuation coefficient of water. Although the CT number is dimensionless, its value is usually said to be in Hounsfield Units (HU). Typical CT numbers are −1000 HU for air, 0 HU for water and above +1000 HU for dense bone, while CT numbers of soft tissues are relatively close to zero. CT is able to distinguish between similar tissues with relatively close CT numbers. For display purposes, the contrast of the image can be modified so that even small differences in CT number can be visualised. Thus, unlike conventional radiographs, CT can be used to study soft tissues.

X-ray CT has a typical nominal resolution of 200x200x1000 µm [140], insufficient if, for instance, the bone microstructure needs to be displayed. Micro-CT, which is based in the same principles as X-ray CT but uses specialised hardware, can obtain extremely high-resolution images (nominal resolutions up to around 10 µm). However, the very high doses of radiation limit the use of *in vivo* micro-CT, especially in the clinical environment.

Quantitative computed tomography (QCT) is a technique that measures volumetric bone densities non-invasively. The anatomical region of interest and a calibration phantom are simultaneously scanned using X-ray CT. The calibration phantom contains several "bone-equivalent" materials of known density. A quantitative interpolation between the CT numbers from these materials and from the region of interest is performed to derive bone-equivalent density values for the region scanned. This technique is widely used in the clinical environment to assess the bone mineral content in patients with bone disorders such as osteoporosis.

APPENDIX B

PILOT STUDY ON THE ASSESSMENT OF COMPRESSION THROUGH THE ARHTRODESIS SITE

Introduction

Compression across the fusion site has been considered an important factor for the success of ankle arthrodesis [17,35,47,178]. However, as mentioned in Chapter 4 (section 4.1.1), the effect of compression in bone fusion is not fully understood and the optimal degree of compression for each type of arthrodesis is unknown.

Screws, with or without fixation plates, are used to apply compression in internal fixation of fractures or arthrodesis. Compression can be assessed by measuring the axial tension generated when the screw is tightened. Two *in vivo* studies measured the axial force developed when using cortical screws to fix long bone fractures. Cortical screws are a type of screw designed with a shallow thread to bite cortical bone. Blümlein et al.[8] measured the axial force produced by cortical screws inserted through internal fixation plates. They implanted and fixed the plates on intact tibial shafts of sheep and measured the screw axial force placing a loadcell washer between the screw head and the plate. Data recording started after wound closure and lasted up to 18 weeks. Initial axial forces up to almost 2000 N were measured (Figure B-1).

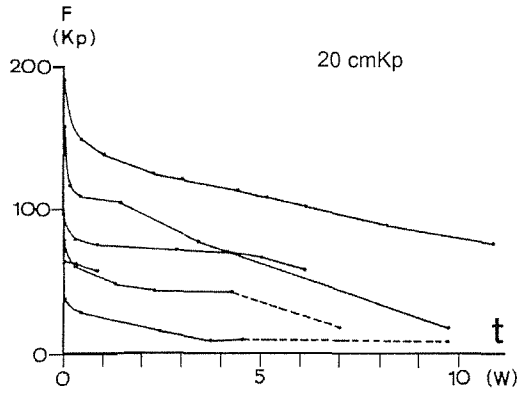

Figure B-1 Change of screw axial force with time for screw insertion torque of approximately 2 Nm (Blümlein et al.[8]). 1 Kp = 9.8 N.

The axial force initially showed a rapid drop during the first day/days, followed by a slower decrease. An appreciable amount of axial force was still present in most of the cases at the time of the last measurements. The fast initial drop of axial force was attributed to the viscoelasticity of bone, whereas the later slow decrease was attributed to the remodelling of cortical bone under pressure. They calculated the ratio of axial force *versus* initial axial force and observed that the higher the screw insertion torque, the slower the decrease of the ratio was.

Cordey et al.[26] performed a similar experiment, also in sheep, comparing the change with time of the screw axial force with and without fixation plates. Cortical screws were inserted through intact tibial diaphyses and loadcell washers placed either between the screw head and the bone or between the screw head and a plate (Figure B-2). Measurements were taken regularly during eight and a half weeks after the operation. The axial force followed the same trend as in Blümlein et al.[8]: A rapid initial drop during the first week, followed by a lower decrease thereafter (Figure B-3). The axial force decrease during the first three weeks was attributed to the viscoelasticity of the bone. From histological data obtained in the study, they observed that between the third and the fourth week after the operation, bone remodelling became the main cause for the decrease. They found that the decrease of axial force was proportional to the initial force. No differences in the decrease were observed between the plate screw and the isolated screw.

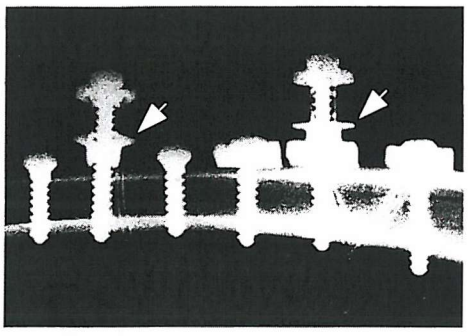

Figure B-2 Cortical screws inserted through a tibial shaft. The three screws on the right are holding a plate against the bone. Arrows mark loadcell locations (Cordey et al.[26])

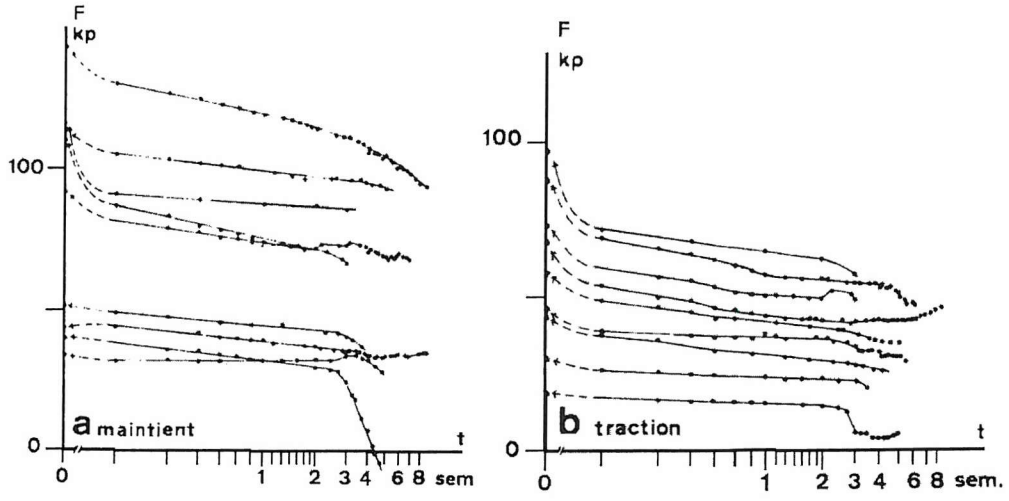

Figure B-3 Change of screw axial force with time (weeks). **a** Plate screws. **b** Screws without plate (Cordey et al.[26]). 1 Kp = 9.8 N.

Blümlein et al.[8] and Cordey et al.[26] used intact tibiae for their experiments, therefore representing ideal cases of bone stability. The effect of possible interfragmentary displacement on the change of the screw compression was not accounted for, as they did not produce any fracture or osteotomy in the tested tibiae. Based on these *in vivo* measurements, Perren et al.[124] stated that one can assume that the screw force in plate fixation is lost around six months after the operation.

Regarding ankle arthrodesis with screw internal fixation, no data have been found in the literature referring to the compression achieved by tightening of the screws at the time of surgery and its change with time. Ankle arthrodesis fixed with screws is generally performed with lagged cancellous screws. Cancellous screws are screws designed to bite cancellous bone and, in general, have a larger thread diameter and a larger pitch than cortical screws. In the field of bone fracture fixation, Wheeler and McLoughlin [169] compared the compression between bone fracture fragments fixed with cancellous screws, before and after cyclic loading. Scaphoid† bone fragments were fixed with three different types of cancellous screws; due to the varying sizes of the bone specimens, different screw lengths were used. A ring load cell was placed between the bone fragments to measure the initial compression after screw tightening. The constructs were then mounted into a materials testing machine, where cyclic bimodal tests simulated physiologic situations of cyclic torsion and axial loading. Final fragment compression was measured after loading. Two types of headless cancellous screws maintained averages of 72 and 91% of the initial compression, whilst the lag screws maintained an average 65%.

The aim of this study was to assess the interfragmentary compression generated by cancellous screws used in ankle arthrodesis by measuring the change of screw axial strain with time in *in vitro* simulated arthrodeses. The information obtained will be used in further developments of the FE models of ankle arthrodesis with internal fixation used to assess the initial stability at the fusion site.

Method

Although using ankle bones would have been preferable, femoral heads were chosen to carry out the experiment, as they are more readily available than ankle bone samples. Ten human femoral heads were collected during hip joint replacement operations and kept frozen till the day before the experiment. The femoral heads came from osteoarthritic patients, although no other data about the patients' history was known. An orthopaedic surgeon (Dr Lauge-Pedersen, Lund University Hospital, Sweden) performed flat

† The scaphoid is a small bone that forms part of the wrist.

osteotomies, approximately perpendicular to the femoral neck, dividing the heads in two halves (Figure B-4). Using standard lag techniques, instrumented 7 mm stainless steel cannulated cancellous screws (Ø 7 mm, length 50 mm, thread length 16 mm) were inserted from the proximal half of the head towards the distal half, approximately in the direction of the femoral neck (Figure B-4). Dr. Lauge Pedersen carried out the screw tightening in accordance to his experience in the surgical theatre. Although no bone density measures were taken, it is worth noting that the osteoarthritic femoral heads showed relatively dense cancellous bone and a considerable thickness of cortical bone. Excellent screw grip was achieved in all the cases.

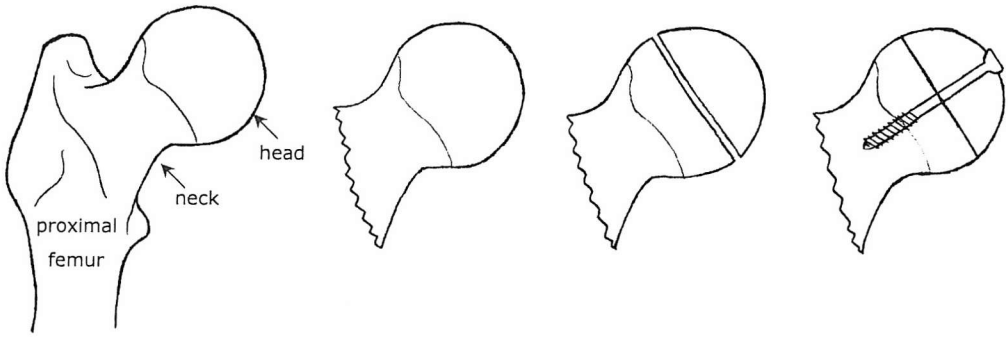

Figure B-4 Femoral head resected from femur, flat cut in two halves and fixed with a lagged cancellous screw.

Two rosette strain gauges (N2A-06-S153R-35B, Vishay Measurements Group UK Ltd., Basingstoke, UK) had been attached to the shaft of each screw, approximately between 10 and 20 mm from the head (Figure B-5), to measure the axial strain generated when the screw was tightened. Each strain-gauged screw was calibrated using a testing machine (M30k, JJ Lloyd Instruments Ltd.), by applying increasing longitudinal tensile loads to the screws and registering the corresponding voltages. An example of typical calibration data is shown in Figure B-6.

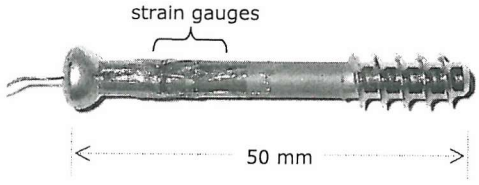

Figure B-5 Cancellous screw instrumented with 2 rosette strain gauges and wiring.

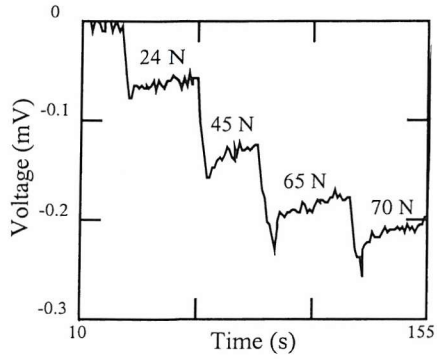

Figure B-6 Calibration curve of one of the instrumented cancellous screws.

A data acquisition card (DAQCard-AI-16XE-50, National Instruments Co.) was used, connected to a portable PC. Figure B-7 shows the experiment set-up. Data logging (at 1 Hz) started prior to the final tightening of each screw and lasted for 22 hours. The femoral head constructs were kept at room temperature, with seven of the ten constructs wrapped with gauze soaked in saline solution.

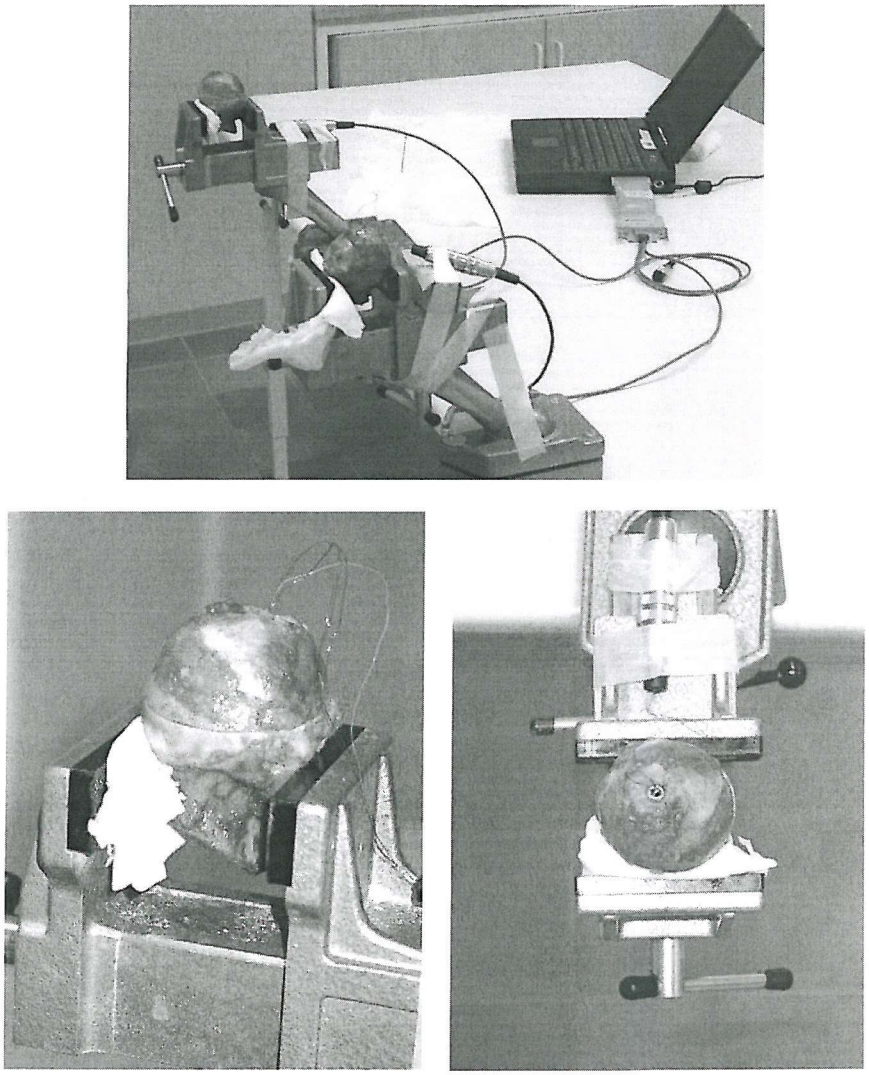

Figure B-7 Experimental set-up (above) and details of one of the samples (lateral view, bottom left; superior view, bottom right).

Results and Discussion

The axial force measured in all the specimens followed very similar trends. Figure B-8 shows a typical trace until 5 minutes after the screw tightening. A clearly distinctive peak value, corresponding to the last turn during screw tightening, was followed by a rapid drop during the first minutes and a slower decrease thereafter. This behaviour is qualitatively similar to the stress relaxation reported in the literature for cancellous and cortical bone specimens tested in various load modes [33,143,176].

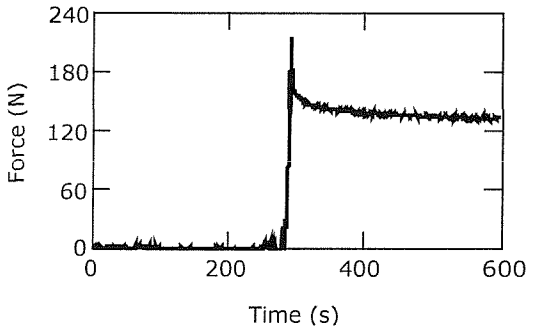

Figure B-8 Example of the axial force measured before and during the first 5 min after the screw tightening.

The peak values measured ranged from 53 to 263 N, with a median of 108 N (Figure B-9). Compression force values reported in the literature vary depending on several factors such as the type of screw, the screw dimensions and the material properties of the bone or bone substitute employed. For instance, Brown et al.[9] measured the compressive force generated by five 4 mm cancellous screws (45-46 mm long, with thread length between 15 and 20 mm) holding blocks of artificial bone; a load washer was placed between the two blocks. Mean compressive forces between approximately 145 and 205 N were measured with the screw that were cannulated. Compressive force was defined as the peak force measured prior to the screw stripping out of the blocks. These values, as well as those obtained in the current test, are substantially lower than those predicted by Blümlein et al.[8] and Cordey et al.[26] when using cortical screws inserted in ovine tibial diaphysis (see pages B-1 and B-2).

The measured percentages of the remaining to maximum axial force ranged from 30 to 79% after 120 seconds, with an average of (64±16)%. At that time, axial forces ranged from 21 to 195 N (Figure B-9). Deliglianni et al.[33] reported remaining stress after 100 s relaxation ranging from 55 to 85%. They tested cancellous bone specimens from human femoral heads by applying a constant compressive strain and measuring the stress relaxation with time. An average percentage of (79.86±3.98)% was reported for

compression perpendicular to the femoral head articular surface. They also suggested that more prominent viscoelastic behaviour was likely if larger specimens, or the intact femoral head, were used.

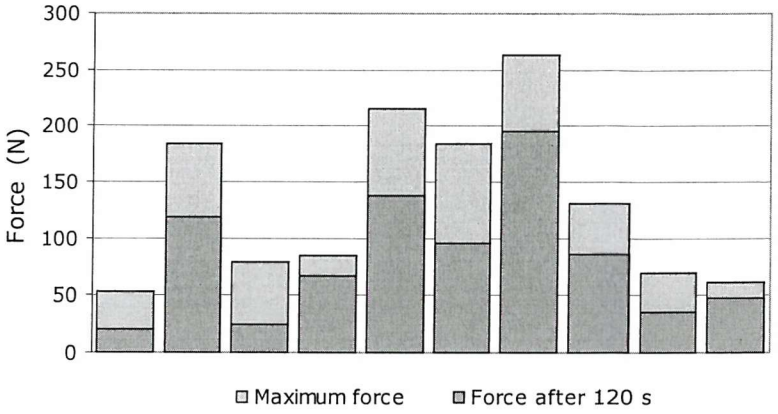

Figure B-9 Peak axial force and axial force after 120 s, measured in each specimen.

The long term decrease (within 1 and 22 hours) of the measured axial force showed an unexpected behaviour in eight out of ten specimens. The axial force gradually decreased to zero with time but then continued its decrease until the end of the test, as shown in Figure B-10. A number of factors may have caused this behaviour and need further investigation. They include: room temperature and specimen temperature changes during the duration of the test; incorrect strain gauge fixation; or the effect of a saline environment on the strain gauge performance.

In summary, this study has showed promising initial results in the assessment of the compression achieved at the arthrodesis site by cancellous screws and its change with time. An estimate of the maximum compression at the fusion site can be made from the peak axial force generated by a lag screw inserted perpendicular to the arthrodesis plane in osteoarthritic femoral heads. Similar qualitative results to those reported in the literature have been obtained in the early stages of bone relaxation. They showed a substantial decrease of the maximum compression after the first minutes. Nevertheless, these results ought to be re-examined after the conclusion of the investigation on the anomalous longer-term results is obtained.

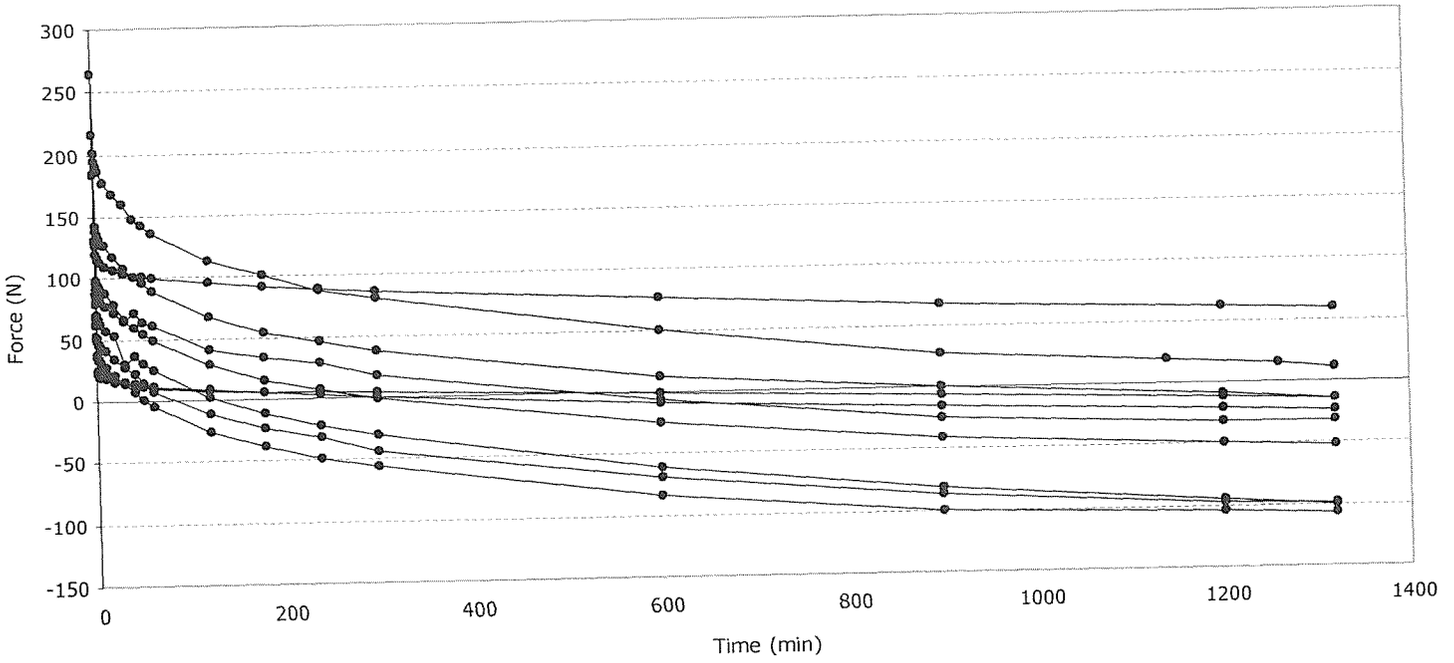

Figure B-10 Axial force measured in each specimen during 22 hours.

APPENDIX C

PUBLICATIONS

As a result of the research carried out to complete this thesis and the collaboration with colleagues within the author's research unit (Bioengineering Sciences Research Group, School of Engineering Sciences, University of Southampton) and with the Department of Orthopaedics of the University Hospital (Lund, Sweden), several pieces of research work have been presented at international conferences or published in international journals. A list of them is given below.

Part of the research material presented in Chapter 7 was submitted and accepted as an oral presentation at the 12th Annual Meeting of the European Orthopaedic Research Society (2002) [(b)]; an extended version of this material was later submitted and published in Clinical Biomechanics [(a)] and is included in this appendix. Results from the early stages of the development of a finite element model of ankle arthrodesis were submitted and accepted for poster presentation at the XVIIIth Congress of the International Society of Biomechanics (2001) [(c)]. Finally, the author took part in related studies carried out within the research group, resulting in the scientific publication referred to in (d).

(a) Alonso Vázquez A, Lauge-Pedersen H, Lidgren L and Taylor M. Finite element analysis of the initial stability of ankle arthrodesis with internal fixation: flat cut versus intact joint contours. *Clin Biomech* 18(3): 244-53, 2003.

(b) Alonso Vázquez A, Lauge-Pedersen H, Lidgren L and Taylor M. Initial stability of ankle arthrodesis with internal fixation. Finite element comparison of two methods of joint surface preparation. Transactions of the 12th Annual Meeting of the European Orthopaedic Research Society. Lausanne (Switzerland), October 2002.

(c) Alonso Vázquez A, Lauge-Pedersen H, Lidgren L and Taylor M. Stability of ankle arthrodesis with internal fixation. A preliminary finite element study. Proceedings of the XVIIIth Congress of the International Society of Biomechanics. ETH Zurich (Switzerland), July 2001.

(d) Perillo-Marcone A, Alonso Vázquez A and Taylor M. Assessment of the effect of mesh density on the material property discretisation within QCT based FE models: A practical example using the implanted proximal tibia. *Comput Methods Biomech Biomed Engin* 6(1): 17-26, 2003.